

A Contribution to the Design of Textile Reinforced Concrete Structures

Thèse n.7490

présenté le 19 juin 2020

à la Faculté de l'environnement naturel, architectural et construit
laboratoire de construction en béton

programme doctoral en génie civile et environnement

École Polytechnique Fédérale de Lausanne

pour l'obtention du grade de Docteur ès Sciences

par

Patrick Lorenzo VALERI

The logo of the École Polytechnique Fédérale de Lausanne (EPFL), consisting of the letters 'EPFL' in a bold, red, sans-serif font.

acceptée sur proposition du jury:

Prof. Dimitrios Lignos, président du jury

Prof. Aurelio Muttoni, directeur de thèse

Dr. Miguel Fernández Ruiz, co-directeur de thèse

Prof. Corentin Fivet, rapporteur

Prof. Boyan Mihaylov, rapporteur

Prof. Marco Di Prisco, rapporteur

Lausanne, EPFL, 2020

Foreword

One of the most significant challenges that concrete construction will face in the coming years is to demonstrate its potential towards a more sustainable approach for construction. This aspect will require a holistic revision on the use of this material: from the amount of clinker and composition of cement used (directly related to its CO₂ footprint) to the amount of material required for building a given element. In this context, one of the most promising approaches emerging in concrete construction is the use of Textile Reinforced Concrete (TRC). This material combines the use of a non-metallic fabric as reinforcement and a cementitious mortar matrix. Due to the fact that the fabric is insensitive to corrosion and that no passivation of the reinforcement is required, lower amounts of clinker can be used. Also, TRC allows for building very thin members, without the necessity of respecting minimum cover dimensions for protection of the reinforcement against corrosion (provided that fire protection is not required or ensured otherwise). The amount of material (and of clinker for the cement production) can thus be significantly reduced with respect to conventional designs, largely limiting the CO₂ footprint associated to concrete construction.

Within this frame, this thesis presents a research performed on TRC, both addressed at its fundamental response, its structural behaviour and its potential as building material. The work performed by Mr Valeri contributes to the current state-of-knowledge by proposing a series of original approaches for the tension and shear response of cracked TRC members verified by means of specific tests. These approaches are based on physical models, clearly explaining the observed behaviour and reproducing available experimental observations. They are also based on similar principles as those used for design of ordinary concrete elements, allowing for their future implementation in design codes. The research also outlines the potential of this material to develop a suitable and tailored architectural language, with a strong potential on light and modular construction. This thesis has been funded by cemsuisse, whose support in financial and technical terms is greatly acknowledged.

Lausanne, May 2020

Prof. Aurelio Muttoni

Dr Miguel Fernández Ruiz

Acknowledgements

First of all, the work presented in this dissertation would not have been possible without the financial support the association of Swiss cement producers (*cemsuisse* research projects #201407 and #201801). In addition, *cemsuisse* provided a substantial amount (more than 10 tons) of high-performance mortar. The assistance of Kerstin Wassmann is particularly acknowledged for the organisation of the sponsored mortar premix and superplasticizer. In addition, also the other members of the *Cemsuisse-Reserach-Commission* are acknowledged for the very fruitful technical discussions (K. Wassmann; H. Widmer; C. Pilloud; M. Tschan; I. Haefeli). The yearly meetings constituted major mile-stones of the present work and allowed to continuously adjust the direction of this investigation.

Secondly, the financial support of the School of Architecture, Civil and Environmental Engineering **ENAC** is sincerely acknowledged. The *Design Together* programme provides common ground for students, professionals and researchers to foster cutting-edge solutions for the build environment. Thanks to the encouragement of this interdisciplinary program a series of practical, hands-on, courses have been established. These have significantly contributed to generate the knowledge necessary to build the TRC Prototype Pavilion financed by the *ENAC Exploratory Grant*.

Along these lines, I would like to thank Patricia Guaita and Raffael Baur for our joyful collaboration. Their genuine devotion to architecture and teaching played a fundamental role in my doctoral-programme. Thanks to Patricia's temper I discovered the beauty of transmitting knowledge on a practical basis and humanity as the central value of our profession. On the other hand, Raffael clearly was the cornerstone of our collaboration. His abstract ideas were often the genesis of our collective materialisation. This collaboration, including the expeditions to South-America, have been one of my main driving forces during the last five years.

Accordingly, I would also like to thank all the enthusiastic professionals I encountered within these interdisciplinary collaborations: Prof. Sérgio K. Ekerman and Prof. Minho (Faculdade de Arquitetura UFBA, Salvador da Bahia, Brazil); Prof. David Jolly (Ead PUC Valparaíso, Chile); Dr. David Fernández-Ordóñez (International Federation for Structural Concrete, *fib*)

In addition I would like to thank the pool of technicians of the **GIS** (Groupe d'ingénierie des structures) and especially Jean-Claude Alain Jacot (*Blue Factory Hall*, Fribourg) for his intensive collaboration and devotion to our projects. Their experience and help made the experimental works presented in this dissertation viable.

Indubitably I would like to thank my thesis director, Prof. Aurelio Muttoni. First of all, for the acquisition of this research project and his interest in an innovative construction material. Thereafter, I deeply acknowledge his approach to construction, civil engineering and science, which has been an example-to-follow for my personal and professional development. Finally, Prof. Muttoni has been genuinely capable of pushing me continuously beyond my limits and boundaries.

By the same token, I would like to thank Dr. Miguel Fernández Ruiz, co-supervisor of the present dissertation. Most of the following work would not have been possible without his assistance, brilliant guidance, insightful supervision, critical analysis and smooth mediation. Through his passion and devotion to engineering, Dr. Fernández Ruiz has been an admirable mentor during my doctoral-journey.

Similarly, I would like to thank the jury-members of my oral thesis exam, for the useful suggestions to improve this work, as well as the fruitful discussion.

Additionally, I would like to thank all my collaborators and colleagues of the structural concrete laboratory **IBETON** of the Swiss Federal Institute of Technology **EPFL**. Not only the technical conversations, but also the broader discussions on concrete, finance, podcasting, culinary culture and the universe have been dominated by objectivity and method. Our time spend together strongly contributed to my personal development, the way I address science problems, life challenges as well as the style of this dissertation.

In particular, I would like to thank Dr. Olivier Burdet for the technical support for the experiments and the IT-infrastructure. Yvonne Bühl for her support in all administrative tasks and for tightly holding together our research group. Thereafter my office-mates: Xhsemsi, Eduardo, and especially, João who guided and supported me at the beginning of my work as well as during the hardest periods at the institute. Finally, I would like to thank Raffaele and Max for their support and all our activities outside the school.

Also, I would like to thank my friends for their sincere support. Every year, our cycling-week has been my revitalising summer-interlude. Fabio, Gianni, Alessandro, Gabriele, Stefano, Bart and Peter have helped me to take a healthy distance to my daily routine, allowing me to digest experimental and numerical findings and thus to redefine my goals and next steps.

Finally, I want to thank my family: my grandfather, for transmitting a broad curiosity in our surrounding world and teaching me how to change it by virtuous action, discipline and rational thinking; my grandmother, for her unconditional love and devotion; and my mother, for continuously encouraging me to follow my passions, her unlimited love and support in the steepest sections of this uphill climb. Eventually I would like to thank my girl-friend and partner, Noura, for her love, patience, the french lectures and for taking the lead whenever a far-reaching vision was required.

In the very end, I would like to shortly mention the professors and mentors who contributed most to shape my temperament and ideology throughout their honourable passion and trustworthy conduct: Luca Bertolini; Alberto Taliercio; Alessandro Lazzarin; Pietro Gambarova; Patrick Bamente; Roberto Nova; Marco Valente; Wulf Shubert; Richard Greiner; Werner Guggenberger; Federico Perotti; Antonio Capsoni; Gianpaolo Rosati; Conrad Jauslin; Markus Hennecke and Roberto Gargiani.

Abstract

The reduction of green-house gas emissions is one of the global challenges that our society is facing and the production of cement plays a major role because concrete is the most used material worldwide. For every 1000 kg of cement produced, 900 kg of CO₂, are released in the atmosphere. In addition, for structural concrete, the generous concrete cover, prescribed by current codes of practice, yields to robust but also to relatively heavy and massive members.

Textile Reinforced Concrete (TRC) is a novel building material made of high-strength fabrics embedded in a fine grained mortar matrix. The implementation of non-corrosive reinforcement materials allows to reduce drastically the concrete cover requirements. That empowers to cast extremely thin-walled structural elements and to reduce the structural dead-load up to 90 % (with respect to conventional Reinforced Concrete). In addition to substantial material savings associated to the structure and its foundations, low-clinker-content cements can be used, since no passivation of the reinforcement is required. That, reduces further the environmental footprint and allows to build more sustainable load-bearing structures. Despite its advantages, TRC is hardly implemented in current engineering practice. On one hand there is a lack of design regulations, but on the other, there is also a shortage of construction experiences. With the aim to promote the widespread of TRC, this work addresses both hurdles at three different levels of analysis:

First, the tensile response of TRC is investigated by means of an extensive experimental programme. It includes, tests on bare fabrics, the plain mortar and composite tension ties. On the basis of the experimental observations and the coaxial ring analogy, a mechanical model has been derived, allowing to predict the deformation capacity and resistance in a unified manner. That is fundamental to understand the effects of fabric-coating, impregnation, tie- and load introduction length on the load-bearing behavior at a micro-level.

More complex loading conditions have been investigated at a meso-scale. Full-scale load tests of thin-walled flanged members have been instrumented with external photogrammetric measurements. These have allowed to validate and adapt the Elastic-Cracked-Stress-Field approach for TRC linear members. The method allows to model beam- and discontinuity regions in a comprehensive manner as well as predicting the response under serviceability conditions and at failure in a unified way, while accounting for both, bending and shear.

Finally, the application potential of TRC is addressed at a macro-level. Starting from previous ferrocement works, different formworking materials, casting methods and connections of thin walled members have been explored. The obtained results have been condensed to design, build and erect a full-scale, demountable, prototype pavilion within a three-weeks workshop.

Eventually, a proper architectural language has been derived for light-weight structures made of thin-walled TRC members. The structural design can be performed in a comprehensive manner with the Elastic-Cracked-Stress-Field approach, while the resistance of the composite can be estimated with the coaxial ring model. That contributes to the development of code-like prescriptions for TRC and its future implementation in common construction practice for sustainable structures.

Zusammenfassung

Die Reduzierung der Treibhausgasemissionen ist eine der globalen Herausforderungen unserer Gesellschaft. Hierbei spielt die Zementherstellung eine zentrale Rolle, da Beton der am meisten verwendete Baustoff der Welt ist und für jede Tonne Zement, 900 kg CO₂ in die Atmosphäre freigesetzt werden. Hinzu kommt, dass gegenwärtige Regelwerke eine relativ großzügige Betondeckung für Stahlbetonbauwerke vorschreiben. Dies führt einerseits zu dauerhaften und robusten Bauwerken, aber andererseits auch zu massiven und relativ schweren Bauteilabmessungen.

Textilbeton ist ein neuer Baustoff, bestehend aus einer Feinbetonmatrix und endlosen Hochleistungsfasern (Multifilamentgarne). Der Einsatz einer rostfreien Bewehrung erlaubt es die notwendige Betondeckung drastisch zu reduzieren und somit extrem schlanke Betonelemente herzustellen, was zu einer Eigengewichtsreduktion von bis zu 90 % führen kann. Außerdem können auch Zemente mit niedrigem Klinkergehalt eingesetzt werden, wodurch der ökologische Fußabdruck zusätzlich reduziert werden kann. Trotz des vielversprechenden Potentials kann Textilbeton noch nicht alltäglich eingesetzt werden. Zum einen fehlen normative Bemessungsvorschriften und zum anderen ist die Anzahl der praktischen Umsetzungen im Baugewerbe noch ungenügend. Um die Verbreitung von nachhaltigen Betonkonstruktionen zu unterstützen, werden in dieser Arbeit beide Thematiken auf drei verschiedenen Ebenen abgehandelt:

Das einaxiale Zugtragverhalten ist anhand von umfangreichen Experimenten untersucht worden (Garnzugversuche, Verbundversuche und Dehnkörperversuche). Auf Basis der experimentellen Beobachtungen wurde ein mechanisches Modell auf Mikroskala-Ebene hergeleitet, um das Verformungsvermögen sowie die Tragfähigkeit des Verbundwerkstoffs einheitlich zu erfassen. Hiermit lassen sich auch die Auswirkungen von Imprägnierung, Oberflächenbeschichtung, Zugglied- und Lasteinleitungslänge anhand physikalischer Größen ganzheitlich beschreiben.

Das Biegetragverhalten wurde an schlanken Textilbetonträgern in Drei-Punkt-Biegeversuchen untersucht. Mittels optischen Messungen konnte festgestellt werden, dass die Verteilung der Hauptdehnungsrichtungen mit klassischen Spannungsfeldern übereinstimmen. Dementsprechend wurde die Spannungsfeldtheorie für Textilbeton auf einer Mesoskala angepasst. Mit diesem Ansatz können Stab- und Diskontinuitätsbereiche, sowie der Grenzzustand der Tragfähigkeit und Gebrauchstauglichkeit von Biegebalken einheitlich bemessen werden.

Die sinngemäße Bauwerksgestaltung aus textilbewehrtem Beton ist auf einer Makroskala erkundet worden. Basierend auf bestehenden Ferrozementbauwerken, sowie einer Vergleichsstudie von verschiedenen Schalungsmaterialien, Gieß- und Montageverfahren wurde ein Pavillon aus Textilbeton erstellt. Die modulare Tragkonstruktion besteht aus ausgesprochen schlanken Betonbauteilen, die mittels Schraubverbindungen zusammengebaut und demontiert werden können.

In dieser Arbeit wurde eine maßgeschnittene Bauform für schlanke Textilbetonglieder entwickelt, welche mit der Spannungsfeldtheorie nachgewiesen werden können. Dadurch wird sowohl zur Entwicklung von Bemessungsvorschriften, als auch zur Konstruktionserfahrung beigetragen, um zukünftig nachhaltigere Betontragwerke in die gängige Ingenieurpraxis besser einbinden zu können.

Riassunto

La riduzione delle emissioni di gas serra è una delle sfide globali che la nostra società sta affrontando e la produzione di cemento gioca un ruolo cruciale perché il calcestruzzo è il materiale da costruzione più utilizzato al mondo. Per ogni 1000 kg di cemento prodotto, 900 kg di CO₂ vengono rilasciati nell'atmosfera. Inoltre, per il cemento armato le normative vigenti prescrivono elevati valori di copriferro, che consentono di ottenere un sufficiente livello di durabilità strutturale, ma che conducono inevitabilmente a membrature relativamente pesanti e massicce.

Il Fibrorinforzato Tessile (FRT) è un nuovo materiale da costruzione, costituito da tessuti ad alta resistenza incorporati in una matrice cementizia. Armature con bassa sensibilità alla corrosione permettono di ridurre drasticamente il copriferro. Ciò consente la realizzazione di elementi strutturali in parete sottile e di ridurre il peso proprio fino al 90 %. Inoltre è possibile impiegare cementi a basso contenuto di clinker, in quanto non è necessario promuovere la passivazione delle armature. Questo riduce ulteriormente il suo impatto ambientale, e permette di costruire strutture decisamente più ecosostenibili. Nonostante i suoi vantaggi, la progettazione di elementi strutturali in FRT presenta ancora svariati ostacoli. Da un lato si riscontra l'assenza di prescrizioni normative, a cui si aggiunge la carenza di applicazioni pratiche. Nel presente elaborato, con l'obiettivo di promuovere la diffusione del FRT, le due problematiche sono affrontate a tre livelli di analisi:

In primo luogo, è stata studiata la risposta a trazione, attraverso un'esteso programma sperimentale che comprende prove su fibre isolate, unitamente alla caratterizzazione della malta e di tiranti compositi. Sulla base delle osservazioni sperimentali e sfruttando l'analogia del modello ad anelli concentrici è stato possibile ricavare un modello micro-meccanico che permette di predire in modo univoco sia la capacità di deformazione che la resistenza del composito. Questo costituisce un passo essenziale per comprendere l'influenza del rivestimento e dell'impregnazione delle fibre, nonché della lunghezza libera e di ancoraggio dei tiranti, sulla resistenza a trazione del composito.

Condizioni di carico più generali sono state studiate a scala maggiore, tramite prove di carico su profili sottili aperti. Le misure di deformazione sono state effettuate tramite fotogrammetria esterna, e i dati raccolti hanno permesso di validare l'approccio mediante campi di sforzo per elementi lineari in FRT. Il metodo permette di modellare le regioni tipo trave e le zone di discontinuità in modo accurato e di determinare la risposta in condizioni di esercizio e a rottura in modo univoco.

Infine, il potenziale del FRT per applicazioni strutturali è stato investigato a livello macroscopico. Sulla base di strutture in ferrocemento esistenti, è stata svolta un'indagine su diversi materiali da cassero, modalità di getto e connessioni di elementi a parete sottile. I risultati ottenuti sono stati sintetizzati per progettare, costruire ed assemblare un padiglione modulare in scala reale.

Questa ricerca ha permesso di sviluppare un nuovo linguaggio architettonico idoneo per le strutture composte da membrature a profilo sottile. La progettazione strutturale di tali membrature può essere svolta in modo esaustivo tramite la teoria dei campi di sforzo, mentre la resistenza del composito può essere stimata mediante il modello coassiale. I risultati ottenuti, contribuiscono allo sviluppo di norme progettuali e alla promozione di strutture più ecosostenibili.

Résumé

La réduction des émissions de gaz à effet de serre est l'un des défis mondiaux auxquels notre société est confrontée et la production de ciment joue un rôle crucial car le béton est le matériau de construction le plus utilisé dans le monde. Pour chaque tonne de ciment produit, 900 kg de CO₂ sont libérés dans l'atmosphère. En outre, les réglementations actuelles prescrivent des valeurs d'enrobage relativement élevées pour le béton armé assurant un niveau suffisant de durabilité structurelle, mais conduisent inévitablement à des éléments relativement lourds et massifs.

Le béton textile (BT) est un nouveau matériau de construction composé de tissus d'armature à haute résistance incorporée dans une matrice de ciment. L'insensibilité de l'armature à la corrosion permet de réduire considérablement l'enrobage. Cela rend possible la construction d'éléments structurels minces et réduit le poids propre jusqu'à 90 %. Outre les économies de matériaux, il est également possible d'utiliser des ciments à faible teneur en clinker, car il n'est pas nécessaire de favoriser la passivation de l'armature. Cela réduit encore son empreinte écologique et permet la construction d'ouvrages plus durables. Malgré ses avantages, la conception des éléments structurels en BT présente encore plusieurs obstacles. D'une part, il y a l'absence de prescriptions normatives et d'autre part le manque, d'applications pratiques. Dans ce travail qui a pour but de promouvoir la diffusion du BT, ces deux problématiques sont abordées à trois niveaux d'analyse:

Tout d'abord, la réponse à la traction du BT a été étudiée, grâce à un vaste programme expérimental qui comprend des essais sur des fibres isolées du tissu, ainsi que la caractérisation du mortier et des tirants composites. Sur la base des observations expérimentales et en exploitant l'analogie du modèle à anneaux concentriques il a été possible de dériver un modèle micromécanique qui permet de prédire, de manière unifiée, la capacité de déformation et la résistance du composite. C'est une étape essentielle pour comprendre l'influence du revêtement et de l'imprégnation des fibres, ainsi que de la longueur libre et de l'ancrage des tirants, sur la résistance à la traction du composite.

Des cas de charge plus générales ont été étudiées à plus grande échelle, avec des essais de charge sur des sections minces. Des mesures de déformation ont été effectuées par photogrammétrie qui ont permis de valider l'approche des champs de contrainte pour les éléments linéaires en BT. La méthode permet de modéliser les régions de type poutre (Bernoulli) et de discontinuité ainsi que de déterminer la réponse à l'état limite de service et à la rupture de manière unifiée.

Enfin, le potentiel du BT pour des applications structurelles a été étudié à au niveau macroscopique. Sur la base des structures existant en ferrociment, une étude des différents matériaux de coffrage, moyens de coulage et des connexions d'éléments a été réalisée. Les résultats obtenus ont permis de réaliser la conception, la construction et l'assemblage d'un pavillon modulaire de taille réelle.

Cette recherche a permis de développer un nouveau langage architectural adapté aux structures composées d'éléments minces en BT. Le dimensionnement de ces éléments structurels peut être effectué de manière générale à l'aide de la théorie des champs de contrainte, tandis que la résistance du composite peut être estimée à l'aide du modèle coaxial. Les résultats obtenus contribuent à l'élaboration de normes de conception et à la promotion de structures plus écologiquement durables.

Resumen

La reducción de las emisiones de gases de efecto invernadero constituye un desafío global para nuestra sociedad y la producción de cemento juega un papel central dado que el hormigón es el material de construcción más usado mundialmente. Por cada 1000 kg de cemento producidos, 900 kg de CO₂ son liberados a la atmósfera. La normativa vigente prescribe recubrimientos elevados para elementos de hormigón estructural con el objetivo de mejorar su durabilidad, lo que da lugar a elementos robustos, pero pesados y masivos

El Hormigón Textil (HT) es un novedoso material de construcción compuesto de fibras de alta resistencia incorporadas a un mortero de granulometría fina. El empleo de materiales de refuerzo no corrosibles permite reducir el recubrimiento, haciendo posible la construcción de elementos finos, así como la reducción de su peso propio hasta en un 90 %. Además del ahorro en material, el HT permite el uso de cementos con bajo contenido en clínker, dado que la pasivación de la armadura no es necesaria. Esto reduce la huella ecológica, y permite construir estructuras más sostenibles. A pesar de estas ventajas, el diseño de elementos estructurales con HT se enfrenta con ciertos obstáculos. Por una parte, no hay normativas disponibles, a lo que hay que añadir que actualmente se dispone de muy pocas experiencias con este material. Con el objetivo de extender el uso del HT, el presente trabajo aborda ambas limitaciones en tres distintos niveles de análisis:

En primer lugar, se investiga el comportamiento del HT en tracción mediante un programa experimental extenso. Dicho programa incluye ensayos de las propias fibras textiles, del mortero, y de tirantes fabricados con el compuesto. Sobre la base de observaciones experimentales y la analogía de los anillos concéntricos, se ha desarrollado un modelo micro-mecánico que permite predecir de forma unívoca su capacidad de deformación y su resistencia. Esto constituye un paso fundamental para comprender la influencia del revestimiento e impregnación de las fibras, así como la longitud libre y de anclaje de los tirantes, en la resistencia a tracción del compuesto.

A una escala mayor se investigan los estados de carga más generales. Ensayos de perfiles finos abiertos han sido instrumentados mediante medidas fotogramétricas. Dichos ensayos han permitido adaptar el método de los Campos de Tensiones Elásticos Fisurados a elementos lineales en HT. Gracias a este método, se ha conseguido modelizar elementos tipo viga y regiones de discontinuidad, así como predecir su respuesta en régimen de servicio y en rotura.

Finalmente, el potencial de aplicación del HT se analiza a nivel macroscópico. A partir de trabajos existentes con ferrocemento, distintos materiales de encofrado, metodologías de hormigonado y conexiones entre elementos de paredes delgadas han sido investigados. Los resultados extraídos se han sintetizado para diseñar, construir y montar un pabellón a escala real.

Este proceso ha permitido desarrollar un nuevo lenguaje arquitectónico para estructuras ligeras construidas con perfiles finos en HT. El diseño estructural se puede desarrollar mediante el método de los Campos de Tensiones, mientras que la resistencia del compuesto puede ser estimada con el modelo de anillos concéntricos. Los resultados obtenidos contribuyen a la elaboración de normas para el HT y a su promoción para la construcción de sistemas estructurales más sostenibles.

Contents

Foreword	ii
Acknowledgements	iii
Abstract	v
Zusammenfassung	vi
Riassunto	vii
Résumé	viii
Resumen	ix
1 General introduction	1
1.1 Context of this research	1
1.2 Objectives of the thesis	4
1.3 Structure of the thesis	5
1.4 List of publications	7
2 Tensile response	15
2.1 Introduction	16
2.2 Mortar, textile and pull-out tests	18
2.2.1 Cementitious mortar	18
2.2.2 Textile reinforcement	19
2.2.3 Bond properties	22
2.3 Experimental programme on TRC tension specimens	23
2.3.1 Specimen preparation	23
2.3.2 Test set-up and experimental programme	23
2.3.3 Load-deformation and load-crack-opening response	25
2.3.4 Cracking pattern	26
2.3.5 Failure	27
2.4 Analytical modelling	30
2.4.1 Interpretation of experimental results	30
2.4.2 Coaxial ring models	30
2.4.3 Response of TRC in tension (stabilised cracking stage)	34
2.4.4 Calculation of cracking load	37
2.5 Comparison to test results	37
2.5.1 Own experimental programme	37
2.5.2 Comparison to tests from the literature	38
2.5.3 General comments and outlook	39
2.6 Parametric studies	39

2.6.1	Influence of coating	39
2.6.2	Influence of anchorage and tie length	40
2.7	Conclusions	42
2.8	Appendix: Bond lag model equations	46
2.9	Appendix: symbols	49
3	Flexural behaviour	51
3.1	Introduction	52
3.2	Experimental programme	53
3.2.1	Specimen preparation and test setup	55
3.2.2	Load-deformation response	56
3.2.3	Crack pattern	56
3.2.4	Failure	57
3.3	Application of Elastic-Cracked Stress Fields to the modelling of TRC	58
3.3.1	Basic principles	58
3.3.2	Flexural response	59
3.3.3	Shear in flanged members	60
3.3.4	Implementation based on finite elements	63
3.4	Shear resistance	64
3.5	Comparison to available tests	66
3.6	Conclusions	70
3.7	Appendix: Detailed development of ECSF equations	76
3.8	Appendix: Calculation of shear resistance	77
4	Application potential	79
4.1	Introduction	80
4.2	TRC: material and structural response	81
4.2.1	Fabric reinforcement	81
4.2.2	Concentrated reinforcement	81
4.2.3	Cementitious based matrix	82
4.2.4	TRC composite	82
4.2.5	Structural response of beams: bending and shear	83
4.3	A prototype pavilion in TRC	86
4.3.1	Historical background and context of <i>ferrocement</i> and <i>argamassa armada</i>	86
4.3.2	Revisiting social construction of <i>argamassa armada</i> in TRC: a case study	87
4.3.3	Conceptual design of the TRC pavilion	89
4.4	Conclusions and outlook	96
5	General discussion	101
5.1	Conclusions	101
5.2	Outlook	106
	Appendix	115
	Curriculum Vitae	132

Chapter 1

General introduction

In 2019 concrete was the most used construction material worldwide [1, 2, 3]. Thanks to large availability of raw-materials, its structural performance and excellent durability, Reinforced Concrete (RC) is often the first choice for a wide range of structural applications (large residential structures, tall buildings, bridges, tunnels, retaining walls, foundations, canals and many others).

In order to fulfil durability requirements a minimum concrete cover ($c_{nom} = 25 - 55$ mm, according to the application) is typically prescribed by the current codes of practice [4, 5]. That, combined with the space required for the vibration and compacting of fresh concrete, leads to structural elements that are hardly thinner than 10 cm. Consequently, RC is usually associated to massive and robust constructions.

Textile Reinforced Concrete (TRC), is a new cementitious composite that allows building high-performance concrete members with enhanced durability properties [6, 7]. It is made of several layers of high-strength fabrics embedded in a fine-grained mortar [8]. The non-corrosive nature of the fabrics allow to drastically reduce cover requirements and thus to cast thin-walled elements with thicknesses below 15 mm.

1.1 Context of this research

For structural applications, Textile Reinforced Concrete presents a series of advantages:

- The fabric reinforcement is usually made of a high-strength and light-weight material (carbon, alkali-resistant glass, or basalt fibres) that is usually lighter and stronger when compared to ordinary reinforcement steel;
- Due to the non-corrosive nature of the reinforcement, cover requirements can be significantly reduced (to values between 2 and 10 mm, depending on the type of textile reinforcement) without significant influence on the durability of the structural component;
- Fine grained mortars with sufficient amount of superplasticizer achieve self-compacting properties. That, in combination with the previous point, allows casting thin-walled members with thicknesses below 15 mm;
- This allows to significantly reduce the self-weight of structural components with respect to ordinary RC and consequently massive material savings can be achieved (for both, the structure and its foundations). That reduces the environmental footprint of the construction, by reducing the consumption of raw materials;
- Additionally, no passivation of the fabric reinforcement is required to ensure its durability. Thus, low-clinker-content cements can be used which reduces further the environmental

footprint of the material;

- Fabric reinforcement typically consists of a bidirectional (orthotropic) grid of rovings. These are bundles of thousands of homogeneous filaments made of the raw material (typically alkali resistant glass, carbon or basalt). The workability (or form-stability) of the fabric depends on the degree and type of coating or impregnation of the rovings. In this context, flexible textiles can be used to reinforce complex geometries and are found to be particularly suited for the construction of double-curved shell structures;
- Also, the orientation of the reinforcement-grid can be easily aligned with the principal direction of stresses and the number of layers can be tailored according to the inner force demand;
- Thin-walled TRC elements are most suited to be realised within a prefabrication facility. In such environment, high performance materials can be handled more easily when compared to exposed construction sites and thus higher quality can be expected. That allows for better working conditions and a further reduction of the environmental footprint, since no heavy machinery is requested on site for the assembly of TRC elements [9, 10, 11];
- To exploit further the potential of TRC, lightweight components can be assembled by means of demountable connections. In such manner, structural elements can be demounted or replaced if necessary;
- Finally, lightweight TRC-elements are also suitable for the construction of prototypes, models and mock-ups. The material can be integrated within practical university courses and replace timber for the construction of full-scale prototypes [12].

Following these characteristics TRC has attracted a series of industrial and academic researches. During the past decades the material experienced a rapid evolution and at the same time various aspects related to the load-bearing behaviour have been investigated:

- First of all, the material experienced an important evolution especially with respect to the reinforcement. The first textiles used for TRC were made of uncoated alkali-resistant glass or carbon fabrics [13]. In order to improve their efficiency, bond performance and workability, specific secondary coatings and impregnations (mainly based on epoxy resins) have been developed [14]. In addition, the geometry of the rovings has been optimised in order to maximise the mechanical bond to the surrounding matrix [15, 16];
- Secondly, a significant amount of research has been dedicated to find a suitable testing system to characterise TRC in tension (tensile forces aligned to the direction of the reinforcement [17, 18, 19]). These works are very important for the development of a standardised testing method that minimises the effects of boundary conditions (length of the load introduction and degree of freedom at the extremities). In such manner, different composites can be tested independently and their performance compared with minimum bias;
- The performance of different systems and compositions has been studied: notably, the addition of short fibres in the matrix mix, and the effect of prestressing of the fabric reinforcement [20, 21, 22];
- Other fundamental works have focused on the bond between reinforcement and matrix [23, 24, 25] and the development length of the textile reinforcement [26];
- On the basis of the experimental works described above, several models have been developed that allow predicting the uniaxial tensile response of TRC. These comprise both, numerical [27, 28] and analytical approaches [29, 30, 31] that aim to predict: (1) the average crack

spacing and opening; (2) the deformation capacity of the composite; and (3) its failure load (and mechanism);

- The response of TRC in uniaxial tension is used to characterise the performance of the composite. Differently, modelling the tensile behaviour is a fundamental tool to understand the load-bearing mechanism of the composite material. However, in structures, principal tensile stresses are not always aligned with the orientation of the reinforcement and thus experimental campaigns investigating bi-axial loading conditions have been performed in order to study the behaviour and strength of: (1) thin TRC plates subjected to bi-axial-tension [32, 33], and (2) tension specimen with inclined reinforcement [34, 35]. Based on these experiments, empirical formulations have been derived, that allow to account for the orientation of the reinforcement with respect to the loading direction [34, 36, 37];
- Structures are in general made to withstand external loads. The load-bearing mechanism can be described by a set of internal forces respecting equilibrium within the member and between the components of the structure. Internal actions only very rarely correspond to pure tension but comprise also compression, bending, shear or any given combination of those. The structural behaviour of Textile Reinforced Concrete linear members has been studied from an experimental and analytical standpoint [38, 39, 40]. Both, bending and shear-failures have been examined in order to derive formulations for flexural members [41, 42];
- Aside from folded linear members, TRC is particularly attractive for the construction of thin-walled shell structures. These are characterised by predominant axial (or membrane) actions with respect to out-of-plane bending. Different researches have addressed the design, optimisation and verification of such structures by combining numerical modelling approaches with experimental evidences and prototypes [43, 44, 45];
- The conceptual design of structures is usually not based on structural optimisation only, but accounts also for the construction and erection procedures. Further research on these topics has been performed with particular focus on the implementation of flexible formworks [46, 47];
- When TRC is implemented as part of the load-bearing structure, also other aspects need to be considered:
 - The performance of the material under elevated temperature (for example in case of fire in buildings [48, 49, 50]);
 - The fatigue behaviour and the resistance under cyclic loading conditions (for instance traffic actions on bridges [51, 52, 53]);
 - The durability of the material when exposed to weathering conditions [54, 55, 56, 57].
- A reliable design also requires an adequate safety format in order to guarantee the recommended level of structural safety. To fulfil this aspect, some authors have performed reliability analyses and proposed partial safety factors for the fabric reinforcement that allows to perform a safe design for TRC structural members with the partial safety format method [58, 59, 60];

In parallel to these researches, also the application potential of TRC has been widely explored. Particular attention has been dedicated to sandwich-panels (mainly for facade elements, [61, 62, 63, 64, 65]); parking slabs [66]; bridge-decks [67, 68]; precast formworks [69, 70] and thin-walled shell structures [37, 71, 72].

Nowadays, TRC is starting to widespread within the construction industry and by the current year 2020, several applications have been realised. These include pedestrian bridges [73, 74], pavilions

[75, 76, 77, 78], facade elements [79, 80, 81], as well as numerous retrofitting works [82, 83, 84]. However, at the current state, there exist no code-like prescription nor national guidelines for the design of TRC structural members. That is a major obstacle for designers, engineers and practitioners willing to implement the material in future design practice without an individual approval [85]. In parallel, also contractors need to develop consistent construction experiences so that TRC can be implemented as a competitive structural solution on a larger scale.

1.2 Objectives of the thesis

As described in the previous section, the specific implementation of TRC as a structural construction material can lead to a series of benefits. Therefore, the main objective of this thesis is to contribute to the widespread of the material for structural applications. The problem is tackled from two different perspectives that comprise different levels of analysis (see Fig. 1.1):

1. The material and structural behaviour is investigated on a fundamental level in order to support the advancement of design prescriptions for TRC. Major attention is dedicated to the development of mechanical models (strictly speaking based on physics and mechanics) which allows to understand, replicate and predict the response of TRC at different levels of analysis:
 - i At the **micro-level**, the load-bearing behaviour of TRC under uniaxial tension is investigated, accounting for the interactions between filaments that compose the fabric reinforcement;
 - ii More complex loading conditions (bending and shear) are addressed at a **meso-scale**. At this level, the composite is mainly characterised by the mechanical properties of the composite and specific efficiency factors;

The aim is to derive a unique approach for each level of analysis, that is valid for different TRC-composites without the need to calibrate tailored efficiency factors for various fabric reinforcements. A consistent research approach has been adopted for the different levels of investigation. That comprises: (1) experimental works in combination with photogrammetric measurements; (2) modelling based on conventional mechanics and previously established approaches; (3) validation of the proposed models with the performed tests and other independent, experimental programs performed by other researchers; and (4) parametric studies to investigate the robustness of the proposed models for specific limit cases.

2. In parallel, the potential of modular construction methodologies for lightweight TRC structures has been investigated in a broader manner at a **macro-scale**. In this context, the aim is to encourage investors, designers and contractors to implement new solutions based on prefabricated TRC-elements. That comprises the development of suitable formworking methods for linear folded members and vaults, as well as investigations concerning suitable connections between structural components and their construction and erection procedures.

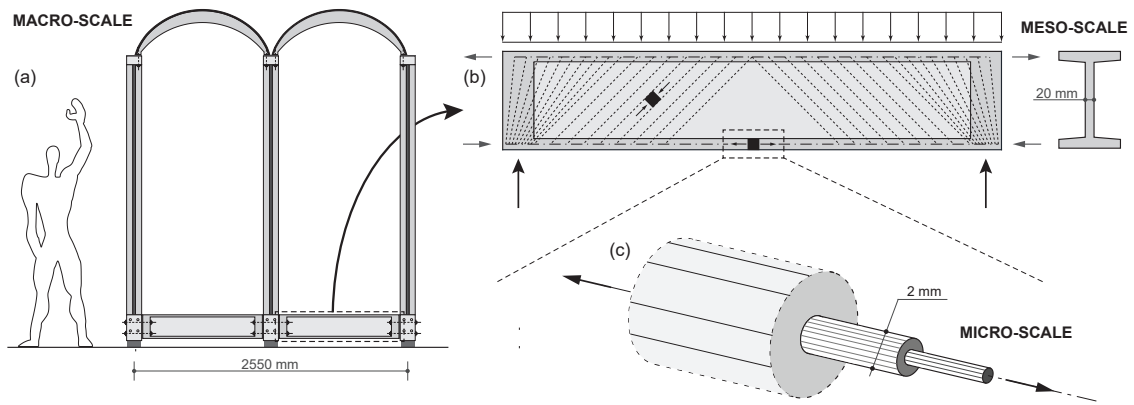


Figure 1.1: Three levels of investigations: (a) macro-scale; (b) meso-scale; and (c) micro-scale.

1.3 Structure of the thesis

The present work is structured in three parts that correspond to a series of scientific publications (see Section 1.4). Within these, the structural behaviour of Textile Reinforced Concrete under different loading conditions and at different levels of analysis is studied:

- The uniaxial response in tension (fabric reinforcement aligned to the loading direction) is investigated in **chapter 2**. For that purpose, a comprehensive experimental programme has been carried out consisting of: 300 tension tests of different rovings; 50 pull-out tests under different conditions to characterise the interface behaviour between reinforcement and matrix; and 28 composite tension ties. The first part of the chapter illustrates the mechanical behaviour of the composite and its components (fabric reinforcement in tension, mortar in tension and compression and the interface response). In the second part of the chapter, a mechanical model at the **micro-level** has been derived on the basis of the co-axial ring analogy (separate treatment of core and sleeve filaments). Within that framework, a novel interface-relationship has been incorporated (accounting for an engagement-slip for the activation of bond stresses between the layers). That, allows to account for the differential activation of filaments within the rovings (variable stress-profile). In such manner, the deformation capacity and failure can be predicted in a unified manner, without the necessity to calibrate empirical efficiency factors (strictly speaking all parameters have a physical background with consistent units). The proposed model is formulated in an analytical manner, but it can be implemented also in a numerical framework. Its performance has been validated against 49 tests performed by other researchers (with different fabrics). The global performance of the model is thus assessed on a total of 77 tests, showing consistent results and fine agreement (with a low coefficient of variation). Finally, the robustness of the model is investigated by analysing a series of case-studies (size effect, anchorage conditions of the tie and influence of fabric coating, impregnation and waviness);
- In **chapter 3**, the flexural response of linear TRC-members is investigated. For that aim, two full-scale double-T beams were tested in a three-point-bending configuration. Tracking of deformations and displacements by means of photogrammetry (Digital Image Correlation), allowed to determine the orientation of principal strains during loading and at failure. Based on these experimental observations, the Elastic-Cracked-Stress-Field (ECSF) method has been adapted, accounting for the peculiar behaviour of TRC at the **meso-level** (linear-elastic response of the reinforcement in tension with brittle failure). The proposed framework allows to treat bending and shear in a unified and manner, and so to predict the response at serviceability and failure of the member. In particular, the proposed set of equations (section 3.3.3)

allows to calculate the inclination of the principal strains and stresses for linear members. On that basis, and accounting for the reduced resistance due to concrete spalling, the shear capacity can be assessed by considering separately the failure of transverse reinforcement and crushing of concrete. The consistency of the proposed model has been validated against other tests of the scientific literature showing sound and fine agreement;

- The application potential of Textile Reinforced Concrete, **chapter 4**, has been extensively explored at the **macro-level** within a series of different activities:
 - A practical course given to undergraduate students (6th semester of civil engineering and architecture). In the *Unité d'enseignement: Argamassa Armada en Salvador de Bahia* (PENS-308), ferrocement works are studied and re-interpreted in Textile Reinforced Concrete. Within the period 2016 - 2020, more than 20 segments and 5 full-scale TRC elements were casted and subjected to load tests [78, 86];
 - In the *Semaine ENAC: Making Structural Logic* (PENS-201) undergraduate students (4th semester of civil engineering and architecture) have realised a series of TRC elements. In order to investigate the efficiency of different formworking methods (timber, steel and geotextile moulds) a series of 15 full-scale members have been realised between 2017 and 2019;
 - Design and construction of a demountable, post-tensioned concrete Canoe. The *Kånöepfl* was build by a group of 8 students (7th semester of civil engineering) for the participation at the international concrete canoe regatta in Cologne (DE);
 - Design of a segmental tube in Textile Reinforced Concrete: The *alphaShell* was designed for high-speed magnetic levitation trains that run in vacuum tunnels (for instance hyperloop). For a proof-of-concept a short segment of 1.5 m of length, 1.8 m of diameter and a thickness of 20 mm has been build by a group of 7 students (7th semester of civil engineering);
 - During the *Summer School: Open City Research Platform*, edition 2019, Valparaiso (Chile) a group of three students build two full-scale shells (1.8 × 1.8 m and 3.6 × 3.6 m respectively). By using flexible fabric formworks, a minimal thickness of approximately 15 mm could be achieved;
 - A structural system in TRC was developed by a visiting student from Politecnico di Milano (Italy). The system made of modular elements was mainly designed for social-housing applications in unformal cities [87]. A full-scale module of a floor segment has been build and subjected to load-testing to verify its performance [78, 88];
 - Two master works (2018 and 2020 respectively) have focused on the design and construction of modular outdoor shelters for sport equipment (bicycles, canoes, surf-boards, and so forth). Each one of these works comprised the design, construction and testing of a single module in full-scale (four and five meters in length respectively). Based on this experience the concept was then extrapolated for larger structural elements (car-parking's, beach-stands, bus-stations, and others).

Based on these experiences, in September 2019 a full-scale pavilion was built within a three-weeks workshop by 24 students (17 of EPFL, Switzerland and 7 from the FAUFBA, Brasil). The techniques, methods and knowledge accumulated in the experiences described above were integrated in the design, construction and erection of the modular structure that is described and discussed in **chapter 4**.

1.4 List of publications

The present work has been realised at the structural concrete laboratory **IBETON** of the Swiss Federal Institute of Technology Lausanne **EPFL**. Within this PhD-thesis, a series of publications have been composed that comprise this dissertation or are stricly related to it:

- 2020 **Textile Reinforced Concrete for sustainable structures: futures perspectives and application to a prototype pavilion** *Valeri, P.; Guaita, P.; Baur, R.; Fernández Ruiz, M.; Fernández-Ordóñez Hernández, D.; Muttoni, A.* Structural Concrete
- 2020 **Modelling of Textile Reinforced Concrete in bending and shear with Elastic-Cracked Stress Fields** *Valeri, P.; Fernández Ruiz, M.; Muttoni, A.* Engineering Structures
- 2020 **Tensile Response of Textile Reinforced Concrete** *Valeri, P.; Fernández Ruiz, M.; Muttoni, A.* Construction and Building Materials
- 2019 **The potential of Textile Reinforced Concrete for design of innovative structures** *Valeri, P.; Guaita, P.; Baur, R.; Fernández Ruiz, M.; Muttoni, A.* fib-Conceptual design Symposium, Madrid, Spain
- 2019 **New perspectives for design of lightweight structures by using textile reinforced concrete;** *Valeri, P.; Fernández Ruiz, M.; Muttoni, A.* fib-Symposium, Krakaw, Poland
- 2018 **Experimental research on Textile Reinforced Concrete for the development of design tools;** *Valeri, P.; Fernández Ruiz, M.; Muttoni, A.* 12th. International fib-PhD-Symposium, Prague, Czech-Republic
- 2018 **Pedagogy thorough artisanal construction of thin-walled concrete elements: a dialogue between engineering and architecture** *Valeri, P.; Guaita, P.; Baur, R.; Fernández Ruiz, M.; Muttoni, A.* IV Int. Conference on Structural Engineering Education Without Borders, Madrid, Spain
- 2017 **Building in a lighter and more sustainable manner: textile reinforced concrete for thin structural elements** *Valeri, P.; Fernández Ruiz, M.; Muttoni, A.* Technical Report *cemsuisse*

Bibliography

- [1] PF Tunji-Olayeni, IO Omuh, AO Afolabi, RA Ojelabi, and EE Eshofonie. Effects of construction activities on the planetary boundaries. In *Journal of Physics: Conference Series*, volume 1299, page 012005. IOP Publishing, 2019.
- [2] Yurong Zhang, Wei Luo, Jingjing Wang, Yuanfeng Wang, Yaqin Xu, and Jianzhuang Xiao. A review of life cycle assessment of recycled aggregate concrete. *Construction and Building Materials*, 209:115–125, 2019.
- [3] Raili Kajaste and Markku Hurme. Cement industry greenhouse gas emissions–management options and abatement cost. *Journal of Cleaner Production*, 112:4041–4052, 2016.
- [4] *EN 1992-1-1 Eurocode 2: Design of concrete structures - Part 1-1: General rules and rules for buildings*, Brussels, 2005. EN, CEN.
- [5] fib (The International Federation for Structural Concrete). *fib Model Code for concrete structures 2010*. Ernst und Sohn Verlag Germany, 2013.
- [6] Wolfgang Brameshuber. Textile Reinforced Concrete. State-of-the-Art Report. Technical report, RILEM Technical Committee TC201-TRC, Aachen, 2009.
- [7] Alva Peled, Arnon Bentur, and Barzin Mobasher. *Textile Reinforced Concrete - Modern Concrete Technology*. Boca Raton : CRC Press, Taylor & Francis Group, 1st edition edition, 2017. ISBN 9780367866914.
- [8] Chokri Cherif. *Textile materials for lightweight constructions: Technologies - methods - materials - properties*. Springer, 2016.
- [9] Ying Chen, Gül E Okudan, and David R Riley. Sustainable performance criteria for construction method selection in concrete buildings. *Automation in construction*, 19(2):235–244, 2010.
- [10] Oriol Pons and Gerardo Wadel. Environmental impacts of prefabricated school buildings in catalonia. *Habitat International*, 35(4):553–563, 2011.
- [11] Xinying Cao, Xiaodong Li, Yimin Zhu, and Zhihui Zhang. A comparative study of environmental performance between prefabricated and traditional residential buildings in china. *Journal of cleaner production*, 109:131–143, 2015.
- [12] Patrick Valeri, Patricia Guaita, Raffael Baur, and Miguel Fernández Ruiz. Pedagogy through artisanal construction of thin-walled concrete elements: a dialogue between engineering and architecture. In ACHE, editor, *Proceedings of the IV Int. Conference on Structural Engineering Education*, pages 1–10, Madrid, 2018. ACHE.
- [13] Manfred Curbach and Frank Jesse. High-performance textile-reinforced concrete. *Structural engineering international*, 9(4):289–291, 1999.
- [14] Christian Kulas. *Zum Tragverhalten getränkter textiler Bewehrungselemente für Betonbauteile*. PhD thesis, RWTH, 2013.
- [15] Philipp Preinstorfer, Benjamin Kromoser, and Johann Kollegger. Einflussparameter auf die spaltrissbildung in textilbeton. *Beton-und Stahlbetonbau*, 113(12):877–885, 2018.
- [16] Philipp Preinstorfer and Johann Kollegger. New insights into the splitting failure of textile-reinforced concrete. *Composite Structures*, page 112203, 2020.

- [17] Diana Arboleda, Francesca Giulia Carozzi, Antonio Nanni, and Carlo Poggi. Testing procedures for the uniaxial tensile characterization of fabric-reinforced cementitious matrix composites. *Journal of Composites for Construction*, 20(3):04015063, 2016.
- [18] Rilem Technical Committee. Recommendation of RILEM TC 232-TDT: test methods and design of textile reinforced concrete. *Materials and Structures*, 49(12):4923–4927, 2016.
- [19] Elisabeth Schütze, Jan Bielak, Silke Scheerer, Josef Hegger, and Manfred Curbach. Einaxialer Zugversuch für Carbonbeton mit textiler Bewehrung. *Beton- und Stahlbetonbau*, 113(1):33–47, 2018.
- [20] HW Reinhardt and M Krüger. Vorgespannte dünne platten aus textilbeton. *Textilbeton-1. Fachkolloquium der Sonderforschungsbereiche*, 528:165–174, 2001.
- [21] Rabea Barhum and Viktor Mechtcherine. Influence of short dispersed and short integral glass fibres on the mechanical behaviour of textile-reinforced concrete. *Materials and structures*, 46(4):557–572, 2013.
- [22] Deju Zhu, Sai Liu, Yiming Yao, Gaosheng Li, Yunxing Du, and Caijun Shi. Effects of short fiber and pre-tension on the tensile behavior of basalt textile reinforced concrete. *Cement and Concrete Composites*, 96:33–45, 2019.
- [23] S Sueki, C Soranakom, B Mobasher, and A Peled. Pullout-Slip Response of Fabrics Embedded in a Cement Paste Matrix. *Journal of materials in civil engineering*, 19(September):718–727, 2005.
- [24] Hana Aljewifi, Bruno Fiorio, and Jean-Louis Gallias. Pull-out behaviour of a glass multifilaments yarn embedded in a cementitious matrix. *EURO-C 2010 – Computational Modelling of Concrete Structures, Schladming, Austria*, 2010.
- [25] Natalie Williams Portal, Ignasi Fernandez Perez, Lars Nyholm Thrane, and Karin Lundgren. Pull-out of textile reinforcement in concrete. *Construction and Building Materials*, 71:63–71, 2014.
- [26] Enrico Lorenz. *Endverankerung und übergreifung textiler bewehrungen in betonmatrices*. PhD thesis, Technische Universität Dresden, 2014.
- [27] Pello Larrinaga, Carlos Chastre, Hugo C Biscaia, and José T San-José. Experimental and numerical modeling of basalt textile reinforced mortar behavior under uniaxial tensile stress. *Materials & Design*, 55:66–74, 2014.
- [28] Elisa Bertolesi, Francesca Giulia Carozzi, Gabriele Milani, and Carlo Poggi. Numerical modeling of fabric reinforce cementitious matrix composites (frcm) in tension. *Construction and Building Materials*, 70:531–548, 2014.
- [29] J. Aveston and A. Kelly. Theory of multiple fracture of fibrous composites. *Journal of Materials Science*, 8(3):352–362, 1973.
- [30] S. Ohno and D. J. Hannant. Modeling the Stress-Strain Response of Continuous Fiber Reinforced Cement Composites. *ACI Materials Journal*, 91(3):306–312, 1994.
- [31] Yiska Goldfeld. Structural modelling of textile-reinforced concrete elements under uniaxial tensile loading. *Composite Structures*, 235:111805, 2020.
- [32] Dirk Jesse. *Tragverhalten von textilbewehrtem beton unter zweiachialer zugbeanspruchung*. 2012.

- [33] J Hegger, S Voss, M di Prisco, R Felicetti, and GA Plizzari. 135. textile reinforced concrete under biaxial loading. In *6th International RILEM Symposium on Fibre Reinforced Concretes*, pages 1463–1472. RILEM Publications SARL, 2004.
- [34] J Hegger, N Will, Oliver Bruckermann, and Stefan Voss. Load-bearing behaviour and simulation of textile reinforced concrete. *Materials and structures*, 39(8):765–776, 2006.
- [35] Stefan Voss. *Ingenieurmodelle zum Tragverhalten von textildbewehrtem Beton*. PhD thesis, Fakultät für Bauingenieurwesen der Rheinisch-Westfälischen Technischen Hochschule Aachen, 2008.
- [36] Oliver Bruckermann, Josef Hegger, and Alaa G Sherif. Modeling of textile-reinforced concrete with inclined textile orientation. *ACI Materials Journal*, 104(5):511, 2007.
- [37] R Chudoba, E Sharei, and A Scholzen. A strain-hardening microplane damage model for thin-walled textile-reinforced concrete shells, calibration procedure, and experimental validation. *Composite Structures*, 152:913–928, 2016.
- [38] J Hegger and S Voss. Investigations on the bearing behaviour and application potential of textile reinforced concrete. *Engineering structures*, 30(7):2050–2056, 2008.
- [39] Natalie Williams Portal, Lars Nyholm Thrane, and Karin Lundgren. Flexural behaviour of textile reinforced concrete composites: experimental and numerical evaluation. *Materials and Structures*, 50(1):1–14, 2017.
- [40] Philipp Preinstorfer, Benjamin Kromoser, and Johann Kollegger. Flexural behaviour of filigree slab elements made of carbon reinforced UHPC. *Construction and Building Materials*, 199: 416–423, 2019.
- [41] Barzin MobasherP. Flexural design of strain hardening cement composites. *BEFIB2012–Fiber reinforced concrete Joaquim Barros et al., UM, Guimarães*.
- [42] Sergej Rempel, Marcus Ricker, and Josef Hegger. Design model with an iterative and closed approach for textile reinforced concrete structures with bending load-clear bending load and a combination with normal force. *Beton-Und Stahlbetonbau*, 2020.
- [43] Tine Tysmans, Sigrid Adriaenssens, Heidi Cuypers, and Jan Wastiels. Structural analysis of small span textile reinforced concrete shells with double curvature. *Composites science and technology*, 69(11-12):1790–1796, 2009.
- [44] Josef Hegger, Manfred Curbach, Alexander Stark, Sebastian Wilhelm, and Kristina Farwig. Innovative design concepts: Application of textile reinforced concrete to shell structures. *Structural Concrete*, (August):1–10, 2017.
- [45] Will Hawkins, John Orr, Paul Shepherd, Tim Ibell, and Julie Bregulla. Thin-shell textile-reinforced concrete floors for sustainable buildings. In *Proceedings of IASS Annual Symposia*, number 7, pages 1–9. International Association for Shell and Spatial Structures (IASS), 2017.
- [46] Niki Cauberg, Tine Tysmans, Sigrid Adriaenssens, Jan Wastiels, Marijke Mollaert, and Bachir Belkassem. Shell elements of textile reinforced concrete using fabric formwork: a case study. *Advances in Structural Engineering*, 15(4):677–689, 2012.
- [47] Sandra Gelbrich, Henrik L Funke, Andreas Ehrlich, and Lothar Kroll. Flexible fiber-reinforced plastic formworks for the production of curved textile-reinforced concrete. *Advances in Structural Engineering*, 21(4):580–588, 2018.

- [48] H-W Reinhardt, M Krüger, M Raupach, and J Orlowsky. Behavior of textile-reinforced concrete in fire. *Special Publication*, 250:99–110, 2008.
- [49] D Ehlig, F Jesse, and M Curbach. High temperature tests on textile reinforced concrete (trc) strain specimens. In *International RILEM Conference on Material Science*, pages 141–151. RILEM Publications SARL, 2010.
- [50] Isabella Colombo, Matteo Colombo, Anna Magri, Giulio Zani, and Marco di Prisco. Textile reinforced mortar at high temperatures. In *Applied mechanics and materials*, volume 82, pages 202–207. Trans Tech Publ, 2011.
- [51] S Ortlepp and F Jesse. Experimental investigation of static fatigue strength of textile reinforced concrete. In *ICTRC'2006-1st International RILEM Conference on Textile Reinforced Concrete*, pages 131–140. RILEM Publications SARL, 2006.
- [52] Deju Zhu, Alva Peled, and Barzin Mobasher. Dynamic tensile testing of fabric–cement composites. *Construction and Building Materials*, 25(1):385–395, 2011.
- [53] Flávio de Andrade Silva, Marko Butler, Viktor Mechtcherine, Deju Zhu, and Barzin Mobasher. Strain rate effect on the tensile behaviour of textile-reinforced concrete under static and dynamic loading. *Materials Science and Engineering: A*, 528(3):1727–1734, 2011.
- [54] Heidi Cuypers, Jeanette Orlowsky, Michael Raupach, and Till Büttner. Durability aspects of ar-glass-reinforcement in textile reinforced concrete, part 1: Material behaviour. In Christian U. Grosse, editor, *Advances in Construction Materials 2007*, pages 381–388, Berlin, Heidelberg, 2007. Springer Berlin Heidelberg.
- [55] J. Orlowsky and M. Raupach. Durability model for AR-glass fibres in textile reinforced concrete. *Materials and Structures/Materiaux et Constructions*, 41(7):1225–1233, 2008.
- [56] Marko Butler, Viktor Mechtcherine, and Simone Hempel. Experimental investigations on the durability of fibre-matrix interfaces in textile-reinforced concrete. *Cement and Concrete Composites*, 31(4):221–231, 2009.
- [57] Marko Butler, Viktor Mechtcherine, and Simone Hempel. Durability of textile reinforced concrete made with ar glass fibre: effect of the matrix composition. *Materials and structures*, 43(10):1351–1368, 2010.
- [58] Sergej Rempel. *Zur Zuverlässigkeit der Bemessung von biegebeanspruchten Betonbauteilen mit textiler Bewehrung*. PhD thesis, Ph. D. Thesis, RWTH Aachen University, Aachen, Germany, 2018.
- [59] Ulrich Häußler-combe, Jörg Weselek, and Frank Jesse. A Safety Concept for Non-Metallic Reinforcement for Concrete under Bending. *ACI Structural Journal*, (116):151–160, 2019.
- [60] CEN TC250. Sc2: Eurocode 2–commentary. *European Concrete Platform*, 2008.
- [61] Isabella Giorgia Colombo, Matteo Colombo, and Marco Prisco. Bending behaviour of Textile Reinforced Concrete sandwich beams. *Construction and Building Materials*, 95:675–685, 2015.
- [62] Zakaria Ilyes Djamaï, Myriam Bahrar, Ferdinando Salvatore, Amir Si Larbi, and Mohammed El Mankibi. Textile reinforced concrete multiscale mechanical modelling: Application to TRC sandwich panels. *Finite Elements in Analysis and Design*, 135(June):22–35, 2017.
- [63] Isabella Giorgia Colombo, Matteo Colombo, Marco di Prisco, and Farhang Pouyaei. Analytical and numerical prediction of the bending behaviour of textile reinforced concrete sandwich beams. *Journal of Building Engineering*, 17:183–195, 2018.

- [64] Christian Kulas. solidian GmbH. <https://www.solidian.com/en/references/>, 2019. [Online; accessed 22-November-2019].
- [65] Matthias De Munck, Tine Tysmans, Jan Wastiels, Panagiotis Kapsalis, Jolien Vervloet, Michael El Kadi, and Olivier Remy. Fatigue behaviour of textile reinforced cementitious composites and their application in sandwich elements. *Applied Sciences (Switzerland)*, 9(7):19, 2019.
- [66] Alexander Schumann, Harald Michler, Frank Schladitz, and Manfred Curbach. Parking slabs made of carbon reinforced concrete. *Structural Concrete*, (October):1–9, 2017.
- [67] Sophia Kueres, Norbert Will, and Josef Hegger. Flexural design of a modular footbridge system with pretensioned carbon fiber reinforced polymer reinforcement. *Structural Concrete*, (April):1–13, 2019.
- [68] Jan Bielak, Sarah Bergmann, and Josef Hegger. Querkrafttragfähigkeit von Carbonbeton-Plattenbrücken mit C-förmiger Querkraftbewehrung. *Beton- und Stahlbetonbau*, 114:1–11, 2019.
- [69] S Verbruggen, O Remy, and J Wastiels. Structural stay-in-place formwork of textile reinforced cement for concrete beams. In *International Conference on Material Science and 64th RILEM Annual Week in Aachen-MATSCI*, volume 1, pages 185–192, 2010.
- [70] IC Papantoniou and CG Papanicolaou. Textile reinforced concrete (trc) for precast stay-in-place formwork elements. *Tailor made concrete structures*, pages 475–481, 2008.
- [71] Alexander Scholzen, Rostislav Chudoba, Josef Hegger, and Norbert Will. Leichte Dachschalen aus Carbonbeton: Fertigteilproduktion, experimentelle Untersuchungen und Anwendungspotenzial. *Beton- und Stahlbetonbau*, 111(10):663–675, 2016.
- [72] Will Hawkins, John Orr, Tim Ibell, and Paul Shepherd. An Analytical Failure Envelope for the Design of Textile Reinforced Concrete Shells. *Structures*, 15(March):56–65, 2018.
- [73] Harald Michler. Verstärken mit Carbonbeton im Brückenbau. In *26. Dresdner Brückenbausymposium*, pages 235–247, Dresden, 2016.
- [74] Thorsten Helbig, Kay Unterer, Christian Kulas, Sergej Rempel, and Josef Hegger. Fuss- und Radwegbrücke aus Carbonbeton in Albstadt-Ebingen: Die weltweit erste ausschliesslich carbonfaserbewehrte Betonbrücke. *Beton- und Stahlbetonbau*, 111(10):676–685, 2016.
- [75] Alexander Scholzen, Rostislav Chudoba, and Josef Hegger. Thin-walled shell structures made of textile-reinforced concrete: Part I: Structural design and construction. *Structural Concrete*, 16:106–114, 2015.
- [76] Alexander Scholzen, Rostislav Chudoba, and Josef Hegger. Thin-walled shell structures made of textile-reinforced concrete: Part II: Experimental characterization, ultimate limit state assessment and numerical simulation. *Structural Concrete*, 16(1):115–124, 2015.
- [77] A. Liew, Y. R. Stürz, S. Guillaume, T. Van Mele, R. S. Smith, and P. Block. Active control of a rod-net formwork system prototype. *Automation in Construction*, 96(November 2016):128–140, 2018.
- [78] Patrick Valeri, Patricia Guaita, Raffael Baur, Miguel Fernández Ruiz, David Fernández-Ordóñez, and Aurelio Muttoni. Textile reinforced concrete for sustainable structures: Future perspectives and application to a prototype pavilion. *Structural Concrete*, 2020.

- [79] E Engberts. Large-size facade elements of textile reinforced concrete. In *ICTRC'2006-1st International RILEM Conference on Textile Reinforced Concrete*, pages 309–318. RILEM Publications SARL, 2006.
- [80] J Hegger, M Zell, and M Horstmann. Textile reinforced concrete–realization in applications. In *Proceedings: international fib symposium tailor made concrete structures: new solutions for our society*, pages 357–362, 2008.
- [81] Josef Hegger, Christian Kulas, and Michael Horstmann. Realization of trc façades with impregnated ar-glass textiles. In *Key Engineering Materials*, volume 466, pages 121–130. Trans Tech Publ, 2011.
- [82] Frank Schladitz, Enrico Lorenz, Frank Jesse, and Manfred Curbach. Verstärkung einer denkmalgeschützten tonnenschale mit textilbeton. *Beton-und Stahlbetonbau*, 104(7):432–437, 2009.
- [83] Silvio Weiland, Frank Schladitz, Elisabeth Schütze, Regine Timmers, and Manfred Curbach. Rissinstandsetzung eines zuckersilos: Tudalit®(textilbeton) zur instandsetzung. *Bautechnik*, 90(8):498–504, 2013.
- [84] Erich Erhard, Silvio Weiland, Enrico Lorenz, Frank Schladitz, Birgit Beckmann, and Manfred Curbach. Anwendungsbeispiele für textilbetonverstärkung: Instandsetzung und verstärkung bestehender tragwerke mit textilbeton. *Beton-und Stahlbetonbau*, 110(S1):74–82, 2015.
- [85] Zulassungsnummer Z-201431 DIBt. 31.10-182. verfahren zur verstärkung von stahlbeton mit tudalit, 2014.
- [86] Patrick Valeri, Miguel Fernández Ruiz, and Aurelio Muttoni. cemsuisse report 201407: Building in a lighter and more sustainable manner : textile reinforced concrete for thin structural elements. Technical report, IBETON, Ecole Polytechnique Fédérale de Lausanne, Lausanne, 2017.
- [87] Francesca Perego. Argamassa armada: Textile Reinforced Concrete, social inclusion through technology and design. Master thesis, Politecnico di Milano, 2019.
- [88] Patrick Valeri, Patricia Guaita, Raffael Baur, Miguel Fernández Ruiz, and Aurelio Muttoni. The potential of textile reinforced concrete for design of innovative structures. In *Proc. of the International fib Symposium on Conceptual Design of Structures*, 2019.

Chapter 2

Tensile response

This chapter deals with the tensile response of Textile Reinforced Concrete from a **micro-level** perspective. It corresponds to the post-print version of the following article:

Tensile Response of Textile Reinforced Concrete *Valeri, P.; Fernández Ruiz, M.; Muttoni, A.* Construction and Building Materials, 2020.
<https://doi.org/10.1016/j.conbuildmat.2020.119517>

The first author (Patrick Valeri) conducted the experimental campaign presented in this chapter: selection of suitable fabrics; identification of test set-ups (for bare rovings, pull-out tests and composite tensile tests); specimen preparation, handling, and execution of all tests (including all measurements). Furthermore he performed the analysis of the experimental data obtained with conventional and photogrammetric measurements for the mortar, reinforcement, pull-out, and composite tests. Based on the experimental results, different constitutive laws were investigated with the coaxial ring model approach (in an analytical manner): (1) delayed response of core filaments by considering an activation strain (ε_0); and (2) delayed activation of bond stresses between sleeve and core filaments following an engagement slip (δ_A). The first author derived all the required analytical formulations and performed their implementation with a numerical tool (MatLab). In addition he performed a literature-review and assembled a database of independent tests available in the scientific literature that is used to validate the model. Finally, the first draft of the manuscript, including all tables and figures, was prepared by the first author.

The second author (Miguel Fernández Ruiz) performed a close supervision off all experimental and theoretical works. He helped assessing the outcomes of the numerical simulations and performed the necessary simplifications of the constitutive laws so that the model could be implemented in an analytical manner. In addition, he helped in the assembly of the data-base and suggested the necessary case-studies to test the robustness of the fundamental model assumptions. Finally, he performed several proof-reads of the manuscript, suggested modifications of the text and figures. Eventually, he was also Principal Investigator of the research project (*cemsuisse* research project #201407), for which he provided the necessary management and coordination.

The third author (Aurelio Muttoni) supervised the works with special focus on the theoretical section. He provided valuable input by critically assessing the fundamental assumptions and the implemented constitutive laws. In addition, he performed some proof-reads of the manuscript prior to its submission and suggested several improvements (especially for the figures). Finally, he was also responsible for the acquisition of the project funding that allowed to perform this research (*cemsuisse* research project #201407).

Abstract

Textile Reinforced Concrete (TRC) is a cementitious composite material where a carbon or glass fabric is embedded as reinforcement. The use of TRC allows building thin and light structures, with reduced concrete covers and an enhanced durability due to the absence of corrosion problems. In this chapter, the response of TRC elements subjected to tension is reviewed by means of an experimental and theoretical investigation. A test programme comprising 28 specimens reinforced with uncoated and coated carbon textile fabrics is presented. Detailed measurements were performed by using Digital Image Correlation allowing to investigate on the crack development and failure in tension of the specimens. On this basis, a comprehensive approach to address the tensile response of TRC is presented based on a coaxial ring model incorporating different constitutive laws for the core and sleeve filaments and their interfaces. The model is observed to consistently predict the various responses measured experimentally, both in terms of the stabilised cracking phase and failure load, avoiding the need to consider empirical efficiency factors. The results are finally compared to available tests in the scientific literature showing consistent and fine agreement.

2.1 Introduction

Conventional reinforced concrete can be considered as one of the most widely used construction materials, with a synergic use of its components: the steel rebars provide the required tensile strength, while the concrete carries the compressive stresses and protects the steel against corrosion. To ensure the performance and durability of reinforced concrete, current codes of practice prescribe a minimum concrete cover (typically between 10 and 60 mm depending on the exposure class). Such cover requirement, together with the spacing between reinforcement layers necessary for compacting and vibrating needs, leads eventually to relatively thick members and in many cases has associated concrete construction to a massive building technique.

In the last decades, Textile Reinforced Concrete (TRC) has emerged as an interesting alternative to reinforced concrete for elements where it is important to reduce weight. Particularly, they have shown a high potential of application for shells or lightweight folded structures [1]. In TRC, conventional steel reinforcement bars are replaced by a fabric reinforcement. The fabric is typically composed by a planar and bidirectional assembly of rovings (also called yarns) [2]. As shown in Fig. 2.1, the rovings are bundles of filaments made of a raw material (such as carbon, alkali-resistant glass or basalt) that does not corrode or degrade in contact with ambient air or chlorides (degradation of the textiles due to the chemical interaction between the fabric and the cementitious matrix may however require to be addressed [3, 4, 5]). As the fabric has no need for passivation by the concrete, low-clinker content cements can be used and the cover thickness can be reduced to minimum static values (unless requirements under fire conditions are governing). Consequently, depending on the element type and by making use of a sufficiently fluid mortar, the thickness of the elements can be significantly reduced, normally up to values between 10 and 30 mm. [6, 7, 8]. This allows to build light and efficient structures. Also, the use of low-clinker content cement ensures a reduction in the CO₂ footprint for production of the elements, contributing to a sustainable construction technique.

Significant research efforts have been devoted in the past to develop consistent design approaches for this material (detailed state-of-the-art can be consulted elsewhere [2, 9, 10]). Within this frame, the understanding of the composite response of TRC in uniaxial tension is an instrumental topic and has concentrated many previous works. The first analytical approaches can be traced back to the 1970's [11] and 1990's [12], and had been followed by many recent researches. Several specific experimental programmes have been carried out (Jesse [13], Molter [14], Bruckermann, [15], Lepenies [16], Colombo et al [17], Larrinaga et al. [18] and Contamine et al. [19]). Despite

these efforts, there is yet no clear agreement on the tensile testing methods for TRC. Brameshuber [20] and Contamine et al. [21] propose a hinged set-up. More recently, partially clamped boundary conditions are suggested by Schütze et al. [22] and De Santis et al. [23]. According to systematic studies performed by Hartig et al. [24], there are clear differences between rigid and soft load introductions which vary with the coating degree of the fabric reinforcement. A similar analysis performed on a larger database by Leone et al. [25], comparing 14 different testing systems, shows that uncoated fabrics are more sensitive to variations of the boundary conditions with respect to coated or impregnated textiles.

With respect to the influence of the fabric type on the response, most works have concentrated on carbon fibres due to their availability and performance. Yet the response of glass or basalt fibres has also been investigated [26, 27]. As described in [28], the impregnation conditions of the fabrics play a significant role in their mechanical response. Namely, the distribution of stresses of the filaments in a roving for a given cross-section (stress-profile) is influenced by the degree of coating and impregnation. Uncoated rovings present a higher non-uniform stress profile (Fig. 2.1d) due to poorer bond properties between filaments. On the other hand, fully-impregnated rovings tend towards more homogeneous stress profiles (Fig. 2.1g), whereas providing an external coating leads to an intermediate response (Fig. 2.1e-f). Based upon these observations and potential responses, different modelling approaches have been proposed at various levels: micro-level, starting from the behaviour of single filaments [29]; meso-level, considering the behaviour of entire rovings [27]; and macro-level dealing with the material as a composite without considering its single components [13]. In addition to analytical models [11, 12, 30], also numerical simulations have shown to be a promising approach to analyse the tensile behaviour of the composite [18, 31, 32].

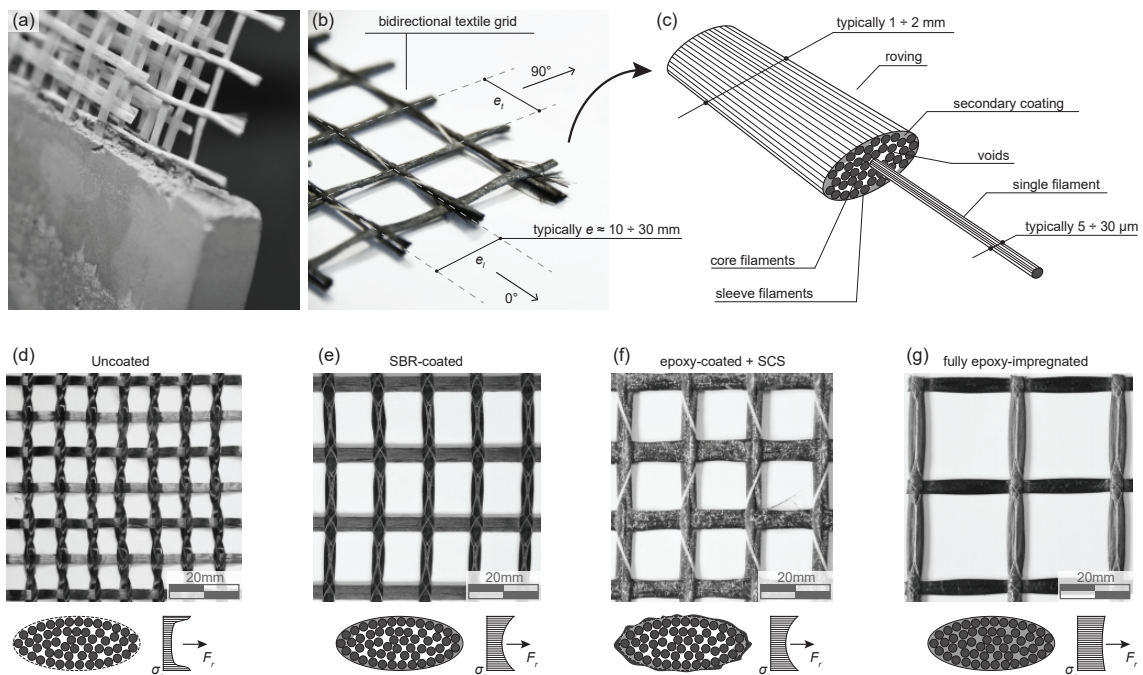


Figure 2.1: TRC: (a) composite; (b) fabric; (c) roving; (d) uncoated fabric; (e) Stereo Butene Rubber coated fabric; (f) fabric with Sand Coated Surface; (g) fully impregnated fabric.

Despite the previous research efforts, design approaches still rely mostly on the calibration of efficiency factors [17, 30, 33, 34] tailored for a given composite and mortar. These approaches are easy to apply in practice but do not allow for a clear understanding of the mechanics of the tensile response of TRC. Also, such approaches do not allow for a consistent treatment of both, the response at serviceability limit state and at failure. In order to improve the current state-of-the-art and to lead to more consistent and comprehensive design approaches, this chapter presents the results of

a test programme addressed at the tensile response of TRC where detailed test measurements were performed on fundamental issues as bond, filament response and composite behaviour. On that basis, a physical model based on the coaxial ring analogy is proposed incorporating the potential straightening of core filaments and introducing the concept of bond-lag (delayed activation of bond stresses for core filaments) between the core and sleeve filaments. The approach is shown to explain the response at serviceability state and at failure in tension without the need of introducing any efficiency factors. The consistency of the proposed approach is verified eventually with the test results presented in this chapter and those available in the scientific literature showing fine agreement.

2.2 Mortar, textile and pull-out tests

In this section the results of material tests performed within this research are presented. These include compressive and tensile tests on the unreinforced mortar matrix and tensile tests on rovings extracted from the fabric grid. In addition, the results of pull-out tests used to characterise the roving-to-mortar interface response are also introduced.

2.2.1 Cementitious mortar

Casting of a thin element requires a mortar with sufficient fluidity to penetrate between the rovings composing the fabric layers. To satisfy these requirements, a mortar mix composed of nearly 40 % binder (with low carbon blast furnace cement) and nearly 60 % aggregate was used. The small aggregate size ensured a uniform penetration of the matrix even for dense fabric reinforcement arrangements (see Table 2.1).

Binder (CEM III/B)	860	kg/m ³
Aggregates (quartz powder and various quartz sands)	1290	kg/m ³
Maximum aggregate size ($d_{g,max}$)	1.6	mm

Table 2.1: Mortar composition and maximum aggregate size.

The mortar showed a high mechanical performance due to the low water-to-cement ratio ($w/c \approx 0.25$) combined with a superplasticizer to ensure the required fluidity.

The compressive mortar strength (f_c) was measured on standard cylinders $D = 70 \times H = 120$ mm (height after sample rectification) and each test lasted typically two minutes to reach the peak strength. Tests on the compressive strength were performed during the complete duration of the testing programme (Fig. 2a-b). The tensile strength (f_{ct}) of the mortar was measured on small clamped dog-bone specimen (Fig. 2c-d), reaching failure in approximately one minute. Details on the measured material parameters can be consulted in Table 2.2. The strength evolution in compression can be satisfactorily approximated by the Model Code 2010 equation [35]:

$$f_c(t) = f_{c,28} \cdot e^{s \cdot \left(1 - \sqrt{\frac{28}{t}}\right)} \quad (2.1)$$

Where $s = 0.2$ can be assumed and t refers to the time in days (see Fig. 2.2a,b). Also the strength in tension is suitably approximated by the Model-Code 2010 expression, as shown in Fig. 2.2c,d. At 68 days, three tension tests on larger dog bones instrumented with Digital Image Correlation were performed. These tests allowed to determine the modulus of elasticity of the mortar (E_c) before cracking in tension and the stress crack opening response ($\sigma_c - w$) in the softening stage (see Fig. 2.3 and Table 2.2)

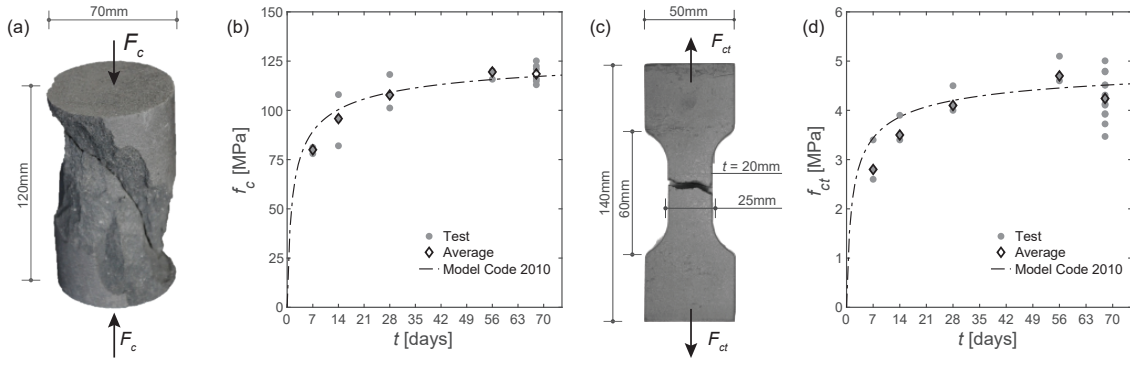


Figure 2.2: Mechanical behaviour of mortar: (a) cylinder for compression tests after failure; (b) evolution of compressive strength (f_c) as a function of time; (c) dog-bone for tensile tests after failure; (d) evolution of tensile strength (f_{ct}) as a function of time.

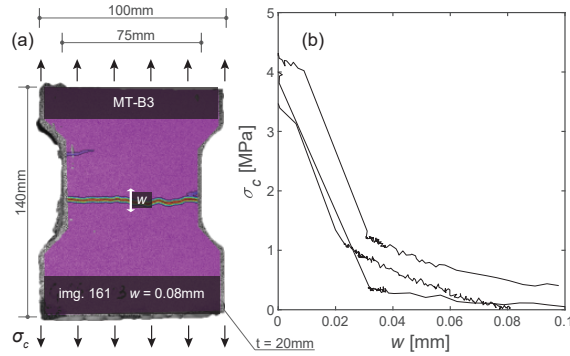


Figure 2.3: Tensile behaviour of mortar: (a) dog-bone specimen; (b) softening response.

2.2.2 Textile reinforcement

Within this research, several carbon fibre (CF) fabrics were used. Fabric CF01 is uncoated, while fabrics CF02 and CF03 are coated with an additional layer of quartz-sand applied to the surface and CF04 is a Stereo Butene Rubber coated fabric (more details on the fabric coating are given in the next section 2.2.3). The roving geometry of selected fabrics (CF01-CF04) is in addition depicted in Fig. 2.5.

All investigated fabrics are ortotropic, thus tension tests on bare rovings of both directions were performed (main direction named 0° and transverse direction named 90° in the following). To perform the tensile tests, single rovings were extracted from the fabric-grid and tested according to the set-up shown in Fig. 2.4a. It can be noted that, for such tests, coated rovings tend to keep an undulated shape even after separation from the mesh and the filaments within the rovings are not perfectly straight. As a consequence, when the load test is performed, the removal of the filament undulation is associated with some initial deformation (refer to roving straightening strain ε_0 , in Fig. 2.5). This phase is followed by a response governed by the modulus of elasticity of the

t [days]	f_c [MPa]	f_{ct} [MPa]	E_c [GPa]
8	80.0 (3, 1.6)	2.8 (3, 0.4)	
14	95.8 (3, 9.2)	3.5 (3, 0.2)	
28	107.8 (3, 8.6)	4.1 (3, 0.2)	
56	119.5 (3, 2.3)	4.7 (3, 0.2)	
68	118.5 (3, 4.8)	4.241 (14, 0.4)	31.0 (3, 0.8)

Table 2.2: Average mechanical mortar properties as a function of time (values in brackets refer to number of tests and standard deviation respectively).

filament (E_r) and its tensile strength (f_r). It can be noted that the initial straightening phase measured during the tests is potentially sensitive to the initial configuration of the roving (which might explain some of the scatter observed in Fig. 2.5c). The observed value of the modulus of elasticity after straightening is however almost not affected by the initial state of the fibre. Cyclic loading tests (Fig. 2.4c) confirm that after the first cycle (once the initial undulation is removed), the response can be considered approximately linear until failure. The mechanical performance of several fabric reinforcements in longitudinal and transverse direction is given in Table 2.3 (average values based on at least 10 tests for each fabric and direction).

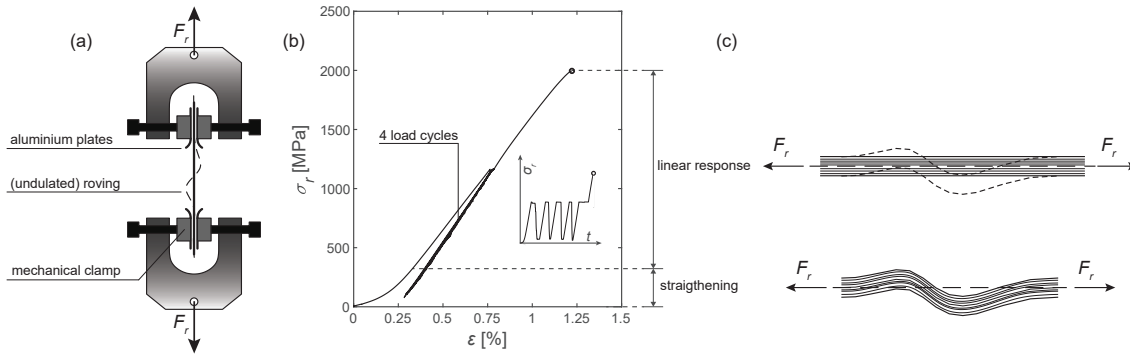


Figure 2.4: Tensile tests of single rovings extracted from the reinforcement grid: (a) test set-up; (b) behaviour of single rovings in cyclic tensile tests; (c) roving straightening process.

The tensile response of the fabrics used for the TRC composite are shown in Fig. 2.5 (CF01, CF02 and CF03). In addition, a bi-linear approximation is also depicted. The latter consists of a linear elastic response delayed by the initial straightening strain ϵ_0 . It can be noted that straightening is more pronounced for coated rovings (CF02) with respect to uncoated ones (CF01) and for those with a marked undulation (compare Fig. 2.5a and b). Further details on the geometry of the rovings and their mechanical response are presented and discussed later (Section 2.4).

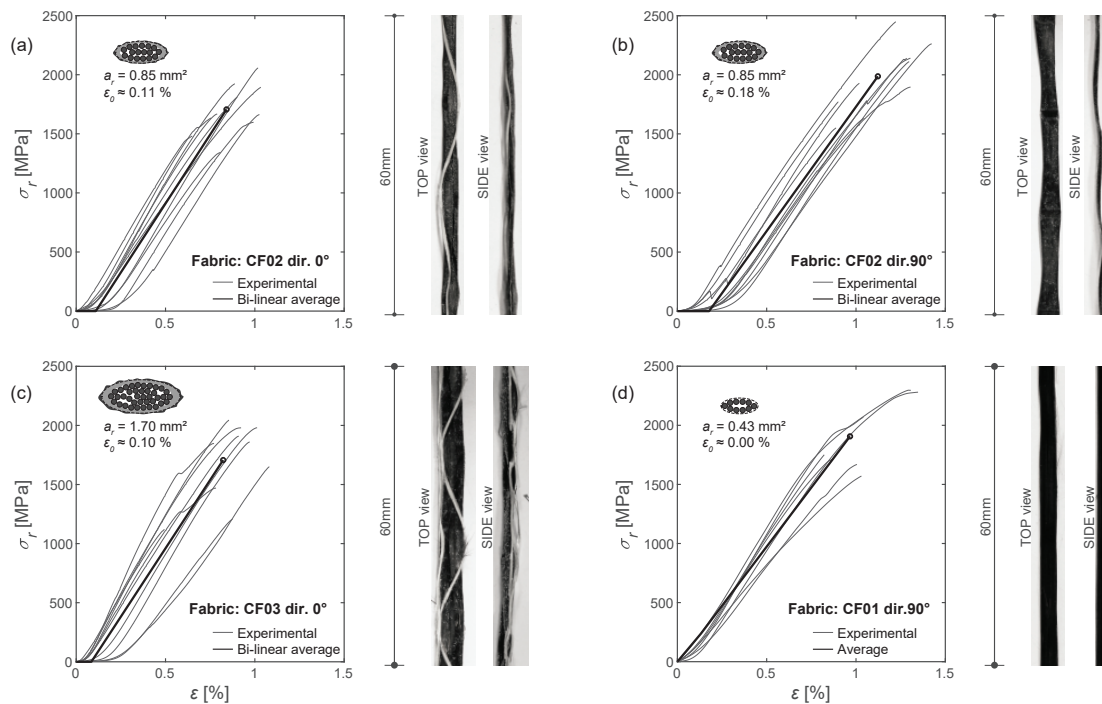


Figure 2.5: Tensile response and geometry of selected rovings: (a) fabric CF02, dir.0°; (b) fabric CF02, dir.90°; (c) fabric CF03, dir.00°; (d) fabric CF01, dir.90°.

Fabric	CF01	CF01	CF02	CF02	CF03	CF03	CF04	CF04
Coating	-	-	SCS	SCS	SCS	SCS	SBR	SBR
Direction	α_r	90°	00°	90°	00°	90°	00°	90°
Linear density	λ_r [tex]	2×800	2×800	1600	2×1600	3200	3200	800
Net cross section	a_r [mm ²]	0.85	0.85	0.85	1.70	1.70	1.70	0.425
Strength	f_r [MPa]	1900 (337)	1700 (226)	2000 (288)	1700 (351)	2000 (157)	1550 (280)	1700 (112)
Grid spacing	e_r [mm]	10.0	20.0	20.0	17.0	17.0	12.5	18.0
Elastic modulus	E_r [GPa]	200 (41.2)	230 (18.8)	210 (14.3)	250 (22.3)	210 (32.3)	220 (68.5)	245 (13.4)
Nominal perimeter	U_r [mm]	7	7	8	11	12	6	4
Peak bond strength	$\tau_{b,max}$ [MPa]	-	0.95 (0.16)	2.9 (0.48)	-	-	1.25	-
Peak bond slip	$\delta_{b,max}$ [mm]	-	0.19	0.029	0.027	-	0.025	-
Manufacturer	Tissa	Tissa	S+P	S+P	S+P	S+P	Fraas	Fraas

Table 2.3: Mechanical properties of the tested carbon fabrics. Average values from tests and standard deviation in brackets. The net cross-section a_r of a single roving is calculated on the basis of its linear density λ_r [36].

2.2.3 Bond properties

Contrary to conventional reinforced concrete, where bond stresses between the reinforcement and concrete develop mostly due to mechanical engagement (ribs of reinforcement bars), the bond stresses between smooth textile fabrics and the mortar are governed by adhesion and friction [37, 38, 39, 40]. Because of their relatively smooth surface, coated and impregnated rovings have rather poor bond properties and several manufacturers have developed products with Sand-Coated Surface rovings (SCS) to enhance its roughness and bond response. Within this research, pull-out tests on rovings embedded in small cylindrical mortar specimens (Fig. 2.6a) have been performed to investigate on the bond properties of the single rovings. The average bond stress is calculated by dividing the pull-out force F_r by the nominal contact surface: $\tau_b = F_r / (U_r \cdot l_e)$. Where l_e refers to the embedment length of the roving within the cementitious matrix (see Fig. 2.6) and U_r to the contact perimeter which was measured on microscope images of saw-cuts. The slip was measured at the unloaded roving end. The experimentally observed bond behaviour, both for uncoated and coated rovings can be divided into three stages (Fig. 2.6b):

- At low slips, the response is rather linear (stage I) with increasing bond stresses for increasing slips. The peak bond stress is characterized by the maximum bond stress ($\tau_{b,max}$) and its associated slip ($\delta_{b,max}$);
- After the peak bond strength is reached, a softening response is observed (stage II) with decreasing bond stress for increasing slip;
- Eventually, only a frictional bond stress remains available (stage III) at a stress about 15-30 % that of the peak bond stress (depending on the surface treatment of the rovings);

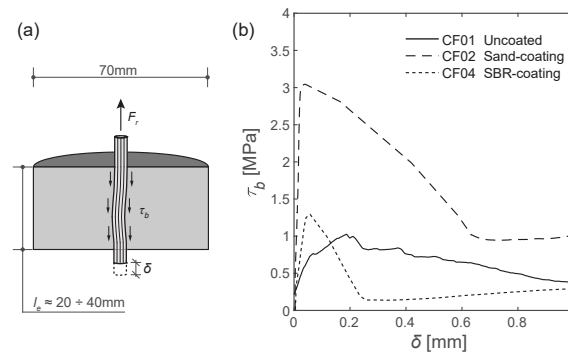


Figure 2.6: Comparison of the pull-out response of rovings with different coatings: (a) specimen geometry; (b) experimental bond-slip response.

The experimental test results in terms of bond-slip response (Fig. 2.6b) show that the roving surface coating has a significant influence on the mechanical interface properties. SCS rovings present higher peak bond strength with respect to Stereo Butene Rubber (SBR) coated and uncoated rovings. For the latter, a good adhesion between sleeve filaments and matrix was observed and a significant differential displacement between core and sleeve filaments was observed at the end of the experiment. Differently, coated rovings are characterised by a more homogeneous behaviour, with no noticeable slip between filaments at the unloaded end observed.

With respect to the investigated bonded lengths, no significant difference could be noticed within the tested range of 20-40 mm when the resistance is normalised to the average bond strength.

To investigate the influence of transverse pressure on the bond behaviour, additional pull-out tests were performed on prismatic specimens, see. Fig. 2.7a (changing from a cylinder segment to a prism was necessary to simplify the introduction of transverse compression). Fig. 2.7 shows that the transverse pressure does not influence significantly the pull-out strength and bond behaviour. This can be justified by the fact that the rovings are rather soft in their radial direction and

the compression stresses are carried by the mortar without any significant change in the interface response.

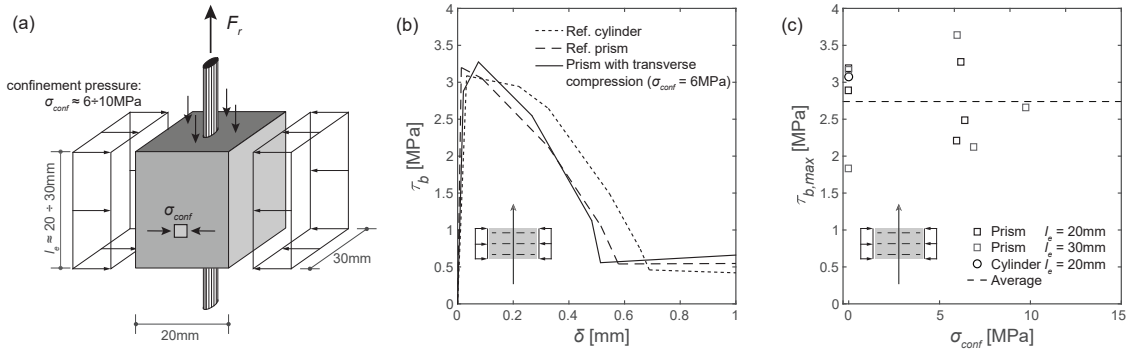


Figure 2.7: Pull-out tests under confinement pressure: (a) specimen geometry; (b) bond-slip response; (c) peak bond strength.

2.3 Experimental programme on TRC tension specimens

In this section, the tensile behaviour of the TRC composite (fabric embedded in the concrete matrix) is investigated by means of a number of tests on TRC tension ties.

2.3.1 Specimen preparation

The tension specimens were obtained from TRC-plates where the distance between textile layers was controlled by means of spacers. For fabric CF01 (relatively deformable due to the absence of any coating or impregnation), the plates were cast with the lamination process (fabric plane arranged horizontally during casting). Differently, for fabrics CF02 and CF03 (relatively stiff thanks to the coating of the rovings), they were cast vertically. The plates were demoulded after three days and rectangular specimens aligned to the fabrics were cut by means of high-pressure water jetting. Thereafter, the specimens were stored in a humid chamber for curing and tested at a minimum age of 30 days.

The nominal longitudinal reinforcement ratio of the tensile specimen is defined as:

$$\rho = \frac{A_r}{A} = \frac{n_r \cdot a_r}{b \cdot t} \quad (2.2)$$

Where A_r refers to the net cross-section of fabric reinforcement, A to the gross cross-section area of tensile specimen, n_r to the number of rovings in the considered cross-section, a_r to the net cross-section of a single roving, b to the specimen width and t to its thickness.

2.3.2 Test set-up and experimental programme

A semi-clamped set-up was used providing timber plates at the ends. This set-up allowed introducing the anchorage transverse pressure (6-8 MPa) but also for a small level of rotation capacity (Fig. 2.8). All tests were loaded under displacement-controlled conditions with a rate of 1 mm/min. Local displacements were measured with Digital Image Correlation (DIC) at a frequency of 0.5 Hz. The DIC speckle was painted on the front-side of the specimen and on the load-introduction plates (refer to Fig. 2.8). This allowed tracking the displacements, strains and crack openings of the specimen as well as verifying that no relative slip occurred between the clamps and the specimen. The results from DIC were also checked by means of a Linear Variable Displacement Transformer (LVDT) arranged on the back-side of the specimen.

Within the present experimental programme, 28 composite specimens were tested in tension. They were reinforced with fabrics CF01, CF02 and CF03 previously described (refer to Table 2.3). The acronym for each specimen describes the orientation of the fabrics with respect to the loading direction (T00 or T90 when the fabric is tested in the longitudinal and transversal directions respectively), the casting batch (named from A to J) and a number for each specimen of a certain batch. Within this programme, the influence of a number of parameters was investigated, namely: the amount of longitudinal and transversal reinforcement, the concrete cover and the influence of coating type. Details for the 28 specimens tested are given in Table 2.4.

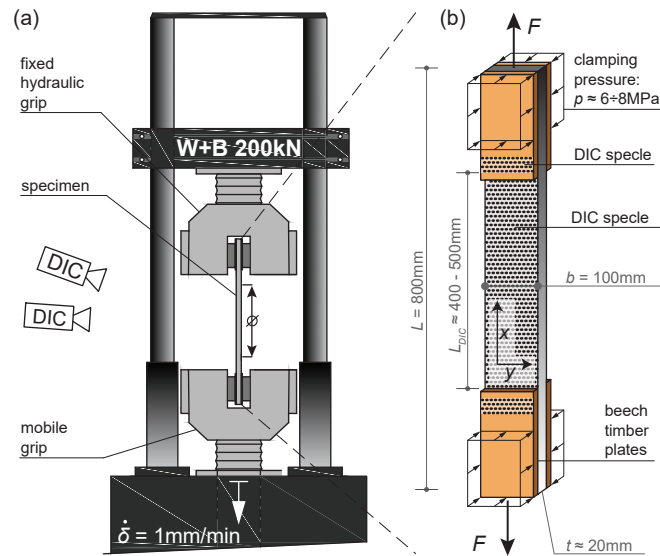


Figure 2.8: Test set-up: (a) test machine and measurement system; (b) specimen.

specimen	batch	fabric	t	b	α_r	layers	ρ_l	ρ_t	c
[...]	[...]	[...]	[mm]	[mm]	[°]	[nr]	[%]	[%]	[mm]
T00-A1	A	CF02	17.1	100	0	6	1.49	1.49	3.0
T00-A2	A	CF02	17.8	100	0	6	1.43	1.43	3.0
T00-A3	A	CF02	16.6	100	0	6	1.54	1.54	3.0
T00-A4	A	CF02	17.5	100	0	6	1.46	1.46	3.0
T00-B1	B	CF02	18.2	100	0	6	1.40	1.40	3.0
T00-B2	B	CF02	18.3	100	0	6	1.39	1.39	3.0
T00-B3	B	CF02	17.2	100	0	6	1.49	1.49	3.0
T00-C4	C	CF02	15.9	100	0	2	0.64	0.64	3.0
T00-C5	C	CF02	16.3	100	0	2	0.63	0.63	3.0
T00-F1	F	CF02	16.6	100	0	6	1.54	1.54	0.2
T00-F2	F	CF02	18.1	100	0	6	1.41	1.41	0.2
T00-F3	F	CF02	16.6	100	0	6	1.54	1.54	0.2
T00-F4	F	CF02	18.3	100	0	6	1.40	1.40	0.2
T00-G1	G	CF02	15.5	100	0	3	0.66	0.66	3.0
T00-G2	G	CF02	17.2	100	0	3	0.59	0.59	3.0
T90-C2	C	CF02	16.6	100	90	2	0.61	0.61	3.0
T90-C3	C	CF02	16.1	100	90	2	0.63	0.63	3.0
T90-D1	D	CF02	17.9	107	90	4	1.07	1.07	3.0
T90-D2	D	CF02	19.5	97	90	4	0.90	0.00	3.0
T90-D3	D	CF02	18.6	100	90	4	1.10	1.10	3.0
T90-E1	E	CF02	11.0	100	90	2	0.77	0.77	3.0
T90-E2	E	CF02	11.4	100	90	2	0.75	0.75	3.0
T90-E3	E	CF02	11.2	100	90	2	0.76	0.76	3.0
T90-E4	E	CF02	10.9	100	90	2	0.78	0.78	3.0
T90-I1	I	CF01	21.0	100	90	6	1.25	2.50	2.0
T90-I2	I	CF01	21.0	100	90	6	1.25	2.50	2.0
T00-J1	J	CF03	20.5	100	90	6	2.90	2.90	3.0
T00-J2	J	CF03	19.7	100	90	6	3.02	3.02	3.0

Table 2.4: Properties of tensile TRC specimens (c refers to the concrete cover).

2.3.3 Load-deformation and load-crack-opening response

The DIC postprocessing software (VIC 3D) allows tracking the strain between two arbitrary points by means of virtual extensometers. For each specimen, several virtual extensometers were defined to investigate the longitudinal strains (typically 5 - 10, at different locations and crossing at least two cracks). The average strain for each specimen was thereafter calculated as the average of the extensometers of the specimen. The results in terms of load (F) versus average strain (ε) are plotted in Fig. 2.9, where specimens with same reinforcement type and similar reinforcement ratio are grouped.

In a similar manner, for each specimen, virtual extensometers (located at the specimen axis) were used to measure the opening of each crack. The average crack opening is calculated on this basis as the average of all virtual extensometers. The average load (F) crack opening (w) response is plotted in Fig. 2.10.

Both, the load-deformation ($F - \varepsilon$) and the load-crack-opening ($F - w$) relationships (Fig. 2.9 and 2.10) show that the tensile response of all composite specimen can be divided in the following three stages: uncracked response (stage I); crack development phase (stage II) and stabilized cracking (stage III). Failure occurred in all cases in a brittle manner at the end of stage III. More details can be found in Table 2.5.

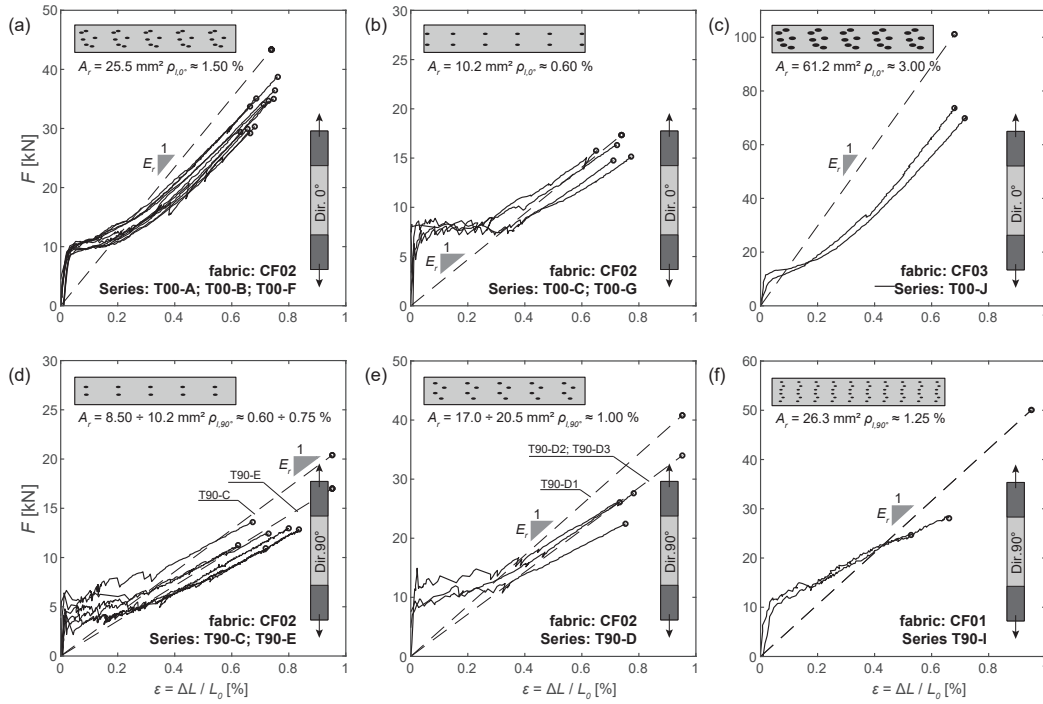


Figure 2.9: Experimental load strain response for all specimens: average specimen response and theoretical fabric response (dashed).

2.3.4 Cracking pattern

All specimens were characterised by a regularly-distributed cracking pattern. The average crack spacing at the end of stage II (s_{rm}) as well as the crack opening just before failure (w_u) are reported in Table 2.5. Close examination of the crack development was performed by making use of the DIC measurements.

Fig. 2.11 presents for instance specimen T00-F3 (with low concrete cover) where interesting phenomena could be observed. First cracks develop at the edges (Fig. 2.11b-A) and progress toward the longitudinal axis of the specimen (2.11b-B). At the end of stage II (Fig. 2.11b-C), a primary set of cracks is fully developed at locations coincident with the position of the transverse reinforcement rovings. This can be explained by the section weakening due to the presence of transverse rovings as visible at the lateral face (Fig. 2.11c). Thereafter, cracks open progressively (Fig. 2.11b-D,E,F) and even secondary cracks may develop at higher load levels at locations where other (intermediate) transverse reinforcements are located (Fig. 2.11b-E,F).

The illustrated case (T00-F3) is representative for all specimens reinforced with coated carbon fabrics (CF02, CF03) and with a significant transverse reinforcement ratio (ρ_t): series T00-A, T00-B, T00-F, and T90-D, T90-E. For specimens with lower reinforcement ratios (series T90-C), cracks still develop in correspondence to the transverse rovings. A narrow crack pattern develops in case transverse rovings are located in the same cross-section (see Fig. 2.12c) resulting in an average crack spacing close to the spacing of transverse rovings ($s_{rm} \approx e_r$, refer to Table 2.5). Differently, when no superposition occurs and when the specimen has a low transverse reinforcement ratio, cracks develop again in correspondence to transverse rovings, but resulting in a wider spacing: for specimen T90-C2, $s_{rm} \approx 1.5 \times e_r$ (see Table 2.5 and Fig. 2.12b).

Since the presence of transverse rovings seems to govern the crack spacing, a comparison was made between specimens with and without transverse rovings (see Fig. 2.12d showing specimen T90-D2 where the transverse rovings were removed and Fig. 2.12e showing specimen T90-D3 with an identical longitudinal reinforcement, but with transverse rovings). It can be noted that specimen

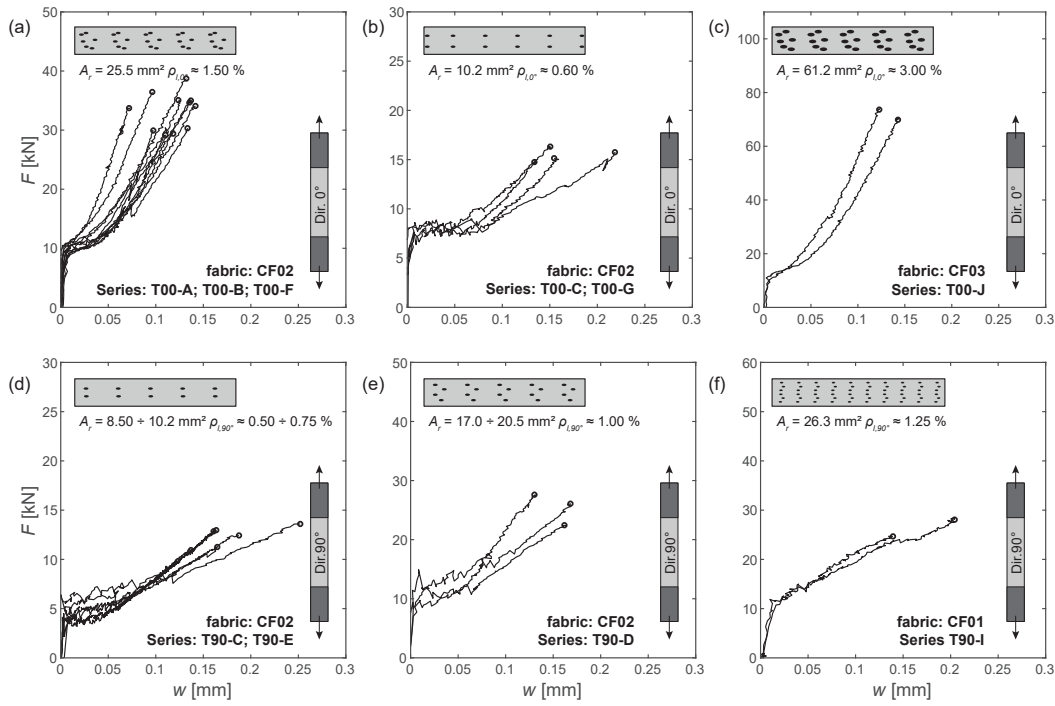


Figure 2.10: Experimental load crack-opening response for all specimens (average crack opening of each specimen).

T90-D2 is characterised by slightly wider spaced cracks and that these cracks do not always develop orthogonally to the loading direction. Differently, specimen T90-D3 is characterised by the typical crack pattern recorded for most of the specimens.

A similar behaviour is observed for specimens reinforced with uncoated fabrics CF01, series T90-I, where cracks develop every three transverse rovings (Fig. 2.12f).

2.3.5 Failure

The tensile failure of the composite (Fig. 2.13) arises in a brittle manner at the end of stage III without any apparent warning sign. For the investigated composites, three types of failure can be distinguished with respect to the location of the failure zone (see also [23]):

- Failure type 1: failure occurs within the measurement region, in a section far from the load introduction zone (Fig. 2.13a). All rovings fail close to the failure crack with filaments failing within a distance lower than 20 mm from the crack tip). As shown in Fig. 2.12a, the failure crack is not always the one associated to the largest crack opening;
- Failure type 2: same as failure type 1, but close to the load introduction zone (Fig. 2.13b);
- Failure type 3: failure occurs at the edge or even within the load introduction zone. In this case, sleeve filaments fail close to the crack tip whereas core filaments are pulled out of the anchorage zone (Fig. 2.13c).

The observed failure types of every specimen are reported in Table 2.5.

specimen [...]	F_{cr} [kN]	σ_{cr} [MPa]	s_{rm} [mm]	s_{rm}/e_r [-]	w_u [mm]	ε_u [%]	F_u [kN]	$\sigma_{r,u}$ [MPa]	failure [type]
T00-A1	9.60	5.6	21	1.1	0.13	0.76	38.7	1519	1
T00-A2	10.2	5.7	19	1.0	0.12	0.69	35.1	1376	2
T00-A3	10.1	6.1	13	0.7	0.07	0.66	33.7	1322	2
T00-A4	9.90	5.7	15	0.8	0.10	0.75	36.5	1430	2
T00-B1	9.80	5.4	20	1.0	0.14	0.71	34.1	1337	3
T00-B2	9.10	5.0	22	1.1	0.14	0.75	35.0	1373	3
T00-B3	8.80	5.2	22	1.1	0.14	0.73	34.7	1360	3
T00-C4	6.30	4.0	22	1.1	0.13	0.71	14.8	1447	2
T00-C5	7.70	4.7	23	1.2	0.15	0.72	16.3	1600	2
T00-F1	7.50	4.5	21	1.1	0.13	0.68	30.3	1189	2
T00-F2	9.50	5.3	20	1.0	0.12	0.63	29.4	1154	2
T00-F3	9.50	5.7	19	1.0	0.11	0.66	29.2	1145	2
T00-F4	9.60	5.3	19	1.0	0.10	0.66	29.9	1174	2
T00-G1	8.60	5.6	20	1.0	0.15	0.77	15.1	1485	2
T00-G2	8.30	4.8	30	1.5	0.22	0.65	15.8	1544	2
T90-C2	6.70	4.0	35	1.8	0.25	0.67	13.6	1333	1
T90-C3	6.40	4.0	23	1.2	0.19	0.73	12.4	1219	1
T90-D1	11.4	6.0	25	1.1	0.17	0.73	26.1	1279	2
T90-D2	9.40	5.0	26	1.6	0.16	0.75	22.4	1320	2
T90-D3	7.00	3.8	23	1.0	0.13	0.78	27.6	1354	2
T90-E1	3.80	3.5	21	1.1	0.16	0.84	12.9	1514	2
T90-E2	4.50	4.0	20	1.0	0.16	0.80	13.0	1526	2
T90-E3	3.80	3.4	29	1.5	0.16	0.62	11.3	1325	2
T90-E4	4.00	3.7	20	1.0	0.14	0.72	10.9	1288	2
T90-I1	11.9	5.7	29	2.9	0.14	0.53	24.7	938	2
T90-I2	12.3	5.9	29	2.9	0.20	0.66	28.5	1083	2
T00-J1	11.5	5.6	19	1.1	0.14	0.72	70.5	1184	2
T00-J2	10.1	5.2	18	1.1	0.12	0.68	73.9	1242	2

Table 2.5: Experimental results of the tested tensile TRC specimens (where s_{rm} refers to the average crack spacing, e_r to the roving spacing, and w_u to the maximum crack-opening at failure).

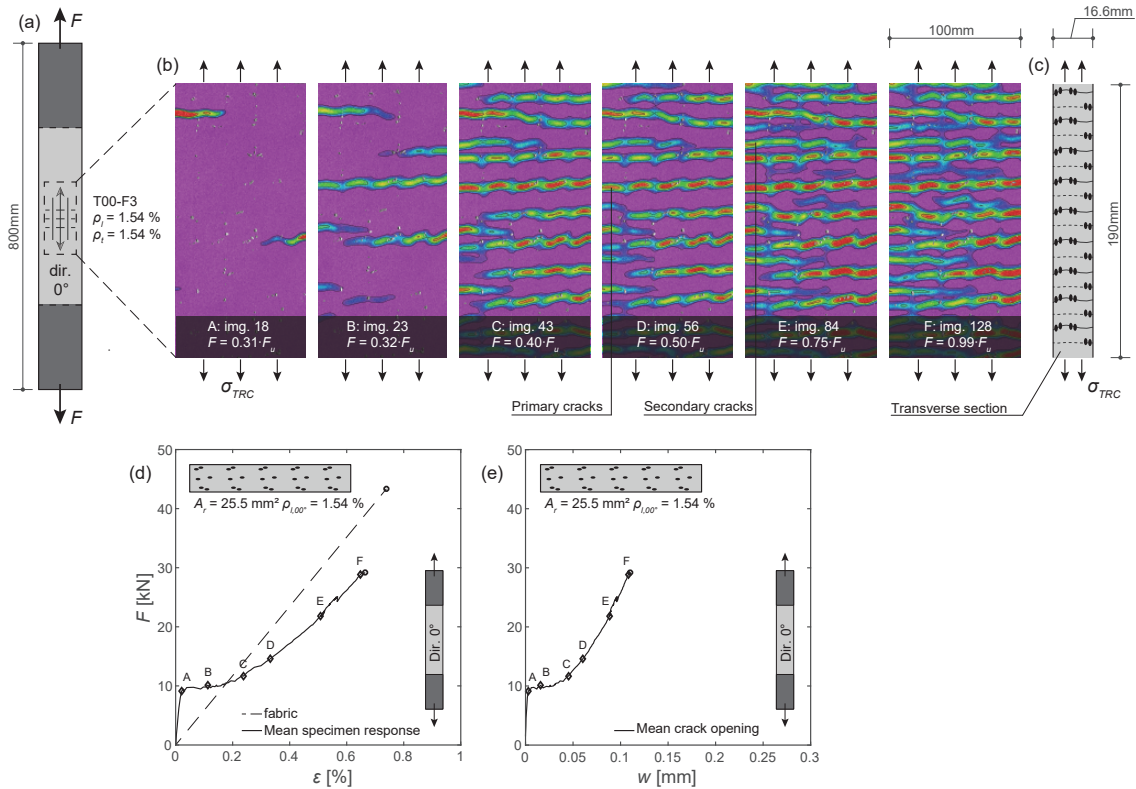


Figure 2.11: Photogrammetric measurements of specimen T00-F3: (a) DIC region; (b) principal tensile strains at selected load steps (A-F from left to right); (c) longitudinal cross-section showing the lateral face and the position of the transverse rovings; (d) load-strain and; (e) load-crack opening relationships.

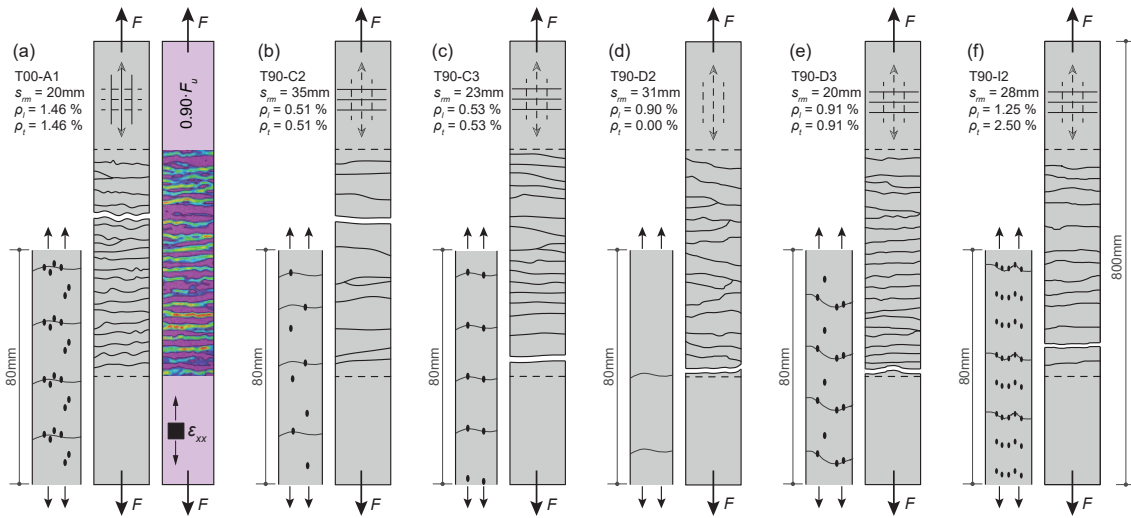


Figure 2.12: (a-f) crack patterns of specimens with various longitudinal and transverse reinforcement ratios.

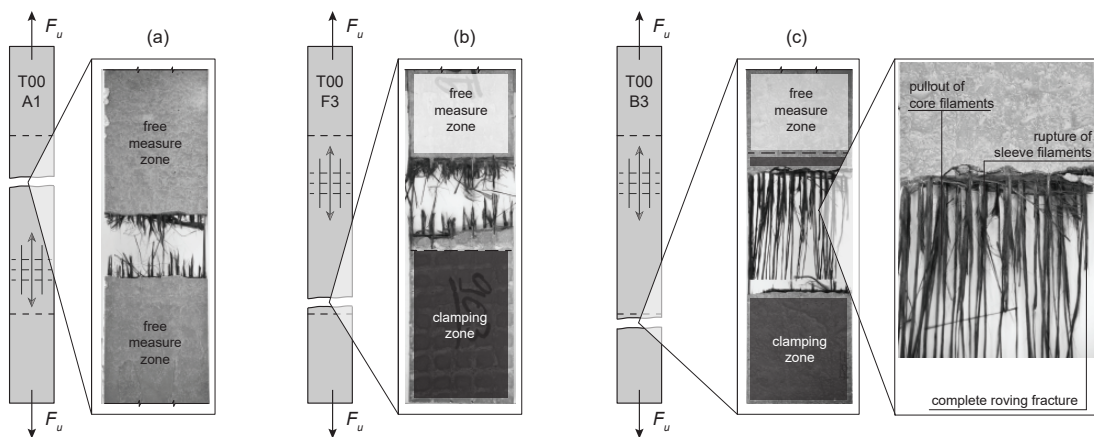


Figure 2.13: Different failure types: (a) type 1; (b) type 2; (c) type 3.

2.4 Analytical modelling

2.4.1 Interpretation of experimental results

The experimental load-deformation response (Fig. 2.9) of the tensile members shows that, at stage I, the stiffness of the composite is mainly governed by the stiffness of the uncracked matrix and by the linear response of the materials (as for ordinary reinforced concrete).

On the contrary, in the cracked stages II and III, the response of the tensile member is mainly governed by the stiffness of the reinforcement and bond properties. As shown in Fig. 2.9, the response in this case deviates from the one theoretically corresponding to a straight bare roving (dashed line in Fig. 2.9).

1. During the cracked phase (stage III) the tangent stiffness of the TRC (slope of the force-strain response at a given point) varies. For coated fabrics, it reaches eventually a value similar to that of the bare fabric (see Fig. 2.9a-e). However, for fabrics without impregnation or coating, the tangent stiffness of the TRC remains in most cases clearly lower than the one of the bare fabrics (see Figure 2.9f).
2. The failure load is usually lower than that of the bare fabric.

These effects can be attributed to the differential activation of filaments within the rovings (not all filaments of the roving are activated identically and are thus subjected to different levels of stress). The tensile strength and stiffness of rovings is usually determined by performing tension tests on single rovings, which are clamped with load introduction plates or capstan grips [41] (see Fig. 2.14a). Both test setups produce significant transverse pressure between the filaments (Fig. 2.14b) and allow for a relatively uniform activation of the section (Fig. 2.14b). The case of TRC is however different as the composite specimen is mechanically gripped at the load introduction zone (Fig. 2.14c). In this case, the transverse pressure p introduced by the grips at the anchorage regions of the specimens is applied to the mortar matrix (Fig. 2.14d) and not on the fabric directly (as for a tension test of a single roving, Fig. 2.14a-b). Due to the low radial stiffness of the rovings with respect to the surrounding matrix, the filaments do not experience a high level of transverse pressure (see Fig. 2.14e). This condition is thus very different to the one for a bare roving test (Fig. 2.14b, with high transverse pressures between filaments). As a consequence, the friction stresses between filaments decreases significantly with respect to the conditions of a simple roving test and a less uniform stress distribution develops (Fig. 2.14e). This assumption is clearly confirmed by the pull-out tests with transverse pressure described in section 2.2.3 and Fig. 2.7, showing that no improvement on bond was achieved by means of a confining pressure applied to the mortar.

2.4.2 Coaxial ring models

To model the tensile behaviour of multifilament-rovings embedded in a cementitious matrix, a ring model approach can be used [42]. The concept of dividing rovings into two coaxial parts traces back to first works performed by Ohno and Hannant [12] and was further devolved by Bruckermann and Voss [15], [34] by means of the two sub-roving model. As shown in Fig. 2.15, the textile roving is divided into a core and a sleeve ring. Each part is assumed to have a constant, but different, level of stress. This constitutes a simplification of reality but allows for a simple analytical treatment of the phenomenon.

Within such framework, the stress difference between core and sleeve filaments are governed by the constitutive laws of core and sleeve layers, as well as by the bond stress-slip relationships at the two interfaces (between the core and the sleeve ring and between the matrix and the sleeve ring). By providing consistent material laws and representative boundary conditions, the response

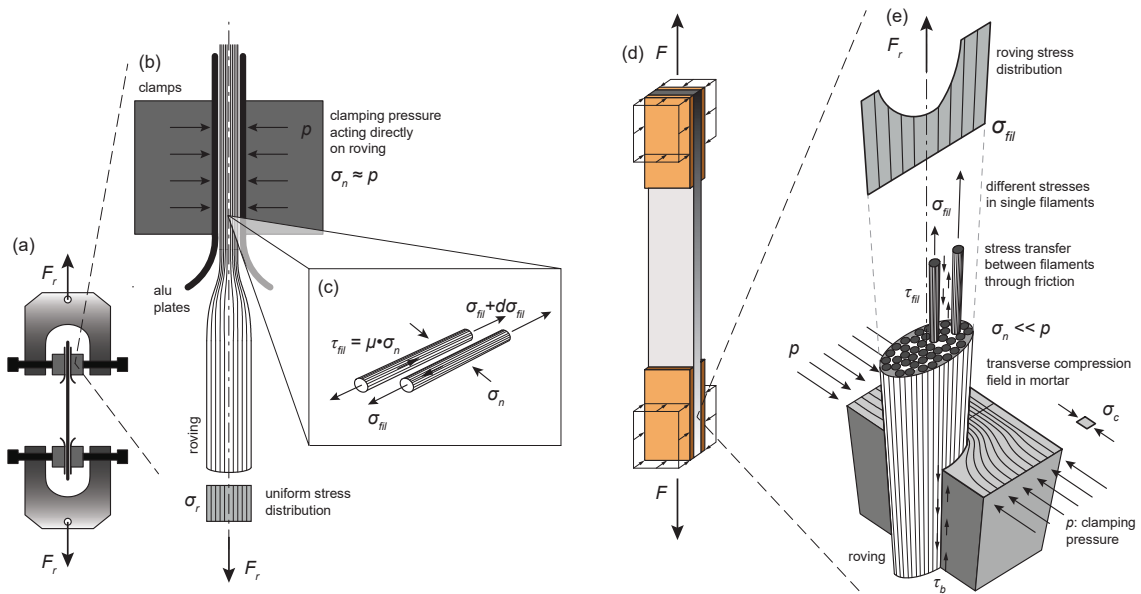


Figure 2.14: Load introduction mechanism: (a) simple roving test set-up; (b) Load introduction for simple roving test; (c) bond between single filaments; (d) composite tensile test; (e) load introduction for composite test.

can be determined in order to obtain the stress distribution for core and sleeve filaments along the member by means of equilibrium and compatibility conditions.

A first step to make the solution more accessible, consists in the selection of simple and consistent constitutive laws. In the following, this is discussed with reference to the material behaviour observed in the first part of this chapter:

1. Due to the chemical adhesion with the matrix, sleeve filaments are assumed to keep their undulated shape when embedded in the mortar. Under tension, these filaments cannot straighten and thus their behaviour can be assumed to be linear-elastic, see Fig. 2.15c.
2. Between matrix and sleeve filaments, a rather strong bond (depending on the type of coating) is ensured on the basis of chemical adhesion. The experimental bond-stress slip relationship is almost tri-linear (refer to pull-out tests in Fig. 2.6) but will be replaced by a rigid-plastic relationship as usually performed in reinforced concrete. This strong simplification can already provide a fairly good estimate of the response [43], see Fig. 2.15f.
3. Differently to the sleeve layer, core filaments can, to a certain extent, straighten within the boundaries provided by the surrounding sleeve and matrix (Fig. 2.15d). Consequently, their response is potentially non-linear in a similar manner as the one shown in the simple roving test (Fig. 2.5) but with a lower degree of straightening (as it is limited by the presence of the matrix and other filaments): $\varepsilon_{rC0} < \varepsilon_0$. This fact is shown in detail in Fig. 2.16 for various cases. In that figure, the response of three cases is presented: the bare undulated filament (see also bare undulated roving, in Fig. 2.5), the embedded undulated filament (Fig. 2.15d) and the theoretical response of a straight filament. As it can be seen, the presence of the matrix limits the straightening process ($\varepsilon_{rC0} < \varepsilon_{r0}$), with a response in-between that of the bare filament and that of a straight filament. The non-linear response is eventually only significant for high levels of undulation and thick fibres (as CF02), but this effect can be neglected in many cases (results in Fig. 2.16 calculated assuming a sinusoidal shape for the bump, fairly matching the experimental results of Fig. 2.5 for a bare roving).
4. The contact between core and sleeve filaments is rather soft when compared to the sleeve-to-

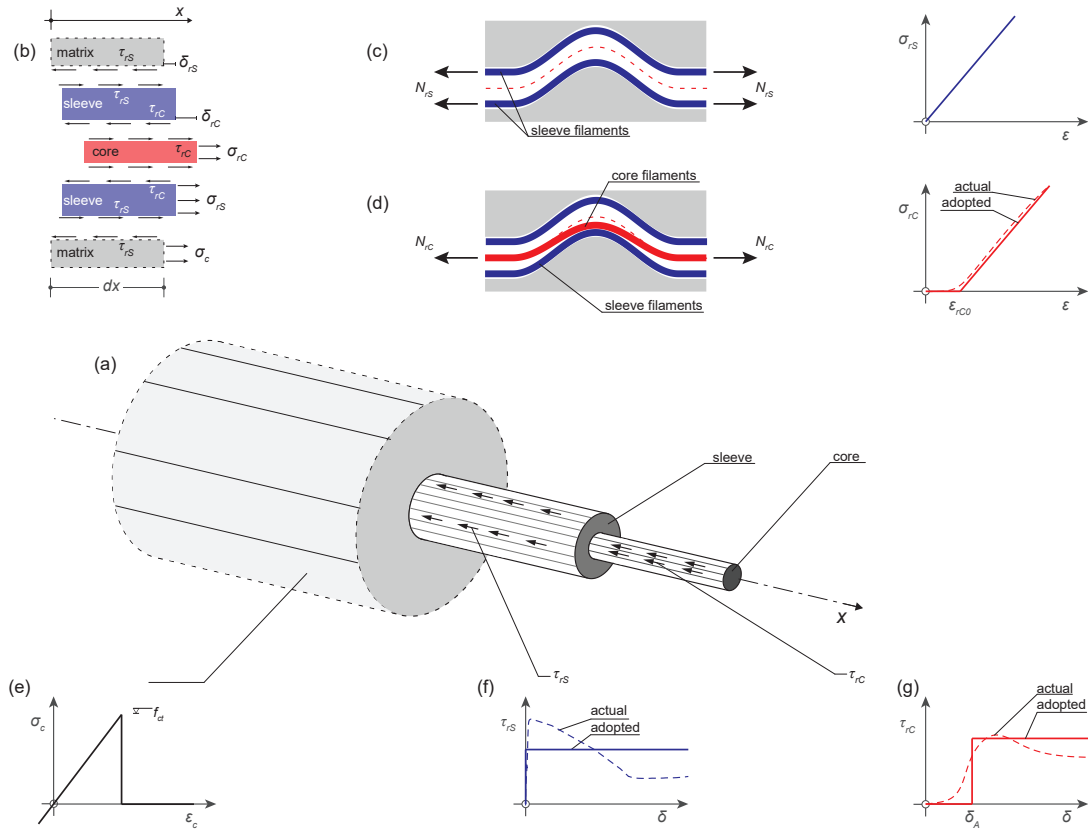


Figure 2.15: Model, experimental and adopted constitutive laws: (a) analysed element; (b) differential elements of core, sleeve and matrix; (c) sleeve and (d) core response; (e) matrix response; (f) sleeve-to-matrix bond response; and (g) core-to-sleeve bond response.

matrix interface, since bond at this level is governed by pure friction only (with the exception of fully-impregnated fabrics). In addition, some level of slip may be required to mechanically engage the contact between the filaments and to develop the bond stresses (straightening of filaments and relative displacement). This results in a more complex, non-linear bond-slip relationship consisting of an incremental hardening until a peak friction is reached (Fig. 2.15g). This response is theoretically softer than that of the sleeve filaments and can be characterised by a *bond-lag* response, delaying the development of bond stresses (see Fig. 2.15g). For modelling purposes, such complex non-linear behaviour can be replaced by a delayed rigid-plastic relationship, where an engagement slip (δ_A) is required to activate the bond stresses between sleeve and core filaments.

- Finally, with respect to the active cross-sections of the sleeve and core filaments (a_{rS} and a_{rC} respectively), they can be expressed by means of a constant k related to the ratio between the nominal active cross-section and the sleeve part: $a_{rS} = k \cdot a_r$ and $a_{rC} = (1 - k) \cdot a_r$. Using the same constant, it is also possible to approximate the contact perimeters assuming that the cross-section of the core and the cross-section of the roving have the same shape: $U_{rC} \approx (1 - k)^{\frac{1}{2}} \cdot U_{rS}$.

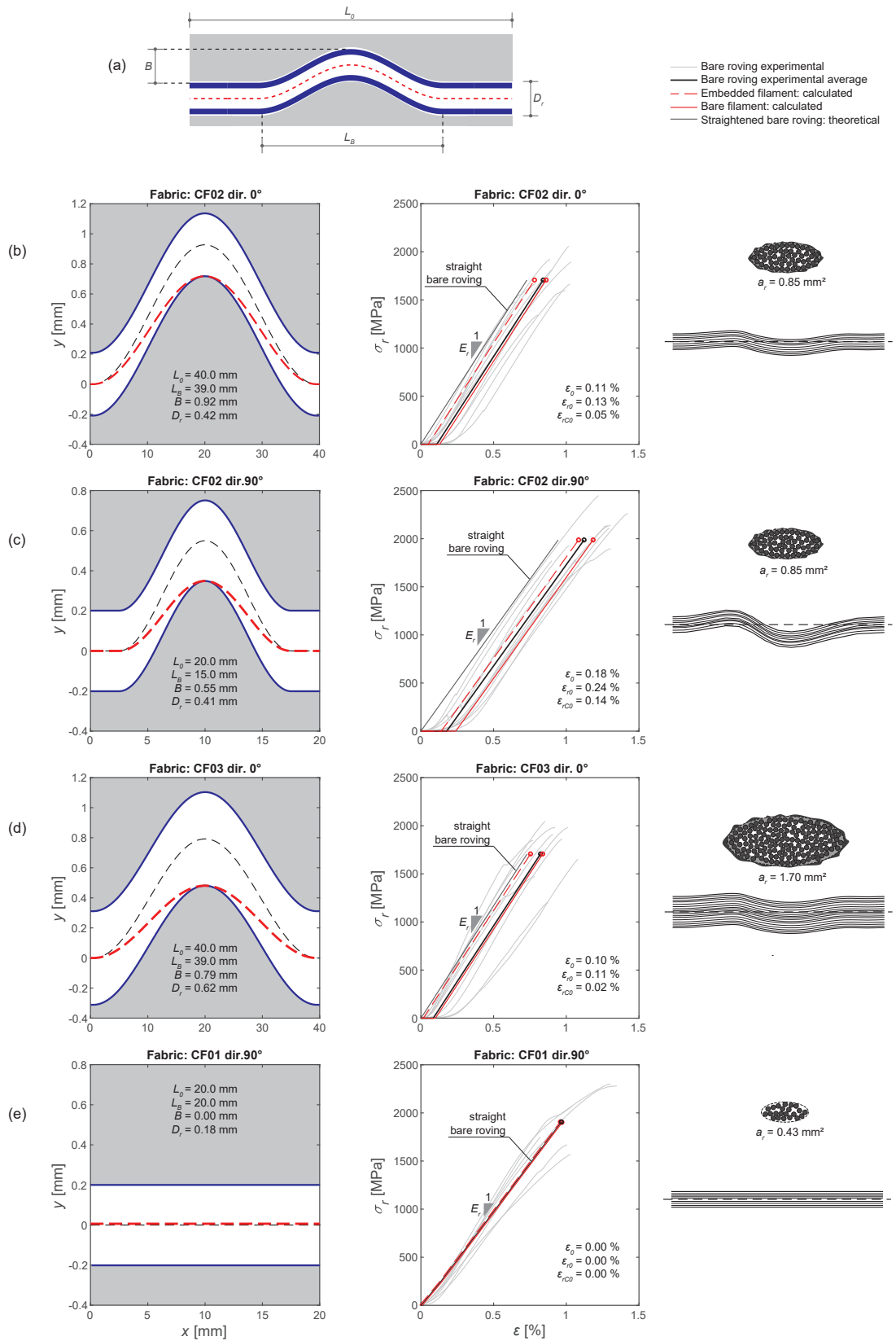


Figure 2.16: Calculated straightening strain for different fabrics based on their measured undulation: (a) definition of the geometric dimensions; (b) fabric CF02, dir. 0° ; (c) fabric CF02, dir. 90° ; (d) fabric CF03, dir. 0° ; (e) fabric CF01, dir. 90° .

2.4.3 Response of TRC in tension (stabilised cracking stage)

As previously discussed, the distribution of stresses in the roving results from two phenomena: the straightening of core filaments and the necessity of a certain level of slip to activate bond stresses between sleeve and core layers. Both phenomena are coupled and occur simultaneously (at least for high levels of loading). However, as shown in Fig. 2.16, the core straightening strain ε_{rC0} is fairly low in most cases and contributes in a limited manner to the delayed response of the composite. Thus, for simplicity reasons, both phenomena will be considered in the following in a condensed manner by means only of the core-to-sleeve bond-slip relationship (more general formulations accounting for both sources of non-linearity are however possible). This simplification allows treating the equations describing the response of a tension member with a linear response for the filaments and a non-linear consideration of the interface responses. In this section, the main equations ruling the response of a TRC tension member are presented and their results are discussed in the next section.

In the following, the origin of the longitudinal axis will be located at the centre of the tensile member (see Fig. 2.17). According to Fig. 2.15, the parameter δ_{rS} refers to the relative displacement between the concrete and the sleeve and δ_{rC} to the relative displacement between the sleeve and the core. In addition, the parameter a_{rS} and a_{rC} refer to the cross-section areas of the sleeve and core respectively while U_{rS} and U_{rC} refer to the contact perimeters between matrix and sleeve, and sleeve and core respectively.

At the location of a crack, the tensile force F carried by a single roving results $F_1 = F/n_r$ (where n_r number of longitudinal rovings in the cross-section of the member). Between cracks, however, a fraction of the axial force is carried by the matrix, leading to smaller deformations of the composite. The force exchanged between one roving and the matrix can be calculated by equilibrium conditions (in the stabilised cracking stage) as:

$$\Delta F_c = \tau_{rS} \cdot U_{rS} \cdot \frac{s_{rm}}{2} \quad (2.3)$$

Thus, the average force carried by the matrix results $\Delta F_c/2$ and for a single roving, the average force in the cracked region results (refer to Fig. 2.17a):

$$N_r = F_1 - \frac{\Delta F_c}{2} = N_{rC} + N_{rS} \quad (2.4)$$

This reduction of the average roving force (and strain) with respect to its maximal value (at cracks) corresponds to the *tension-stiffening* effect in tension ties.

To calculate the distance of the section where sufficient relative slip (δ_A) between core and sleeve has accumulated in order to engage the bond stresses (τ_{rC}), the average strains are integrated along the longitudinal axis of the member. In the following, this section is referred to as activation section and denoted as x_A :

$$\begin{aligned} u_{rC1} &= \int_0^{x_A} \varepsilon_{rC}(x) \cdot dx = \int_0^{x_A} \frac{N_{rC}(x)}{E_r \cdot a_{rC}} dx && \text{Displacements core} \\ u_{rS1} &= \int_0^{x_A} \varepsilon_{rS}(x) \cdot dx = \int_0^{x_A} \frac{N_{rS}(x)}{E_r \cdot a_{rC}} dx && \text{Displacements sleeve} \\ \delta_{SC1} &= u_{rS1} - u_{rC1} = \delta_A && \text{Accumulated slip in } x_A \end{aligned}$$

In a similar manner, the anchorage section of core filaments is located where the condition $\delta_{SC} = 0$

is satisfied:

$$u_{rC2} = \int_0^{x_C} \varepsilon_{rC}(x) \cdot dx \quad \text{Displacements core}$$

$$u_{rS2} = \int_0^{x_C} \varepsilon_{rS}(x) \cdot dx \quad \text{Displacements sleeve}$$

$$\delta_{SC2} = u_{rS2} - u_{rC2} = 0 \quad \text{Accumulated slip in } x_C$$

Depending on the roving type, some residual slip (between core and sleeve) may be necessary to ensure equilibrium and compatibility. This condition yields in: $\delta_{SC2} = u_{rS2} - u_{rC2} = \delta_A$ (more details and the full set of equations are given in 2.8).

According to the type of roving and the applied load, five different cases can be distinguished as presented in Fig. 2.17 (the complete equations necessary to calculate the activation section, anchorage sections and internal forces for each case are given in 2.8):

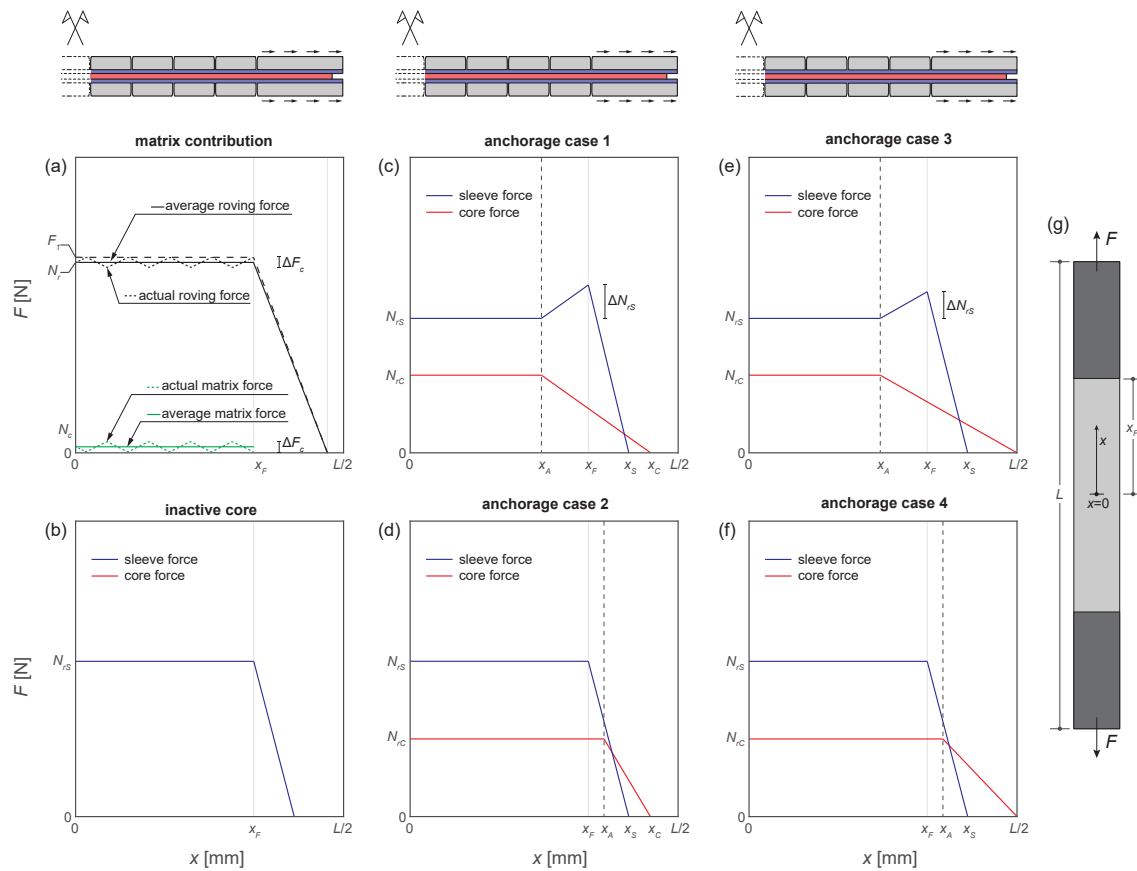


Figure 2.17: Distribution of internal forces for the coaxial ring model: (a) matrix contribution; (b) inactive core; (c) anchorage case 1; (d) anchorage case 2; (e) anchorage case 3; (f) anchorage case 4; (g) specimen and definition of local coordinates.

- Inactive core. In this case, the core is considered inactive since insufficient slip has accumulated along the tensile member to engage bond between inner and outer filaments (typical case for low load levels). At the cracked section, all the tensile force is thus carried by the sleeve, and both, by the sleeve and the matrix between cracks ($N_{rS} = N_r$, see Fig. 2.17b);
- Anchorage case 1: Core and sleeve filaments are anchored within the anchorage zone of the member. The activation section x_A is located within the free length: $x_A < x_F$ (refer to anchorage case 1, Fig. 2.17c). This corresponds to a typical case of coated fabrics with a long tie length and high load levels;

- Anchorage case 2: Both, core and sleeve filaments are anchored within the anchorage zone. Also the activation section x_A is located within the anchorage zone of the tie: $x_F < x_A < L/2$ (refer to anchorage case 2, Fig. 2.17d). This corresponds to a typical case of coated fabrics with a short tie length and low load levels;
- Anchorage case 3: Sleeve filaments are anchored within the anchorage zone while core filaments are only partially anchored in this region (slip at the end of tie higher than the engagement slip δ_A). This anchorage case considers that the activation section is within the free length of the member: $x_A < x_F$ (Fig. 2.17e). This corresponds to a typical case of uncoated fabrics with a long tie length and high load levels;
- Anchorage case 4: Sleeve filaments are anchored within the anchorage zone of the member and core filaments only partially anchored. The activation section is located beyond the free length of the tie: $x_F < x_A < L/2$ (see anchorage case 4, Fig. 2.17f). This corresponds to a typical case of uncoated fabrics with a short tie length and low load levels.

These cases allow calculating the stresses and strains in the layers of the composite member along its longitudinal axis for a given level of load. The tensile response of the member in the cracked stage in terms of force-strain relationship can thus be determined by calculating the stress distribution of the composite for a series of load steps. The complete set of equations to be solved for each case is given in 2.8. For each load level, it can be solved numerically (for instance by means of an iterative procedure). This allows identifying the governing anchorage case for the given load-step, the location of the activation section x_A and the stress distribution of the core and sleeve ring along the longitudinal axis of the member. Following this methodology, the response of the TRC composite can be determined and the stiffness of the tie can in some cases be lower with respect to that of the bare fabric. This is due to the non-homogeneous activation of filaments, without the need of introducing any efficiency factor on the area or stiffness of the rovings.

The deformation of the tensile element is assumed to correspond to the average one of the sleeve layer (ε_{rS}). It shall be noted that ε_{rS} accounts for tension-stiffening and bond-lag effects between the core and sleeve layers. In a similar manner, the crack opening is calculated as:

$$w = \varepsilon_{rS} \cdot s_{rm} \quad (2.5)$$

Failure occurs when at the location of the crack, sleeve stresses attain the strength of roving:

$$\varepsilon_{rS,max} = \max \{ \varepsilon_{rS}(x) \} + \Delta \varepsilon_{rS,c} = \frac{f_r}{E_r} \quad (2.6)$$

Where the term $\Delta \varepsilon_{rS,c}$ refers to the increase of maximum strain with respect to the average one due to tension-stiffening. This term can be estimated in a safe manner as:

$$\Delta \varepsilon_{rS,c} = \frac{\Delta F_c}{2 \cdot a_{rS} \cdot E_r} \quad (2.7)$$

assuming that the force carried by the matrix between cracks is carried only by the sleeve filaments at the location of the crack. This means that the failure load can be calculated directly from the resulting state of strains in the filament (where the sleeve is governing) without the need of considering any additional empirical efficiency factor.

2.4.4 Calculation of cracking load

At low applied stresses, the response can be assumed as linear and the contribution of the fabric can be neglected:

$$\varepsilon \approx \frac{F}{E_c \cdot A_c} \quad (2.8)$$

with A_c referring to the net cross-section area (longitudinal and transversal rovings removed). Due to the variability of the matrix tensile strength, A_c can be simplified by assuming $A_c \approx A$ so that the cracking load can be calculated as:

$$N_{cr} \approx f_{ct} \cdot A \quad (2.9)$$

2.5 Comparison to test results

2.5.1 Own experimental programme

The fundamental model parameters used to compute the tensile response of the tested specimen are reported in Table 2.6. The same parameters were consistently used for identical fabrics and directions. The results for some selected specimen in terms of force-strain, force-crack opening relationships and the stress evolution throughout the loading process are shown in Fig. 2.18 (all results refer to the mid-section of the tie, $x = 0$). The calculated response shows consistent agreement with the experimental one for different types of fabric and confirm the validity of the approach. Both the apparent softer response after cracking and the failure load are correctly reproduced, with an average of ratio $N_{R,test}/N_{R,calc}$ close to unity and a coefficient of variation of 10%. Moreover, in practically all cases, the failure type of the member is correctly reproduced, as a consequence from the calculated stress concentrations of sleeve filaments close to the physical anchorage zone.

specimen [type]	tests [nr]	τ_{rS} [MPa]	s_{rm} [mm]	ΔF_c [N]	k [-]	δ_A [mm]	τ_{rC} [MPa]	F_u [kN]	N_R [kN]	F_u/N_R [-]
T00-A	4	2.6	20	224	0.60	0.65	1.50	36.0	34.4	1.05
T00-B	3	2.6	20	224	0.60	0.65	1.50	34.6	34.4	1.01
T00-C	2	2.9	30	336	0.60	0.65	1.50	15.5	13.2	1.17
T00-F	4	2.6	10	56	0.60	0.65	1.50	29.7	35.2	0.84
T00-G	2	2.6	20	224	0.60	0.65	1.50	15.5	13.8	1.12
T90-C	2	2.3	30	336	0.50	0.35	1.50	13.0	14.1	0.92
T90-D	3	2.3	20	224	0.50	0.35	1.50	25.4	27.2	0.93
T90-E	4	2.3	20	224	0.50	0.35	1.50	11.7	12.0	0.98
T90-I	2	0.8	30	140	0.45	0.20	0.10	26.6	24.4	1.09
T90-J	2	2.3	17	272	0.55	0.80	1.00	72.2	71.1	1.02
V-31.Z2	5	0.7	60	180	0.45	0.20	0.10	6.9	7.4	0.93
V-31.Z2	5	0.7	60	180	0.45	0.20	0.10	16.3	14.9	1.09
TC1-1	7	0.8	40	300	0.45	0.20	0.10	9.7	9.2	1.05
TCB-1	5	0.8	75	120	0.45	0.20	0.10	3.9	3.5	1.11
TCB-2	7	0.8	35	140	0.45	0.20	0.10	8.8	7.1	1.24
TCB-3	7	0.8	23	92	0.45	0.20	0.10	12.5	10.7	1.17
TCB-4	7	0.8	21	84	0.45	0.20	0.10	16.7	14.3	1.17
V3-T01-K3	5	4.5	40	1120	0.80	0.00	0.00	63.7	62.6	1.02
V3-T01-K30	1	4.5	40	1120	0.80	0.00	0.00	20.0	19.9	1.01
									Average	1.06
									COV	0.12

Table 2.6: Model parameters and results.

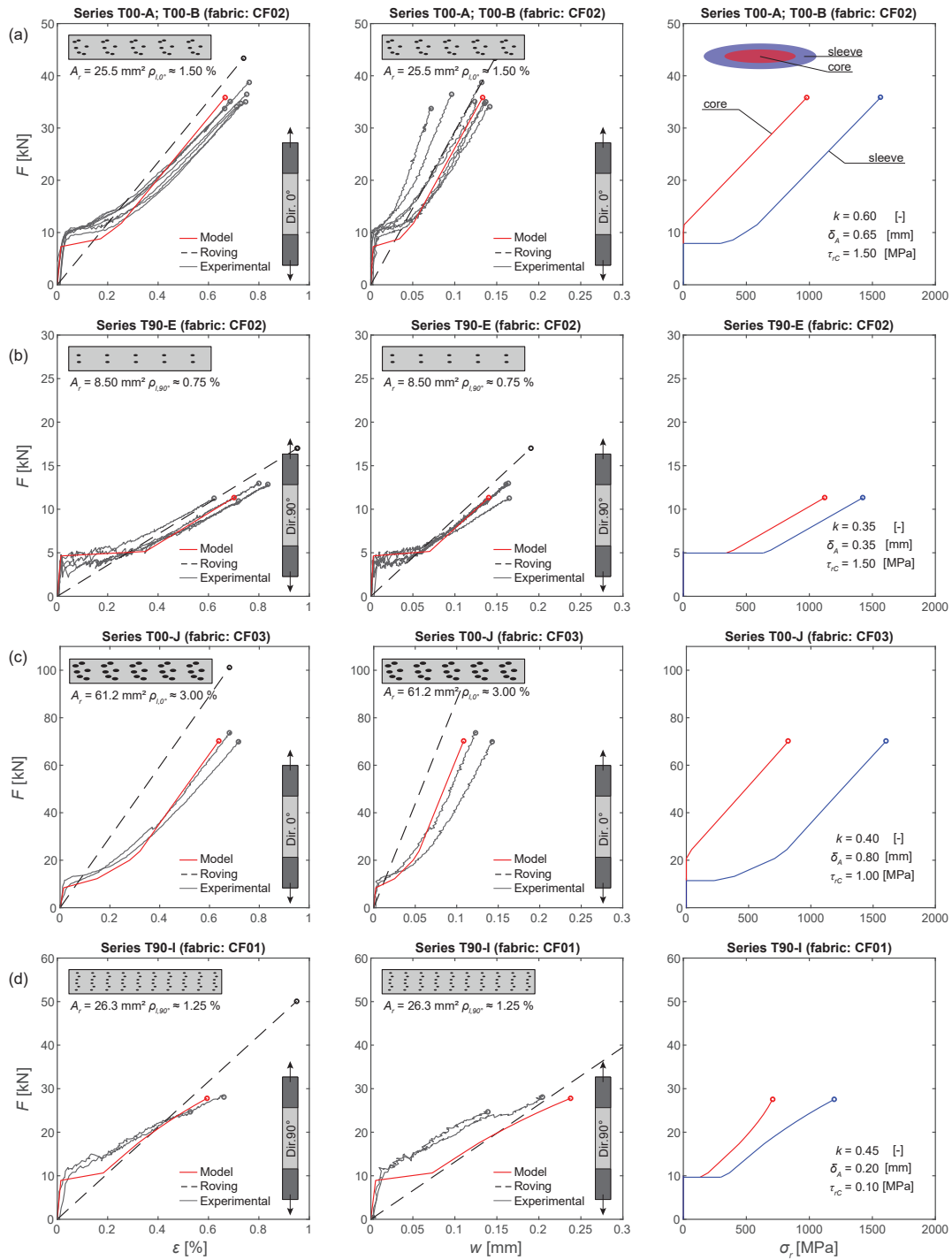


Figure 2.18: Experimental and calculated tensile response of selected members with varying impregnation and cross-section. Force-strain, force-crack opening and evolution of roving stresses (core and sleeve) at the central section of the member $x = 0$: (a) series T00-A and B; (b) series T90-E; (c) series T00-J; (d) series T90-I;

2.5.2 Comparison to tests from the literature

To validate the proposed approach on a larger basis, the model was also used to compute the response of 49 tests available in scientific literature [34, 44, 45]. For the uncoated carbon fabrics (series V-31.Z2 [34] and TC1 [44]), the same values for the parameters were used with respect to the ones of the testing programme introduced in this chapter (refer to Table 2.6). Differently, for impregnated carbon fabrics [45], part of the roving cross-section is considered as inactive (series

V3-T01-K30, Table 2.6). As shown in Fig. 2.19, both the load-strain response and the resistance of the members are reproduced with good accuracy (average measured-to-calculated strength equal to 1.02, coefficient of variation equal to 11%, similar values as for own tests).

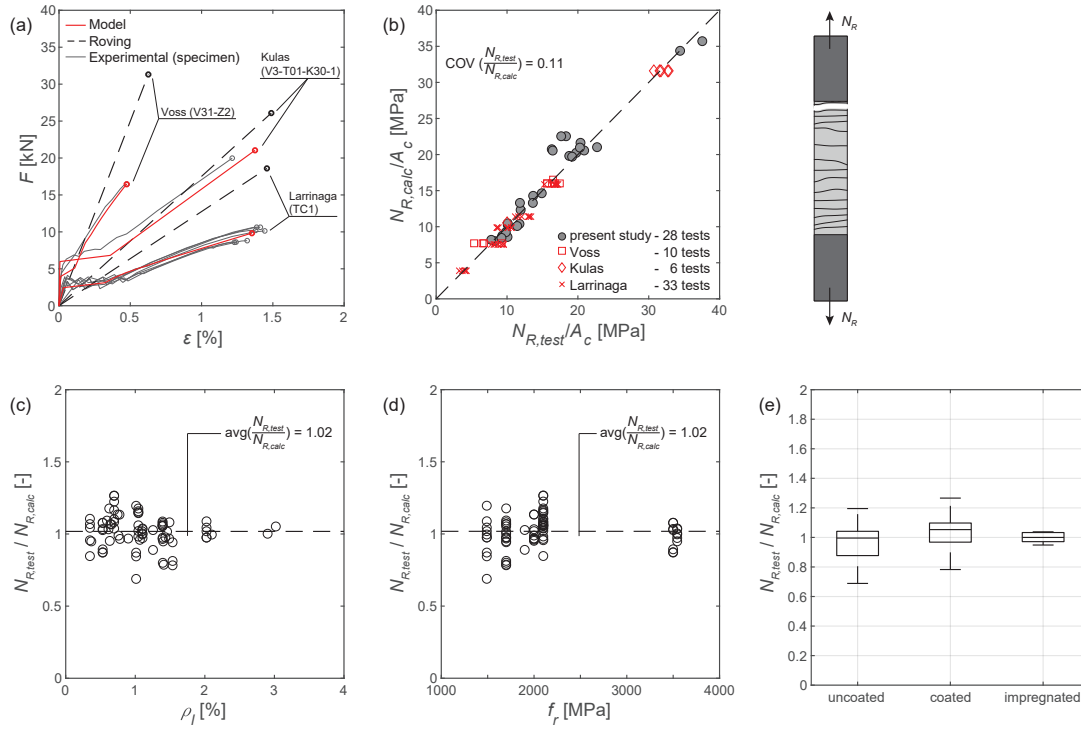


Figure 2.19: Comparison to literature: (a) comparison of load-strain deformation responses for selected specimens; (b) comparison of failure loads; (c-e) comparison for selected parameters.

2.5.3 General comments and outlook

The comparison of the presented model and the results from the literature shows fine agreement. The available ranges of several parameters are however limited, particularly in terms of member length and coating properties. In the following some parametric studies will be presented, but additional experimental work is judged to be required to confirm and better calibrate the assumptions of the proposed model (mainly the assumed core-to-sleeve bond law and response of the core filaments).

2.6 Parametric studies

Taking advantage of the developed model, the role of some parameters is investigated in this section to better understand the response of TRC in tension. In this context it will be referred to the mean composite stress, which is defined as:

$$\sigma_{TRC} = \frac{F}{b \cdot t} \quad (2.10)$$

2.6.1 Influence of coating

As mentioned earlier, the response of TRC and its resistance is significantly influenced by the coating degree of the fabric. Such differences can be taken into account in a condensed manner through the bond behaviour between core and sleeve filaments. Fig. 2.20 shows the theoretical response of three fundamental cases:

- Unbonded core, with no friction between filaments (Fig. 2.20a). This situation corresponds mainly to uncoated fabrics with low undulation. The response of the composite is governed by the sleeve filaments while the core filaments remain inactive;
- Delayed activation of bond stresses (Fig. 2.20b). This type of behaviour was observed for coated fabrics with some degree of undulation. The global response is delayed with respect to the bare reinforcement and the full strength of the rovings cannot be attained;
- Completely bonded rovings (Fig. 2.20c) as it would be the case for fully impregnated fabrics. In this case, the reinforcement behaves in a homogeneous manner and the full strength of the fabric can be exploited.

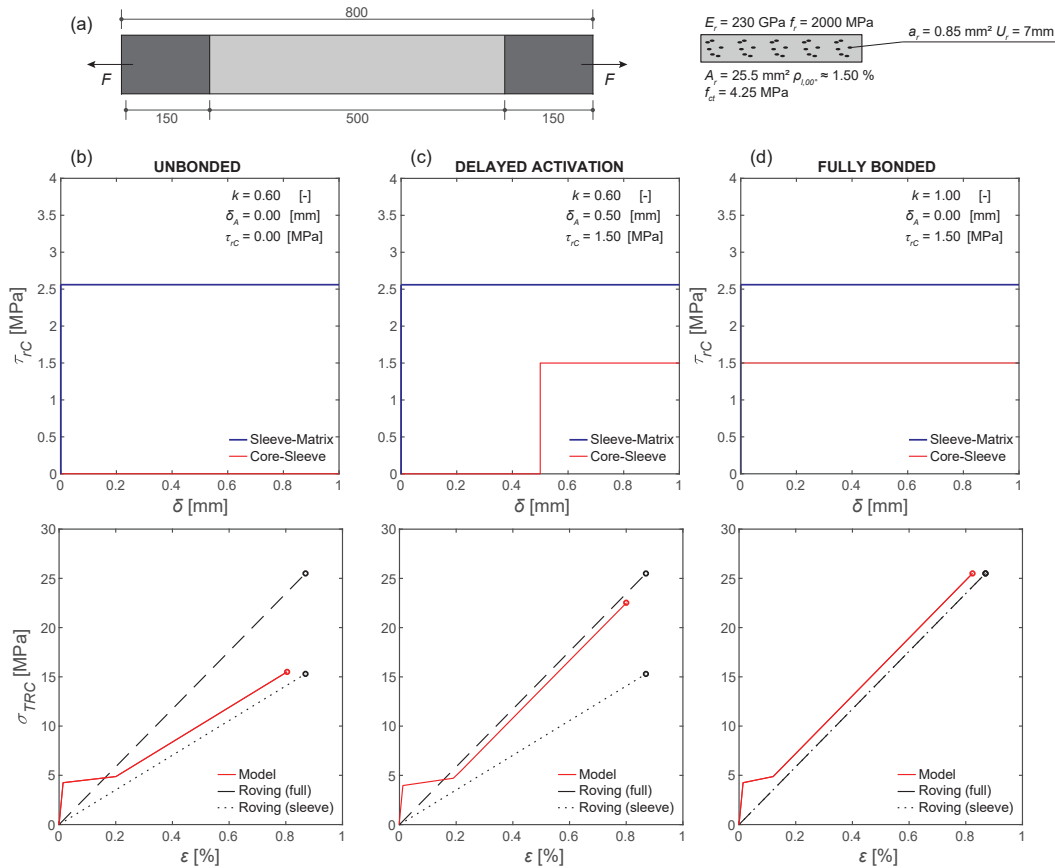


Figure 2.20: Parametric study of bond laws allowing to consider different types of fabric: (a) investigated case; interface bond laws (top) and composite response (bottom) for: (b) unbonded core; (c) delayed bond activation; and (d) fully bonded response.

2.6.2 Influence of anchorage and tie length

The stress distribution in the rovings and the resulting stiffness reduction of the composite depend significantly on the length of the member and the length of the load introduction zone. In Fig. 2.21, the effect of the tie and anchorage length is investigated for different fabrics, focusing on the effect of coating and impregnation. Five different cases are examined for two types of fabric:

1. Long tie with long anchorage zone (case A);
2. Long tie with short anchorage zone (same anchorage length as the tested specimens presented in this chapter, case B);
3. Medium size member (with an overall length corresponding to that of the tested specimens

presented in this chapter) with long anchorage zone (case C);

4. Medium length member with short anchorage zone (with the dimensions corresponding to the tested specimens presented in this chapter, case D);
5. Short member with short free length (anchorage length corresponding to the one used in the specimens presented in this chapter, case E).

The results in terms of stress-strain of the parametric study are shown in Fig. 2.21. It can be noted that the variation of anchorage and tie length has a different effect according to the fabric type. For the cases under investigation, the following observations can be performed:

- Coated fabrics with a significant undulation and strong core-to-sleeve bond are mainly influenced by the free length of the tie. For longer members, sufficient slip to engage core-to-sleeve bond stresses accumulates already at low load levels. Bond-lag effects thus are limited for long members and the response in terms of stiffness tends towards the one of the bare fabric. Yet the full strength of the fabric cannot be attained due to stress concentrations in the sleeve layer close to the anchorage zone. On the contrary, for members with short length, bond-lag effects are significant with an overall reduction of the stiffness and resistance. For the limit case E (see Fig. 2.21), only the sleeve filaments contribute to the load-bearing capacity and the core filaments remain inactive during the whole loading process. As a conclusion, the strength (and stiffness) is dominated by the free length of the tie (distance between anchorages) with higher resistances associated to higher free lengths (strengths of case B and D higher than those of cases A and C respectively). This is justified by the fact that longer free lengths are associated to more uniform stress profiles between core and sleeve (as the core filaments can be activated at earlier load stages);
- For uncoated fabrics with a low degree of undulation and a weak core-to-sleeve bond capacity, the response is on the contrary more dominated by the anchorage lengths. Similar to coated fabrics, when the free length increases, sufficient slip can accumulate already at low load stages and the stiffness of the member tends towards the one of the bare fabric. However, due to the weak core-to-sleeve bond strength, a longer anchorage length is required in order to correctly develop the core filaments. Also in this case, the full resistance cannot be attained due to the stress concentrations in the sleeve layer close to the anchorage zone. As a result, the strength of the tie is highly dependent on the anchorage length, with longer anchorage lengths associated to higher resistances (strength of cases A and C higher than B and D respectively), as the anchorage length limits the load that can be introduced in the tie.

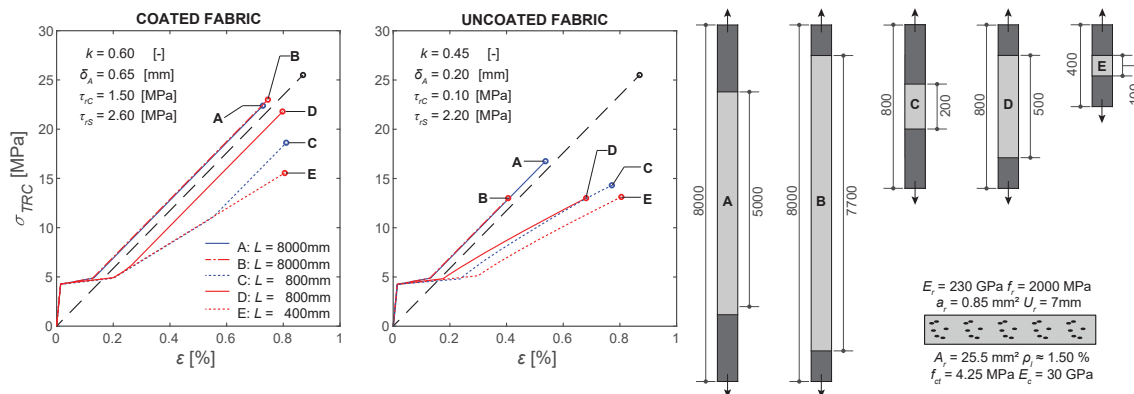


Figure 2.21: Parametric study of anchorage and tie length for different textile types.

2.7 Conclusions

This chapter investigates the response of Textile Reinforced Concrete (TRC) in tension on the basis of an experimental programme and analytical approach. Its main conclusions are summarised as follows:

1. TRC can be suitably used in tension. Crack widths remain limited due to the narrow crack spacing and generally high resistances can be obtained. Its main drawback refers to the brittle nature of its failure;
2. Crack spacing is mostly controlled by the reinforcement amount and distance of transverse rovings, particularly when several layers have coincident locations (weakening of the section);
3. Bond in TRC is not particularly influenced by the presence of transverse confining pressures. This is justified by the low radial stiffness of the rovings, which yields the transverse pressure compression to be carried by the mortar;
4. As a consequence of the previous point, one can conclude that bond between the matrix and fabric is mostly originated by adhesion and friction;
5. The undulated shape of the filaments embedded in TRC and the soft response of the rovings in radial direction has two effects. The first one related to a non-linear filament response (during filament straightening) and the second to the fact that some level of slip is required between core and sleeve filaments prior to activation the bond of the core filaments. These phenomena can be implemented in a condensed manner with a *bond-lag* response between core and sleeve filaments (delayed activation of bond stresses) in a coaxial ring model;
6. Modelling by accounting for the bond-lag phenomenon allows describing in a consistent manner the serviceability limit state (crack-openings) and the failure load, without the need of efficiency factors. Also, such approach allows understanding the influence of the tie and the anchorage length in the overall response of the element;
7. A systematic comparison of such approach to 77 test results confirms its soundness with an average measured-to-calculated strength of 1.02 and a coefficient of variation of $COV = 0.11$.

Acknowledgements

The authors would like to sincerely acknowledge the support given by the association of the swiss cement producers *cemsuisse* (research project #201407) for their financial support, providing the concrete mix and technical discussions.

Bibliography

- [1] Josef Hegger, Manfred Curbach, Alexander Stark, Sebastian Wilhelm, and Kristina Farwig. Innovative design concepts: Application of textile reinforced concrete to shell structures. *Structural Concrete*, (August):1–10, 2017.
- [2] Wolfgang Brameshuber. Textile Reinforced Concrete. State-of-the-Art Report. Technical report, RILEM Technical Committee TC201-TRC, Aachen, 2009.
- [3] J. Orlowsky and M. Raupach. Durability model for AR-glass fibres in textile reinforced concrete. *Materials and Structures/Materiaux et Constructions*, 41(7):1225–1233, 2008.
- [4] Marko Butler, Viktor Mechtcherine, and Simone Hempel. Experimental investigations on the durability of fibre-matrix interfaces in textile-reinforced concrete. *Cement and Concrete Composites*, 31(4):221–231, 2009.
- [5] Heidi Cuypers, Jeanette Orlowsky, Michael Raupach, and Till Büttner. Durability aspects of ar-glass-reinforcement in textile reinforced concrete, part 1: Material behaviour. In Christian U. Grosse, editor, *Advances in Construction Materials 2007*, pages 381–388, Berlin, Heidelberg, 2007. Springer Berlin Heidelberg.
- [6] S. Scheerer, R. Chudoba, M.P. Garibaldi, and M. Curbach. Shells Made of Textile Reinforced Concrete - Applications in Germany. *Journal of the International Association for Shell and Spatial Structures*, 58(1):79–93, 2017.
- [7] Philipp Preinstorfer, Benjamin Kromoser, and Johann Kollegger. Flexural behaviour of filigree slab elements made of carbon reinforced UHPC. *Construction and Building Materials*, 199: 416–423, 2019.
- [8] Alexander Scholzen, Rostislav Chudoba, Josef Hegger, and Norbert Will. Leichte Dachschalen aus Carbonbeton: Fertigteilproduktion, experimentelle Untersuchungen und Anwendungspotenzial. *Beton- und Stahlbetonbau*, 111(10):663–675, 2016.
- [9] Alva Peled, Arnon Bentur, and Barzin Mobasher. *Textile Reinforced Concrete - Modern Concrete Technology*. Boca Raton : CRC Press, Taylor & Francis Group, 1st edition edition, 2017. ISBN 9780367866914.
- [10] Josef Hegger, Wolfgang Brameshuber, and Norbert Will. Textile Reinforced Concrete. In *1st international RILEM Symposium*, page 406, Aachen, 2006. RILEM.
- [11] J. Aveston and A. Kelly. Theory of multiple fracture of fibrous composites. *Journal of Materials Science*, 8(3):352–362, 1973.
- [12] S. Ohno and D. J. Hannant. Modeling the Stress-Strain Response of Continuous Fiber Reinforced Cement Composites. *ACI Materials Journal*, 91(3):306–312, 1994.
- [13] Frank Jesse. *Load Bearing Behaviour of Filament Yarns in cementitious matrix*. PhD thesis, Fakultät Bauingenieurwesen der Technischen Universität Dresden, 2004.
- [14] M Molter. *Zum Tragverhalten von textildbewehrtem Beton*. PhD thesis, Fakultät für Bauingenieurwesen der Rheinisch-Westfälischen Technischen Hochschule Aachen, 2005.
- [15] Oliver Bruckermann. *Zur Modellierung des Zugtragverhaltens von textildbewehrtem Beton*. PhD thesis, Fakultät für Bauingenieurwesen der Rheinisch-Westfälischen Technischen Hochschule Aachen, 2007.
- [16] I Lepenies. *Zur hierarchischen und simultanen Multi-Skalen-Analyse von Textilbeton*. PhD thesis, Fakultät Bauingenieurwesen der Technischen Universität Dresden, 2007.

-
- [17] Isabella Giorgia Colombo, Anna Magri, Giulio Zani, Matteo Colombo, and Marco di Prisco. Textile Reinforced Concrete: experimental investigation on design parameters. *Materials and Structures*, 46(11):1933–1951, 2013.
- [18] Pello Larrinaga, Carlos Chastre, Hugo C. Biscaia, and Jose T. San-Jose. Experimental and numerical modeling of basalt textile reinforced mortar behavior under uniaxial tensile stress. *Materials and Design*, 55:66–74, 2014.
- [19] Raphaël Contamine, Angel Junes, and Amir Si Larbi. Tensile and in-plane shear behaviour of textile reinforced concrete: Analysis of a new multiscale reinforcement. *Construction and Building Materials*, 51:405–413, 2014.
- [20] Rilem Technical Committee. Recommendation of RILEM TC 232-TDT: test methods and design of textile reinforced concrete. *Materials and Structures*, 49(12):4923–4927, 2016.
- [21] R. Contamine, A. Si Larbi, and P. Hamelin. Contribution to direct tensile testing of textile reinforced concrete (TRC) composites. *Materials Science and Engineering A*, 528(29-30): 8589–8598, 2011.
- [22] Elisabeth Schütze, Jan Bielak, Silke Scheerer, Josef Hegger, and Manfred Curbach. Einaxialer Zugversuch für Carbonbeton mit textiler Bewehrung. *Beton- und Stahlbetonbau*, 113(1):33–47, 2018.
- [23] Stefano De Santis, Francesca Giulia Carozzi, Gianmarco de Felice, and Carlo Poggi. Test methods for Textile Reinforced Mortar systems. *Composites Part B: Engineering*, 127:121–132, 2017.
- [24] J. Hartig, F. Jesse, K. Schick Tanz, and U. Häukler-Combe. Influence of experimental setups on the apparent uniaxial tensile load-bearing capacity of Textile Reinforced Concrete specimens. *Materials and Structures*, 45(3):433–446, 2012.
- [25] Marianovella Leone, Maria Antonietta Aiello, Alberto Balsamo, Francesca Giulia Carozzi, Francesca Ceroni, Marco Corradi, Matija Gams, Enrico Garbin, Natalino Gattesco, Piotr Krajewski, Claudio Mazzotti, Daniel Oliveira, Catherine Papanicolaou, Giovanna Ranocchiai, Francesca Roscini, and Dorothea Saenger. Glass fabric reinforced cementitious matrix: Tensile properties and bond performance on masonry substrate. *Composites Part B: Engineering*, 127: 196–214, 2017.
- [26] Carmelo Caggegi, Emma Lanoye, Khaled Djama, Antoine Bassil, and Aron Gabor. Tensile behaviour of a basalt TRM strengthening system: Influence of mortar and reinforcing textile ratios. *Composites Part B: Engineering*, 130:90–102, 2017.
- [27] Josef Hegger, Michael Horstmann, Stefan Voss, and Norbert Will. Textilbewehrter Beton Tragverhalten, Bemessung und Anwendung. *Beton- und Stahlbetonbau*, 102(6):362–370, 2007.
- [28] Chokri Cherif. *Textile materials for lightweight constructions: Technologies - methods - materials - properties*. Springer, 2016.
- [29] Bong-gu Kang. *Modellierung von Textilbeton auf der Mikroskalenebene*. PhD thesis, Fakultät für Bauingenieurwesen der Rheinisch-Westfälischen Technischen Hochschule Aachen, 2011.
- [30] Pello Larrinaga, Carlos Chastre, Jose T. San-Jose, and Leire Garmendia. Non-linear analytical model of composites based on basalt textile reinforced mortar under uniaxial tension. *Composites Part B: Engineering*, 55:518–527, 2013.

- [31] Francesca Giulia Carozzi, Gabriele Milani, and Carlo Poggi. Mechanical properties and numerical modeling of Fabric Reinforced Cementitious Matrix (FRCM) systems for strengthening of masonry structures. *Composite Structures*, 107:711–725, 2014.
- [32] Viktor Mechtcherine, Volker Slowik, and Petr Kabele. Strain-hardening cement-based composites: SHCC4. *RILEM Bookseries*, 15:418 – 426, 2018.
- [33] J Hegger, N Will, O Bruckermann, and S Voss. Investigations on the bearing behaviour and application potential of textile reinforced concrete. *Engineering Structures*, 30(7):2050–2056, 2008.
- [34] Stefan Voss. *Ingenieurmodelle zum Tragverhalten von textildbewehrtem Beton*. PhD thesis, Fakultät für Bauingenieurwesen der Rheinisch-Westfälischen Technischen Hochschule Aachen, 2008.
- [35] fib (The International Federation for Structural Concrete). *fib Model Code for concrete structures 2010*. Ernst und Sohn Verlag Germany, 2013.
- [36] Patrick Valeri, Patricia Guaita, Raffael Baur, and Miguel Fernández Ruiz. Pedagogy through artisanal construction of thin-walled concrete elements: a dialogue between engineering and architecture. In ACHE, editor, *Proceedings of the IV Int. Conference on Structural Engineering Education*, pages 1–10, Madrid, 2018. ACHE.
- [37] S Sueki, C Soranakom, B Mobasher, and A Peled. Pullout-Slip Response of Fabrics Embedded in a Cement Paste Matrix. *Journal of materials in civil engineering*, 19(September):718–727, 2005.
- [38] Natalie Williams Portal, Ignasi Fernandez Perez, Lars Nyholm Thrane, and Karin Lundgren. Pull-out of textile reinforcement in concrete. *Construction and Building Materials*, 71:63–71, 2014.
- [39] Hana Aljewifi, Bruno Fiorio, and Jean-Louis Gallias. Pull-out behaviour of a glass multi-filaments yarn embedded in a cementitious matrix. *EURO-C 2010 – Computational Modelling of Concrete Structures, Schladming, Austria*, 2010.
- [40] Ali Dalalbashi, Bahman Ghiassi, Daniel V. Oliveira, and Ana Freitas. Effect of test setup on the fiber-to-mortar pull-out response in TRM composites: Experimental and analytical modeling. *Composites Part B: Engineering*, 143(December 2017):250–268, 2018.
- [41] V Eckers, R Rypl, R Chudoba, T Gries, and J Hegger. Modified Tensile Test Setup for High-Modulus Multi-Filament Yarns. In *International RILEM Conference on Material Science*, volume I, pages 111–116, 2010.
- [42] B. W. Zastrau, I. Lepenies, and M. Richter. Entwicklung konstitutiver Gesetze für Feinbeton mit textiler Bewehrung. *Arbeitsbericht des Sonderforschungsbereiches 528*, pages 164–212, 2001.
- [43] Peter Marti, Manuel Alvarez, Walter Kaufmann, and Viktor Sigrist. Tension Chord Model for Structural Concrete. *Structural Engineering International*, 98(1998), 1998.
- [44] P. Larrinaga. *Flexural strengthening of low grade concrete through the use of new cement-based composite materials*. PhD thesis, Faculty of Engineering, Bilbao, 2011.
- [45] Christian Kulas. *Zum Tragverhalten getränkter textiler Bewehrungselemente für Betonbauteile*. PhD thesis, RWTH, 2013.

2.8 Appendix: Bond lag model equations

Anchorage case 1

It is considered: $x_A < x_F$ and $x_C < L/2$ refer to Fig. 2.17b:

$$N_{rC} = a_{rC} \cdot \sigma_{rC} \quad (2.11)$$

$$N_{rS} = a_{rS} \cdot \sigma_{rS} \quad (2.12)$$

$$\sigma_{rC} = \varepsilon_{rC} \cdot E_r \quad (2.13)$$

$$\sigma_{rS} = \varepsilon_{rS} \cdot E_r \quad (2.14)$$

$$u_{rC1} = \varepsilon_{rC} \cdot x_A \quad (2.15)$$

$$u_{rS1} = \varepsilon_{rS} \cdot x_A \quad (2.16)$$

$$\delta_{SC1} = u_{rS1} - u_{rC1} = \delta_A \quad (2.17)$$

$$u_{rC2} = \varepsilon_{rC} \cdot x_A + \frac{1}{2} \cdot \varepsilon_{rC} \cdot (x_C - x_A) \quad (2.18)$$

$$u_{rS2} = \varepsilon_{rS} \cdot x_F + \frac{1}{2} \cdot \Delta\varepsilon_{rS} \cdot (x_F - x_A) + \frac{1}{2} \cdot (\varepsilon_{rS} + \Delta\varepsilon_{rS}) \cdot (x_S - x_F) \quad (2.19)$$

$$\Delta\varepsilon_{rS} = \frac{\tau_{rC} \cdot U_{rC} \cdot (x_F - x_A)}{a_{rS} \cdot E_r} \quad (2.20)$$

$$\delta_{SC2} = u_{rS2} - u_{rC2} = 0 \quad (2.21)$$

$$N_r = N_{rC} + N_{rS} \quad (2.22)$$

$$N_r = \tau_{rC} \cdot U_{rC} \cdot (x_C - x_F) + \tau_{rS} \cdot U_{rS} \cdot (x_S - x_F) \quad (2.23)$$

$$N_{rC} = \tau_{rC} \cdot U_{rC} \cdot (x_C - x_A) \quad (2.24)$$

For non-real solutions to the above system of equations, equation 2.21 is replaced by: $\delta_{SC2} = u_{rS2} - u_{rC2} = \delta_A$.

Anchorage case 2

It is considered: $x_A > x_F$ and $x_C < L/2$ refer to Fig. 2.17e:

$$N_{rC} = a_{rC} \cdot \sigma_{rC} \quad (2.25)$$

$$N_{rS} = a_{rS} \cdot \sigma_{rS} \quad (2.26)$$

$$\sigma_{rC} = \varepsilon_{rC} \cdot E_r \quad (2.27)$$

$$\sigma_{rS} = \varepsilon_{rS} \cdot E_r \quad (2.28)$$

$$u_{rC1} = \varepsilon_{rC} \cdot x_A \quad (2.29)$$

$$u_{rS1} = \varepsilon_{rS} \cdot x_A - \frac{1}{2} \cdot \frac{\tau_{rS} \cdot U_{rS} \cdot (x_A - x_F)^2}{a_{rS} \cdot E_r} \quad (2.30)$$

$$\delta_{SC1} = u_{rS1} - u_{rC1} = \delta_A \quad (2.31)$$

$$u_{rC2} = \varepsilon_{rC} \cdot x_A + \frac{1}{2} \cdot \varepsilon_{rC} \cdot (x_C - x_A) \quad (2.32)$$

$$u_{rS2} = \varepsilon_{rS} \cdot x_F + \frac{1}{2} \cdot \varepsilon_{rS} \cdot (x_S - x_F) \quad (2.33)$$

$$\delta_{SC2} = u_{rS2} - u_{rC2} = 0 \quad (2.34)$$

$$N_r = N_{rC} + N_{rS} \quad (2.35)$$

$$N_{rS} = \tau_{rS} \cdot U_{rS} \cdot (x_S - x_F) \quad (2.36)$$

$$N_{rC} = \tau_{rC} \cdot U_{rC} \cdot (x_C - x_A) \quad (2.37)$$

For non-real solutions to the above system of equations, equation 2.34 is replaced by: $\delta_{SC2} = u_{rS2} - u_{rC2} = \delta_A$.

Anchorage case 3

It is considered: $x_A < x_F$ and $x_C = L/2$ refer to Fig. 2.17d:

$$N_{rC} = a_{rC} \cdot \sigma_{rC} \quad (2.38)$$

$$N_{rS} = a_{rS} \cdot \sigma_{rS} \quad (2.39)$$

$$\sigma_{rC} = \varepsilon_{rC} \cdot E_r \quad (2.40)$$

$$\sigma_{rS} = \varepsilon_{rS} \cdot E_r \quad (2.41)$$

$$u_{rC} = x_A \cdot \varepsilon_{rC} \quad (2.42)$$

$$u_{rS} = \varepsilon_{rS} \cdot x_A \quad (2.43)$$

$$\delta_{SC} = u_{rS} - u_{rC} = \delta_A \quad (2.44)$$

$$N_{rC} = \tau_{rC} \cdot U_{rC} \cdot (x_C - x_A) \quad (2.45)$$

$$N_r = \tau_{rC} \cdot U_{rC} \cdot (x_C - x_F) + \tau_{rS} \cdot U_{rS} \cdot (x_S - x_F) \quad (2.46)$$

$$N_r = N_{rC} + N_{rS} \quad (2.47)$$

Anchorage case 4

It is considered: $x_A > x_F$ and $x_C > L/2$ refer to Fig. 2.17d:

$$N_{rC} = a_{rC} \cdot \sigma_{rC} \quad (2.48)$$

$$N_{rS} = a_{rS} \cdot \sigma_{rS} \quad (2.49)$$

$$\sigma_{rC} = \varepsilon_{rC} \cdot E_r \quad (2.50)$$

$$\sigma_{rS} = \varepsilon_{rS} \cdot E_r \quad (2.51)$$

$$u_{rC} = \varepsilon_{rC} \cdot x_A \quad (2.52)$$

$$u_{rS} = \varepsilon_{rS} \cdot x_A - \frac{1}{2} \cdot \frac{\tau_{rS} \cdot U_{rS} \cdot (x_A - x_F)^2}{a_{rS} \cdot E_r} \quad (2.53)$$

$$\delta_{SC} = u_{rS} - u_{rC} = \delta_A \quad (2.54)$$

$$N_{rS} = \tau_{rS} \cdot U_{rS} \cdot (x_S - x_F) \quad (2.55)$$

$$N_{rC} = \tau_{rC} \cdot U_{rC} \cdot (x_C - x_A) \quad (2.56)$$

$$N_r = N_{rC} + N_{rS} \quad (2.57)$$

Model parameters

The bond-lag model consists of a coarse abstraction of reality. Although all parameters have a mechanical background and the model is consistent in terms of its physical units, it still requires for three values that cannot be measured in an experimental manner (due to the consequential simplification of reality). Those are: the engagement slip δ_A ; the ratio between core and sleeve filaments k ; and the core-to-sleeve bond strength τ_{rC} .

The numerical values of these parameters were calibrated based on the composite tensile tests presented in this chapter and validated by means of other tests performed independently by other researchers (same parameters used for similar fabrics that show similar or same degree of coating or impregnation). In order to assess the robustness of the proposed bond-lag-model, future investigations should also include a sensitivity analysis of the calibrated parameters.

2.9 Appendix: symbols

Capital latin symbols

Symbol	Unit	Description
A	[mm ²]	Gross cross-section area
A_c	[mm ²]	Concrete net cross-section
A_r	[mm ²]	Roving cross-section area
B	[mm]	Bump amplitude
D	[mm]	Diameter
D_r	[mm]	Roving diameter
E_c	[MPa]	Modulus of elasticity of concrete
E_r	[MPa]	Modulus of elasticity of rovings
F	[kN]	Force
F_{ct}	[kN]	Concrete tensile resistance
F_1	[kN]	Calculated composite force
F_c	[kN]	Concrete compressive resistance
F_{cr}	[kN]	Force at cracking (experimental)
F_f	[kN/m]	Fabric strength
F_r	[kN]	Force applied on a single roving
F_u	[kN]	Experimental force at failure
H	[mm]	Height
L	[mm]	Length (of tensile member)
ΔL	[mm]	Displacement
L_{DIC}	[mm]	Length of measurement zone
L_0	[mm]	Base length
L_B	[mm]	Length of bump
N_{cr}	[kN]	Calculated cracking force
$N_{R,calc}$	[kN]	Calculated resistance of member
$N_{R,test}$	[kN]	Experimental resistance of member
N_{rC}	[N]	Calculated core force (single roving)
N_{rS}	[N]	Calculated sleeve force (single roving)
N_r	[N]	Calculated roving force (per roving)
U_{rC}	[mm]	Core layer perimeter
U_{rS}	[mm]	Sleeve layer perimeter
U_r	[mm]	Roving perimeter

Small latin symbols

Symbol	Unit	Description
a_{rC}	[mm ²]	Net cross-section of core
a_{rS}	[mm ²]	Net cross-section of sleeve
a_r	[mm ²]	Net cross-section of single roving
b	[mm]	Width
c	[mm]	Concrete cover
e_r	[mm]	Roving spacing
$f_{c,28}$	[MPa]	Concrete strength at 28 days
f_{ct}	[MPa]	Concrete tensile strength
f_c	[MPa]	Concrete compressive strength
f_r	[MPa]	Roving tensile strength
l_e	[mm]	Embedment length;
k	[-]	Ratio between sleeve and net roving
n_r	[-]	Number of rovings in a cross-section
p	[MPa]	(Clamping) pressure
s_{rm}	[mm]	Average crack spacing
t	[mm]	Thickness of member; time
u_{rC}	[mm]	Calculated core displacement
u_{rS}	[mm]	Calculated sleeve displacement
w	[mm]	Crack opening
w_u	[mm]	Crack opening at failure
x	[mm]	Longitudinal axis
x_A	[mm]	Location of activation section
x_C	[mm]	Anchorage section of core filaments
x_F	[mm]	Section of physical anchorage
x_S	[mm]	Anchorage section of sleeve filaments

Small greek symbols

Symbol	Unit	Description
α_r	[°]	Fabric orientation
δ	[mm]	Slip
$\delta_{b,max}$	[mm]	Experimental slip at peak bond strength
δ_{rC}	[mm]	Displacement between sleeve and core
δ_{rS}	[mm]	Displacement between concrete and sleeve
δ_{SC}	[mm]	Slip between sleeve and core filaments
δ_A	[mm]	Engagement slip
λ_r	[tex]	Linear density of rovings
ν	[-]	Friction coefficient
ρ	[%]	Reinforcement ratio
ρ_l	[%]	Longitudinal reinforcement ratio
ρ_t	[%]	Transversal reinforcement ratio
σ_{conf}	[MPa]	Confining transverse pressure
σ_{cr}	[MPa]	Cracking stress (experimental)
σ_{fil}	[MPa]	Filament stress
$\sigma_{r,u}$	[MPa]	Ultimate nominal roving stress
σ_{rC}	[MPa]	Calculated core roving stress
σ_{rS}	[MPa]	Calculated sleeve roving stress
σ_{TRC}	[MPa]	Composite stress
σ_c	[MPa]	Concrete stress
σ_n	[MPa]	Transverse stress
$\tau_{b,max}$	[MPa]	Peak bond stress
τ_{fil}	[MPa]	Frictional bond stresses (filaments)
τ_{rC}	[MPa]	Core-to-sleeve bond stress
τ_{rS}	[MPa]	Sleeve-to-matrix bond stress
τ_b	[MPa]	Bond stress
ε	[%]	Strain
$\varepsilon_{rC,0}$	[%]	Calculated initial strain of core
ε_{rC}	[%]	Calculated core strain
$\varepsilon_{r,0}$	[%]	Calculated initial strain of roving
$\Delta\varepsilon_{rS,c}$	[%]	Calculated tension stiffening strain
$\varepsilon_{rS,max}$	[%]	Maximum calculated sleeve strain
ε_{rS}	[%]	Calculated sleeve strain
ε_{xx}	[%]	Strain in longitudinal, x -direction
ε_0	[%]	Initial strain (experimental)
ε_u	[%]	Ultimate strain (experimental)

Acronyms

Acronym	Description
CF	Carbon Fibre
DIC	Digital Image Correlation
LVDT	Linear Variable Displacement Transformer
SBR	Stereo Butene Rubber
SCS	Sand Coated Surface
TRC	Textile Reinforced Concrete

Chapter 3

Flexural behaviour

In this chapter, the flexural behaviour of TRC linear elements is studied at a meso-scale, with special focus on their shear-capacity. The findings reported in this chapter correspond to the post-print version of the following paper:

Modelling of Textile Reinforced Concrete in bending and shear with Elastic-Cracked Stress Fields *Valeri, P.; Fernández Ruiz, M.; Muttoni, A.*
Engineering Structures, 2020. <https://doi.org/10.1016/j.engstruct.2020.110664>

The first author (Patrick Valeri) was responsible for the production and handling of the specimen. He performed all tests reported in this chapter including all measurements and Digital Image Correlation. Thereafter, he performed the post-processing of the experimental data: calculation of the principal strains recorded by means of photogrammetry and analysis of failure mechanisms. The first author also performed most of the analytical works presented in this chapter: (1) verification of stress-field equations for Reinforced Concrete and adaptation for TRC; (2) implementation of the analytical model based on Elastic-Cracked-Stress-Fields; (3) performing of numerical calculations with the Elastic-Plastic-Stress-Field approach; (4) collection of databasis for the validation of the model. Finally, the first author prepared the manuscript including all figures, tables and the appendix.

The second author (Miguel Fernández Ruiz) was closely involved in all works: design of the experimental programme; analysis of test results and failure modes; input and suggestions concerning the modelling framework (with major focus on the efficiency factors for concrete); verification of analytical equations; and correction of the manuscript (including figures and tables). Finally, Miguel Fernández Ruiz, was also the Principal Investigator of the research project that supplied the funding for this chapter.

The third author (Aurelio Muttoni) supervised the experimental programme (including the design of the beams and test set-up) and the analytical works. He provided valuable input for the mechanical approach pursued and the calibration of the efficiency factors suggested in this chapter. In addition he performed a proof-read of the manuscript that allowed to improve the English grammar and several figures. Finally he is also responsible for acquiring the funding on which this chapter is based (*cemsuisse* research project #201407).

Abstract

Textile Reinforced Concrete (TRC) is emerging as a promising alternative to ordinary Reinforced Concrete for the construction of durable, lightweight and more sustainable structures, with a large potential particularly in shells and thin members. Research on the response of TRC in bending and shear has so far been performed on the basis of different approaches: plain section analysis with compatibility conditions for bending and mostly empirical strength formulas for shear. This chapter explores a comprehensive approach for modelling the TRC response both for bending and shear on the basis of the Elastic-Cracked Stress Field (ECSF) method. The results of two full-scale flanged members in TRC tested in three-point-bending are presented. The tests are investigated by using Digital Image Correlation and the results are used to validate the assumptions of the ECSF. This approach allows accounting for the peculiarities of the material (notably for the linear-brittle response of the fabric) and leads to consistent results, accurately predicting the structural response in terms of strength and deformation capacity. The method is finally validated with other tests from the scientific literature, showing consistent agreement with a low coefficient of variation.

3.1 Introduction

Currently, Reinforced Concrete (RC) is one of the most popular construction materials. This is not only due to large availability of raw materials, but also due to the possibility to cast tailored shapes and the potential to integrate the structure as part of the architecture satisfying building physics requirements. To ensure the durability of RC, codes of practice prescribe a minimal concrete cover, typically 20 - 60 mm depending on the exposure class, in order to protect the steel rebars against corrosion. Yet, these cover requirements together with the spacing required for vibration and compacting needs lead in many cases to relatively large thicknesses of the elements when compared to the dimensions required for static needs. As a consequence, RC construction is frequently associated to a heavy and massive construction technique.

A promising approach to reduce cover requirements and thus the thickness of concrete members, not designed to resist fire, has been identified as the use of non-corrosive reinforcement. Such reinforcement can be in the form of bars [1, 2, 3] but also in the form of textile fabrics [4, 5, 6]. In the latter, bundles of continuous filaments (rovings) are assembled to form a fabric which can be embedded in a high-performance mortar. The resulting material, commonly known as Textile Reinforced Concrete (TRC) allows casting thin-walled elements (10 - 50 mm thickness) where in principle, the reinforcement can be oriented and the number of fabric layers can be tailored according to the internal force demand [7, 8, 9]. In addition to corrosion endurance, low clinker cements can also be used for the concrete mix, since no passivation of the reinforcement is required. This results in a reduction of the environmental footprint associated to the CO₂ emissions of cement production with respect to ordinary RC and to a more sustainable material [10, 11].

To date, there exists several applications built in TRC, whose number is increasing rapidly. Worth mentioning are: the TRC-pavilion on the RWTH-University campus in Aachen (Germany) [12] [13], the pedestrian bridge in Kempten (Germany) [14], the pedestrian footbridge in Albstadt (Germany) [15], the roof structure of the NEST building in Switzerland [16], the prototype pavilion in Fribourg (Switzerland) [17], and a series of precast elements, such as facade panels and deck-slabs [18]. The material is also attracting a number of research efforts to develop consistent design models that can eventually be implemented in codes of practice [19, 20, 21, 22, 23, 24]. Within this frame, the present chapter explores the possibility of using the stress field method for design of TRC. This method, widely used for RC [25, 26, 27, 28], allows performing design for beam or discontinuity regions in a comprehensive and rational manner. Its application to RC is based on limit analysis and presumes sufficient deformation capacity of the materials. Such large deformation capacity

is however not necessarily ensured in TRC as this material exhibits brittle failures in tension [29, 30] and limited deformation capacity in compression. Accounting for this fact, in this chapter, Elastic-Cracked-Stress-Field (ECSF) solutions are derived [31], respecting the potentially brittle response of the materials and their limited redistribution capacity. These solutions are shown to be applicable both for bending and shear design in a general manner.

First, an experimental programme consisting of two full scale double-T beams is presented and the results of the structural load tests are discussed with respect to their response and failure modes (bending and shear). In bending, the ECSF leads to consistent results to sectional design models based on compatibility of deformations for a plane-section analysis [32, 33, 34, 35]. For shear, ECSF allows predicting the angle of the compression field and the level of deformation of the fabric. A comparison of the measured inclination of the principal strains of the tests (by means of Digital Image Correlation) and the predictions of ECSF as well as the agreement on the failure loads confirm the soundness of the approach. At the end of this chapter, a systematic comparison to tests performed by other researchers is also presented, showing consistent results and general agreement with the current literature.

3.2 Experimental programme

An experimental programme has been conducted to investigate the response in bending and shear of flanged TRC members. It consists of two I-shaped beams with a depth of 290 mm and a total length of $L = 2900$ mm. One beam was reinforced with a carbon textile fabric only (BV1), while the other (BV2) presented an additional concentrated flexural reinforcement made of high-strength stainless steel rebars (see Fig 3.1).

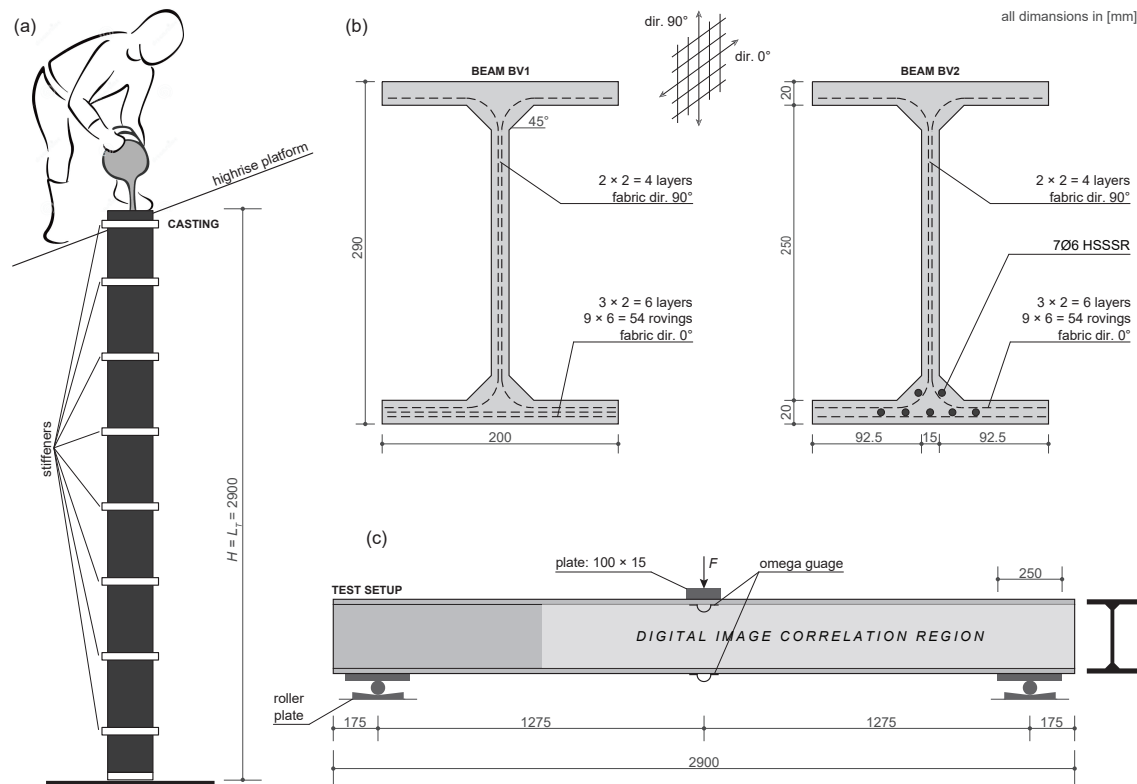


Figure 3.1: Tested members: (a) casting procedure; (b) sectional geometry; and (c) test set-up.

The mechanical properties of the materials are given in Tables 3.1, 3.2 and 3.3. Their response, in terms of stress-strain curves, are also depicted in Fig. 3.2 and additional information can be found in [36].

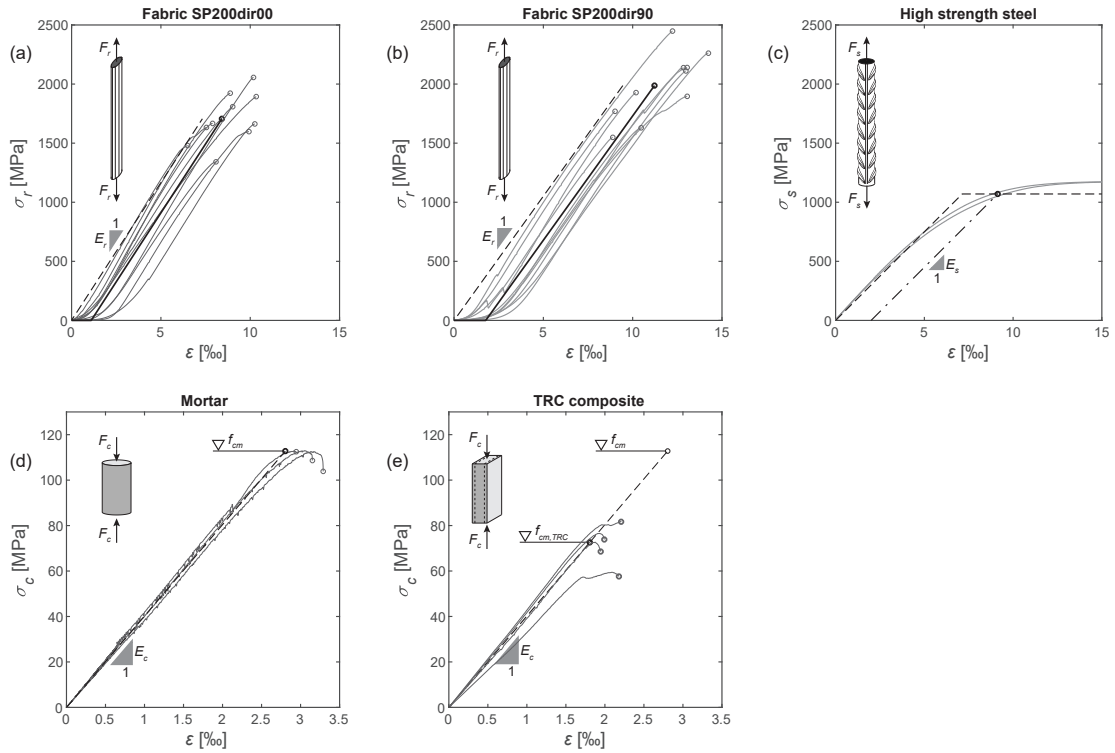


Figure 3.2: Material response: (a-b) carbon fabric textile reinforcement in longitudinal and transverse direction in tension; (c) stainless steel in tension; (d) mortar in compression; (e) TRC in compression.

		average	# tests	CoV
Elastic Modulus of mortar	E_c [GPa]	40.0	3	0.066
Mortar tensile strength	f_{ct} [MPa]	4.10	3	0.063
Mortar compressive strength	f_c [MPa]	112	3	0.0019
TRC compressive strength	$f_{c,TRC}$ [MPa]	72.6	4	0.110

Table 3.1: Mechanical material properties of high performance mortar and TRC.

The textile fabric used in this research (type S&P ARMO-mesh[®]200/200) presents an external epoxy coating. Compared to fully-impregnated (rigid) fabrics, it remains relatively soft and can be easily folded. However, with respect to uncoated fabrics, the secondary coating ensures a minimal form-stability. On top of the external epoxy coating, an additional layer of quartz-sand ensures sufficient bond with the surrounding matrix [37]. Tests of the bare textile (single rovings extracted from the grid) were performed by clamping single rovings between grips (with conventional or capstan grips configurations [38] leading to virtually identical results). A first phase of hardening response can be observed, corresponding to the removal of the fabric waviness (slack). This phase is followed by a linear response until failure of the fabric, see Fig. 3.2 and [39].

Compressive tests on the mortar were carried out on cylinders ($H = 120 \times D = 70$ mm) and

		dir.0°			dir.90°		
		average	# tests	CoV	average	# tests	CoV
Linear density	λ_r [tex]	2×800	-	-	1600	-	-
Net cross-section	a_r [mm ²]	0.85	-	-	0.85	-	-
Fabric spacing	s_r [mm]	20	-	-	20	-	-
Roving elastic modulus	E_r [GPa]	230	20	0.081	210	20	0.068
Roving tensile strength	f_r [MPa]	1700	20	0.13	2000	20	0.14

Table 3.2: Mechanical material properties of fabric in longitudinal (dir.0°) and transversal (dir.90°) direction in tension.

		average	# tests
Bar diameter	\varnothing [mm]	6	2
Elastic modulus	E_s [GPa]	150	2
Nominal yield strength	$f_{y,0.2}$ [MPa]	1070	2
Ultimate strength	f_u [MPa]	1170	2

Table 3.3: Mechanical material properties of high strength stainless steel in tension.

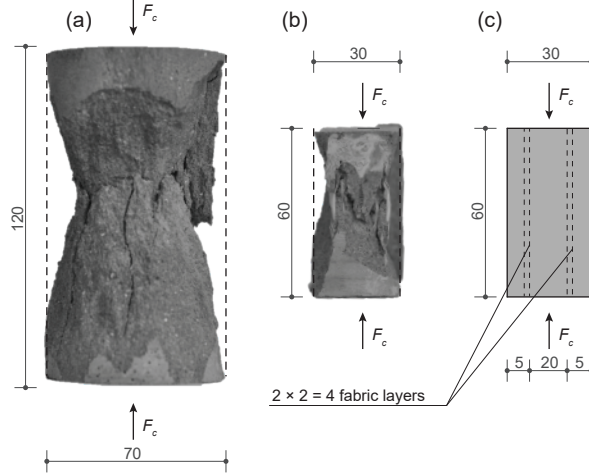


Figure 3.3: Compressive tests of mortar and TRC (dimensions in [mm]): (a) cylinder; (b) TRC-prism; and (c) reinforcement layout.

TRC prisms ($H = 60 \times b = 60 \times t = 30$ mm) reinforced with two fabric layers at each side of the prism (see Fig. 3.3). As shown in Fig. 3.3, when the mortar is reinforced with textile fabrics, discontinuity planes are generated. That can lead to premature spalling of the concrete cover and thus a reduction of the compressive strength (see Figs. 3.2, 3.3, Table 3.1 and [40, 41]).

3.2.1 Specimen preparation and test setup

Both beam specimens were cast in the same formwork with concrete poured in the longitudinal direction (Fig. 3.1a). The vertical casting direction ensures sufficient hydrostatic pressure to develop inside the formwork and thus assures homogeneous penetration of the mortar in-between the fabric rovings. The position of the reinforcement was ensured by the coating of the fabric an additional set of spacers [42]. Specimen BV1 was reinforced only with textile fabrics both in the web and flanges, while specimen BV2 had additional stainless steel bars in the tension flange, see Fig. 3.1. The correct spacing of the fabric layers was ensured by means of spacers. The cross-section and reinforcement layout is shown in Fig. 3.1. The 45° gusset between web and flange was arranged to avoid spalling of concrete due to deviating forces resulting from the folding of the transverse reinforcement.

The members were tested in three-point bending with a span of $L = 2550$ mm. The force was applied at mid-span through a plate 100×15 mm. The hydraulic jack was displacement-controlled with a rate equal to 0.015 mm/s. Two Linear Variable Differential Transformers (LVDTs) were used to track the mid-span deflection v . Two omega-gauges ($L_0 = 100$ mm) were used to measure deformations of the tension and compression flange at mid-span (installed at the bottom of the flanges see Fig. 3.1). In addition to conventional instrumentation, also photogrammetric measurements based on Digital Image Correlation were used to record cracking patterns and deformations at a frequency of 0.1 Hz close to failure.

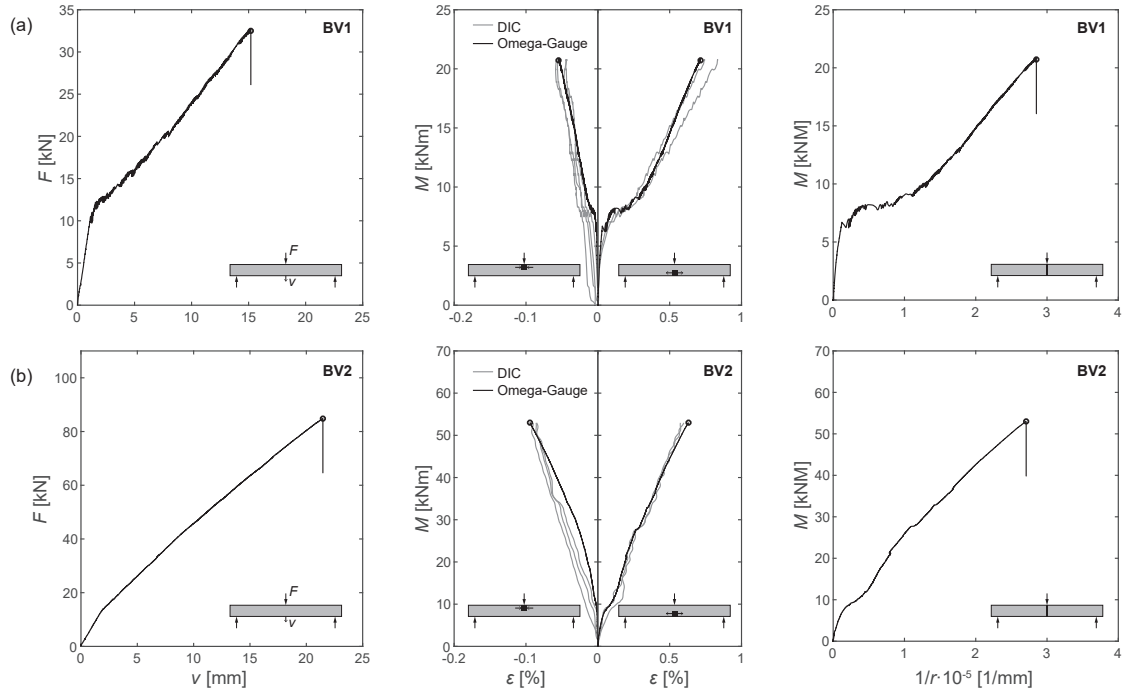


Figure 3.4: Experimental results of the tested members in terms of load-deflection, moment-strain and moment-curvature: (a) specimen BV1; and (b) specimen BV2.

3.2.2 Load-deformation response

The mid-span force-deflection and sectional response in terms of moment-curvature are shown in Fig. 3.4. For low levels of load, a linear response is observed until the cracking moment is reached. For increasing levels of load, the response becomes softer due to the cracking of concrete and is governed by the tensile reinforcement (only carbon fabric for specimen BV1 and fabric plus stainless steel bars for specimen BV2). Failure occurred eventually in a brittle manner for both specimens. For specimen BV1 it was due to a bending failure (rupture of tension flange) while it was due to shear for specimen BV2 (more details given later). In Fig. 3.4, the diagrams corresponding to the moment-chord strain and moment-curvature are also depicted for the section at mid-span.

3.2.3 Crack pattern

Both members developed a uniformly distributed cracking pattern during the test (see Fig. 3.5a). Beam BV1 was characterised by a flexural cracking pattern, with cracks developing vertically almost until the upper flange. For beam BV2, a similar pattern was observed at low load levels. Due to the higher flexural capacity of this specimen (resulting from the concentrated tensile reinforcement), the load could be significantly increased with respect to beam BV1. At higher load levels, shear cracks developed in an inclined and smeared manner (see Fig. 3.5a). These inclined cracks merged at the level of the gussets, leading to longitudinal delamination cracks both at the top and bottom flanges (see Figs. 3.5 and 3.6).

The Digital Image Correlation (DIC) analysis allows calculating the direction of the principal compressive strains. As shown in Fig. 3.5b the angle of the principal compressive strain direction θ_ϵ is variable (values taken at 99 % of the failure load). Near the load introduction region, it varies from almost vertical to about 45° . In the central part of the shear span, its value is particularly constant for beam BV2 (about 35° , refer to Fig. 3.5c) and shows some level of scatter for BV1 (generally between 60° and 30° , refer to Fig. 3.5c). This observation, particularly for specimen BV2, failing at a higher level of shear force, has clear analogies with a classical stress field for RC

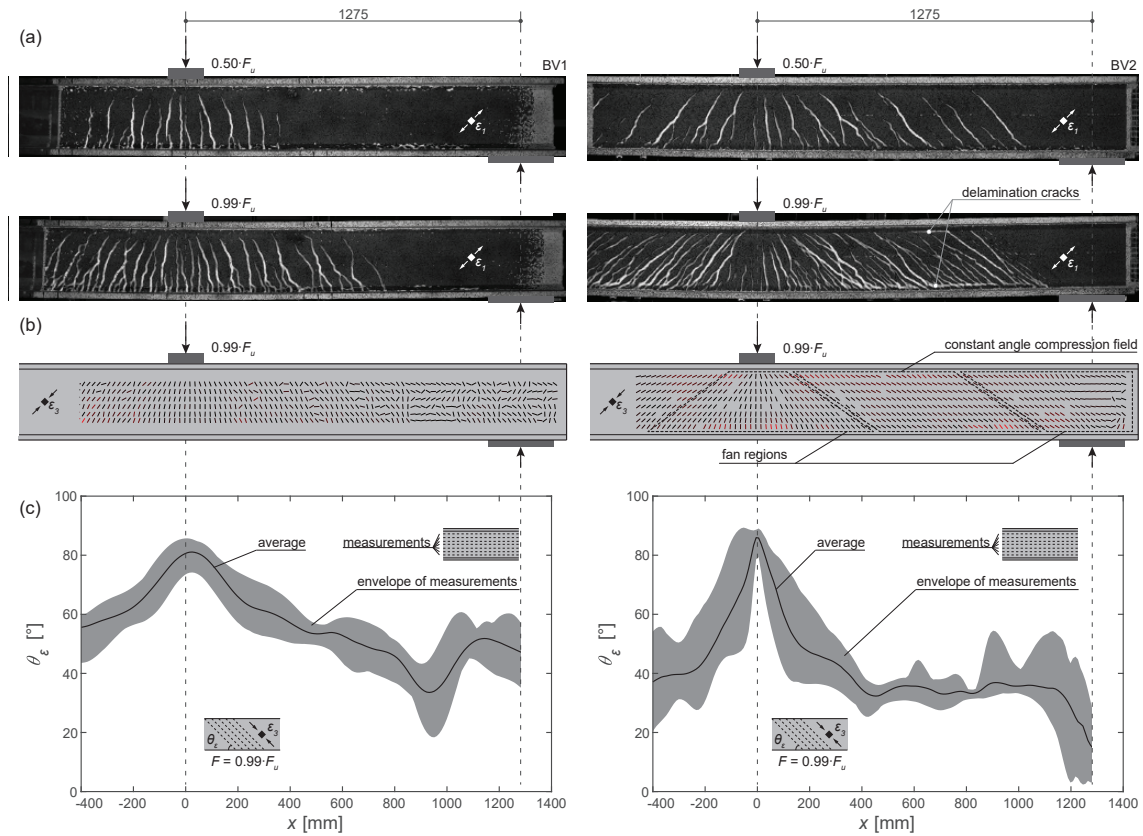


Figure 3.5: Deformation analysis with DIC at different load levels: (a) principal tensile stains; (b) direction of compressive strain field; and (c) inclination of compression field in the web.

beams [25] comprising fan regions and a constant-angle compression field in-between them (see Fig. 3.5b).

3.2.4 Failure

Both members were characterised by a sudden and brittle loss of their bearing capacity (Fig. 3.4). Beam BV1 failed in bending due to the rupture of the longitudinal reinforcement in the tension flange. Rupture of the textile occurred for a vertical crack located at mid-span (see Fig. 3.6a). At failure, small crack openings were observed (lower than 0.2 mm as also observed for TRC ties at failure [36, 43, 44]) and failure occurred without warning signs (absence of plastic deformation, large deflections or cracks). The failure of beam BV2 can also be described as brittle, since no visible plastic deformations or large increase of deflections announcing failure could be observed (Fig. 3.4). In this case, failure was due to a combined crushing of the web and sliding along delamination cracks (vertical detachment of the flanges from the web, see Figs. 3.5 and 3.6). The development of the final failure mechanism is completed by four local plastic hinges in the flanges and a quasi vertical crack allowing for the relative sliding of the web panel with respect to the top flange (see Fig. 3.6b).

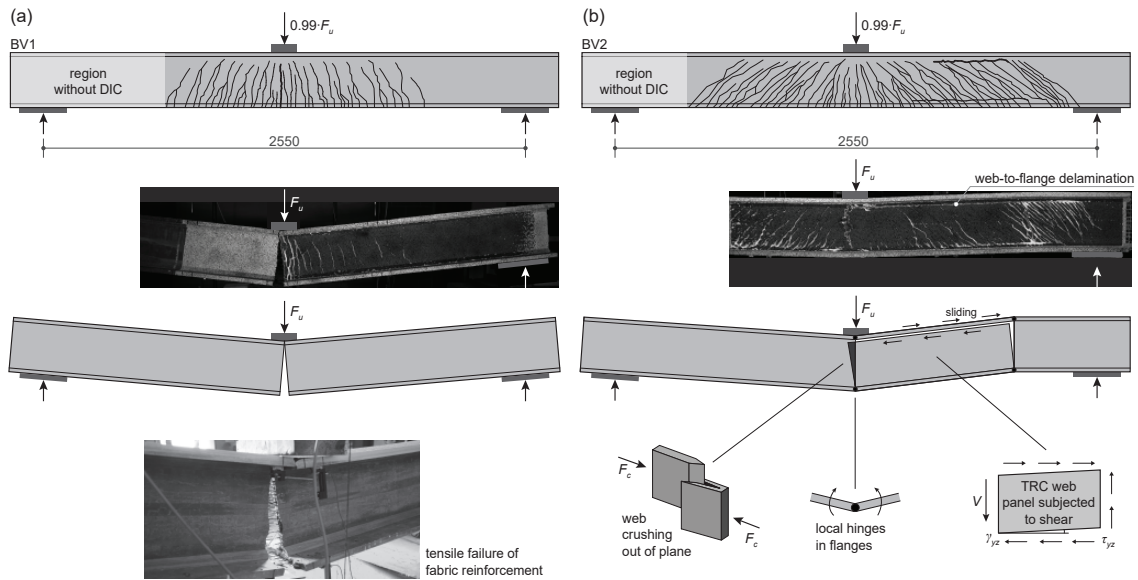


Figure 3.6: Crack pattern and sketch of mechanisms of the tested members: (a) specimen BV1; and (b) specimen BV2.

3.3 Application of Elastic-Cracked Stress Fields to the modelling of TRC

In the following, the response of the tested specimens is investigated by means of Elastic-Cracked Stress Fields (ECSF). This technique can be seen as an evolution of the method developed by Kupfer [31] for shear panels by making use of the minimisation of internal work but accounting for the compression softening behaviour of concrete under transverse cracking (see Vecchio and Collins [45]). In the following, its basic assumptions are summarised and its application to bending and shear in the case of TRC is discussed.

3.3.1 Basic principles

For development of ECSF, a number of assumptions will be adopted:

- Concrete is assumed to behave in an elastic-plastic manner in compression, with no tensile strength (Fig. 3.7a);
- The uniaxial compressive strength of concrete is reduced to $f_{cp} = f_c \cdot \eta_{cc}$ in order to consider an elastic-plastic response of the material [27]. The efficiency factor η_{cc} accounts for the material brittleness in compression (consideration of stress redistribution in a quasi-brittle material [46]) and can be estimated as [47]:

$$\eta_{cc} = \left(\frac{f_{c,ref}}{f_c} \right)^{1/3} \leq 1 \quad (3.1)$$

where a value of $f_{c,ref} = 30$ MPa is usually adopted for structural concrete elements [47].

- In biaxial compression, concrete behaves with a Mohr-Coulomb plasticity surface with a tension cut-off. Under plane-stress conditions, this criterion is presented in Fig. 3.7d (considering normality of plastic strains to the yield surface). The direction of principal strains is in addition assumed to be parallel to the direction of principal stresses [27].
- When subjected to transverse tension, a compression field reduces its strength to a value of $f_{ce} = f_{cp} \cdot \eta_\varepsilon$ [27], where η_ε is a strength reduction factor accounting for transverse strains

and crack widths. In absence of more precise data, the compression-softening law formulated by Vecchio and Collins [45] for RC will be adopted assuming smeared cracking and fully rotational crack response. In this case, for a uniform (or quasi-uniform) strain field, one can assume [45]:

$$\eta_\varepsilon = \frac{1}{0.8 + 170 \cdot \varepsilon_1} \leq 1 \quad (3.2)$$

- Textile reinforcement is assumed to present a linear-elastic response in tension with a brittle failure (no plastic behaviour). Its contribution to compression is not considered (Fig. 3.7b) [40, 41]. It shall be noted that when an embedded textile is subjected to tension, its stiffness in the cracked stage with respect to the bare fabric depends to a large extent on the type of fabric (impregnation, surface treatment, production process, bumpiness...) and on its anchorage conditions (length and properties) [39, 48, 49, 50, 51, 52]. This response is implemented in the following manner [53, 54]:
 - A linear response is assumed for the fabric (the straightening of an embedded fabric is neglected [39, 53, 54]);
 - The stiffness of the textile is reduced by a coefficient k_e [39, 50, 53, 54, 55] to account for the non-uniform profile of stresses (activation of inner filaments via bond stresses) by considering a reduced effective reinforcement area;
 - The strength of the embedded fabric is reduced with respect to the bare roving (additionally to the previous effect) by means of an efficiency factor η_b . This factor accounts, amongst others, for bond conditions of the roving (resulting in non-uniform stress profiles [56]) and the statistical size effect (length dependency) [57, 58];
- For the concentrated steel reinforcement (bars), an elastic-plastic behaviour is assumed (see Fig. 3.7c).
- Perfect bond is assumed between the reinforcement (fabric or bars) and the cement matrix. Nevertheless, due to the low crack spacing and bond stresses, tension-stiffening effects are neglected.

To determine the stress-state, the analysis considers a displacement field acting on the member [27]. On that basis, the strains of the materials are determined and the stresses calculated by using the constitutive material laws (Fig. 3.7). The displacement field is varied until equilibrium with the external loads and boundary conditions is ensured.

In RC structures, with ductile behaviour, this technique leads to exact solutions according to limit analysis [28]. This is justified in this case by the fact that the equilibrium conditions are respected together with the yield criteria of the materials (lower bound of strength) but also by the consideration of compatibility of deformations (allowing for a licit mechanism at failure). However, in the case of TRC, the approach cannot be claimed to be an exact solution as the lack of ductile response of the materials potentially makes the failure load to depend upon the initial state of strains of the member (requiring consideration for instance of loading history and self-stresses).

3.3.2 Flexural response

The case of ECSF for the flexural response is equivalent to the consideration of a plane-section analysis accounting for compatibility of deformations, see Fig. 3.8. This assumption has in fact been extensively investigated in previous researches, with several experimental programmes [1, 9, 32, 34, 59, 60] showing the consistency of this approach. In the present case, the differential activation of filaments due to the delayed activation of bond stresses (bond-lag) is taken into account by means of the efficiency factors defined in the previous sections and consistently with

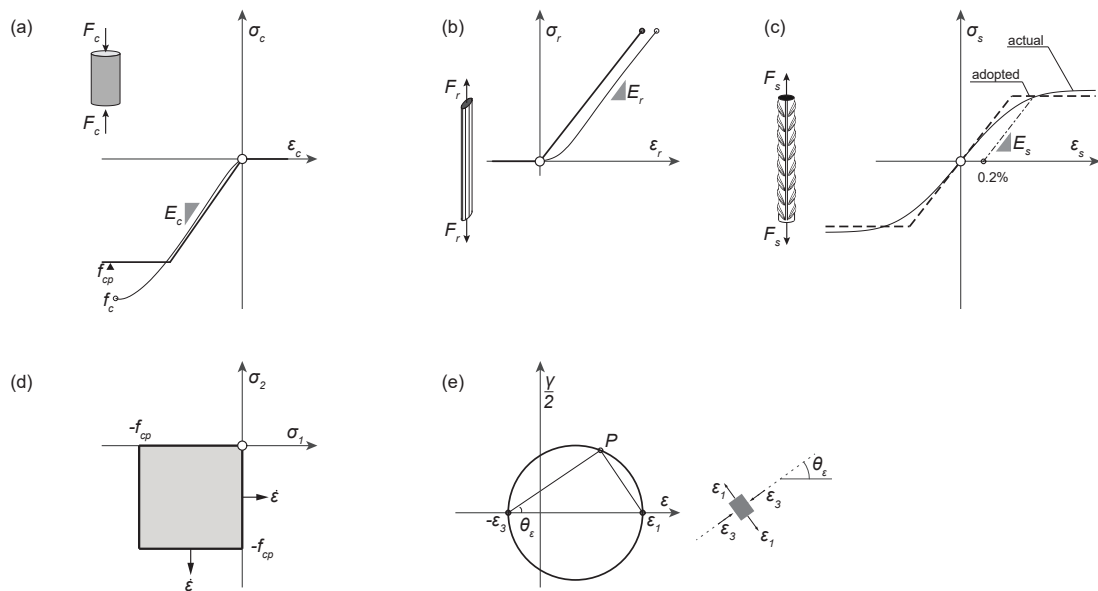


Figure 3.7: Basic model assumptions: (a) concrete behaviour; (b) roving response; (c) response of concentrated reinforcement; (d) yield surface; and (e) strain state.

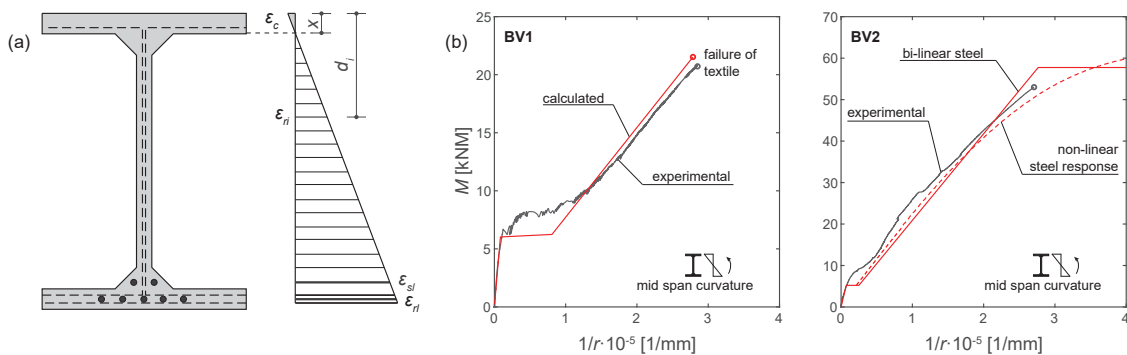


Figure 3.8: Sectional analysis and bending design of the tested members: (a) model; (b) results for specimens BV1 and BV2.

[53, 54]. These parameters allow a satisfactory prediction of the deformation and bending capacity of the TRC section (refer to Fig. 3.8, beam BV1).

For beam BV2, the contribution of the carbon fabric reinforcement is neglected for the calculation of the flexural strength. This is justified by the fact that the stainless steel reinforcement has a significantly higher contribution to the strength. As shown in Fig. 3.8 such assumptions give again satisfactory results. The consistency of this approach has also been verified based on similar assumptions by other researchers [9, 32, 34, 59].

3.3.3 Shear in flanged members

As observed from the DIC measurements (Fig. 3.5b), the response of the web in the tested flanged members can be reproduced by considering a stress field with fan regions near the load-introduction zones and a constant-angle stress field in the span region, see Figs. 3.5 and 3.9 [25]. The critical regions are typically located outside the fan regions [61, 62] due to the more unfavourable strain state in the concrete. In that region (constant angle field, see Fig. 3.9), a panel approach can be used, with the flanges acting as the compression and tension stringers and the web as the panel carrying shear. The panel (Fig. 3.9b) can be considered with a constant inclination of the

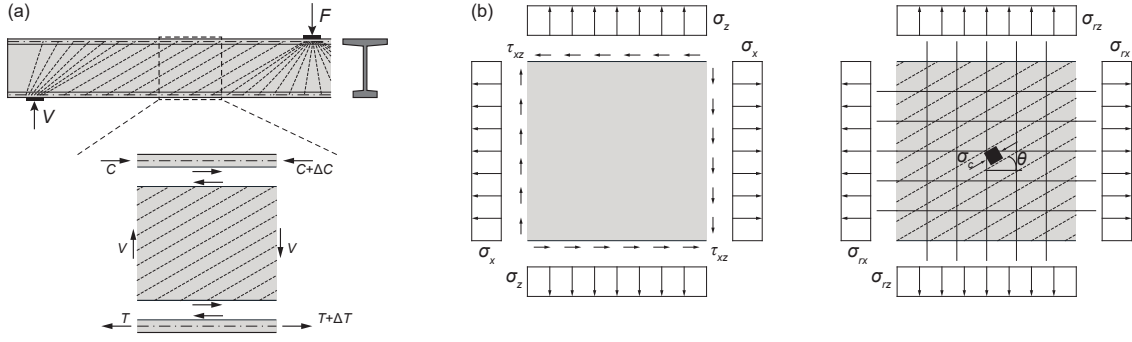


Figure 3.9: Stress fields in linear members: (a) stringer-panel model; (b) equilibrium of cracked panel.

compression field θ_σ (see Figs. 3.5 and 3.9). As shown in Fig. 3.9, the panel is subjected to longitudinal (σ_x), vertical (σ_z) and shear stresses (τ_{xz}). Neglecting the tensile strength of concrete these actions are equilibrated by the internal forces in the panel: compressive stresses in the concrete (σ_c , compression negative) and tensile stresses in the reinforcement (σ_{rx}, σ_{rz}). Assuming vertical and horizontal reinforcement, the equilibrium conditions can be expressed as:

$$\sigma_x = \sigma_c \cdot \cos^2 \theta_\sigma + \rho_{rx,eff} \cdot \sigma_{rx} \quad (3.3)$$

$$\sigma_z = \sigma_c \cdot \sin^2 \theta_\sigma + \rho_{rz,eff} \cdot \sigma_{rz} \quad (3.4)$$

$$\tau_{xz} = -\sigma_c \cdot \sin \theta_\sigma \cdot \cos \theta_\sigma \quad (3.5)$$

Where the effective reinforcement ratios are defined as:

$$\rho_{rx,eff} = \frac{k_{ex} \cdot a_{rx} \cdot n_{lx}}{s_{rx} \cdot b_w} \quad (3.6)$$

$$\rho_{rz,eff} = \frac{k_{ez} \cdot a_{rz} \cdot n_{lz}}{s_{rz} \cdot b_w} \quad (3.7)$$

Where a_r refers to the cross-section of the roving, s_r to its spacing, and n_{lx} and n_{lz} refer to the number of layers of the fabric in x and z direction respectively.

The compatibility conditions are given by:

$$\varepsilon_x = \varepsilon_1 \cdot \sin^2 \theta_\varepsilon + \varepsilon_3 \cdot \cos^2 \theta_\varepsilon \quad (3.8)$$

$$\varepsilon_z = \varepsilon_1 \cdot \cos^2 \theta_\varepsilon + \varepsilon_3 \cdot \sin^2 \theta_\varepsilon \quad (3.9)$$

$$\gamma_{xz} = 2 \cdot (\varepsilon_1 - \varepsilon_3) \cdot \sin \theta_\varepsilon \cdot \cos \theta_\varepsilon \quad (3.10)$$

Where ε_1 is the principal tensile strain, ε_3 the principal compressive strain (see Fig. 3.9) and θ_ε is the angle of the principal compressive strain. The constitutive laws for the materials (see Fig. 3.7) are given by:

$$\sigma_c = E_c \cdot \varepsilon_3 \leq \eta_\varepsilon \cdot \eta_{cc} \cdot f_c \quad (3.11)$$

$$\sigma_{rx} = E_{rx} \cdot \varepsilon_x \text{ with failure at } \sigma_{rx} = \eta_{bx} \cdot f_{rx} \quad (3.12)$$

$$\sigma_{rz} = E_{rz} \cdot \varepsilon_z \text{ with failure at } \sigma_{rz} = \eta_{bz} \cdot f_{rz} \quad (3.13)$$

For flanged members, vertical membrane stresses can be neglected ($\sigma_z = 0$). In addition, the inclination of the compression field can be assumed parallel to the principal strains ($\theta_\varepsilon = \theta_\sigma = \theta$) and can be calculated for a defined level of shear force and a given ratio of longitudinal-to-transversal strains ($\varepsilon_x/\varepsilon_z$). Assuming that all materials remain elastic (this hypothesis will be

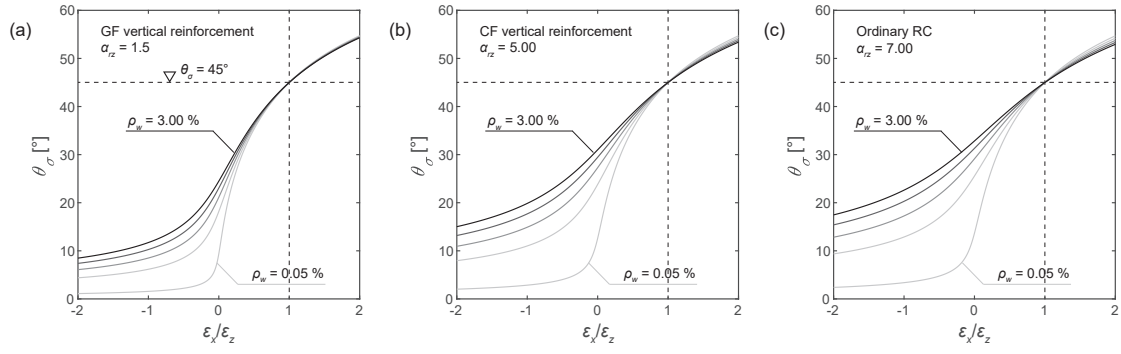


Figure 3.10: Calculated inclination of compression field: (a) TRC with vertical Glass-Fibre (GF) reinforcement; (b) TRC with vertical Carbon-Fibre (CF) reinforcement and (c) Ordinary Reinforced Concrete (RC).

discussed later), $\sigma_z = 0$ in Equation 3.4 and by using Equations 3.11 and 3.13, it results:

$$\varepsilon_3 = -\rho_{rz,eff} \cdot \alpha_{rz} \cdot \frac{\varepsilon_z}{\sin^2 \theta} = -\rho_{rz,eff} \cdot \alpha_{rz} \cdot \frac{\varepsilon_z}{\tan^2 \theta} \cdot (1 + \tan^2 \theta) \quad (3.14)$$

Where $\alpha_{rz} = E_{rz}/E_c$ is the ratio between the moduli of elasticity of the vertical reinforcement and that of the concrete matrix. From the strain conditions (Equations 3.8 and 3.9) one can derive that:

$$\varepsilon_3 = \frac{\varepsilon_x - \varepsilon_z \cdot \tan^2 \theta}{1 - \tan^2 \theta} \quad (3.15)$$

And thus:

$$\tan^4 \theta - \frac{\varepsilon_x}{\varepsilon_z} \cdot \tan^2 \theta - \alpha_{rz} \cdot \rho_{rz,eff} \cdot (1 - \tan^4 \theta) = 0 \quad (3.16)$$

Which leads to:

$$\tan^2 \theta = \frac{\frac{\varepsilon_x}{\varepsilon_z} + \sqrt{\left(\frac{\varepsilon_x}{\varepsilon_z}\right)^2 + 4 \cdot \alpha_{rz} \cdot \rho_{rz,eff} \cdot (1 + \alpha_{rz} \cdot \rho_{rz,eff})}}{2 \cdot (1 + \alpha_{rz} \cdot \rho_{rz,eff})} \quad (3.17)$$

The detailed development of the ECSF equations is given in 3.7. Equation 3.17 can be approximated (with an error lower than 5 % for the practical range of application) as:

$$\tan^2 \theta \approx \frac{1}{2} \cdot \left[\frac{\varepsilon_x}{\varepsilon_z} + \sqrt{\left(\frac{\varepsilon_x}{\varepsilon_z}\right)^2 + 4 \cdot \alpha_{rz} \cdot \rho_{rz,eff}} \right] \quad (3.18)$$

Figure 3.10 shows the relationship between the calculated inclination of the compression field θ_σ and the ratio of longitudinal-to-transversal strains $\varepsilon_x/\varepsilon_z$ for different reinforcement ratios and some selected values of α_{rz} .

For a given level of shear force (V), the corresponding shear stresses can be calculated as: $\tau_{xz} = V/(z \cdot b_w)$. On this basis, the concrete stress σ_c can be determined with Equation 3.5 and the principal strain ε_3 with the constitutive law of concrete (Equation 3.11). This allows to eventually calculate the longitudinal strain ε_x (for the given ratio $\varepsilon_x/\varepsilon_z$ and by using using Equation 3.15) as:

$$\varepsilon_x = \varepsilon_3 \cdot \frac{1 - \tan^2 \theta}{1 - \frac{\varepsilon_x}{\varepsilon_z} \cdot \tan^2 \theta} \quad (3.19)$$

The ratio $\varepsilon_x/\varepsilon_z$ is to be varied for a given section and level of applied shear force until the panel strain of Equation 3.19 equals the one calculated at the centre of the panel according to a plane (cracked) section analysis. This consideration is consistent with the Model Code 2010 approach for shear design [47]. It can be formulated in a simplified manner by neglecting the strains in the

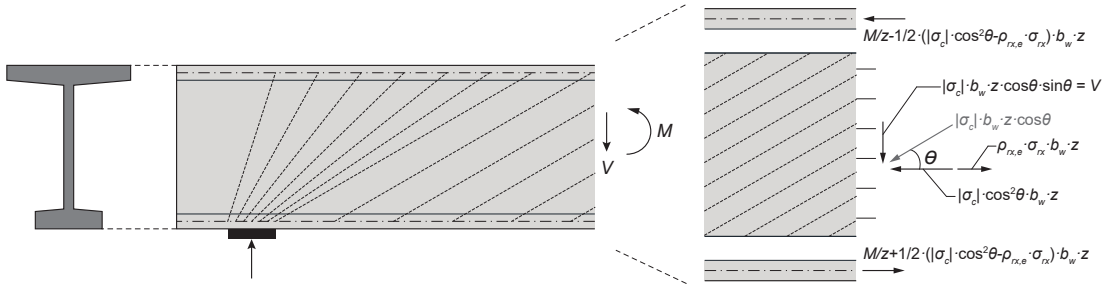


Figure 3.11: Equilibrium of stresses.

compression chord as: $\varepsilon_x \approx \varepsilon_l/2$. Where ε_l refers to the longitudinal strain in the tension chord that can be calculated on the basis of the tie force derived on equilibrium considerations (Fig. 3.11) as:

$$\varepsilon_l = \frac{\frac{M}{z} + \frac{V \cdot \cot \theta}{2}}{A_{l,eff} \cdot E_l + \frac{\rho_{rx,eff}}{4} \cdot E_{rx} \cdot b_w \cdot z} \quad (3.20)$$

Where $A_{l,eff}$ is the effective reinforcement of the tension chord: $A_{l,eff} = k_{el} \cdot n_l \cdot a_l$ (with a_l being the the cross-section of one roving or bar and n_l the number of longitudinal bars or rovings).

It can be noted that other effects (prestressing or normal forces) can also be consistently accounted for in this analysis. In addition, accounting for the range of variation of $\varepsilon_x/\varepsilon_z$ for practical cases, assuming an inclination of the compression field of $\theta_\sigma = 45^\circ$ leads already to a reasonable estimate of its actual value (see Fig. 3.10).

3.3.4 Implementation based on finite elements

As an alternative to the previous analytical approach, a numerical implementation of the principles of the ECSF is also possible to consistently model the behaviour of TRC. This can for instance be performed within the frame of the Elastic-Plastic Stress Fields (EPSF), by means of the finite element method [27] accounting for the peculiarities of the material previously discussed.

Figure 3.12 shows the results of a general EPSF model and the analytically-determined angle of the compression fields (Equation 3.17). Both reproduce in an accurate manner the orientation of the principal compressive strains measured by means of the DIC (Fig. 3.12). It is for instance interesting to note that the inclination of the compression field is steeper for higher levels of axial deformation ε_x , refer to Equations 3.17 and 3.18 (Fig. 3.10) and this fact is clearly confirmed by the test measurements (see Figs. 3.5 and 3.12).

The inclination of the compression field θ_σ determined by analytical and numerical means is roughly similar (slightly higher angles for the analytical approach), particularly in the region of constant-angle compression field. Furthermore it can be noted that the condition of a plastic response of concrete may lead to deviations with respect to the angle θ_σ calculated with elastic-cracked stress fields (Equation 3.17, where concrete is assumed to have a linear response). These deviations are yet limited (larger redistributions in RC are mostly associated to yielding of the reinforcement). In any case, the EPSF approach implemented by means of finite elements (refer to Fig. 3.12) will remain valid and general allowing to identify the location of the maximum stress in the fabric reinforcement. Such information can be used to determine the resistance of TRC linear members and to predict their failure mechanism and ultimate capacity.

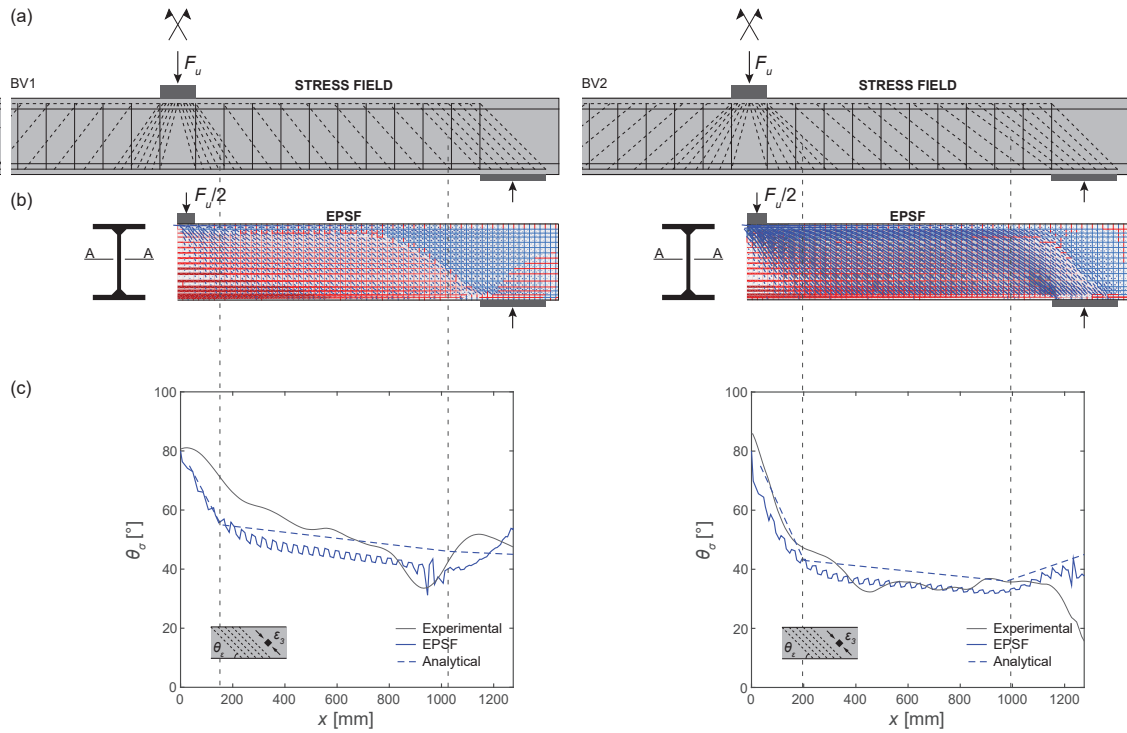


Figure 3.12: Numerical analysis of tested beams: (a) stress field; (b) EPSF analysis with finite elements; (c) comparison of the compression field angle.

3.4 Shear resistance

The shear resistance of TRC linear members can be determined using the ECSF approach (details on the implementation of the procedure are given in 3.8). For slender members, the resistance of the member can be calculated from the governing free-body (see Fig. 3.13) as: $V_R = \min\{V_{Rc}, V_{Rr}\}$, corresponding to the crushing of the compression field and to the rupture of transverse reinforcement respectively.

For the vertical reinforcement (Fig. 3.13a), the maximum capacity can be calculated by considering equilibrium on a section with inclination θ (angle of the principal direction of the compression field) and rupture of the textile:

$$V_{Rr} = \rho_{rz,eff} \cdot b_w \cdot z \cdot \cot \theta \cdot \eta_{bz} \cdot f_{rz} \quad (3.21)$$

where $\eta_{b,z}$ is the efficiency factor characterising the reduced resistance of the textile accounting the anchorage region (development length, delamination cracks, potential shearing of rovings). This factor is to be determined experimentally and its values are discussed in the next section.

The maximum capacity of the compression field associated to crushing can be determined as follows

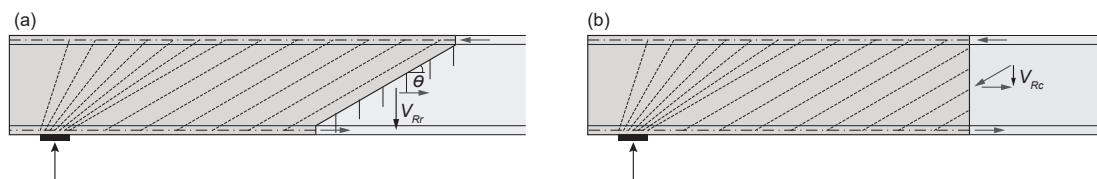


Figure 3.13: Free body: (a) resistance of transverse reinforcement; and (b) resistance of concrete carrying the inclined compression field.

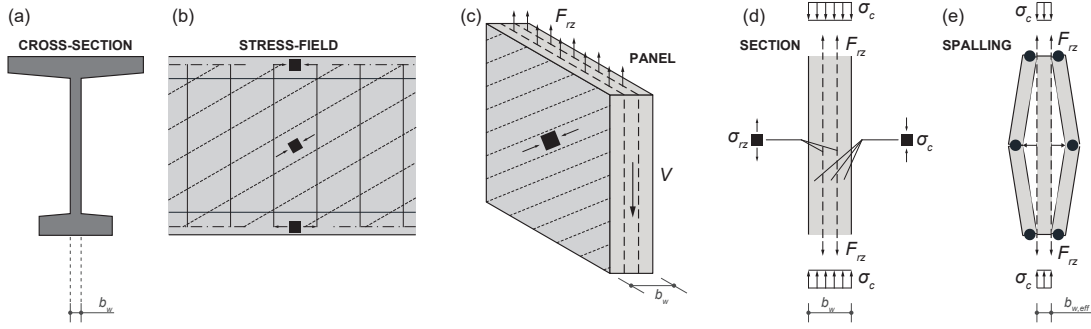


Figure 3.14: Effective width: (a) cross-section of flanged member; (b) stress-field; (c) web-panel; (d) stresses acting in the web; (e) rupture due to premature spalling of concrete cover.

(Fig. 3.13b):

$$V_{Rc} = \eta_{\varepsilon,panel} \cdot \eta_{cc} \cdot f_c \cdot b_{w,eff} \cdot z \cdot \sin \theta \cdot \cos \theta \quad (3.22)$$

where $\eta_{\varepsilon,panel}$ is the efficiency factor for concrete subjected to transverse tension. This factor is calculated for a panel according to Model Code 2010 [47, 63] (integration of local η_{ε} -factor accounting for strain-field gradients in a panel):

$$\eta_{\varepsilon,panel} = \frac{1}{1.2 + 55 \cdot \varepsilon_1} \leq 0.65 \quad (3.23)$$

where ε_1 is calculated from the state of strains in the panel as:

$$\varepsilon_1 = \varepsilon_x + (\varepsilon_x + 0.002) \cdot \cot^2 \theta \quad (3.24)$$

and ε_x refers to the average strain in the panel calculated according to Equation 3.20 for the control section (assumed to be located at a distance equal to z from the load introduction region). In addition, the resistance of the compression field is calculated on an effective web width $b_{w,eff}$. As already well established for RC, disturbances in the web (as the presence of prestressing ducts) lead to reductions of the strength of the compression field developing in the web (see Fig. 3.14a-c, and [64]). This is usually considered in reinforced concrete modelling by reducing the thickness of the web [61, 62]. With respect to TRC, the dense nature of the textile fabric may generate a discontinuity plane within the web. This can lead to premature spalling of the concrete cover of the web (see Fig. 3.14), which has been experimentally reported and extensively discussed by Kromoser et al. (see Fig. 3.15 and [65]) and Preinstorfer et al. [66]. This phenomenon is also in agreement to the tests on TRC prisms presented in Fig. 2c-d and to the pull-out tests by Preinstorfer et al. [66] (where spalling was triggered by high splitting forces orthogonally to the layer of the textile reinforcement). To account for this phenomena in thin-walled elements, as a safe assumption, it is suggested to consider only the width of the panel $b_{w,eff} \leq b_w$ confined between the textile sheets as the effective portion of the web carrying shear (Fig. 3.14e).

It shall be noted that this effect is additional to the strength reduction factor due to material brittleness and stress redistribution (η_{cc}). This is justified by the fact that, after initiation of a cover spalling, potential stress redistributions occur within the region of the web between fabric layers.

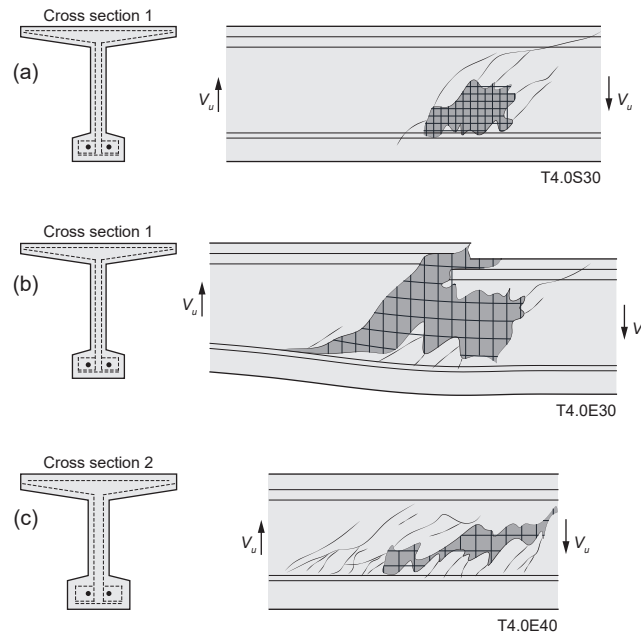


Figure 3.15: Spalling of concrete cover observed in the experimental campaign conducted by Kromoser et al. [65]: (a) specimen T4.0S30; (b) specimen T4.0E30; and (c) specimen T4.0E40.

3.5 Comparison to available tests

To validate the proposed ECSF approach in shear (similar approaches in bending have been extensively validated by other researchers [32, 34, 39]) the results of 18 tests available in the scientific literature will be used. The main parameters of these tests are summarised in Table 3.5 and Fig. 3.16.

The considered beams vary significantly in size and cross-section type and consider also a solid (not-flanged) section type. Similar to beam BV2, also the members tested by Kromoser [65] are characterised by a concentrated reinforcement in the bottom flange. Others, as the beams tested by Kulas [39] are reinforced with textile fabric only (high-strength carbon fabrics as bottom reinforcement and glass fibre fabric as web reinforcement). Several other shear tests performed by Kulas are characterised by failure due to insufficient anchorage or delamination of the bottom flange due to insufficient cover at the web-to-flange connection [39]. Those tests were excluded from the database since failure occurred by detailing issues. Eventually, also the tests performed by Molter [67] and Voss [68] are not considered, since the failure modes are not described in the available documents.

The model parameters for the stiffness (k_e) and the efficiency (η_b) of the reinforcement are given in Table 3.5 and discussed below:

- With respect to the reduction factors of the textiles k_e :
 - For the tests of Kromoser [65] and Bielak [69], a value of $k_{el} = k_{ex} = 1.00$ (fibres in the longitudinal direction were stretched during the impregnation process [70]) and $k_{ez} = 0.80$ (fibres in the vertical direction were loose during the impregnation process [70]). These values are in agreement to those suggested by Kulas [39];
 - For the tests of Kulas, a value of $k_{el} = k_{ex} = k_{ez} = 0.80$ is adopted (considering the non-industrial manufacturing process of the textile and in agreement to [39]);
 - For the tests presented in the present experimental programme, $k_{el} = k_{ex} = k_{ez} = 0.80$ are adopted (non-stretched fibre during impregnation, consistent value to [39, 70]).

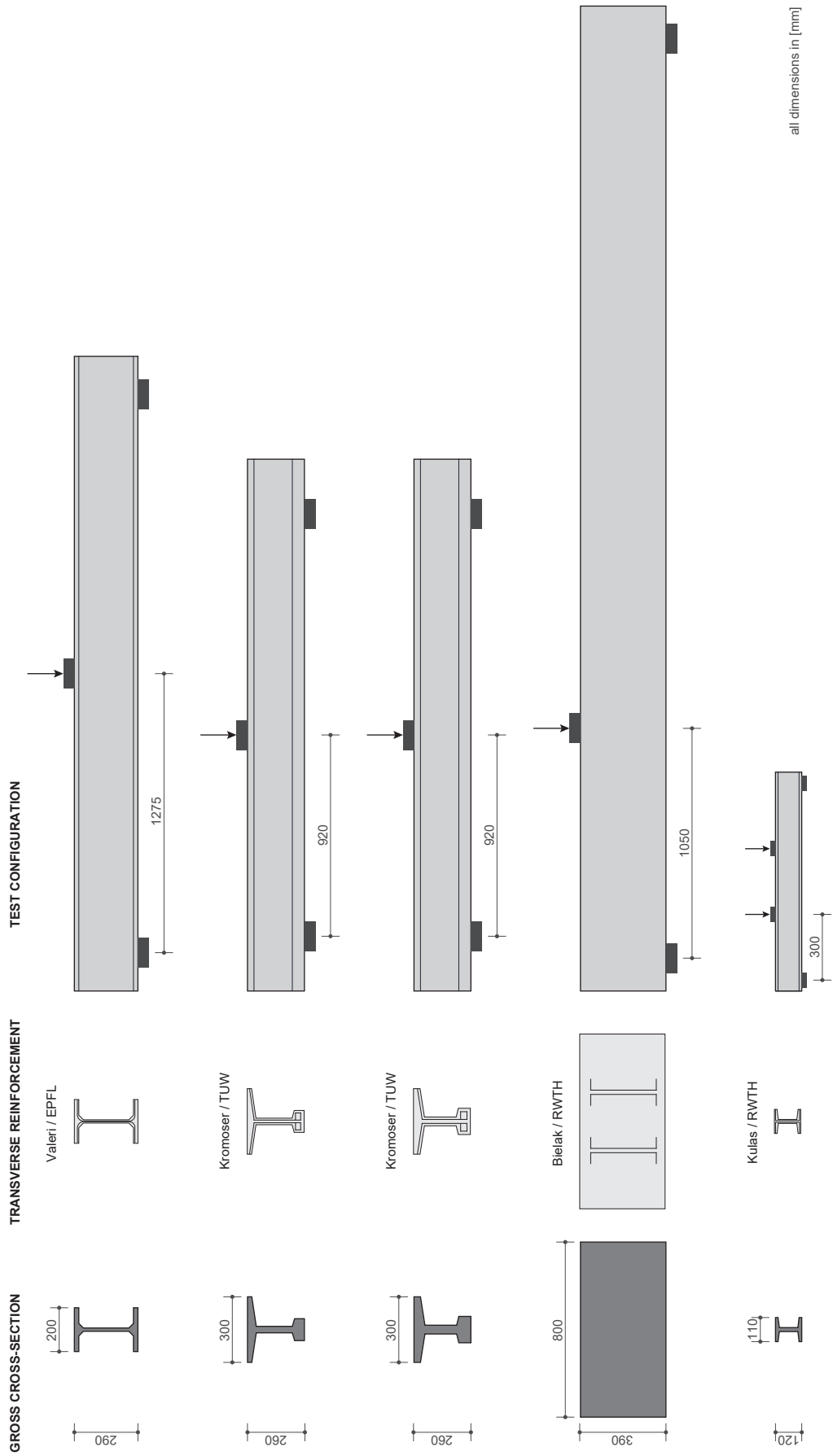


Figure 3.16: Sectional geometry and reinforcement of test beams.

- With respect to the strength reduction factor η_b , it is not observed to be necessary for the coated and impregnated textiles considered in this investigation. Its value is thus set to $\eta_b = 1$.

Table 3.4 shows that the proposed approach leads to consistent results with an average measured-to-calculated resistance of 1.04 and a coefficient of variation of 13 % (inclination of the compression field calculated according to equation 3.17). These values are comparable to those obtained for ordinary reinforced concrete members [63] with a slightly higher value of the scatter. In addition, the prediction of the failure modes shows consistent agreement to the one observed experimentally (for all tests, except those of Bielak with rectangular cross-section, where distributed cracking cannot be clearly appreciated). Thus, future comparisons will be required in order to clarify the limits of applicability of the model (as control of crack localisation).

Author	Test	$b_{w,eff}$ [mm]	k_{el} [-]	k_{ex} [-]	k_{ez} [-]	V_R [kN]	Failure	$V_{R,test}/V_{R,calc}$ [-]
Valeri	BV2	7.5	0.80	0.80	0.80	41.8	crushing	0.99
Kromoser	T2.5E30	8.0	1.00	1.00	0.80	46.3	crushing	0.84
Kromoser	T3.0E30	8.0	1.00	1.00	0.80	45.4	crushing	0.83
Kromoser	T3.5E30	8.0	1.00	1.00	0.80	44.3	crushing	1.07
Kromoser	T4.0E30	8.0	1.00	1.00	0.80	43.3	crushing	1.00
Kromoser	T2.5E40	9.0	1.00	1.00	0.80	51.5	crushing	0.73
Kromoser	T3.0E40	9.0	1.00	1.00	0.80	51.1	crushing	0.91
Kromoser	T3.5E40	9.0	1.00	1.00	0.80	50.6	crushing	0.93
Kromoser	T4.0E40	9.0	1.00	1.00	0.80	50.0	crushing	1.04
Bielak	V1b	391.0	1.00	1.00	0.80	318.9	roving failure	1.06
Bielak	V2b	392.0	1.00	1.00	0.80	321.2	roving failure	1.11
Bielak	V3b	392.0	1.00	1.00	0.80	314.8	roving failure	1.08
Bielak	V4a	390.0	1.00	1.00	0.80	321.2	roving failure	1.09
Bielak	V4b	392.0	1.00	1.00	0.80	322.6	roving failure	1.15
Kulas	V6-T95-K1-1	6.0	0.80	0.80	0.80	5.7	roving failure	0.98
Kulas	V6-T95-K1-2	6.0	0.80	0.80	0.80	5.7	roving failure	0.82
Kulas	V6-T95-K1-3	6.0	0.80	0.80	0.80	5.7	roving failure	0.89
Kulas	V6-T95-K1-4	6.0	0.80	0.80	0.80	5.7	roving failure	1.05
Average								1.04
COV								0.13

Table 3.4: Model parameters and results for the considered shear tests.

Author	Test	V_u [kN]	L [mm]	a [mm]	d [mm]	a/d [-]	b_w [mm]	E_c [GPa]	f_c [MPa]	n_L [nr]	a_L [mm ²]	E_L [GPa]	f_L [MPa]	n_{lx} [nr]	a_{rx} [mm ²]	s_{rx} [mm]	E_{rx} [GPa]	f_{rx} [MPa]	n_{lz} [nr]	a_{rz} [mm ²]	s_{rz} [mm]	E_{rz} [GPa]	f_{rz} [MPa]
Valeri	BV2	42.4	2550	1275	270	4.7	15	40.0	120	7	28.3	150	1050	4	0.85	20	230	2000	4	0.85	20	210	1700
Kromoser	T2.5E30	55.0	1930	579	234	2.5	30	48.5	166	2	50.3	161	2048	2	3.62	38	240	2824	2	3.60	38	192	2824
Kromoser	T3.0E30	54.4	2296	689	234	3.0	30	48.5	166	2	50.3	161	2048	2	3.62	38	240	2824	2	3.60	38	192	2824
Kromoser	T3.5E30	41.5	2693	808	234	3.5	30	48.5	166	2	50.3	161	2048	2	3.62	38	240	2824	2	3.60	38	192	2824
Kromoser	T4.0E30	43.2	3059	918	234	3.9	30	48.5	166	2	50.3	161	2048	2	3.62	38	240	2824	2	3.60	38	192	2824
Kromoser	T2.5E40	70.3	1932	580	230	2.5	40	48.5	166	2	78.5	161	2048	2	3.62	38	240	2824	2	3.60	38	192	2824
Kromoser	T3.0E40	56.4	2300	690	230	3.0	40	48.5	166	2	78.5	161	2048	2	3.62	38	240	2824	2	3.60	38	192	2824
Kromoser	T3.5E40	54.2	2699	810	230	3.5	40	48.5	166	2	78.5	161	2048	2	3.62	38	240	2824	2	3.60	38	192	2824
Kromoser	T4.0E40	48.3	3067	920	230	4.0	40	48.5	166	2	78.5	161	2048	2	3.62	38	240	2824	2	3.60	38	192	2824
Bielak	V1b	302.1	2400	1047	355	3.0	391	28.0	52	40	3.6	246	3221	4	3.62	38	246	3221	4	3.62	38	195	3334
Bielak	V2b	288.5	2500	1052	359	2.9	392	28.0	52	40	3.6	246	3221	4	3.62	38	246	3221	4	3.62	38	195	3334
Bielak	V3b	292.3	2500	1056	352	3.0	392	28.0	52	40	3.6	246	3221	4	3.62	38	246	3221	4	3.62	38	195	3334
Bielak	V4a	293.8	4200	1052	359	2.9	390	28.0	54	40	3.6	246	3221	4	3.62	38	246	3221	4	3.62	38	195	3334
Bielak	V4b	280.8	2500	1050	362	2.9	392	28.0	54	40	3.6	246	3221	4	3.62	38	246	3221	4	3.62	38	195	3334
Kulas	V6-T95-K1-1	5.8	1300	400	117	3.4	10	45.4	104	4	1.8	238	3544	1	0.90	21	69	1129	1	0.90	23	66	1072
Kulas	V6-T95-K1-2	6.9	1300	400	117	3.4	10	45.4	104	4	1.8	238	3544	1	0.90	21	69	1129	1	0.90	23	66	1072
Kulas	V6-T95-K1-3	6.4	1300	400	117	3.4	10	45.4	104	4	1.8	238	3544	1	0.90	21	69	1129	1	0.90	23	66	1072
Kulas	V6-T95-K1-4	5.4	1300	400	117	3.4	10	45.4	104	4	1.8	238	3544	1	0.90	21	69	1129	1	0.90	23	66	1072

Table 3.5: Considered shear tests of the scientific literature: failure load, geometry and material properties.

3.6 Conclusions

In this chapter, the response of thin-walled linear members in Textile Reinforced Concrete (TRC) has been investigated with reference to its flexural behaviour and resistance. Two full-scale beams have been tested in a three-point bending configuration allowing to investigate on the applicability of Elastic-Cracked Stress Fields (ECSF) for its design. The main conclusions of this investigation are given below:

1. The bending response is governed by the strength and deformation capacity of the flanges. To enhance the bending resistance and deformation capacity, adding stainless steel reinforcement is a promising solution in terms of strength and deformation capacity (while keeping the resistance to corrosion of the material with small concrete cover);
2. The suitability of modelling TRC in bending by means of ECSF (assuming an elastic-cracked response of concrete and an elastic response of the fabric reinforcement) is confirmed and shown to be equivalent to plane section analysis accounting for compatibility of deformations;
3. The response in shear is governed by the strength of the web panel. Failure in shear in the performed test occurred by simultaneous crushing of the web and delamination of the flanges and is governed by the textile failure;
4. Modelling of the shear response of TRC can be consistently performed by means of ECSF. This considers an elastic-plastic response of concrete in compression and a linear-elastic and brittle material behaviour for the fabric. Such approach in combination with simple efficiency factors for the strength and stiffness allows suitably estimating the angle of the compression field and the resistance of the member;
5. A comparison of other tests failing in shear from the literature plus the tests presented in this chapter (failing in bending and shear) confirms the consistency of using ECSF for modelling of TRC.

Acknowledgements

The authors would like to sincerely acknowledge the support given by the association of the Swiss cement producers *cemsuisse* (research project #201407) for their financial support, providing the concrete mix and technical discussions.

Bibliography

- [1] fib (The International Federation for Structural Concrete). Frp reinforcement for rc structures. technical report on the design and use of fibre reinforced polymer reinforcement (frp) for reinforced concrete structures. Technical report, fib Bulletin 40, 2007.
- [2] ACI Committee 440. Guide for the design and construction of structural concrete reinforced with fiber-reinforced polymer bars. Technical report, American Concrete Institute, 2015.
- [3] Kurth Martin Christof. *Zum Querkrafttragverhalten von Betonbauteilen mit Faserverbundkunststoff-Bewehrung*. PhD thesis, Fakultät für Bauingenieurwesen der Rheinisch-Westfälischen Technischen Hochschule Aachen, 2012.
- [4] Alva Peled, Arnon Bentur, and Barzin Mobasher. *Textile Reinforced Concrete - Modern Concrete Technology*. Boca Raton : CRC Press, Taylor & Francis Group, 1st edition edition, 2017. ISBN 9780367866914.
- [5] Chokri Cherif. *Textile materials for lightweight constructions: Technologies - methods - materials - properties*. Springer, 2016.
- [6] Wolfgang Brameshuber. Textile Reinforced Concrete. State-of-the-Art Report. Technical report, RILEM Technical Committee TC201-TRC, Aachen, 2009.
- [7] J Hegger and S Voss. Investigations on the bearing behaviour and application potential of textile reinforced concrete. *Engineering structures*, 30(7):2050–2056, 2008.
- [8] Will Hawkins, John Orr, Paul Shepherd, Tim Ibell, and Julie Bregulla. Thin-shell textile-reinforced concrete floors for sustainable buildings. In *Proceedings of IASS Annual Symposia*, number 7, pages 1–9. International Association for Shell and Spatial Structures (IASS), 2017.
- [9] Will Hawkins, John Orr, Tim Ibell, and Paul Shepherd. An analytical failure envelope for the design of textile reinforced concrete shells. In *Structures*, volume 15, pages 56–65. Elsevier, 2018.
- [10] Liang Wen-quan, L I Bei-xing, and L I Xiang-guo. Preparation of Super Composite Cement with a Lower Clinker Content and a Larger Amount of Industrial Wastes. *Journal of Wuhan University of Technology*, 17(4):2–5, 2002.
- [11] I Garcia-Lodeir, A Fernández-Jimenez, and A Palomo. Cements with a low clinker content: versatile use of raw materials. *Journal of Sustainable Cement-Based Materials*, 4:140–151, 2015.
- [12] Alexander Scholzen, Rostislav Chudoba, and Josef Hegger. Thin-walled shell structures made of textile-reinforced concrete: Part I: Structural design and construction. *Structural Concrete*, 16:106–114, 2015.
- [13] Alexander Scholzen, Rostislav Chudoba, and Josef Hegger. Thin-walled shell structures made of textile-reinforced concrete: Part II: Experimental characterization, ultimate limit state assessment and numerical simulation. *Structural Concrete*, 16(1):115–124, 2015.
- [14] Harald Michler. Verstärken mit Carbonbeton im Brückenbau. In *26. Dresdner Brückenbausymposium*, pages 235–247, Dresden, 2016.
- [15] Thorsten Helbig, Kay Unterer, Christian Kulas, Sergej Rempel, and Josef Hegger. Fuss- und Radwegbrücke aus Carbonbeton in Albstadt-Ebingen: Die weltweit erste ausschliesslich carbonfaserbewehrte Betonbrücke. *Beton- und Stahlbetonbau*, 111(10):676–685, 2016.

- [16] A. Liew, Y. R. Stürz, S. Guillaume, T. Van Mele, R. S. Smith, and P. Block. Active control of a rod-net formwork system prototype. *Automation in Construction*, 96(November 2016): 128–140, 2018.
- [17] Patrick Valeri, Patricia Guaita, Raffael Baur, Miguel Fernández Ruiz, David Fernández-Ordóñez, and Aurelio Muttoni. Textile reinforced concrete for sustainable structures: Future perspectives and application to a prototype pavilion. *Structural Concrete*, 2020.
- [18] Christian Kulas. solidian GmbH. <https://www.solidian.com/en/references/>, 2019. [Online; accessed 22-November-2019].
- [19] Alexander Schumann, Harald Michler, Frank Schladitz, and Manfred Curbach. Parking slabs made of carbon reinforced concrete. *Structural Concrete*, (October):1–9, 2017.
- [20] Sebastian May, Harald Michler, Frank Schladitz, and Manfred Curbach. Lightweight ceiling system made of carbon reinforced concrete. *Structural Concrete*, 19(6):1862–1872, 2018.
- [21] Benjamin Kromoser, Philipp Preinstorfer, and Johann Kollegger. Building lightweight structures with carbon-fiber-reinforced polymer-reinforced ultra-high-performance concrete: Research approach, construction materials, and conceptual design of three building components. *Structural Concrete*, 20(2):730–744, 2019.
- [22] Isabella Giorgia Colombo, Matteo Colombo, and Marco Prisco. Bending behaviour of Textile Reinforced Concrete sandwich beams. *Construction and Building Materials*, 95:675–685, 2015.
- [23] Tine Tysmans, Maciej Wozniak, Olivier Remy, and John Vantomme. Finite element modelling of the biaxial behaviour of high-performance fibre-reinforced cement composites (hprfcc) using concrete damaged plasticity. *Finite Elements in Analysis and Design*, 100:47–53, 2015.
- [24] Elisabeth Schütze, Jan Bielak, Silke Scheerer, Josef Hegger, and Manfred Curbach. Einaxialer zugversuch für carbonbeton mit textiler bewehrung. *Beton- und Stahlbetonbau*, 113(1):33–47, 2018.
- [25] Aurelio Muttoni, Joseph Joseph, Schwartz, and Bruno Thürlimann. *Design of Concrete Structures with Stress Fields*. Birkhäuser Verlag, 1996.
- [26] P Nielsen, M and C Hoang, L. *Limit Analysis and Concrete Plasticity*. CRC Press, 2010.
- [27] Miguel Fernández Ruiz and Aurelio Muttoni. On Development of Suitable Stress Fields for Structural Concrete. *ACI Structural Journal*, 104:495–502, 2007.
- [28] Aurelio Muttoni, Miguel Fernández Ruiz, and Filip Niketić. Design versus assessment of concrete structures using stress fields and strut-and-tie models. *ACI Structural Journal*, 112(5):605–615, 2015.
- [29] Pello Larrinaga, Carlos Chastre, Hugo C Biscaia, and José T San-José. Experimental and numerical modeling of basalt textile reinforced mortar behavior under uniaxial tensile stress. *Materials & Design*, 55:66–74, 2014.
- [30] Benben Li, Haibei Xiong, Jiafei Jiang, and Xiangxiang Dou. Tensile behavior of basalt textile grid reinforced engineering cementitious composite. *Composites Part B: Engineering*, 156: 185–200, 2019.
- [31] H Kupfer. Erweiterung der Mörsch’schen Fachwerkanalogie mit Hilfe des Prinzips vom Minimum der Formänderungsarbeit. Technical Report 40, Comité Euro-International du Béton (CEB), Paris, France, 1964.

- [32] Philipp Preinstorfer, Benjamin Kromoser, and Johann Kollegger. Flexural behaviour of filigree slab elements made of carbon reinforced UHPC. *Construction and Building Materials*, 199: 416–423, 2019.
- [33] Ulrich Häußler-combe, Jörg Weselek, and Frank Jesse. A Safety Concept for Non-Metallic Reinforcement for Concrete under Bending. *ACI Structural Journal*, (116):151–160, 2019.
- [34] Natalie Williams Portal, Lars Nyholm Thrane, and Karin Lundgren. Flexural behaviour of textile reinforced concrete composites: experimental and numerical evaluation. *Materials and Structures*, 50(1):1–14, 2017.
- [35] Rebecca Mansur de Castro Silva and Flávio de Andrade Silva. Carbon textile reinforced concrete: materials and structural analysis. *Materials and Structures*, 53(1):17, 2020.
- [36] Patrick Valeri, Miguel Fernández Ruiz, and Aurelio Muttoni. Building in a lighter and more sustainable manner: textile reinforced concrete for thin structural elements. Technical report, cemsuisse, 2017.
- [37] Jacopo Donnini, Valeria Corinaldesi, and Antonio Nanni. Mechanical properties of frcm using carbon fabrics with different coating treatments. *Composites Part B: Engineering*, 88:220–228, 2016.
- [38] V Eckers, B Sköck-Hartmann, R Rypl, R Chudoba, T Gries, and J Hegger. Modified tensile test setup for high-modulus multifilament yarns. In *International RILEM Conference on Material Science*, pages 111–116. RILEM Publications SARL, 2010.
- [39] Christian Kulas. *Zum Tragverhalten getränkter textiler Bewehrungselemente für Betonbauteile*. PhD thesis, RWTH, 2013.
- [40] Jakob Bochmann, Manfred Curbach, and Frank Jesse. Carbonbeton unter einaxialer druckbeanspruchung: Ergebnisse systematischer experimenteller untersuchungen. *Beton-und Stahlbetonbau*, 112(5):293–302, 2017.
- [41] Jakob Bochmann, Manfred Curbach, and Frank Jesse. Carbonbeton unter druck: Teil 2: Einfluss von bewehrungsgeometrie und-anordnung. *Beton-und Stahlbetonbau*, 113(1):22–32, 2018.
- [42] Patrick Valeri, Miguel Fernández Ruiz, and Aurelio Muttoni. cemsuisse report 201407: Building in a lighter and more sustainable manner : textile reinforced concrete for thin structural elements. Technical report, IBETON, Ecole Polytechnique Fédérale de Lausanne, Lausanne, 2017.
- [43] Mohamed Saidi and Aron Gabor. Use of distributed optical fibre as a strain sensor in textile reinforced cementitious matrix composites. *Measurement*, 140:323–333, 2019.
- [44] Carmelo Caggegi, Emma Lanoye, Khaled Djama, Antoine Bassil, and Aron Gabor. Tensile behaviour of a basalt trm strengthening system: Influence of mortar and reinforcing textile ratios. *Composites Part B: Engineering*, 130:90–102, 2017.
- [45] F J Vecchio and M P Collins. The modified compression-field theory for reinforced concrete elements subjected to shear. *ACI Structural Journal*, pages 219–231, 1986.
- [46] Aurelio Muttoni. *Die Anwendbarkeit der Plastizitätstheorie in der Bemessung von Stahlbeton*. Birkhäuser Verlag, Institut für Baustatik und Konstruktion ETH Zürich, 1990.
- [47] fib (The International Federation for Structural Concrete). *fib Model Code for concrete structures 2010*. Ernst und Sohn Verlag Germany, 2013.

- [48] Elisa Bertolesi, Francesca Giulia Carozzi, Gabriele Milani, and Carlo Poggi. Numerical modeling of fabric reinforced cementitious matrix composites (frcm) in tension. *Construction and Building Materials*, 70:531–548, 2014.
- [49] Pello Larrinaga, Carlos Chastre, Hugo C. Biscaia, and Jose T. San-Jose. Experimental and numerical modeling of basalt textile reinforced mortar behavior under uniaxial tensile stress. *Materials and Design*, 55:66–74, 2014.
- [50] Josef Hegger, Wolfgang Brameshuber, and Norbert Will. Textile Reinforced Concrete. In *1st international RILEM Symposium*, page 406, Aachen, 2006. RILEM.
- [51] Massimo Messori, Andrea Nobili, Cesare Signorini, and Antonella Sola. Mechanical performance of epoxy coated ar-glass fabric textile reinforced mortar: influence of coating thickness and formulation. *Composites Part B: Engineering*, 149:135–143, 2018.
- [52] R Contamine, A Si Larbi, and P Hamelin. Contribution to direct tensile testing of textile reinforced concrete (trc) composites. *Materials Science and Engineering: A*, 528(29-30):8589–8598, 2011.
- [53] Patrick Valeri, Patricia Guaita, Raffael Baur, and Miguel Fernández Ruiz. Pedagogy through artisanal construction of thin-walled concrete elements: a dialogue between engineering and architecture. In ACHE, editor, *Proceedings of the IV Int. Conference on Structural Engineering Education*, pages 1–10, Madrid, 2018. ACHE.
- [54] Patrick Valeri, Miguel Fernández Ruiz, and Aurelio Muttoni. New perspectives for design of lightweight structures by using Textile Reinforced Concrete. In *fib symposium. Innovations in materials, design and structures*, page 8, Krakow, 2019.
- [55] Diana Arboleda, Francesca Giulia Carozzi, Antonio Nanni, and Carlo Poggi. Testing procedures for the uniaxial tensile characterization of fabric-reinforced cementitious matrix composites. *Journal of Composites for Construction*, 20(3):04015063, 2016.
- [56] Isabella Giorgia Colombo, Anna Magri, Giulio Zani, Matteo Colombo, and Marco Di Prisco. Textile reinforced concrete: experimental investigation on design parameters. *Materials and structures*, 46(11):1953–1971, 2013.
- [57] R Chudoba, M Vořechovský, and M Konrad. Stochastic modeling of multi-filament yarns. i. random properties within the cross-section and size effect. *International Journal of Solids and Structures*, 43(3-4):413–434, 2006.
- [58] Sergej Rempel. *Zur Zuverlässigkeit der Bemessung von biegebeanspruchten Betonbauteilen mit textiler Bewehrung*. PhD thesis, Ph. D. Thesis, RWTH Aachen University, Aachen, Germany, 2018.
- [59] J. Hegger and N. Will. 8 - textile-reinforced concrete: Design models. In Thanasis Triantafillou, editor, *Textile Fibre Composites in Civil Engineering*, pages 189 – 207. Woodhead Publishing, 2016.
- [60] Tine Tysmans, Sigrid Adriaenssens, Heidi Cuyppers, and Jan Wastiels. Structural analysis of small span textile reinforced concrete shells with double curvature. *Composites science and technology*, 69(11-12):1790–1796, 2009.
- [61] Michael Rupf. *Querkraftwiderstand von Stahlbeton- und Spannbetonträgern mittels Spannungsfeldern*. PhD thesis, School of Architecture, Civil and Environmental Engineering ENAC - École polytechnique fédérale de Lausanne EPFL, 2014.

-
- [62] Miguel Fernández Ruiz and Aurelio Muttoni. Shear Strength of Thin-Webbed Post-Tensioned Beams. *ACI Structural Journal*, (May 2014):308–317, 2008.
- [63] Viktor Sigrist, Evan Bentz, Miguel Fernández Ruiz, Stephen Foster, and Muttoni Aurelio. Background to the fib Model Code 2010 shear provisions – part I: beams and slabs. *Structural Concrete*, 14(3):195 – 203, 2013.
- [64] Aurelio Muttoni, Olivier L Burdet, and Eckhart Hars. Effect of duct type on shear strength of thin webs. *ACI Structural Journal*, pages 729–735, 2006.
- [65] Benjamin Kromoser, Patrick Huber, and Philipp Preinstorfer. Experimental study of the shear behaviour of thin walled CFRP reinforced UHPC structures. *5th International fib Congress Melbourne*, 2016.
- [66] Philipp Preinstorfer, Benjamin Kromoser, and Johann Kollegger. Einflussparameter auf die spaltrissbildung in textilbeton. *Beton- und Stahlbetonbau*, 113(12):877–885, 2018.
- [67] M Molter. *Zum Tragverhalten von textiltbewehrtem Beton*. PhD thesis, Fakultät für Bauingenieurwesen der Rheinisch-Westfälischen Technischen Hochschule Aachen, 2005.
- [68] Stefan Voss. *Ingenieurmodelle zum Tragverhalten von textiltbewehrtem Beton*. PhD thesis, Fakultät für Bauingenieurwesen der Rheinisch-Westfälischen Technischen Hochschule Aachen, 2008.
- [69] Jan Bielak, Sarah Bergmann, and Josef Hegger. Querkrafttragfähigkeit von Carbonbeton-Plattenbrücken mit C-förmiger Querkraftbewehrung. *Beton- und Stahlbetonbau*, 114:1–11, 2019.
- [70] J Bielak, J Hegger, and M Schmidt. Shear capacity of carbon fibre textile reinforced concrete slabs with planar and c-shaped shear reinforcement. In *FRPRCS-14*, volume 14, pages 1–5. Queen’s University Belfast, 2019.

3.7 Appendix: Detailed development of ECSF equations

In this section the complete procedure to derive Eq. 3.17 is illustrated. The compatibility conditions given by Eqs. 3.8 and 3.8 are:

$$\begin{aligned}\varepsilon_x &= \varepsilon_1 \cdot \sin^2 \theta_\varepsilon + \varepsilon_3 \cdot \cos^2 \theta_\varepsilon \\ \varepsilon_z &= \varepsilon_1 \cdot \cos^2 \theta_\varepsilon + \varepsilon_3 \cdot \sin^2 \theta_\varepsilon\end{aligned}$$

Those can be rearranged as follows:

$$\varepsilon_3 = \frac{\varepsilon_x - \varepsilon_1 \cdot \sin^2 \theta_\varepsilon}{\cos^2 \theta_\varepsilon} \quad (3.25)$$

$$\varepsilon_1 = \frac{\varepsilon_z - \varepsilon_3 \cdot \sin^2 \theta_\varepsilon}{\cos^2 \theta_\varepsilon} \quad (3.26)$$

Substituting Eq. 3.26 in Eq. 3.25 results in:

$$\varepsilon_3 = \frac{\varepsilon_x - (\varepsilon_z - \varepsilon_3 \cdot \sin^2 \theta_\varepsilon) \cdot \tan^2 \theta_\varepsilon}{\cos^2 \theta_\varepsilon} \quad (3.27)$$

Which equals to Eq. 3.15

$$\varepsilon_3 = \frac{\varepsilon_x - \varepsilon_z \cdot \tan^2 \theta_\varepsilon}{1 - \tan^2 \theta_\varepsilon}$$

The vertical equilibrium and the constitutive relations for concrete and the vertical reinforcement are given by Eqs. 3.4, 3.11 and 3.13:

$$\begin{aligned}\sigma_z &= \sigma_c \cdot \sin^2 \theta_\sigma + \rho_{rz,eff} \cdot \sigma_{rz} \\ \sigma_c &= E_c \cdot \varepsilon_3 \\ \sigma_{rz} &= E_{rz} \cdot \varepsilon_z\end{aligned}$$

By imposing $\sigma_z = 0$ it results:

$$\varepsilon_3 = \frac{-\rho_{rz,eff} \cdot E_{rz} \cdot \varepsilon_z}{E_c \cdot \sin^2 \theta_\sigma} \quad (3.28)$$

By admitting $\theta_\sigma = \theta_\varepsilon$ and by equalising Eq. 3.15 with Eq. 3.28 one obtains:

$$\frac{\varepsilon_x - \varepsilon_z \cdot \tan^2 \theta}{1 - \tan^2 \theta} = \frac{-\rho_{rz,eff} \cdot E_{rz} \cdot \varepsilon_z}{E_c \cdot \sin^2 \theta} \quad (3.29)$$

By defining $\alpha_{rz} = E_{rz}/E_c$ and using the trigonometric identity:

$$\frac{1}{\sin^2 \theta} = \frac{1 + \tan^2 \theta}{\tan^2 \theta} \quad (3.30)$$

Eq. 3.29 results in:

$$\frac{\varepsilon_x - \varepsilon_z \cdot \tan^2 \theta}{1 - \tan^2 \theta} = \frac{-\rho_{rz,eff} \cdot \alpha_{rz} \cdot \varepsilon_z \cdot (1 + \tan^2 \theta)}{\tan^2 \theta} \quad (3.31)$$

And solving this equation gives:

$$\tan^2 \theta = \frac{1}{2} \cdot \frac{\varepsilon_x \cdot \sqrt{\varepsilon_x^2 + 4 \cdot \alpha_{rz} \cdot \varepsilon_z \cdot \rho_{rz,eff} \cdot (\varepsilon_z + \alpha_{rz} \cdot \varepsilon_z \cdot \rho_{rz,eff})}}{\varepsilon_z + \alpha_{rz} \cdot \varepsilon_z \cdot \rho_{rz,eff}} \quad (3.32)$$

$$= \frac{\frac{\varepsilon_x}{\varepsilon_z} + \sqrt{\left(\frac{\varepsilon_x}{\varepsilon_z}\right)^2 + 4 \cdot \alpha_{rz} \cdot \rho_{rz,eff} \cdot (1 + \alpha_{rz} \cdot \rho_{rz,eff})}}{2 \cdot (1 + \alpha_{rz} \cdot \rho_{rz,eff})} \quad (3.33)$$

Which corresponds to Eq. 3.17.

3.8 Appendix: Calculation of shear resistance

The calculation of the shear-resistance can be performed in an iterative manner as follows:

- A number of load-steps V_i can be considered (e.g. 500 load steps). The range can be defined as follows:

$$0 < M_f^i \leq M_R = A_l \cdot f_l \cdot z \quad (3.34)$$

- that allows to calculate the acting shear force (for simply supported members subjected to a single point load) as:

$$V_E^i = \frac{M_f^i}{a} \quad (3.35)$$

- for each load step i , the inclination of the compression field at the edge of the fan regions θ^i can be calculated. This can be done in a numerical manner by using Eqs. 3.17, 3.20 and by imposing $\varepsilon_x \approx \varepsilon_l/2$;
- That allows to calculate the shear resistance at those locations V_R^i with Eqs. 3.21 and 3.22;
- At each load step i , the resistance is verified:

$$V_E^i \leq V_R^i \quad (3.36)$$

As soon as the resistance V_R^i is lower than the action V_E^i , the calculation is stopped.

Chapter 4

Application potential

This chapter presents a synthetic summary of the construction experiences made within the period 02.2016 – 02.2020 (see section 1.3 in chapter 1). Major focus is dedicated to the design, construction and erection of a demountable prototype pavilion in Textile Reinforced Concrete, build in September 2020 within a three weeks workshop, by 24 students and the authors of the following publication:

Textile Reinforced Concrete for sustainable structures: futures perspectives and application to a prototype pavilion *Valeri, P.; Guaita, P.; Baur, R.; Fernández Ruiz, M.; Fernández-Ordóñez Hernández, D.; Muttoni, A.*

Structural Concrete, 2020. <https://doi.org/10.1002/suco.201900511>

The contribution of the first author comprises the design, execution and evaluation of all material and structural tests presented in this chapter. Additionally he provided supervision and technical guidance to students in practical courses PENS-201 (*Semaine ENAC: Making Structural Logic*) and PENS-308 (*Unité d'enseignement: Argamassa Armada en Salvador de Bahia*). The final design of the prototype pavilion is based on the techniques developed by the first three authors within these courses (in the period 2016 – 2020) and under the supervision of the fourth, fifth and sixth authors. Furthermore, the first three authors not only supervised the students during the workshop, but also participated actively in the construction of the formworks, concrete mixing, casting and erection of the prototype pavilion.

The first draft of the manuscript was prepared by the first author (including tables and figures) while the remaining authors helped writing the final version of this contribution.

Abstract

Textile reinforced concrete (TRC) is a cementitious-based material where reinforcement consists of high-strength noncorrosive textile fabrics. Due to the use of a noncorrosive reinforcement, cover requirements can be limited to minimum static values and the amount of clinker in the cement can also be notably reduced. In addition, the simplicity to arrange the fabrics in complex formworks makes the material suited for thin shells or folded structures (typically with thicknesses ranging 10 - 20 mm). Due to the savings in material and to the lower amounts of clinker used for its production, TRC has a higher sustainable potential than conventional reinforced concrete, with a significantly lower CO₂ footprint. To encourage an extensive use of TRC in practice, several topics need however further development. They comprise aspects related to the material and structural response of TRC, but also to the design and to the possibilities to integrate TRC within the architecture and building-physics. In the present research, results of a 4-year research program on TRC performed by researchers in civil engineering and architecture are presented. The response of the material is first investigated in tension, bending, and shear. On this basis, considerations on the potential of TRC for construction are drawn and an example of application is presented with the construction of a full-scale pavilion entirely in TRC.

4.1 Introduction

First patents for modern reinforced concrete were registered at the end of the 19th century [1]. At that time, the availability of raw materials (cement and iron) was relatively limited and the construction was consequently oriented towards material savings and to the use of structural form allowing it. Later in that century, the cost of concrete and iron dropped significantly with respect to labour wages. In addition, codes of practice became more stringent with respect to concrete cover requirements in order to ensure the durability of concrete works (currently requiring 20 – 60 mm depending on the exposure class). These facts yielded to the use of reinforced concrete to cast thicker elements with simpler forms, which was also convenient in many cases for architectural purposes (casting of partition walls and other elements) and in agreement to building physics and acoustics. Yet, the robust but massive construction technique of reinforced concrete is currently under debate mostly due to considerations on the sustainability of construction, encouraging a lower consumption of CO₂ for building.

Within this frame, a new perspective is offered by textile reinforced concrete (TRC), where conventional metallic reinforcement can be replaced by a noncorrosive high-strength fabric reinforcement [2, 3]. This allows to drastically reduce cover requirements (with minimum values normally between 2 and 5 mm depending on the textile type and arrangement) and to cast significantly thinner components with respect to ordinary reinforced concrete ($t \approx 10 - 20$ mm, [4, 5]). In addition, since no passivation of the reinforcement is required, cements with lower contents of clinker can be used (by replacing Portland cement with products of industrial processes as fly ash, ground granulated blast furnace slag, and silica fume [6] with overall significantly lower energy consumption [7]). The use of such thin elements and of low-clinker content cements leads to a reduction of energy-demand related to the concrete production [8].

The practical application of TRC to construction is however still a challenge. This solution requires to consider its architectural integration and potential, requiring a joint effort of engineers and architects in the search of the optimum use of the material. Due to a lack of a normative framework and poor construction experience, currently only a limited number of applications exist. One of the first ones are the TRC-pavilion on the RWTH-University campus in Aachen (Germany) [9, 10] and the pedestrian bridge in Kempten (Germany, [11]). Also for the application of facade panels, the material is rapidly gaining popularity [12]. Some of the most recent projects showing the latest

advancements of the material are the pedestrian footbridge in Albstadt (Germany), built without any use of metallic reinforcement [13] and the large-shell prototype for the roof structure of the NEST building in Switzerland [14].

In this chapter, a collaborative work of researchers in civil engineering and architecture exploring the application potential of this material is presented [15]. After a condensed introduction of the material behaviour and its structural response of linear members, some examples of full-scale elements are presented exploring the potential of TRC. On this basis, the construction of a prototype pavilion in TRC is presented as a synthesis of structural and architectural design. The modular lightweight structure can be assembled and demounted manually and the performances of its key elements are tested and discussed.

4.2 TRC: material and structural response

TRC is composed of one or various fabric layers embedded in a fine-grained high-performance mortar (Fig. 4.1). It can also have the addition of concentrated reinforcement in the form of bars or prestressing wires when high tensile forces need to be carried. Its constituents and composite response are presented in the following.

4.2.1 Fabric reinforcement

Textile fabric reinforcement is usually made of a bidirectional grid consisting of rovings. These are bundles of several thousand filaments made of carbon, glass, or basalt. Filaments have a diameter of $5 - 30 \mu\text{m}$ and their mechanical properties reflect those of their raw material. When bundled together into rovings (typically with a diameter of $1 - 2 \text{ mm}$) the mechanical behaviour is also influenced by the waving procedure, the coating, and impregnation of the fibres [16]. With respect to the coating, the addition of fine sand (normally quartz) on the surface significantly enhances the bond properties with the cementitious matrix [17].

In the present research, a wide number of textiles were investigated. The mechanical properties of the rovings were determined by simple tension tests and are reported in Table 4.1. As shown in Fig. 4.2a, when rovings are subjected to tension, they are characterised by a straightening phase (which can be neglected for the composite [18, 19]) followed by a linear elastic behaviour until their tensile strength is reached.

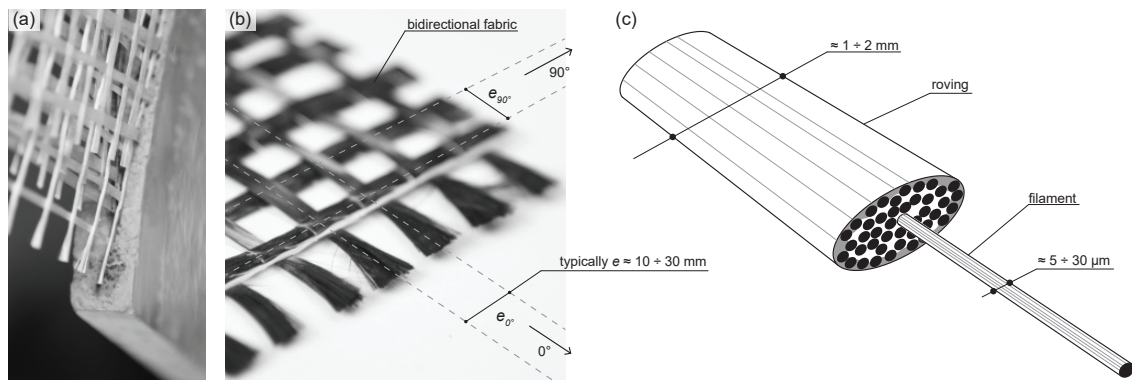


Figure 4.1: Textile reinforced concrete: (a) composite; (b) fabric reinforcement; and (c) roving.

4.2.2 Concentrated reinforcement

In some cases, the arrangement of textile fabrics is inconvenient to withstand high tensile forces as a large number of fabric layers is required (leading to an excessive thickness or to pouring or

casting problems). In these cases, arranging a concentrated reinforcement is a good solution to maintain reduced thicknesses and to avoid fabric congestion.

In this research, high-strength stainless steel (HSSS) and glass-fiber reinforced polymer (GFRP) rebars have been used to reinforce tensile zones of linear members. Their tensile response was experimentally determined and is presented in Fig. 4.2b – d. HSSS rebars do not present a well-defined yield plateau. They are thus characterized in Fig. 4.2b by their conventional yield strength ($f_{y,0.2} \approx 1080$ MPa). Failure in HSSS occurs after a significant plastic deformation, with a rupture strain $\varepsilon_u \approx 1.9$ % at ultimate strength ($f_u \approx 1170$ MPa). Differently, GFRP bars present a linear elastic response followed by a brittle failure (see Fig. 4.2c). The short-term average strength of the tested bars is 615 MPa, significantly lower than that of glass fibres (75 % of glass-fibers in volume with a strength of about 3500 MPa) mainly due to interlaminar stress concentrations at the anchorage [20]. For design, it shall also be noted that its long-term strength is to be considered (design value of the tensile strength $f_{Gd} = 445$ MPa according to the manufacturer [20]).

Threaded bars can also be efficiently used for connections of precast elements. In the present research, GFRP threaded bars [21] were used for this purpose, whose mechanical behaviour and parameters are presented in Fig. 4.2d and Table 4.1 (linear response until brittle failure).

4.2.3 Cementitious based matrix

To penetrate inside the fabric layers, the cementitious matrix typically consists of a grout or mortar with small aggregates and superplasticizer. The mortar is normally characterised by a low water-to-cement ratio ($w/c \approx 0.25$) leading thus to relatively high compressive strengths and enhanced compacity.

For the present research, two types of mortar were used:

- High-performance mortar with high fluidity. Such mortar was used to cast thin elements using closed formworks with casting thicknesses around 15 – 25 mm.
- Ultra-high-performance mortar with enhanced tixotropic qualities. This mix allows to cast curved elements produced with the lamination technique and using single-sided casting moulds. With this practice, the local inclination of the formwork controls the thickness of composite and thicknesses below 10 mm can be achieved.

The mechanical properties of the mortars in compression were determined by tests on cylinders $D = 70 \times H = 120$ mm. The results reported in Table 4.1 refer to the mean values at 28 days (cured in humid chamber until testing).

4.2.4 TRC composite

The tensile response of TRC was investigated on tension ties (thin plates reinforced with several layers of fabric reinforcement, see cross section in Fig. 4.2f and Reference [22]). As shown in Fig. 4.2f, their response can be divided into three stages:

- Stage I: uncracked response, when the stresses in the mortar are below its tensile strength.
- Stage II: crack development stage, characterised by development of an increasing number of cracks.
- Stage III: stabilised cracking stage, characterised by a constant number of cracks in the element, whose widths increase for increasing load.

In all tested cases, the failure mode was brittle and governed by the fabric, occurring at the end of Stage III. The failure load and the cracked stiffness are governed by the response of the fabric reinforcement and its interaction with the surrounding mortar. Since the filaments of the rovings

are not uniformly activated, the stiffness and the failure load of the composite can be lower with respect to that of bare reinforcement [23]. The degree of activation can vary significantly according to the impregnation, coating and undulation of the rovings [24]. For the cases investigated, the serviceability behaviour observed was excellent, with a uniformly distributed cracking pattern (typically between 20 and 35 mm, in most cases with cracks in coincidence with transverse rovings) and low crack openings (crack openings remained below 0.3 mm before failure [25]). More details on the serviceability response of the tested specimens can be found elsewhere [18, 22].

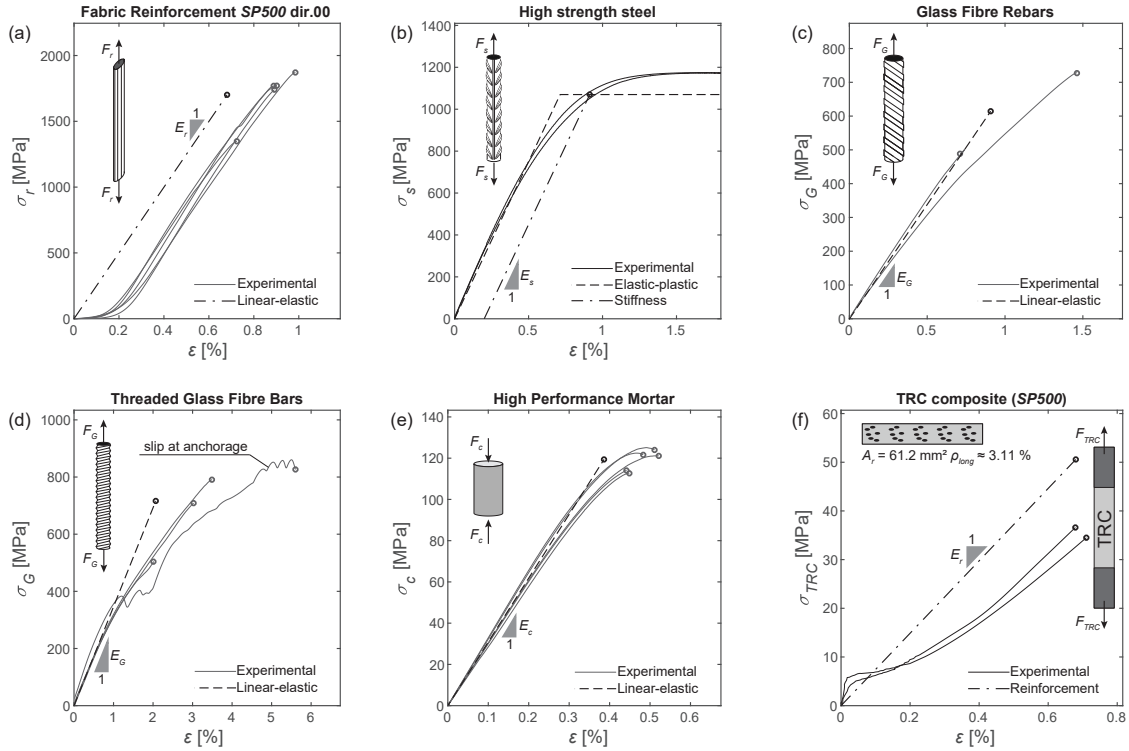


Figure 4.2: Material response in tension: (a) rovings; (b) high-strength stainless steel; (c) GFRP rebars; (d) threaded GFRP bars; (e) high performance mortar; (f) TRC-composite with 6 layers of SP500 fabric.

4.2.5 Structural response of beams: bending and shear

After investigation of TRC response in tension, the structural response of the material was investigated for linear members both in bending and shear. This was performed by means of three-point bending tests. Fig. 4.3 presents three of the tested members. Beams BV1 and BV2 presented an I-shaped cross section with a maximum wall thickness of 20 mm, whereas the plate PV1 consists of a slender unidirectional slab (45 mm of thickness). Beam BV1 was reinforced with several layers of coated carbon fabric (*SP200*), plate PV1 with several layers of uncoated carbon fabric (*TISSA 17M12*) and beam BV2 with coated carbon fabrics (*SP200*) and additional concentrated reinforcement made of HSSS, arranged in the bottom (tension) flange. The arrangement and details of the reinforcement are shown in Fig. 4.3 and complete details comprising the test set-ups and instrumentations with photogrammetric measurements (digital image correlation) can be found in References [18, 22, 26]. For mechanical modelling and design formulations refer to References [27, 28, 29, 30, 31, 32].

The structural response of the tested TRC members (Fig. 4.3) can be summarised as follows:

- Linear members reinforced with carbon fabrics have only a limited capacity in the tension chord. Their failure tends to occur in bending in a brittle manner by failure in tension and for moderate load levels (refer to specimen BV1).

- When the slenderness is significantly increased (as for specimen PV1), the flexural response is softer and, despite the eventual brittle failure, the structure may experience a relatively large deformation capacity.
- The strength can be significantly increased by arrangement of a concentrated reinforcement in the tension chord. This can be done for instance by means of stainless-steel bars, allowing in addition for an enhanced deformation capacity. It can be noted that the increase of the resistance in bending may potentially yield to failures in shear, potentially associated also to limited deformation capacity (as observed in specimen BV2 [18]).

Following the observed behaviour, it can be noted that failures in bending of TRC without concentrated reinforcement can be unsatisfactory, particularly for members requiring a certain level of resistance and/or sufficient deformation capacity. This encourages the use of TRC in combination with concentrated reinforcement. As an alternative approach, also failures in the compression side can enhance the deformation capacity at failure [22]. In both cases, the conceptual design of TRC structures shall yield to an evolution of conventional structural forms optimised for reinforced concrete. In the following, some possibilities will be explored on the basis of a case-based study of a prototype pavilion in TRC.

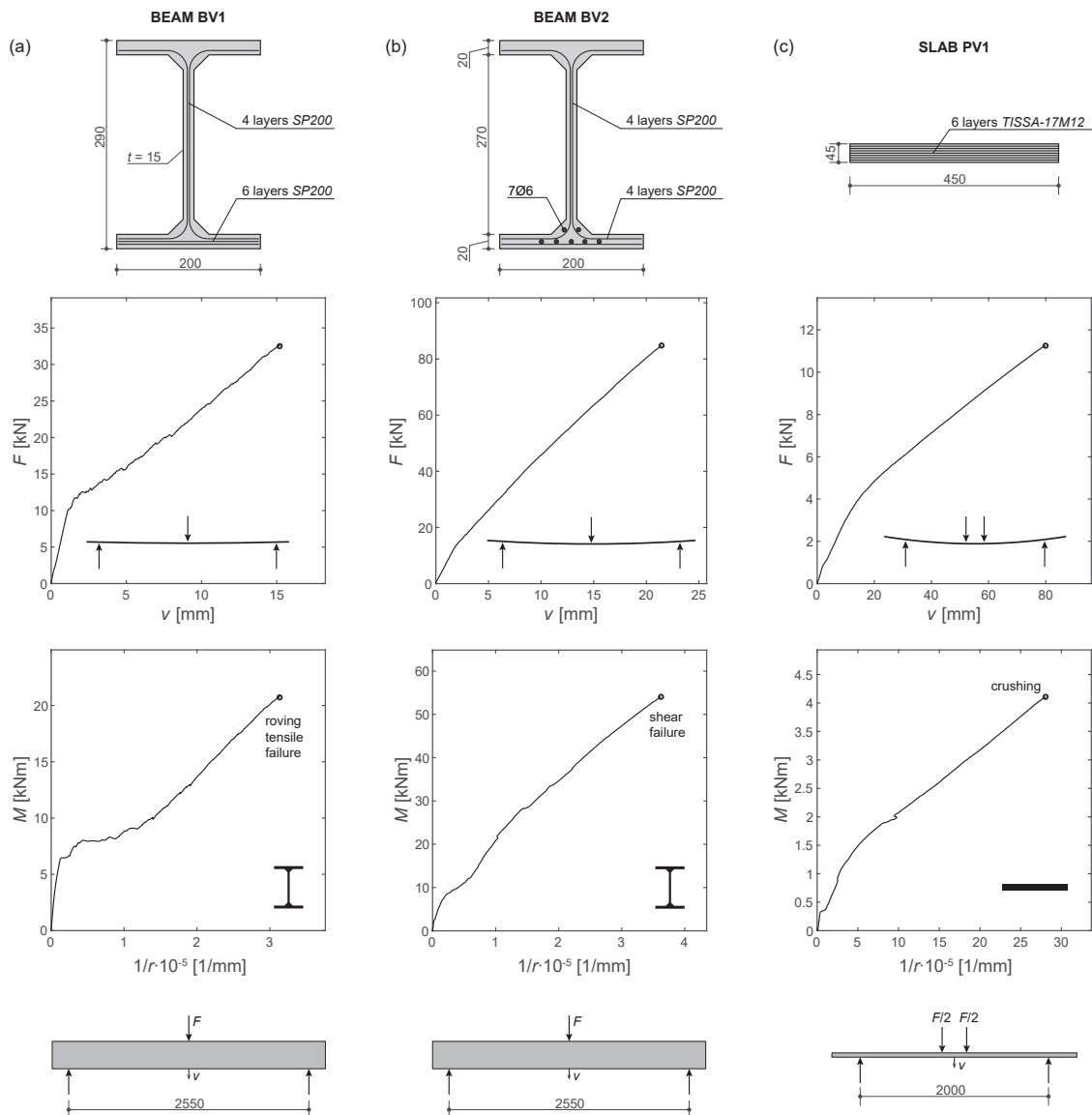


Figure 4.3: Flexural tests of TRC members: (a) beam BV1; (b) beam BV2, and (c) plate PV1.

Material	[...]	<i>SP500</i> (CCF)	<i>SP200</i> (CCF)	<i>TISSA 17M12</i> (UCF)	HSSS rebars	GFRP rebars	GFRP threaded bars	HP-Mortar (compression)	UHP-Mortar (compression)	TRC composite
		dir.0	dir.0	dir.0	($\varnothing 8\text{mm}$)	($\varnothing 8\text{mm}$)	(M10)	($\varnothing 70\text{mm}$)	($\varnothing 70\text{mm}$)	($20.1 \times 100\text{mm}$)
Gross cross-section area	a [mm^2]	1.7	0.85	0.425	50.2	50.2	58	3850	3850	210
Grid spacing	e [mm]	17	20	10	var.	var.	-	-	-	-
Modulus of elasticity	E [GPa]	250	230	200	150	67.7	34.6	30.1	41.2	var.
Strength (referred to gross section)	f [MPa]	1700	1700	1900	1080	615	716	119	148	36.1
Nr. Tests	[-]	10	10	10	2	2	4	5	2	2
COV of strength	[%]	20.6	13.3	15.9	0.18	26	21.5	4.28	2.5	3.32

Abbreviations: CCF, coated carbon fiber; UCF, uncoated carbon fiber.

Table 4.1: Measured mechanical material properties.

4.3 A prototype pavilion in TRC

One of the most promising fields of application of TRC is related to the use of lightweight prefabricated structures, taking advantage of the low thicknesses that can be achieved and accounting for the easiness to fold the fabrics on moulds. To highlight the promising characteristics of the material, a full-scale structure was designed and built within the frame of a three-week student workshop performed at École Polytechnique Fédérale de Lausanne (EPFL, Switzerland). The project was led by the authors of this chapter, following a hands-on pedagogic approach [15] with 24 students of civil engineering and architecture (17 from EPFL and 7 from the School of Architecture in Salvador de Bahia, FAUFBA, Brazil).

4.3.1 Historical background and context of *ferrocement* and *argamassa armada*

The history of reinforced concrete is a wide topic, from first roman puzzolanic cements (opus caementicium) and the concept of reinforcement in tension (already used for pots masonry in middle ages in Europe), it was only after the industrial revolution and the introduction of iron and steel in construction [33] that the concept of reinforced concrete was developed in its modern conception. Such invention followed after a number of independent discoveries already in the 19th century performed by a series of pioneers in different places across Europe. These inventions were aimed at introducing linear elements (reinforcement or iron) to suitably carry tensile stresses that concrete alone failed to withstand: in 1850 William B. Wilkinson used flat iron rods or second-hand wire ropes to reinforce concrete slabs [34]; in 1852 François Coignet used rails to reinforce structural concrete [35]; in 1855 Joseph-Louis Lambot built a concrete boat reinforced with an iron wire mesh [36]; in 1867 Joseph Monier also used an iron grid to reinforce concrete pots [36]; in 1889 Paul Cottancin patented a system consisting of wire meshes embedded in a thin concrete matrix [37]. One of the most important steps towards modern reinforced concrete was probably performed in 1892, when François Hennebique patented his own system (Béton Armé [38]). Dividing the structure into primary and secondary linear elements, Hennebique proposed a complete building system, sufficiently flexible to adapt to different contexts and spreading with a high success.

During the 20th century, the true potential of reinforced concrete was unveiled with masters both on the analysis and building potential of the material. Within this frame, Pier Luigi Nervi in Italy performed several original developments [39, 40]. Particularly, the use of a fine-grain mortar reinforced with several layers of micro-reinforcement [41] was implemented in a systematic manner under the name of *ferrocement*. The construction methodology proved to be faster and more economical with respect to its competitors since it was making large use of prefabrication and avoided the use of heavy machinery.

The development of *ferrocement* followed also outside of Italy. Notably, Nervi went to Brazil in the 1950s (invited by Pietro Maria Bardi, husband of the italo-brazilian architect Lina Bo Bardi) and led to the development of this technique in the Escola de Engenharia de São Carlos by the engineers Dante Martinelli and Frederico Schiel. Schiel came later to Salvador de Bahia to work with the architect João Figueiras Lima (Lelé), helping him in designing the first pieces at the RENURB factory [42].

Between the 1970s and 1990s, Lelé was involved in a number of extensive infrastructure projects in areas of difficult access as favelas. These projects were the basis for the further evolution of the *ferrocement* technology, which was named within the Brazilian context as *argamassa armada* [43, 44, 45] and was oriented to its production in large factories, leading to elements light enough to be carried and assembled by few workers with limited equipment. To reduce the costs associated to formworks, structures were in addition designed with the least possible number of components,

so that each member had typically to fulfil a series of functions (as water tightness and assemblies).

4.3.2 Revisiting social construction of *argamassa armada* in TRC: a case study

From a technical point of view, the multifunctional structural elements in *argamassa armada* designed by Lelé can be considered as one of the most advanced developments of *ferrocement*. Its current application is however debatable as the slender thickness of the members does not allow ensuring sufficient protection of the reinforcement against corrosion. Within this context, the use of TRC offers a suitable possibility to revisit this building technique, taking advantage of the modularity concept and refined laminar cross sections, but with an enhanced structural performance and durability of the works.

Starting from the *argamassa armada* technique required overcoming some challenges in the form-working and casting technology to ensure sufficient geometrical accuracy for elements with low thickness and complex cross section [15, 46]. In total, 35 short segments and 16 large scale elements were produced within this research program (some of the most interesting ones are depicted in Fig. 4.4). The first elements were based on the geometries by Lelé, while latter elements are evolutions taking advantage of TRC properties (trying for instance to promote failures by concrete crushing or with sufficient deformation capacity, see Fig. 4.4). Further valuable experience was gained during a site visit of the precast factories in Salvador de Bahia (Brazil) in collaboration with local experts from the faculty of architecture in Salvador [47, 48].

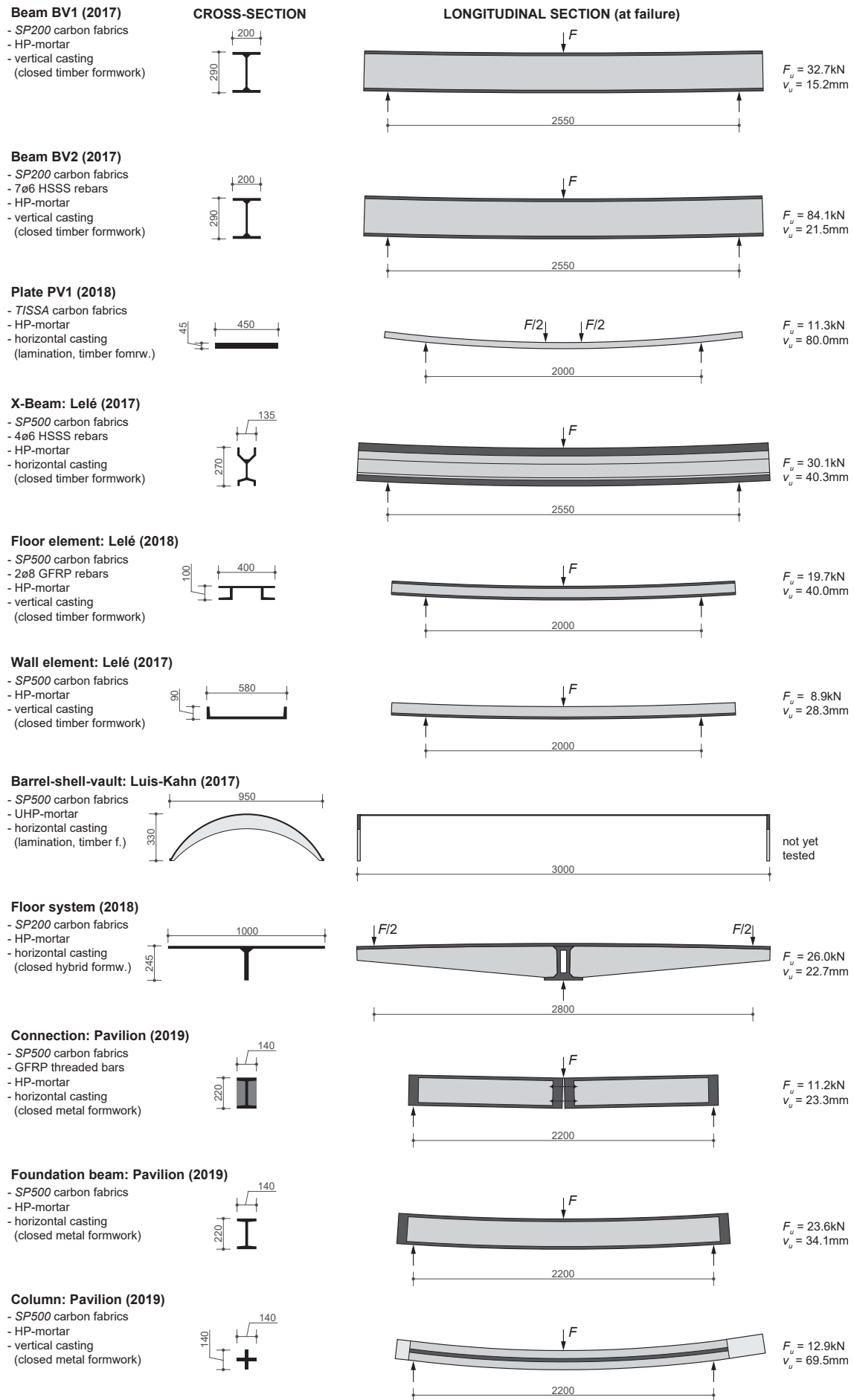


Figure 4.4: Overview of selected elements build and tested with the current investigation.

4.3.3 Conceptual design of the TRC pavilion

The idea of building a pavilion in TRC offered the possibility not only to explore the potential of this material on isolated structural elements, but also on its connections both from a structural (performance) and architectural point of view. The pavilion is also intended to demonstrate the feasibility of TRC as building material and is designed as a modular structure, allowing to expand upon necessity. Currently, only the main structural elements have been assembled (basement's beam grid, columns, roof shells) and will be followed by floor slabs and partitions in a second phase (see Fig. 4.4).

A number of references from sources other than *argamassa armada* were also identified during the conceptual design of the pavilion. A key work was the maison tropicale (Fig. 4.55a) built by Jean Prouve in the 1950s [49, 50], with a clear intention on modularity and expressing the structural elements as part of the architecture. With respect to the roof, the search for an efficient shell structure was guided by the barrel-shaped shells from the Kimbell art museum (Texas) by Kahn and Komendant [51, 52] which were in turn influenced by previous shell elements designed and tested by Franz Dischinger and Ulrich Finsterwalder [53]. The ribs of the shell (see Fig. 4.5b) avoid horizontal reactions at the supports, allowing the roof of the prototype pavilion to be supported on four slender columns.

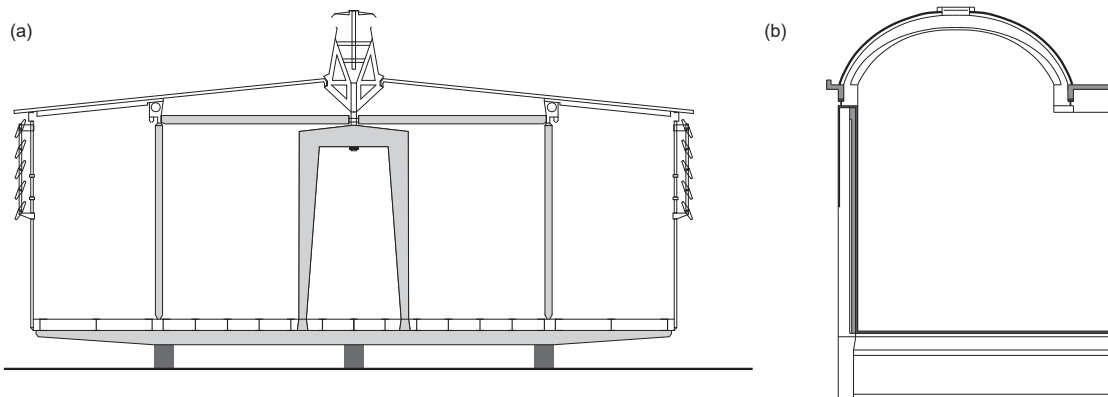


Figure 4.5: Design inspirations: (a) Maison tropicale by Jean Prouve (West Africa, 1949), and (b) Kimbell Art Museum by Louis I. Kahn (Fort Worth, Texas, 1972).

After analysis of these references, a number of decisions were taken on the geometry and building principles of the pavilion:

- The system is based on a constant grid spacing of $2.55 \text{ m} \times 1.275 \text{ m}$ and shall enable for a modular assembly, extension or modification in the future.
- A cross-bracing system shall not be arranged, to allow access to the pavilion from all sides.
- The structural assemblies have to be demountable, including the connections to the basement.
- All elements are built in TRC. For the most stressed elements, the use of concentrated reinforcement in the form of GFRP or HSSS rebars is advised to reduce thicknesses to a minimum.
- The structural elements should not exceed a weight of 60 kg allowing transport and erection by two persons. For the roof shells, the maximum weight is increased to 100 kg, allowing still for erection with simple lifting devices.

The final geometry of the pavilion is shown in Fig. 4.6. In the lower plane (basement), a grid of beams is arranged, allowing to clamp the vertical columns at their basis. Such clamping of

the columns is instrumental as it avoids the necessity of a bracing system. The connection of all elements was performed with GFRP threaded bars and bolts (see Fig. 4.7). The TRC elements are reinforced with carbon textile fabrics and additional concentrated reinforcement is added only when statically required.

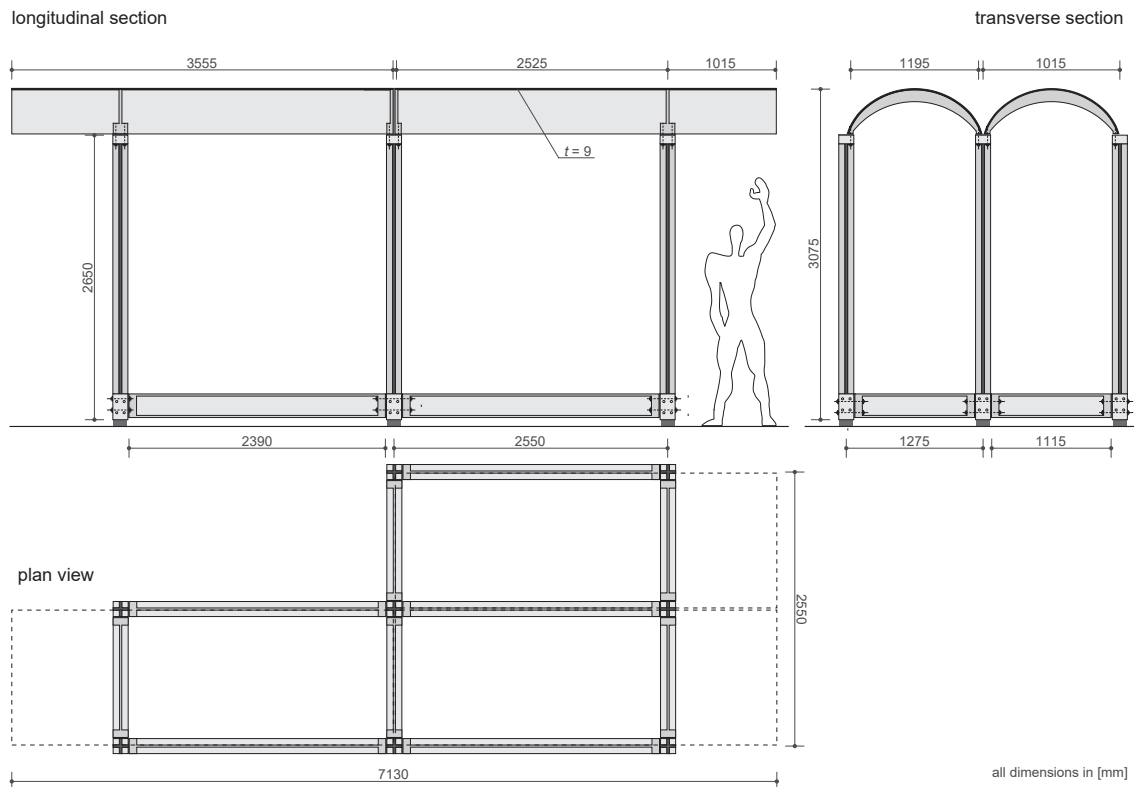


Figure 4.6: Main dimensions of the TRC prototype pavilion.

With respect to the shells, they cover a main span of 2.50 m with an additional cantilever of 1.00 m. Regarding their thickness, the aim was to build the shells as thin as possible while embedding sufficient fabric layers to ensure the load-bearing capacity. The final thickness resulted in 9 mm, without the need of arranging any concentrated reinforcement in the barrel-shaped region. Such reinforcement was however required at the ribs (diaphragms) connecting the shells to the columns due to their high level of internal forces.

The cross section of the columns is a thin cross with a height of 140 mm in both directions and a thickness of 25 mm (see Figs. 4.4 and 4.6). Its shape resulted from the similar bracing actions in the longitudinal and transversal directions. Due to their significant slenderness, concentrated reinforcement bars in the form of high strength stainless steel were required to ensure sufficient flexural capacity.

For the grid of beams in the basement, an I-shaped cross section was selected, with a height of 220 mm and a flange and web thickness of 20 mm (see Fig. 4.4). No concentrated reinforcement was arranged as the significant lever arm allowed to suitably control the internal forces. The length of the solid part at the ends of the basement beams (regions between the discontinuity section and the interface to the column blocks) was determined by anchoring and folding conditions of the textile, adopting a value of 70 mm.

Structural design was based on a linear-elastic analysis of the internal forces. The resistance of the single members and connections was calculated with an elastic cracked analysis and brittle failure for elements with textile reinforcement and the connections. For the elements with ductile reinforcement (columns and ribs of the shell), a plastic behaviour was considered to determine

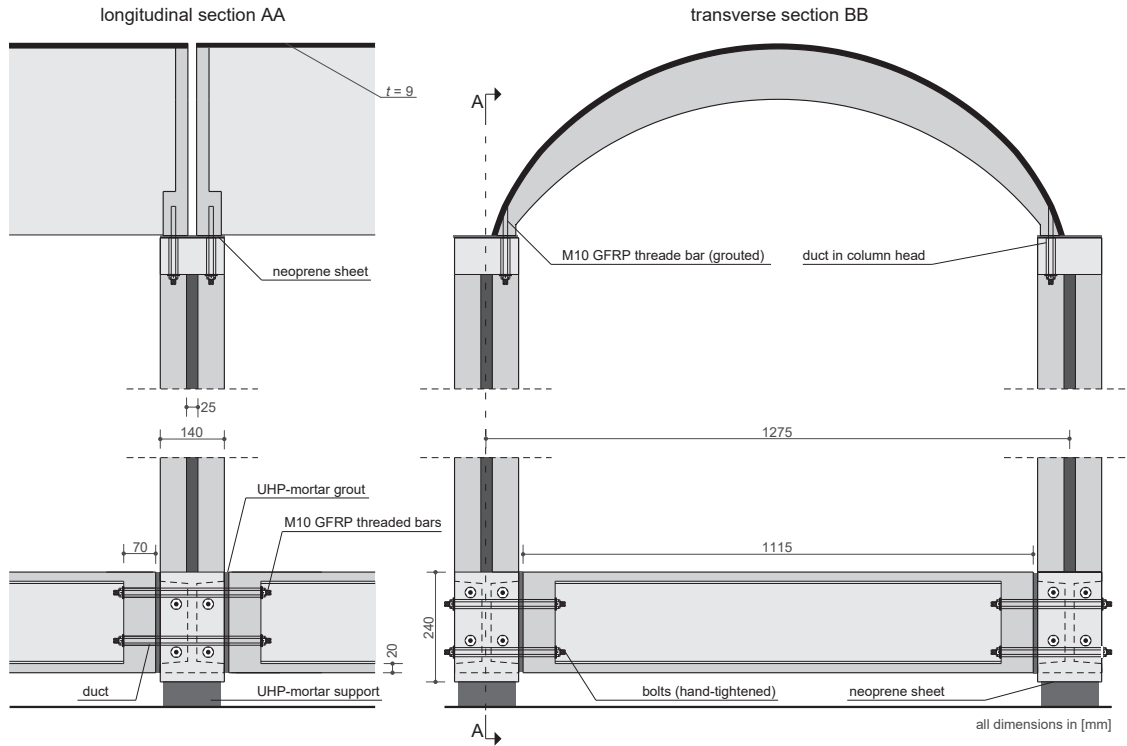


Figure 4.7: Connection details of the TRC elements.

their bending capacity. The flexural strength can be calculated using general design procedures accounting for anchorage and compatibility of deformations [18, 22, 26]. The material properties were determined experimentally (see Table 4.1) and considered in combination with the following partial safety factors:

- $\gamma_c = 1.5$ for the HP- and UHP-mortar.
- $\gamma_s = 1.15$ for HSSS rebars.
- $\gamma_t = 1.30$ for textile reinforcement [54] with an additional efficiency factor $\eta_b = 0.4$ in regions where the fabric was folded or for shear design to account for potential sliding combined with severe crack-openings [18].
- $\gamma_G = 1.30$ safety factor for GFRP bars and bolts [20].

The casting molds were designed and built with different techniques: ordinary timber formworking plates 3000 mm × 1000 mm × 27 mm; steel and stainless-steel sheets 2500 mm × 1500 mm × 1.25 mm and rectangular aluminium profiles 40 mm × 25 mm. For the connections,; $\varnothing 20$ plastic ducts were used to create the required holes. In the following, the casting moulds and technique as well as the detailing of the reinforcement for each element are explained in detail.

Barrel-shaped shells

For construction of the barrel-shaped shells, the ribs were first cast in a closed formwork with protruding textile reinforcement. When the mortar was sufficiently stiff, the counter-formwork of the ribs was removed and the thin shell was completed with the lamination process [32] (see Fig. 4.8a). After casting, the free surface was covered with a plastic sheet to enhance the curing process and the element was demoulded after less than 24 hr.

As for the reinforcement, two layers of *SP500* (see Table 4.1) were embedded in the UHP-mortar. The ribs were reinforced with a single HSSS-rebar ($\varnothing 8$) at their bottom and several small carbon

textile sheets placed underneath the bar, see Fig. 4.8a. These sheets protruded and were overlapped with the fabrics of the shell.

Columns

The formworks consisted of folded steel sheets, tied together with aluminium profiles as shown in Fig. 4.8b. At the upper and lower end, timber boxes with holes were arranged as moulds for the upper capital and basement respectively. Due to the relatively large static demand of the columns for bracing needs, a concentrated reinforcement was arranged in the form of 4 \varnothing 8 HSSS rebars (one in each corner) while the textile fabric was folded enclosing the section. Similarly, also the capital and basement socles were reinforced with cages made of carbon fabrics. Finally, the columns were cast vertically.

Grid of basement beams

The casting moulds of the basement beams were metallic without any timber parts (Fig. 4.8c). Also in this case, the different elements were bolted together, ensuring simple and fast assembly and demoulding. The I-shaped beams were reinforced only with carbon fabrics and detailing was performed by folding the reinforcement at the edges combined with an additional termination cage (see Fig. 4.9c).

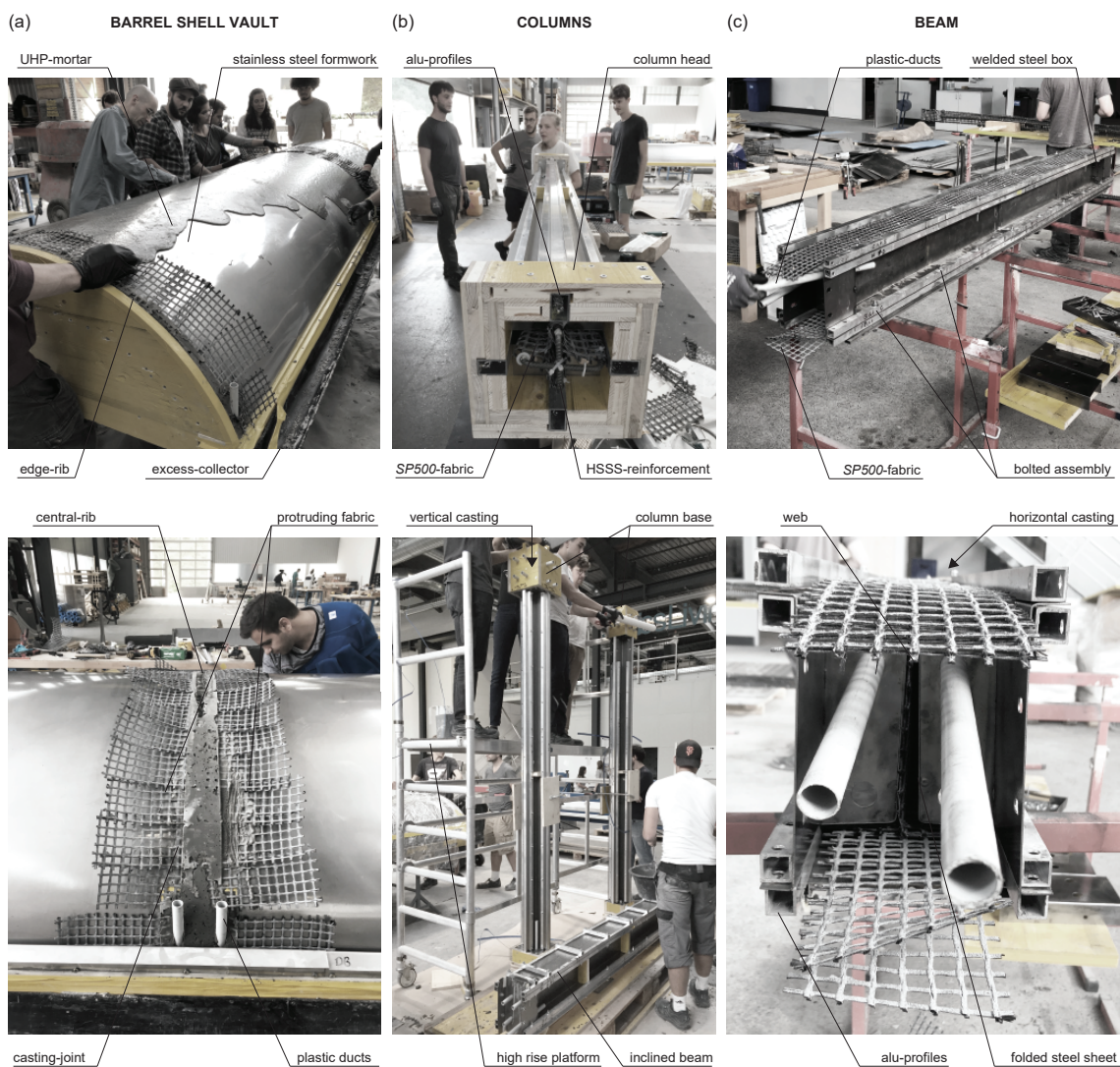


Figure 4.8: Casting procedure and formworks of: (a) barrel-shaped shell; (b) columns, and (c) foundation-frame beams.

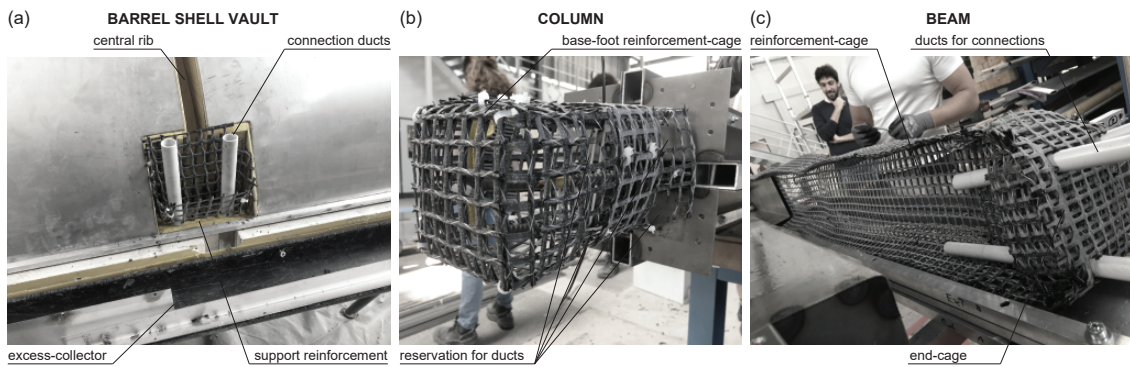


Figure 4.9: Reinforcement detailing of (a) barrel-shaped shell connection; (b) column-head, and (c) beam.

Erection and final state

Small base-foundations (also in TRC) were cast to support the structure and to create a plane level for the basement grid (Fig. 4.10b). The modules were then assembled comprising the following steps:

- Columns were placed on top of the supports (with a neoprene sheet in-between to avoid peaks of contact stresses). A temporary timber bracing was used in this phase to adjust vertical levelling and ensure stability of the elements. Proper alignment was ensured by placing provisory timber templates of the shells (Fig. 4.10a).
- The basement beams were arranged and the connection performed with GFRP-threaded bars. Tolerance gaps between the beams and columns (≈ 10 mm) were grouted with UHP-mortar.
- The timber templates were removed and the barrel-shaped shells were placed with a fork-lifter (Fig. 4.10b).
- Finally, the connection between the shells and columns was performed with GRFP-bolts. These bolts were glued in the shell with an epoxy resin and bolted from the bottom side of the capital (Fig. 4.10c).

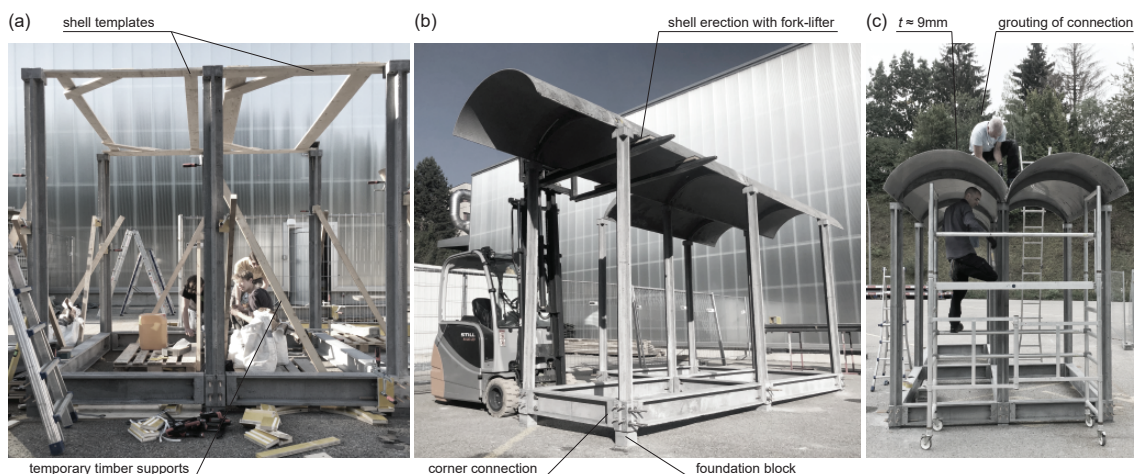


Figure 4.10: Erection process: (a) stabilised pavilion; (b) erection of the vaults, and (c) performing shell connections.

Since completion of the pavilion (Fig. 4.11), the structure has shown excellent performance, without any sign of degradation. Its long-term response will be monitored in the next years while other parts of the pavilion are added.



Figure 4.11: Final structure: (a) three modules; (b) construction staff; (c) column-head connection; (d-f) connections of the base frame.

Structural tests and verification

To verify the structural load-carrying capacity of the elements, a number of specimens were cast and tested in laboratory to verify their performance. In all cases, the observed behaviour corresponded well to the expected one. Fig. 4.12 gives an overview of the performed tests:

- *Connections:* To test the capacity of the connections, two short beams were assembled together to create a longer member. As for the pavilion, the connection at the interface section was performed with M10 GFRP threaded bars with a tolerance gap of 15 mm grouted with UHP-mortar (threaded unbonded bars). The member was then tested in three-point-bending with displacements and deformations recorded with ordinary linear variable displacement transformers. This allowed tracking the curvature at the interface section and at the discontinuity section (see definition of sections in Fig. 4.12a). As shown in Fig. 4.12a, the interface section between the two pieces opens at very low levels of load (explained by the poor adhesion of the surfaces to the mortar). For other sections of the beam, the cracking load is governed by the tensile strength of the mortar and by the inertia of the section. Load was increased after cracking until failure, which took place at the discontinuity section of the beams (where section changes from a solid beam to a I-shape, see Fig. 4.13a). Failure occurred with rupture of the outer filaments and pull-out of the core filaments. The strength of the bare fabric was not attained due to stress concentrations largely related to folding of the fabric at that region.
- *Grid of basement beams:* To investigate the performance of the connection, a long beam was tested under three point bending as shown in Fig. 4.12b. The member attained a relatively high resistance and failed at mid-span in bending (see Fig. 4.13b). The composite developed in this case its full tensile strength (no disturbances due to folding) and the failure was brittle occurring in the stabilised cracking phase.
- *Columns:* The static role of the columns is to support the roof and to provide a bracing capacity of the system. Consequently, the column elements were also tested in bending. Due to the presence of HSSS reinforcement, a significant increase of the deformation capacity was observed, with a failure due to crushing of the compression zone as depicted in Fig. 4.12c.

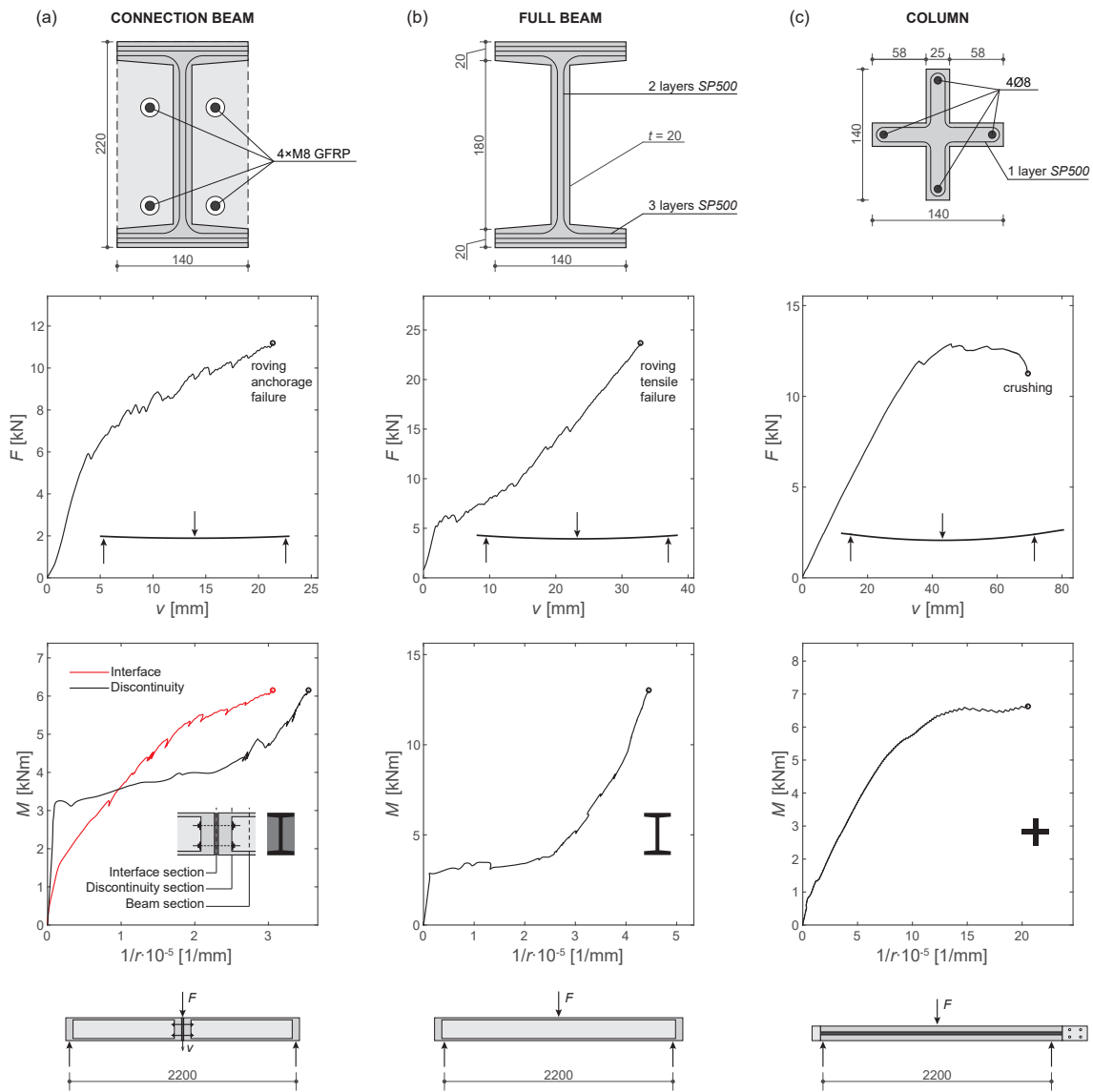


Figure 4.12: Flexural tests of the pavilion elements: (a) connection; (b) foundation beam, and (c) column.

Other elements were not directly tested in laboratory, although their performance was assessed at the construction site. This was for instance the case of the barrel shaped shells that, after casting, were supported on four points and tested by the weight of several students with no signs of apparent damage (see Fig. 4.13c).

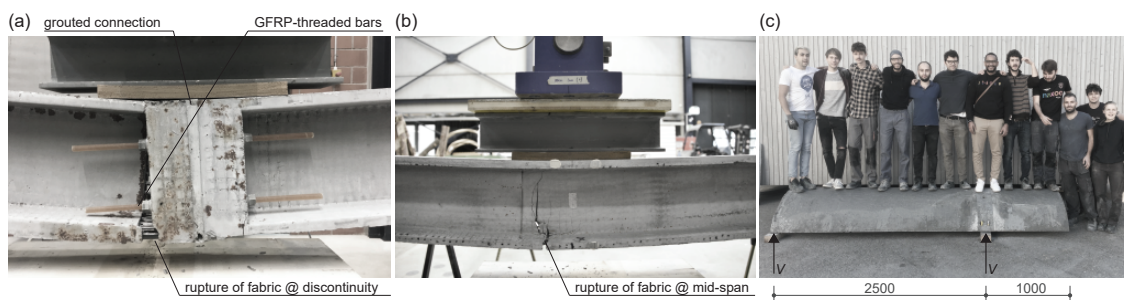


Figure 4.13: Tests of pavilion elements: (a) anchorage failure of the connection; (b) bending failure of the beam, and (c) test of the barrel-shell vault.

4.4 Conclusions and outlook

The potential of TRC as a sustainable building material is explored in this chapter focusing on its material and structural performances as well as on its architectural possibilities. A case-based study on a prototype pavilion in TRC is presented, showing how previous building knowledge on *ferrocement* and *argamassa armada* can be revisited and updated to this technique. The main conclusions of this chapter are listed below:

1. TRC is an efficient material, suitable for structural design and with application to construction.
2. The main potential of TRC is identified for construction of thin elements (shells, laminar, or folded elements). The reduction of thicknesses with respect to ordinary concrete, in combination with its potential for using low-clinker cements, allows enhancing its qualities as a sustainable material.
3. Despite its brittleness in tension, responses with sufficient deformation capacity can be achieved in TRC. Some potential approaches with this respect may consist on promoting failures in compression or designing members with high elastic-cracked deformation capacity.
4. The use of TRC in combination with non-corrosive concentrated reinforcement (in the form of glass-fibre reinforced polymer or high-strength stainless steel bars) is observed as a very promising solution. It allows to locally increase the load-carrying capacity in tension while maintaining low thicknesses and overall good workability.
5. TRC is particularly well-suited for prefabrication. Due to the low thicknesses, the pieces are light to be transported and assembled on site. Also, demountable, modular and reusable systems can be efficiently designed and constructed.
6. TRC has a high potential to merge with architectural needs, yielding to a proper and tailored architectural language.

Acknowledgements

The authors would like to sincerely acknowledge the support given by the association of the Swiss cement producers *cemsuisse* (research projects #201407 and #201801) for their financial support, providing the concrete mix and technical discussions. Also, the realisation of the prototype pavilion would not have been possible without the encouragement to interdisciplinary and financial support from the School of Architecture, Civil and Environmental Engineering (*ENAC exploratory grant*) at EPFL and the program *ENAC Design Together*.

Bibliography

- [1] Cyrille Simonnet. *Le béton. Histoire d'un matériau*. Parenthèses, Marseille, 2005. ISBN 9782953077902.
- [2] Silke Scheerer. Was ist Textilbeton: Eine kurze Einführung in das Thema. *Beton- und Stahlbetonbau*, 110:4–6, 2015.
- [3] Enrico Lorenz, Elisabeth Schütze, Frank Schladitz, and Manfred Curbach. Textilbeton - Grundlegende Untersuchungen im Überblick. *Beton- und Stahlbetonbau*, 108(10):711–722, 2013.
- [4] Alexander Scholzen, Rostislav Chudoba, Josef Hegger, and Norbert Will. Leichte Dachschalen aus Carbonbeton: Fertigteilproduktion, experimentelle Untersuchungen und Anwendungspotenzial. *Beton- und Stahlbetonbau*, 111(10):663–675, 2016.
- [5] S. Scheerer, R. Chudoba, M.P. Garibaldi, and M. Curbach. Shells Made of Textile Reinforced Concrete - Applications in Germany. *Journal of the International Association for Shell and Spatial Structures*, 58(1):79–93, 2017.
- [6] C. Meyer. The greening of the concrete industry. *Cement and Concrete Composites*, 31(8): 601–605, 2009.
- [7] P. Van Den Heede and N. De Belie. Environmental impact and life cycle assessment (LCA) of traditional and 'green' concretes: Literature review and theoretical calculations. *Cement and Concrete Composites*, 34(4):431–442, 2012.
- [8] Natalie Williams Portal, Karin Lundgren, Holger Wallbaum, and Katarina Malaga. Sustainable potential of textile-reinforced concrete. *Journal of materials in civil engineering*, 27(7): 04014207, 2015.
- [9] Alexander Scholzen, Rostislav Chudoba, and Josef Hegger. Thin-walled shell structures made of textile-reinforced concrete: Part I: Structural design and construction. *Structural Concrete*, 16:106–114, 2015.
- [10] Alexander Scholzen, Rostislav Chudoba, and Josef Hegger. Thin-walled shell structures made of textile-reinforced concrete: Part II: Experimental characterization, ultimate limit state assessment and numerical simulation. *Structural Concrete*, 16(1):115–124, 2015.
- [11] Harald Michler. Verstärken mit Carbonbeton im Brückenbau. In *26. Dresdner Brückenbausymposium*, pages 235–247, Dresden, 2016.
- [12] Christian Kulas. solidian GmbH. <https://www.solidian.com/en/references/>, 2019. [Online; accessed 22-November-2019].
- [13] Thorsten Helbig, Kay Unterer, Christian Kulas, Sergej Rempel, and Josef Hegger. Fuss- und Radwegbrücke aus Carbonbeton in Albstadt-Ebingen: Die weltweit erste ausschliesslich carbonfaserbewehrte Betonbrücke. *Beton- und Stahlbetonbau*, 111(10):676–685, 2016.
- [14] A. Liew, Y. R. Stürz, S. Guillaume, T. Van Mele, R. S. Smith, and P. Block. Active control of a rod-net formwork system prototype. *Automation in Construction*, 96(November 2016): 128–140, 2018.
- [15] Patrick Valeri, Patricia Guaita, Raffael Baur, and Miguel Fernández Ruiz. Pedagogy through artisanal construction of thin-walled concrete elements: a dialogue between engineering and architecture. In ACHE, editor, *Proceedings of the IV Int. Conference on Structural Engineering Education*, pages 1–10, Madrid, 2018. ACHE.

- [16] Enrico Lorenz. *Endverankerung und übergreifung textiler bewehrungen in betonmatrices*. PhD thesis, Technische Universität Dresden, 2014.
- [17] Jacopo Donnini, Valeria Corinaldesi, and Antonio Nanni. Mechanical properties of FRCC using carbon fabrics with different coating treatments. *Composites Part B*, 88:220–228, 2016.
- [18] Patrick Valeri, Miguel Fernández Ruiz, and Aurelio Muttoni. cemsuisse report 201407: Building in a lighter and more sustainable manner : textile reinforced concrete for thin structural elements. Technical report, IBETON, Ecole Polytechnique Fédérale de Lausanne, Lausanne, 2017.
- [19] Christian Kulas. *Zum Tragverhalten getränkter textiler Bewehrungselemente für Betonbauteile*. PhD thesis, RWTH, 2013.
- [20] Schöck Bauteile AG. Technische Information Schöck Combar ®. Technical report, Schöck Gruppe, Aarau, 2018.
- [21] DURAtec AG. GFK Gewindestangen, 2019. URL <https://www.duratec.ch/de/composites/gewindestangen-and-bundmuttern>.
- [22] Patrick Valeri, Miguel Fernández Ruiz, and Aurelio Muttoni. New perspectives for design of lightweight structures by using Textile Reinforced Concrete. In *fib symposium. Innovations in materials, design and structures*, page 8, Krakow, 2019.
- [23] Isabella Giorgia Colombo, Anna Magri, Giulio Zani, Matteo Colombo, and Marco di Prisco. Textile Reinforced Concrete: experimental investigation on design parameters. *Materials and Structures*, 46(11):1933–1951, 2013.
- [24] Elisa Bertolesi, Francesca Giulia Carozzi, Gabriele Milani, and Carlo Poggi. Numerical modeling of Fabric Reinforce Cementitious Matrix composites (FRCC) in tension. *Construction and Building Materials*, 70:531–548, 2014.
- [25] Matthias De Munck, Tine Tysmans, Jan Wastiels, Panagiotis Kapsalis, Jolien Vervloet, Michael El Kadi, and Olivier Remy. Fatigue behaviour of textile reinforced cementitious composites and their application in sandwich elements. *Applied Sciences (Switzerland)*, 9(7):19, 2019.
- [26] Patrick Valeri, Miguel Fernández Ruiz, and Aurelio Muttoni. Experimental research on Textile Reinforced Concrete for the development of design tools. In *Proceedings of the 12th International PhD Symposium in Civil Engineering*, pages 169–177, 2018.
- [27] Will Hawkins, John Orr, Tim Ibell, and Paul Shepherd. An Analytical Failure Envelope for the Design of Textile Reinforced Concrete Shells. *Structures*, 15(March):56–65, 2018.
- [28] Sophia Kueres, Norbert Will, and Josef Hegger. Flexural design of a modular footbridge system with pretensioned carbon fiber reinforced polymer reinforcement. *Structural Concrete*, (April):1–13, 2019.
- [29] Sebastian May, Harald Michler, Frank Schladitz, and Manfred Curbach. Lightweight ceiling system made of carbon reinforced concrete. *Structural Concrete*, 19(6):1862–1872, 2018.
- [30] N Williams Portal and K Lundgren. Numerical modelling of textile reinforced concrete. In *VIII International Conference on Fracture Mechanics of Concrete and Concrete Structures*, pages 1–12, 2013.
- [31] Zakaria Ilyes Djamai, Myriam Bahrar, Ferdinando Salvatore, Amir Si Larbi, and Mohammed El Mankibi. Textile reinforced concrete multiscale mechanical modelling: Application to TRC sandwich panels. *Finite Elements in Analysis and Design*, 135(June):22–35, 2017.

- [32] Stefan Voss. *Ingenieurmodelle zum Tragverhalten von textildbewehrtem Beton*. PhD thesis, Fakultät für Bauingenieurwesen der Rheinisch-Westfälischen Technischen Hochschule Aachen, 2008.
- [33] Charlton. *A History of the Theory of Structures in the Nineteenth Century*. Cambridge University Press, Cambridge, 2002.
- [34] Joyce Brown. W. B. Wilkinson (1819-1902) and his place in the History of Reinforced Concrete. *The International Journal for the History of Engineering & Technology*, pages 129–142, 2014.
- [35] Peter Collins. *Concrete: the vision of a new architecture*. McGill-Queen’s Press, 2004.
- [36] Hans Ramler. The Invention of Reinforced Concrete (1848 – 1906). In *High Tech Concrete: Where Technology and Engineering Meet - Proceedings of the 2017 fib Symposium*, pages 2786–2794, 2017.
- [37] Elisabetta Procida. Paul Cottancin, ingénieur, inventeur et constructeur. In *Édifice & Artifice. Histoires constructives*, pages 597–607, Paris, 2010. A. & J. Picard.
- [38] Douglas Mc Beth. Francois Hennebique (1842-1921), Reinforced Concrete Pioneer. In *Proceedings of the Institution of Civil Engineers - Civil Engineering*, pages 86–95, 2015.
- [39] Roberto Gargiani. *The rhetoric of Pier Luigi Nervi. Concrete and ferrocement forms*. EPFL Press, Lausanne, 2016.
- [40] Tullia Iori and Sergio Poretti. The golden age of “italian style” engineering. In *Third International Congress on Construction History, Brandenburg University of Technology Cottbus, Germany, 20th-24th May 2009*, page 1, 2009.
- [41] Daniel Busse and Martin Empelmann. Shear strength of thin-walled concrete members with micro-reinforcement. In *12th fib International PhD Symposium in Civil Engineering*, pages 337–344, Prague, 2018. fib.
- [42] Adalberto Vilela. *Architecture without Applause: The Manufactured Work of João Filgueiras Lima, Lelé*. PhD thesis, Eidgenössische Technische Hochschule Zürich, 2018.
- [43] Cristina Cândia Trigo. *Pré-fabricados em argamassa armada: material, técnica e desenho de componentes desenvolvidos por Lelé*. PhD thesis, Universidad de Sao Paulo, 2009.
- [44] Isa Grinspum Ferraz, Esequias Souza de Freitas, Stuart Birkinshaw, and Katica Szabó. *João Filgueiras Lima, Lelé*. Editorial Blau, 2000.
- [45] José Samuel Giongo. *Argamassa Armada dimensionamento de perfis submito a flexao*. PhD thesis, Universidade de Sao Paulo, 1990.
- [46] Francesca Perego. Argamassa armada: Textile Reinforced Concrete, social inclusion through technology and design. Master thesis, Politecnico di Milano, 2019.
- [47] Sergio K Ekerman. Ferrocement Prefabrication for Selfbuilt Areas : Factories And Casting Molds In The Work Of João Filgueiras Lima (1979-1989). In *12th International symposium on ferrocement and thin cement composites – Ferro 12*, pages 1–10, Belo Horizonte, 2018.
- [48] Sergio Kopinski Ekerman. *Tecnologia e Transformação Pré-fabricação para reestruturação de bairros populares e assistência técnica à autoconstrução*. PhD thesis, Universidade Federal da Bahia, 2018.
- [49] François Moulin. *Jean Prouvé. Le Maître du métal*. La Nuée Bleue, Strasbourg, 2001.
- [50] Peter Sulzer. *Jean Prouvé. Oeuvre complète/Complete Works*. Birkhauser, Basel, 1995.

-
- [51] Anna Rossellini. *Louis I. Kahn - towards the zero degree of concrete*. EPFL Press, Lausanne, 2014.
- [52] Luca Bellinelli and Louis Kahn. *The Construction of the Kimbell Art Museum*. Skiro Editore, Milano, 1999.
- [53] Aurelio Muttoni. *The art of structures*. EPFL Press, Lausanne, 2011.
- [54] Sergej Rempel. *Zur Zuverlässigkeit der Bemessung von biegebeanspruchten Betonbauteilen mit textiler Bewehrung*. PhD thesis, Rheinisch-Westfälischen Technischen Hochschule Aachen, 2018.

Chapter 5

General discussion

Textile Reinforced Concrete is a novel cementitious composite that allows building lightweight, durable and robust load-bearing structures. In this dissertation, TRC has been studied at different levels of analysis:

- The uniaxial response in tension has been investigated at the **micro-level**. In chapter 2, a comprehensive experimental campaign is illustrated, which has been used to derive a mechanical model that can be formulated in an analytical manner;
- Bending and shear of linear members, have been analysed at the **meso-scale**. Full-scale TRC members have been subjected to load-tests and instrumented with photogrammetry (Digital Image Correlation, [1, 2]). The results have allowed to validate the Elastic-Cracked-Stress-Field approach, which can be used for comprehensive modelling of TRC members (see chapter 3);
- And finally, the application potential has been studied in a broader manner at a **macro-scale**. Based on previous ferrocement works [3, 4], a new architectural language has been developed by integrating the peculiar structure of textile reinforcement fabrics. On that basis, in chapter 4, the design and construction of a full-scale pavilion entirely in TRC is reported.

In the next section, the findings of this research are discussed in a broader manner and the previous chapters are being correlated to each other.

5.1 Conclusions

TRC is a composite construction material made of high strength fabrics embedded in a high performance mortar. The material has been evolving rapidly during the last decades and is becoming a competitive alternative to traditional construction materials (especially for lightweight members, [5, 6]). TRC presents a series of analogies to ordinary Reinforced Concrete and ferrocement: the materials have a similar load-bearing mechanism (cracked and uncracked stages); and the reinforcement can be oriented and tailored with respect to the inner force demand. Consequently, within this thesis, similar approaches to structural concrete have been followed for the testing, modelling and design of TRC.

The major difference between the materials obviously consists in the reinforcement. While for ordinary steel rebars there exists well-established standards and prescriptions [7, 8], textile fabrics present a wide spectrum of mechanical properties [9]. First, the rovings constituting the fabrics are not homogeneous, but are made of bundles of fine filaments. Secondly, there exist uncoated, coated

and impregnated rovings with a variety of different impregnation materials and surface treatments (as for instance sand-coated surfaces). In addition, producers are starting to provide impregnated rovings with tailored shapes in order to increase their bond properties and reduce the required development length [10, 11]. Finally, to increase the efficiency of the reinforcement, filaments can also be stretched prior to impregnation of the rovings [12]. This wide range of properties is reflected in the material and structural behaviour. Consequently, a unified treatment is relatively demanding, and thus TRC can hardly follow conventional design prescriptions.

In this work, a unified approach for different types of reinforcement has been pursued:

- By means of a mechanical approach that considers the interaction between core and sleeve (inner and outer) filaments of the rovings at the **micro-level**;
- Based on the type of fabric and its anchorage conditions, the micro-analysis allows to derive integral efficiency factors for the reinforcement that can be implemented at the **meso** and **macro-scale**.

The analytical approaches proposed in this dissertation are funded on a comprehensive experimental campaign investigating the behaviour of TRC at the material and structural level. The **experimental findings** of this thesis summarise as follows:

- The high-performance mortars used in this research presents a linear-elastic response followed by brittle failure (in both, tension and compression). When reinforced with several layers of textile fabrics, the resistance in compression decreases and premature spalling of the concrete cover can be observed;
- The tensile behaviour of bare rovings depends on the material of the filaments, their assembly and coating or impregnation. When tested in tension, rovings can show a first hardening phase (corresponding to the removal their initial waviness) with a subsequent linear-elastic response, followed by brittle failure. Cyclic loading tests have confirmed that once the initial undulation is removed, the response of the fabric follows a linear-elastic unloading- and reloading path;
- Also the bond properties result to be severely influenced by the fabric properties. In general, the interface between rovings and matrix is governed by an adhesive and frictional component (in contrast to ordinary reinforced concrete, where bond stresses are transferred by the mechanical actions of ribs). The conducted pull-out tests have shown that coated fabrics with a smooth surface (for example Stereo Butene Rubber) have relatively poor bond properties. The adhesive bond can be significantly improved by providing the rovings with a sand coated surface. In addition, some manufacturers are exploring the possibility to tailor the shape of the impregnation in order to add a mechanical component to the bonding actions. Novel pull-out tests have shown that transverse stresses have little or no influence on the interface properties (specifically, no improvement of bond strength could be observed);
- TRC is made of fabrics that are embedded in a mortar matrix. The uniaxial tensile response of TRC consists of three stages (uncracked, cracking, and stabilised cracking phase). Stage I is mainly governed by the mortar, while stages II and III are governed by the fabric reinforcement:
 - The results of the present experimental campaign (section 2.3) have shown that a distributed cracking-pattern with narrow crack spacings develops in TRC subjected to tension. The distance between cracks is strongly influenced by the grid spacing of the fabric and the reinforcement ratio;
 - Due to the narrow crack pattern, crack-openings are fairly limited leading to an excellent material behaviour at service-ability;

- The stiffness in the cracked stage is dictated by the reinforcement ratio and the properties of the fabric (geometry, coating, impregnation). With respect to bare rovings, a softer response has been observed for the TRC composites subjected to tension. In general the stiffness appears to be variable (softening, constant or hardening) as a function of the reinforcement type.
- Failure in tension occurs suddenly and without premonitory signs (wide crack openings or plastic deformations). In section 2.3 different failure types have been observed, once again, corresponding to different types of reinforcement (for the given boundary conditions and development length);
- The flexural behaviour has been investigated on several thin-walled flanged members in TRC, tested in three-point-bending. The sectional bending response (in terms of moment-curvature, see sections 3.2 and 4.3) is mainly governed by the linear elastic behaviour of the mortar in compression and the tri-linear response of TRC in tension. The flexural strength and deformation capacity can be increased by adding concentrated reinforcement in the tension flange:
 - Similarly to tension ties, also flexural members develop a narrow crack pattern that is mainly controlled by the fabric reinforcement and the spacing between transverse rovings;
 - All elements tested within this research presented a sufficiently high reinforcement ratio in order to develop distributed cracking prior to failure. Consequently, small crack openings have been observed in the stabilised cracking stage and prior to failure;
 - The cracked flexural stiffness mainly depends upon the stiffness of the cracked TRC composite in the tension chord;
- The observed flexural failures have occurred due to: (a) rupture of the tensile reinforcement; (b) crushing of the compression chord; (c) local buckling of the compression flange; (d) rupture of the reinforcement at the anchorage; and (e) crushing of the web combined to the delamination between the web and the flanges;

In several tests, the force-strain response as well as the development of the cracking patterns has been traced with detailed photogrammetric measurements and analysed with Digital Image Correlation. That allows to measure the principal strains (direction and magnitude) during the loading process and at failure (refer to specimens BV1 and BV2 in section 3.2).

Based on previous researches, the current state of the art and the experimental observations of the present experimental campaign, new modelling approaches have been derived. These deal with the tensile response of TRC at the **micro-level** and the flexural behaviour at a **meso-scale**. The **theoretical findings** of this research can be summarised as follows:

- The response of single rovings in tension can be approximated by a bi-linear stress-strain relationship. A simplification can be performed, by considering a linear-elastic response with delayed activation. That can be taken into account by an initial strain ε_0 (see also [13]);
- Likewise, also the behaviour of the mortar matrix can be accurately approximated by a linear-elastic stress-strain relationship with brittle failure (for both, tension and compression). For numerical purposes (as for example Elastic-Plastic-Stress-Field analysis), also an elastic-plastic relationship, combined with a reduced plastic strength and a tension cut-off has shown to yield consistent results;
- The experimental findings have shown that, the tensile response of TRC is somewhat different to that of the bare rovings. That is mainly due to differences in load-introduction of tensile

forces: bond (adhesion and friction) for embedded rovings, and friction with significant transverse pressure in single roving tests. Consequently, for an appropriate representation of the tensile load-bearing behaviour rovings cannot be considered to be homogeneous.

In this dissertation, the coaxial ring analogy has been used to model the behaviour of TRC at the **micro-scale** (separate treatment of core and sleeve filaments, [14, 15]). Within this framework different constitutive and interface laws have been investigated (activation strain for core filaments and delayed activation of bond stresses). Eventually it was found that the following set of assumptions allow to accurately predict the tensile response of Textile Reinforced Concrete for any degree of fabric impregnation:

- Linear-elastic response for sleeve and core filaments;
- Rigid-plastic interface response between sleeve filaments and mortar matrix;
- Delayed rigid-plastic interface behaviour between sleeve and core filaments.

It is considered that an engagement slip (δ_A) is necessary, in order to activate the inter-laminar bond stresses between inner and outer filaments (*bond-lag*).

These constitutive laws allow to derive a mechanical description of TRC subjected to uniaxial tension that can be formulated in an analytical manner. The present experimental campaign has allowed to calibrate the model parameters: engagement slip (δ_A); core-to-sleeve bond stress (τ_{rc}); sleeve-to-core filaments ratio (k). With these parameters, the model shows to accurately reproduce the experimental load-strain response and resistance of TRC ties. A systematic comparison of the approach to 49 independent tests performed by other researchers confirms the soundness of the approach (average measured-to-calculated strength of 1.02 and a coefficient of variation of $\text{CoV} = 0.11$). In addition, also the experimentally observed failure mechanisms are reproduced with a certain degree of accuracy (stress concentrations in sleeve filaments close to the anchorage region).

Finally, the effects of the modelling assumptions have been investigated on a series of theoretical limit cases: variation of tie length; variation of load introduction length; and degree of fabric impregnation.

Accounting for *bond-lag* phenomena provides a reliable tool to understand the load-bearing mechanism of TRC at the **micro-level**. However, when considering more complex loading conditions, its implementation results to be relatively manifold;

- In order to adequately model realistic loading situations, a **meso-scale** approach has been pursued. For linear members subjected to bending and shear, the reinforcement is considered in a homogeneous manner but with the following peculiarities:
 - Linear-elastic response of rovings in tension;
 - No contribution of the fabric reinforcement to compression [16, 17];
 - The effective fabric area is reduced by means of an efficiency factor k_e [18, 19, 20];
 - Reduced resistance of the fabric according to its anchorage condition by considering an efficiency factor η_b [21];

In addition, the compression-softening behaviour for concrete can be modelled locally according to the Modified Compression Field Theory [22]. On the other hand, also a global approach may be implemented as for instance performed in Model-Code [7].

These assumptions allow a more accessible modelling of TRC flexural members;

- The experimental observations have shown a clear analogy between the measured principal strains and the Elastic-Cracked-Stress-Field (ECSF) modelling approach (comprising constant-angle-stress-fields and fan regions). On that basis, the ECSF approach [23, 24], has

been extended for TRC-linear members by considering the simplified material behaviour of the fabric reinforcement mentioned above:

- For bending the ECSF approach leads to consistent results with a plane section-analysis;
- For shear-panels (for instance webs in beams), the ECSF allows to accurately predict the inclination of compression field (which depends on the geometry, reinforcement and strain-state). On that basis, the maximum shear capacity of the member can be calculated by considering independently the crushing of the compression field and failure of transverse reinforcement;
- As observed experimentally, premature spalling of the concrete cover may reduce the shear strength of the compression field (see also [10, 25]). That is accounted for, by considering a reduced thickness of the web.

Consequently, the ECSF approach allows to model beam- and discontinuity regions in a comprehensive manner (accounting for both, bending and shear) as well as predicting the response under serviceability conditions and at failure in a unified way. Moreover, the equations derived in section 3.3 allow to calculate the inclination of the compression field in an analytical way. In addition, also a numerical implementation has been performed based on Finite Elements [26]. Both approaches show fine and sound agreement when compared to the test results obtained from the experimental programme.

In addition to the tests performed in this experimental campaign, 17 other tests available in the scientific literature have been considered. The data-basis, consists of 18 linear TRC members failing in shear and comprising different reinforcement types. The results show that the ECSF approach is a relatively reliable tool that can be used to predict the shear strength of linear members in a unified manner (average measured-to-calculated strength of 1.04 and a coefficient of variation of $\text{CoV} = 0.13$).

From a broader point-of-view, TRC presents relatively limited construction experience with respect to other, well-established, construction materials [27, 28]. That is also related to the fact that TRC is a high performance material and consequently the conceptual design of TRC structures needs to account for material minimisation and optimisation [29]. Consequently TRC is particularly suitable for the construction of thin-walled folded members and shell structures. In chapter 4, the application potential of TRC has been investigated at the **macro-level**, based on a series of construction experiences. The experimentation with different formworking materials and casting methods has been performed within a series of practical courses, workshops and master projects. The knowledge acquired within the four year teaching programmes (2015 - 2019) was condensed to build a full-scale, prototype pavilion entirely in TRC. The latter was designed, build and erected by a group of 24 students within a three-weeks workshop. From this experience and the know-how gained from others projects (see section 1.3 in chapter 1), the following can be summarised:

- Textile Reinforced Concrete is suitable to build structural members and load-bearing structures. These are likely to be composed by, thin-walled, flanged members and ribbed shell-elements which represent the most competitive application of TRC. Within the mentioned workshop, shell-elements with a thickness below 10 mm have been achieved;
- The implementation of re-usable casting-moulds is imperative for a cost-effective production of TRC components. In the present research, it was found that thin steel plates are particularly suited for the fast assembly of folded formworks. These present adequate precision to control the minimal thickness of the members, but are also sufficiently flexible to relief demoulding after concrete hardening. The folded sheets can be combined with timber or aluminium ribs to rigidify the formwork where needed, and stainless-steel sheets can be implied in order to achieve extremely long-lasting casting moulds.

While the geometry of elements presenting single curvature can be controlled by means of metal sheets, double curved concrete structures require more complex formworks. In this research it was found that flexible formworks (for example geotextile fabrics) can be used to cast double-curved shells in TRC (by means of the lamination process);

- A drastic reduction of structural self-weight is the excellence of TRC. In detail, that allows to build structural elements that can be moved without heavy-weight site equipment (as for instance cranes). This aspect has been stretched to the limit in the prototype pavilion, where all elements can be transported by two persons (four for the barrel-shell vaults);
- Taking advantage of the lightweight members, the concept of modular demountable structural systems has been pursued in this research. That has mainly been implemented in the prototype pavilion by means of bolted connections. It allows to build more resilient structures, where single elements can be replaced once their design life-time is reached or when an increase in load-bearing capacity is necessary (for instance due to a change of use).

Under considerations of these aspects and based on previous ferrocement works a legitimate architectural language has been developed for TRC comprising prefabricated modular elements.

5.2 Outlook

The works presented in this dissertation, seek to improve the current state-of-the-art [30, 31], but still new findings tend to open new questions. Following the results depicted in the previous section a series experimental and theoretical works are suggested below, to validate and extend the findings of the present research:

- The mechanical characterisation of the fabrics was performed on isolated rovings clamped with conventional or capstan grips. For some fabrics, a relative high level of scatter was observed for the strength and stiffness (especially when compared to the values of conventional steel reinforcement). However, the level of scatter varies significantly for different fabrics, which suggests that a standardised testing procedure may not be the finest solution for the characterisation of fabrics with extremely different properties. Consequently, further experimental investigations are highly recommended in order identify suitable testing methods for a comprehensive mechanical characterisation of rovings and fabric reinforcements;
- To strengthen the theoretical findings depicted in section 2.6, an additional experimental programme on TRC tension ties should be performed. This should focus on comparing different tie- and load-introduction lengths as well as different degrees of fabric coatings;
- Recently new measurement techniques based on fibre optics have been developed and are starting to be commercially available [32, 33, 34]. These allow to perform local strain measurements along the axis of the optical fibre. Where possible, such fibres should be incorporated in- and on the surface of rovings (multi-filament-yarns). That would allow to investigate the stress-profile of rovings in an experimental manner. Particular attention could also be dedicated to the variation of the stress profile along the axis of the rovings. That would allow to better understand the stress transfer mechanisms as a function of the anchorage conditions;
- The model proposed in section 2.4 is to be extended for cases of bi-axial and inclined loading conditions (applied tensile forces not parallel to rovings, [15, 35, 36]). For this purpose further theoretical works are necessary that are to be based on additional experiments;
- With respect to the shear strength of linear TRC members, a series of different experimental works are still required:

- A series of full-scale tests on linear members with shorter shear spans [37, 38, 39]. That would allow to investigate on the effects provided by direct arching action, validate the Elastic-Cracked-Stress-Field approach and to extent the database;
- Further full-scale tests with different ratios of transverse reinforcement. These can be used to understand the limits of applicability of the Elastic-Cracked-Stress-Field approach (which assumes distributed cracking);
- Further compression tests on TRC prisms and where possible combined with transverse tension [16, 17, 40, 41]. Such tests would allow to better understand the influence of discontinuity planes in compression zones created by textile fabrics;
- Also, the implementation of the ECSF framework in a numerical tool would be particularly interesting [42, 43]. That would provide simpler access to the ECSF-analysis for a broader community of designers and practitioners;
- Finally, the investigations on the application potential are foreseen to continue in the upcoming years. The planned works aim to complete and enlarge the TRC prototype pavilion (see chapter 4):
 - Addition of floor slabs on top of the existing base-frame. It is currently under investigation weather slab-strips or bidirectional slabs are more suitable. Moreover it is to be investigated if these elements are flat or ribbed and the best way to realise the connection to the existing structure;
 - The formworks for the barrel-shell-vaults will be revised in order to improve the surface quality. For that purpose a double sided (closed) mould is necessary and the casting method has to be changed from lamination to pouring. Within the performed works, casting TRC elements thinner than 20 mm with the pouring method has proven to be extremely manifold. That threshold should be reduced in order to produce more cost-efficient elements with high finishing qualities;
 - Finally, some sides of the pavilion may be closed by means of precast wall panels.

The investigations proposed here above are in direct relation to the works performed in this dissertation. However, from a broader perspective, a series of additional topics should also be addressed:

- First of all, a series of systematic studies on the **anchorage behaviour** of fabric reinforcement should be performed [44, 45, 46]. In particular, comparing straight with folded anchorages, as well as investigating the effects of different folding radii [47, 48]. Along these lines, also the associated transverse pressure needs to be quantified, in order to prevent concrete spalling [49, 50]. In addition, the reinforcement cannot always be anchored in undisturbed zones. Thus, it is necessary to understand the effect of transverse tension or compression on the development length of rovings (for instance flanges of linear members, [51, 51]). On that basis, a more general formulation of the behaviour of D-regions should be derived (perhaps by extending the ECSF framework). These aspects are fundamental for the practical application of TRC and the development of **detailing prescriptions**;
- As mentioned earlier, one of the highlights of TRC is the possibility to build very-thin walled elements. In general, these are more prone to **local instability** (for instance buckling of compression flanges in beams or columns, [52, 53]). Experimental and theoretical works are required to investigate on the load bearing capacity and to understand the limitations of current formulations. Special attention may be dedicated to premature spalling of concrete cover in the compression zone;
- More **complex loading conditions** than the ones studied in this research are not uncom-

mon. These comprise for instance bi-axial bending combined with torsion as well as in and out-of-plane shear [54, 55]. That could for instance be the case for thin-walled shell structures. It is suggested to perform experimental and theoretical studies to investigate the interaction of these combined loading conditions and develop suitable design procedures;

- Textile reinforcement usually consist of non-corrosive fabrics characterised by a linear-brittle response in tension without plastic behaviour. Consequently, the theory of plasticity is not directly applicable for the design of TRC load bearing structures (as usually performed in conventional reinforced concrete structures, [56, 57]).

In **statically redundant structures** internal forces redistribute as soon as cracks start to appear (in other words, the distribution of internal forces deviates from the elastic prediction). In particular, bending moments will redistribute in the structure as a function of the flexural reinforcement ratios. Therefore, only a non-linear analysis can accurately predict the structural resistance (ultimate load). For this reason, future research should also focus on statically redundant systems and identify suitable design procedures for such structures;

- There exist relatively limited experimental knowledge on the **time-dependent behaviour** of TRC. Time effects, such as creep and shrinkage, may result dominant parameters that need to be considered at the serviceability limit state (often resulting as governing in the design-stage). In detail, particular focus may be dedicated to thin-walled elements, as these may dry faster with respect to massive concrete elements and could show higher sensitivity to time effects [58, 59];
- The **cyclic loading and fatigue** behaviour has been mainly investigated on tension ties [60, 61, 62] and represented with numerical tools [63, 64]. Further experimental investigations should be carried out at a larger scale to foster potential damaging effects under different loading conditions and to derive analytical formulations accounting for cyclic loading;
- For the establishment of a comprehensive normative background, a series of related topics also require further research. These include:
 - Investigations on the load-bearing behaviour of TRC under **elevated temperatures** to provide prescriptions regarding fire-safety of TRC members [65, 66, 67]. In detail, non-metallic materials may present relatively good heat-resistance (for instance, bare carbon does not melt below 3550°C and barely no reduction of its strength occurs at temperatures below 200°C [68]). However rovings are often coated and impregnated by means of an epoxic material, that is characterised by a glass transition temperature T_g that can be already lower than 100°C [69];
 - Despite previous research efforts [70, 71], more knowledge regarding **structural reliability** of TRC load bearing members is strictly required in order to derive a unified safety format [72, 73]. Major efforts have been dedicated to the model-uncertainty of members failing in bending. However, also other failure mechanisms should be considered (as for instance shear or more complex loading conditions). In addition, a comparative study of different reinforcements should be addressed (comprising uncoated, coated and impregnated fabrics);
 - Additional investigations may also concern the **durability** of Textile Reinforced Concrete with special focus on the reinforcement and potential degradation of its coating or impregnation [74];

- Finally, further investigations should consider adding a certain level of prestress to TRC. That can be achieved by means of prestressing directly the reinforcement [75, 76] or by adding ferritic Shape Memory Alloys [77] which are particularly suited to prestress thin-

walled concrete members (activation of prestressing integrated within a high-temperature curing process, [78, 79]). These methods would allow to increase the resistance of TRC members as well as their performance under serviceability conditions.

The suggested works, in addition to other studies should be carried-out in parallel to the future evolution of the material. The latter might be driven by the construction industry, but should be incorporated in future investigations, which need to account for a rapidly evolving composite material.

Bibliography

- [1] Analysis of the tensile response of textile reinforced concrete using digital image correlation technique combined with multi-scale stochastic modelling. In *11th International Symposium on Ferrocement (FERRO-11) and 3rd International Conference on Textile Reinforced Concrete (ICTRC-3)*, pages 141–148. RILEM Publications SARL, 2015.
- [2] Bora Gencturk, Kazi Hossain, Aadit Kapadia, Emad Labib, and Yi-Lung Mo. Use of digital image correlation technique in full-scale testing of prestressed concrete structures. *Measurement*, 47:505–515, 2014.
- [3] Pier Luigi Nervi. *Costruire correttamente: caratteristiche e possibilità delle strutture cementizie armate*. U. Hoepli, 1955.
- [4] Isa Grinspum Ferraz, Esequias Souza de Freitas, Stuart Birkinshaw, and Katica Szabó. *João Filgueiras Lima, Lelé*. Editorial Blau, 2000.
- [5] Philipp Preinstorfer, Benjamin Kromoser, and Johann Kollegger. Flexural behaviour of filigree slab elements made of carbon reinforced UHPC. *Construction and Building Materials*, 199: 416–423, 2019.
- [6] Patrick Valeri, Patricia Guaita, Raffael Baur, Miguel Fernández Ruiz, David Fernández-Ordóñez, and Aurelio Muttoni. Textile reinforced concrete for sustainable structures: Future perspectives and application to a prototype pavilion. *Structural Concrete*, 2020.
- [7] fib (The International Federation for Structural Concrete). *fib Model Code for concrete structures 2010*. Ernst und Sohn Verlag Germany, 2013.
- [8] *EN 1992-1-1 Eurocode 2: Design of concrete structures - Part 1-1: General rules and rules for buildings*, Brussels, 2005. EN, CEN.
- [9] Chokri Cherif. *Textile materials for lightweight constructions: Technologies - methods - materials - properties*. Springer, 2016.
- [10] Philipp Preinstorfer and Johann Kollegger. New insights into the splitting failure of textile-reinforced concrete. *Composite Structures*, page 112203, 2020.
- [11] Christian Kulas. solidian GmbH. <https://www.solidian.com/en/references/>, 2019. [Online; accessed 22-November-2019].
- [12] J Bielak, J Hegger, and M Schmidt. Shear capacity of carbon fibre textile reinforced concrete slabs with planar and c-shaped shear reinforcement. In *FRPRCS-14*, volume 14, pages 1–5. Queen’s University Belfast, 2019.
- [13] Yiska Goldfeld. Structural modelling of textile-reinforced concrete elements under uniaxial tensile loading. *Composite Structures*, 235:111805, 2020.
- [14] S. Ohno and D. J. Hannant. Modeling the Stress-Strain Response of Continuous Fiber Reinforced Cement Composites. *ACI Materials Journal*, 91(3):306–312, 1994.
- [15] J Hegger, N Will, Oliver Bruckermann, and Stefan Voss. Load-bearing behaviour and simulation of textile reinforced concrete. *Materials and structures*, 39(8):765–776, 2006.
- [16] Jakob Bochmann, Manfred Curbach, and Frank Jesse. Carbonbeton unter einaxialer druckbeanspruchung: Ergebnisse systematischer experimenteller untersuchungen. *Beton-und Stahlbetonbau*, 112(5):293–302, 2017.

- [17] Jakob Bochmann, Manfred Curbach, and Frank Jesse. Carbonbeton unter druck: Teil 2: Einfluss von bewehrungsgeometrie und-anordnung. *Beton-und Stahlbetonbau*, 113(1):22–32, 2018.
- [18] Christian Kulas. *Zum Tragverhalten getränkter textiler Bewehrungselemente für Betonbauteile*. PhD thesis, RWTH, 2013.
- [19] Josef Hegger, Wolfgang Brameshuber, and Norbert Will. Textile Reinforced Concrete. In *1st international RILEM Symposium*, page 406, Aachen, 2006. RILEM.
- [20] Diana Arboleda, Francesca Giulia Carozzi, Antonio Nanni, and Carlo Poggi. Testing procedures for the uniaxial tensile characterization of fabric-reinforced cementitious matrix composites. *Journal of Composites for Construction*, 20(3):04015063, 2016.
- [21] Isabella Giorgia Colombo, Anna Magri, Giulio Zani, Matteo Colombo, and Marco Di Prisco. Textile reinforced concrete: experimental investigation on design parameters. *Materials and structures*, 46(11):1953–1971, 2013.
- [22] F J Vecchio and M P Collins. The modified compression-field theory for reinforced concrete elements subjected to shear. *ACI Structural Journal*, pages 219–231, 1986.
- [23] H Kupfer. Erweiterung der Mörsch’schen Fachwerkanalogie mit Hilfe des Prinzips vom Minimum der Formänderungsarbeit. Technical Report 40, Comité Euro-International du Béton (CEB), Paris, France, 1964.
- [24] Aurelio Muttoni, Joseph Joseph, Schwartz, and Bruno Thürlimann. *Design of Concrete Structures with Stress Fields*. Birkhäuser Verlag, 1996.
- [25] Benjamin Kromoser, Patrick Huber, and Philipp Preinstorfer. Experimental study of the shear behaviour of thin walled CFRP reinforced UHPC structures. *5th International fib Congress Melbourne*, 2016.
- [26] Miguel Fernández Ruiz and Aurelio Muttoni. On Development of Suitable Stress Fields for Structural Concrete. *ACI Structural Journal*, 104:495–502, 2007.
- [27] J Hegger, M Zell, and M Horstmann. Textile reinforced concrete–realization in applications. In *Proceedings: international fib symposium tailor made concrete structures: new solutions for our society*, pages 357–362, 2008.
- [28] S. Scheerer, R. Chudoba, M.P. Garibaldi, and M. Curbach. Shells Made of Textile Reinforced Concrete - Applications in Germany. *Journal of the International Association for Shell and Spatial Structures*, 58(1):79–93, 2017.
- [29] Will Hawkins, John Orr, Tim Ibell, and Paul Shepherd. A design methodology to reduce the embodied carbon of concrete buildings using thin-shell floors. *Engineering Structures*, 207: 110195, 2020.
- [30] Wolfgang Brameshuber. Textile Reinforced Concrete. State-of-the-Art Report. Technical report, RILEM Technical Committee TC201-TRC, Aachen, 2009.
- [31] Alva Peled, Arnon Bentur, and Barzin Mobasher. *Textile Reinforced Concrete - Modern Concrete Technology*. Boca Raton : CRC Press, Taylor & Francis Group, 1st edition edition, 2017. ISBN 9780367866914.
- [32] Farhad Ansari. State-of-the-art in the applications of fiber-optic sensors to cementitious composites. *Cement and Concrete Composites*, 19(1):3–19, 1997.

- [33] Mohamed Saidi and Aron Gabor. Use of distributed optical fibre as a strain sensor in textile reinforced cementitious matrix composites. *Measurement*, 140:323–333, 2019.
- [34] LUNA. Luna Inc. <https://lunainc.com>, 2019. [Online; accessed 10-April-2020].
- [35] Stefan Voss. *Ingenieurmodelle zum Tragverhalten von textildbewehrtem Beton*. PhD thesis, Fakultät für Bauingenieurwesen der Rheinisch-Westfälischen Technischen Hochschule Aachen, 2008.
- [36] Raphaël Contamine, Angel Junes, and Amir Si Larbi. Tensile and in-plane shear behaviour of textile reinforced concrete: Analysis of a new multiscale reinforcement. *Construction and Building Materials*, 51:405–413, 2014.
- [37] Darko Tasevski, Miguel Fernández Ruiz, and Aurelio Muttoni. Influence of load duration on shear strength of reinforced concrete members. *ACI Structural Journal*, 117(2):157–170, 2020.
- [38] Boyan I Mihaylov, Bradley Hunt, Evan C Bentz, and Michael P Collins. Three-parameter kinematic theory for shear behavior of continuous deep beams. *ACI Structural Journal*, 112(1):47, 2015.
- [39] Jian Liu and Boyan I Mihaylov. A comparative study of models for shear strength of reinforced concrete deep beams. *Engineering Structures*, 112:81–89, 2016.
- [40] Frank J Vecchio and Michael P Collins. Compression response of cracked reinforced concrete. *Journal of structural engineering*, 119(12):3590–3610, 1993.
- [41] Ji-Hyung Lee, Sung-Gul Hong, Changbin Joh, Imjong Kwahk, and Jung-Woo Lee. Biaxial tension–compression strength behaviour of uhpfr in-plane elements. *Materials and structures*, 50(1):20, 2017.
- [42] Jaime Mata-Falcón, Duc Thong Tran, Walter Kaufmann, and Jaroslav Navrátil. Computer-aided stress field analysis of discontinuity concrete regions. *Proc., Computational Modelling of Concrete and Concrete Structures (EURO-C 2018)*, pages 641–650, 2018.
- [43] Miguel Fernández Ruiz, Aurelio Muttoni, and Olivier Burdet. Computer-aided development of stress fields for the analysis of structural concrete. In *fib Symposium, Dubrovnik 2007*, pages 591–598. fib Symposium, Dubrovnik 2007, 2007.
- [44] Enrico Lorenz. *Endverankerung und übergreifung textiler bewehrungen in betonmatrices*. PhD thesis, Technische Universität Dresden, 2014.
- [45] John Cairns et al. *Bond and anchorage of embedded reinforcement: Background to the fib Model Code for Concrete Structures 2010: Technical report*, volume 72. fib-Fédération internationale du béton, 2014.
- [46] Fabio Brantschen. Influence of bond and anchorage conditions of the shear reinforcement on the punching strength of rc slabs. Technical report, EPFL, 2016.
- [47] Otto Graf. *Versuche über die Widerstandsfähigkeit des Betons an den Abbiegestellen der schief abgebogenen Eisen in Eisenbetonbalken*. Ernst, 1933.
- [48] Fritz Leonhardt, René Walther, and Hannes Dieterle. Versuche zur ermittlung der tragfähigkeit von zugschlaufenstößen. *Deutscher Ausschuss für Stahlbeton*, (226), 1973.
- [49] John Minor and James O Jirsa. Behavior of bent bar anchorages. In *Journal Proceedings*, volume 72, pages 141–149, 1975.

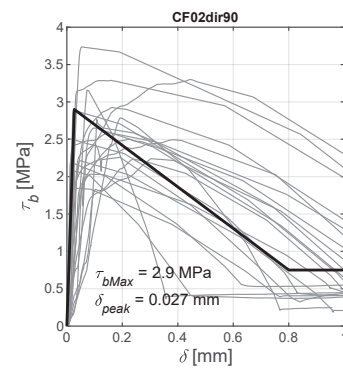
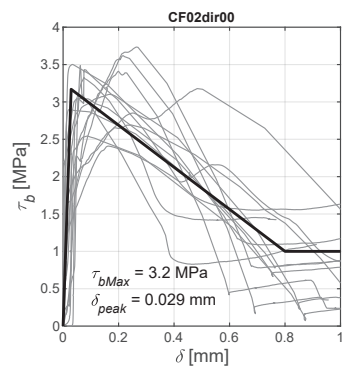
- [50] Ricardo Costa, Paulo Providência, and Alfredo Dias. Anchorage models for reinforced concrete beam-column joints under quasi-static loading. *ACI Structural Journal*, 113(3), 2016.
- [51] PG Gambarova and B Zasso. Aderenza armatura-calcestruzzo e fessurazione longitudinale da spacco: una sintesi di alcuni recenti risultati sperimentali. *Studi e ricerche—Corso di perfezionamento per le costruzioni in cemento armato Fratelli Pasenti*, (7):7–54, 1985.
- [52] A Siev. The lateral buckling of slender reinforced concrete beams. *Magazine of Concrete Research*, 12(36):155–164, 1960.
- [53] P Revathi and Devdas Menon. Estimation of critical buckling moments in slender reinforced concrete beams. *ACI Structural Journal*, 103(2):296, 2006.
- [54] Marie-Rose Backes, Miguel Fernández Ruiz, and Aurelio Muttoni. Interaction between in-plane shear forces and transverse bending moments in concrete bridge webs. In *Proc. of the 10th fib International PhD Symposium in Civil Engineering, Quebec*, pages 403–408. Proc. of the 10th fib International PhD Symposium in Civil Engineering, Quebec, 2014.
- [55] Maria Anna Polak and Frank J Vecchio. Reinforced concrete shell elements subjected to bending and membrane loads. *ACI Structural Journal-American Concrete Institute*, 91(3):261–268, 1994.
- [56] Aurelio Muttoni. *Die Anwendbarkeit der Plastizitätstheorie in der Bemessung von Stahlbeton*. Birkhäuser Verlag, Institut für Baustatik und Konstruktion ETH Zürich, 1990.
- [57] Mogens Peter Nielsen and Linh Cao Hoang. *Limit analysis and concrete plasticity*. CRC press, 2016.
- [58] Raymond Ian Gilbert and Gianluca Ranzi. *Time-dependent behaviour of concrete structures*. CRC Press, 2010.
- [59] Darko Tasevski, Miguel Fernández Ruiz, and Aurelio Muttoni. Compressive strength and deformation capacity of concrete under sustained loading and low stress rates. *Journal of Advanced Concrete Technology*, 16(8):396–415, 2018.
- [60] Flávio de Andrade Silva, Marko Butler, Viktor Mechtcherine, Deju Zhu, and Barzin Mobasher. Strain rate effect on the tensile behaviour of textile-reinforced concrete under static and dynamic loading. *Materials Science and Engineering: A*, 528(3):1727–1734, 2011.
- [61] Z Mesticou, L Bui, A Junes, and A Si Larbi. Experimental investigation of tensile fatigue behaviour of textile-reinforced concrete (trc): Effect of fatigue load and strain rate. *Composite Structures*, 160:1136–1146, 2017.
- [62] Matthias De Munck, Tine Tysmans, Jan Wastiels, Panagiotis Kapsalis, Jolien Vervloet, Michael El Kadi, and Olivier Remy. Fatigue behaviour of textile reinforced cementitious composites and their application in sandwich elements. *Applied Sciences (Switzerland)*, 9(7):19, 2019.
- [63] Martin Konrad, Rostislav Chudoba, and Bong-Gu Kang. Numerical and experimental evaluation of damage parameters for textile reinforced concrete under cyclic loading. In *III European Conference on Computational Mechanics*, pages 367–367. Springer, 2006.
- [64] Aurelio Muttoni and Miguel Fernández Ruiz. Concrete cracking in tension members and application to deck slabs of bridges. *Journal of Bridge Engineering*, 12(5):646–653, 2007.
- [65] VKR Kodur and M Dwaikat. A numerical model for predicting the fire resistance of reinforced concrete beams. *Cement and Concrete Composites*, 30(5):431–443, 2008.

- [66] D Ehlig, F Jesse, and M Curbach. High temperature tests on textile reinforced concrete (trc) strain specimens. In *International RILEM Conference on Material Science*, pages 141–151. RILEM Publications SARL, 2010.
- [67] Isabella Colombo, Matteo Colombo, Anna Magri, Giulio Zani, and Marco di Prisco. Textile reinforced mortar at high temperatures. In *Applied mechanics and materials*, volume 82, pages 202–207. Trans Tech Publ, 2011.
- [68] F Durand, D Rouby, G Fantozzi, B Allard, and D Dumas. Characterization of the high-temperature mechanical behaviour of carbon materials. *Carbon*, 32(5):857–865, 1994.
- [69] Moyeenuddin Ahmad Sawpan, Peter G Holdsworth, and Peter Renshaw. Glass transitions of hygrothermal aged pultruded glass fibre reinforced polymer rebar by dynamic mechanical thermal analysis. *Materials & Design*, 42:272–278, 2012.
- [70] Ulrich Häußler-combe, Jörg Weselek, and Frank Jesse. A Safety Concept for Non-Metallic Reinforcement for Concrete under Bending. *ACI Structural Journal*, (116):151–160, 2019.
- [71] Sergej Rempel. *Zur Zuverlässigkeit der Bemessung von biegebeanspruchten Betonbauteilen mit textiler Bewehrung*. PhD thesis, Ph. D. Thesis, RWTH Aachen University, Aachen, Germany, 2018.
- [72] Jörg Schneider. *Introduction to safety and reliability of structures*, volume 5. Iabse, 2006.
- [73] CEN TC250. Sc2: Eurocode 2–commentary. *European Concrete Platform*, 2008.
- [74] J. Orlowsky and M. Raupach. Durability model for AR-glass fibres in textile reinforced concrete. *Materials and Structures/Materiaux et Constructions*, 41(7):1225–1233, 2008.
- [75] Raymond Ian Gilbert, Neil Colin Mickleborough, and Gianluca Ranzi. *Design of prestressed concrete to Eurocode 2*. CRC Press, 2017.
- [76] HW Reinhardt and M Krüger. Vorgespannte dünne platten aus textilbeton. *Textilbeton–1. Fachkolloquium der Sonderforschungsbereiche*, 528:165–174, 2001.
- [77] Yutaka Moriya, Tetsuya Sanpei, and Hisatoshi Tagawa. Iron-based shape-memory alloy excellent in shape-memory property and corrosion resistance, May 29 1990. US Patent 4,929,289.
- [78] Benjamin Kromoser, Emanuel Strieder, and Johannes Kirnbauer. Self post-tensioning ultra-high performance concrete elements the activation of with iron based shape memory alloys reinforced uhpc elements by thermal follow up treatment. *BETON-UND STAHLBETONBAU*, 114(5):315–326, 2019.
- [79] K Moser, A Bergamini, R Christen, and C Czaderski. Feasibility of concrete prestressed by shape memory alloy short fibers. *Materials and Structures*, 38(5):593–600, 2005.

Appendix

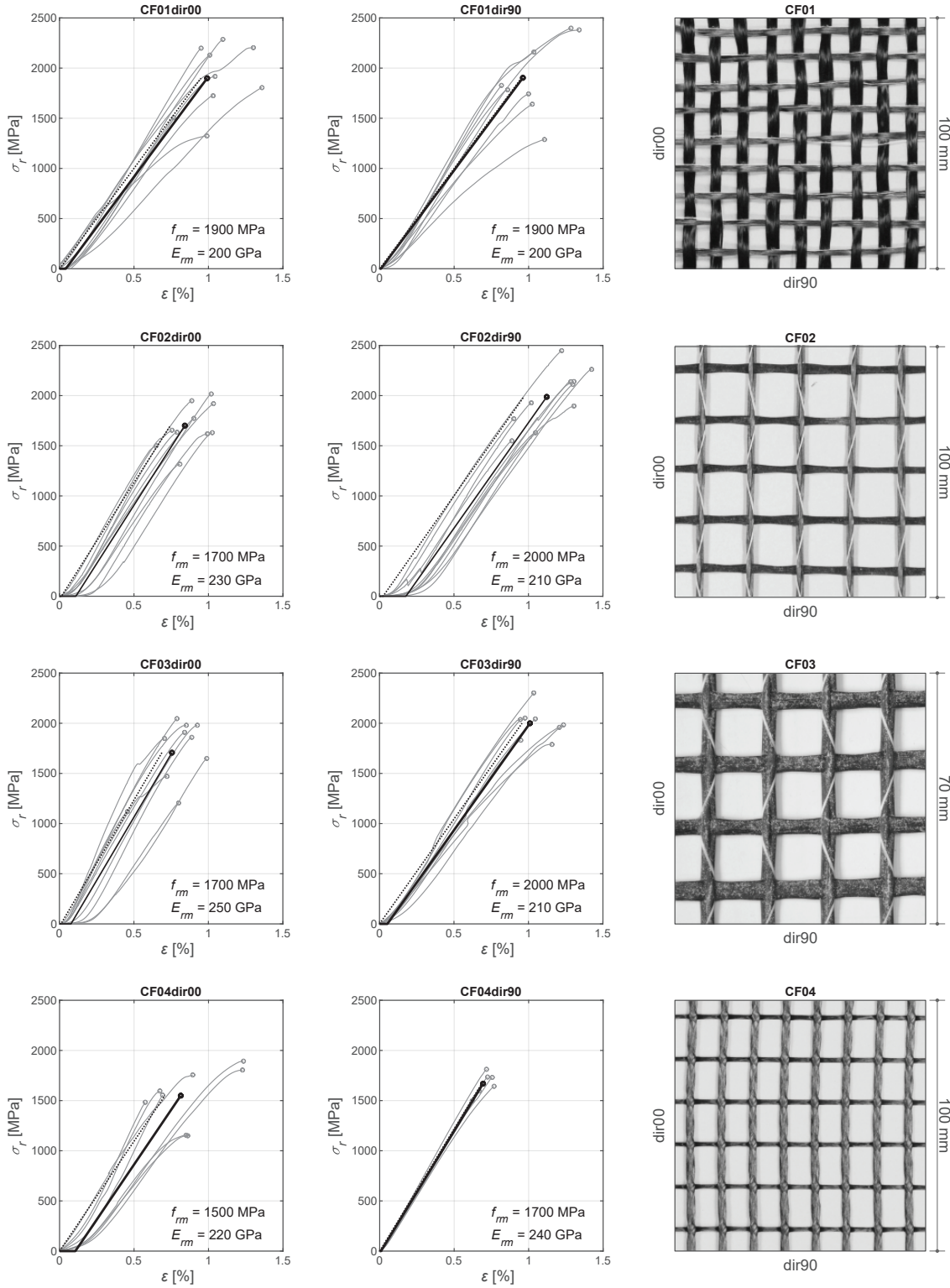
Pull-out tests

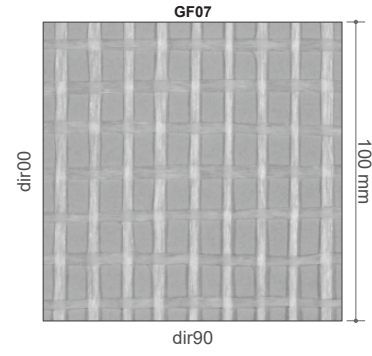
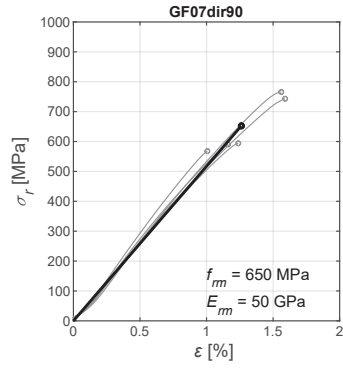
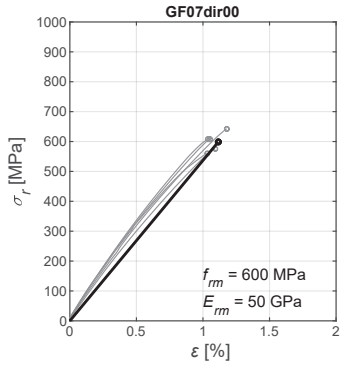
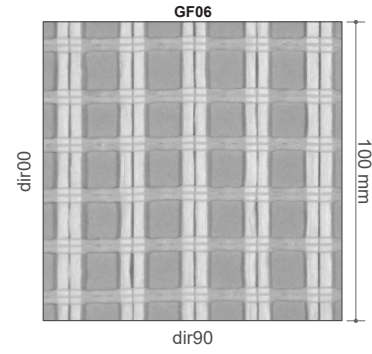
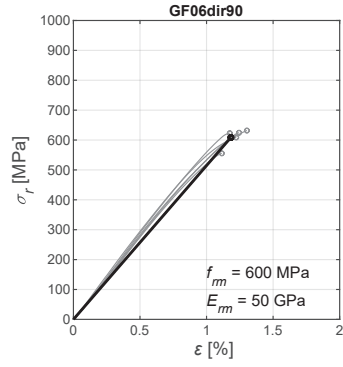
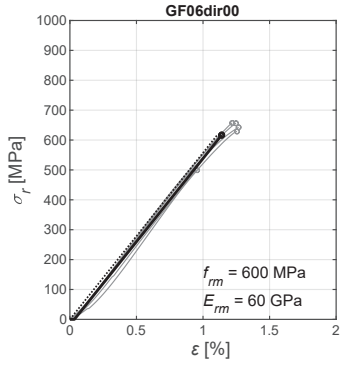
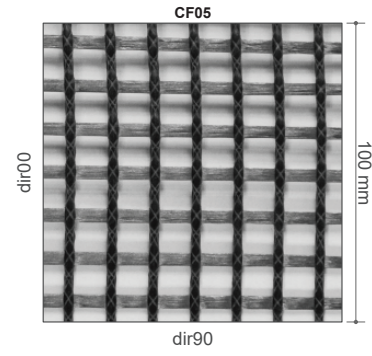
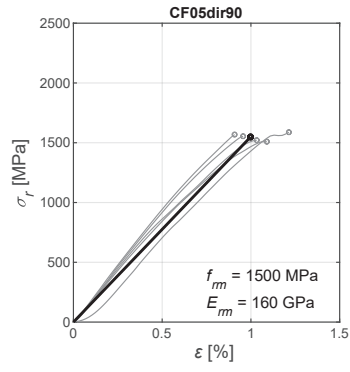
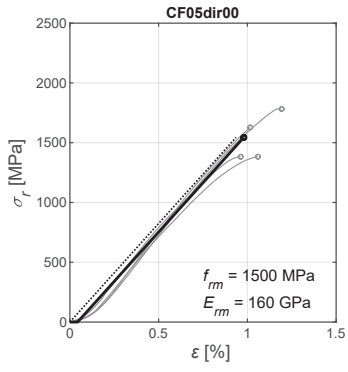
Results of pull-out test for fabric CF02. Single tests in light gray and tri-linear average in black.



Fabrics

Results of tension tests of single rovings extracted from the fabric-grid. Single tests in light gray, bilinear average response in black (considering an activation strain ϵ_0), while the theoretical response of a straight bare roving is represented by the dotted line.

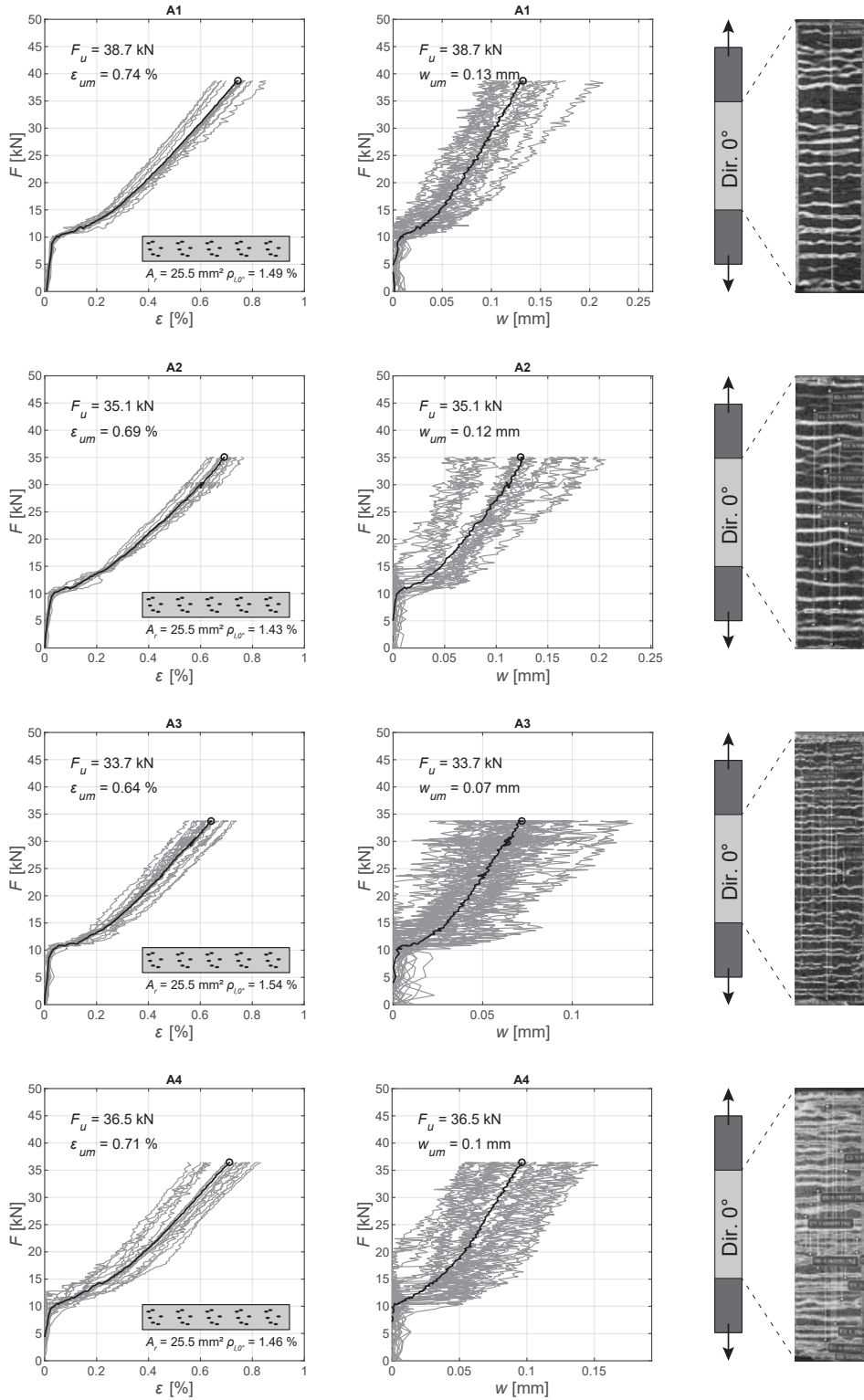


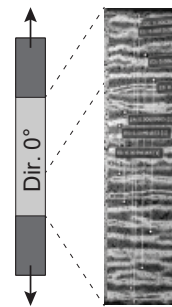
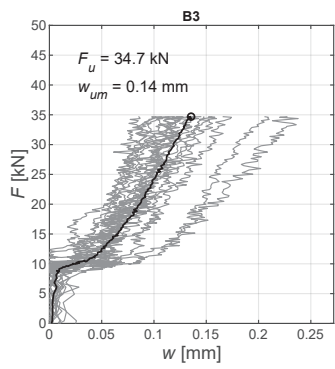
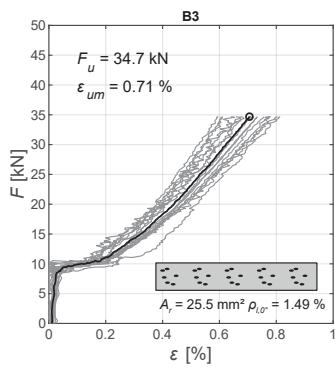
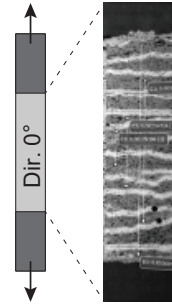
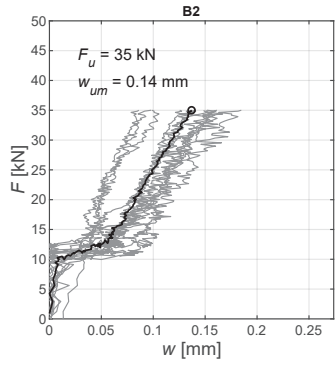
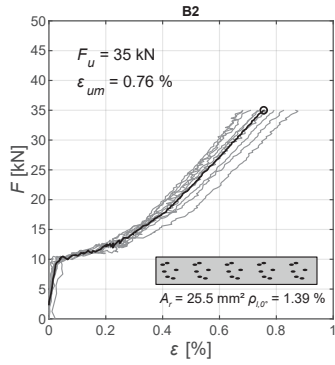
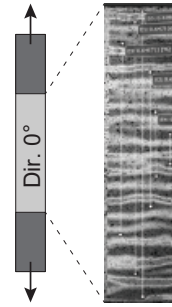
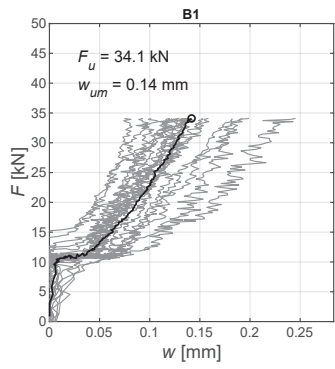
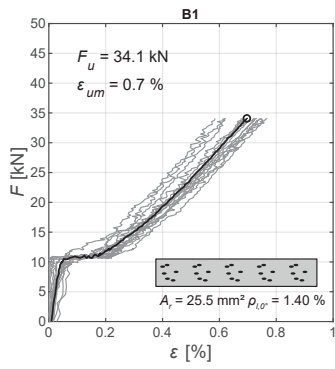


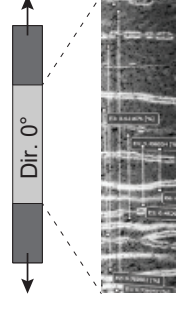
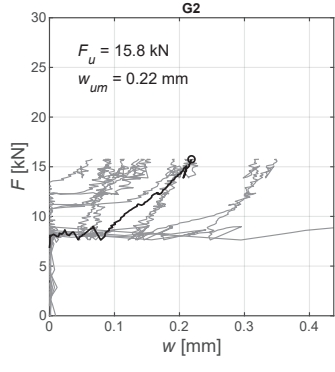
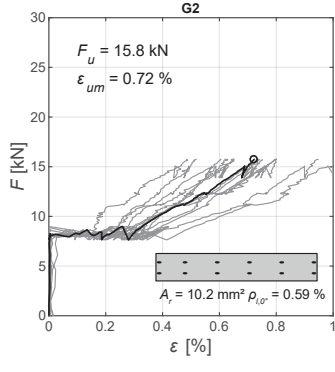
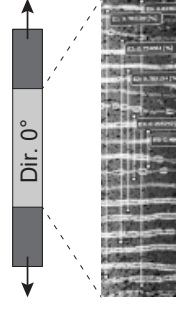
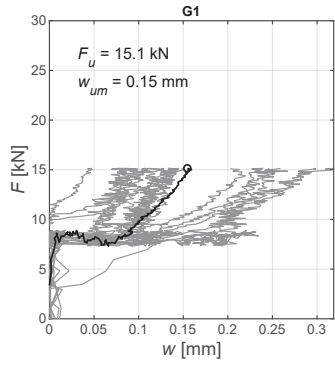
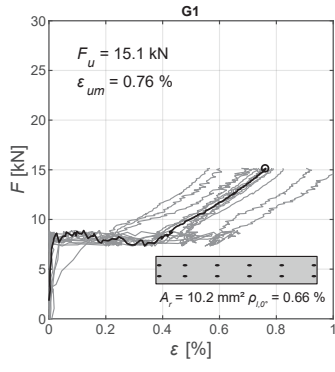
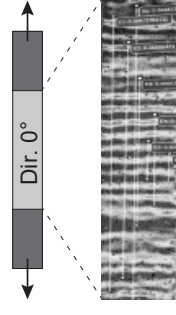
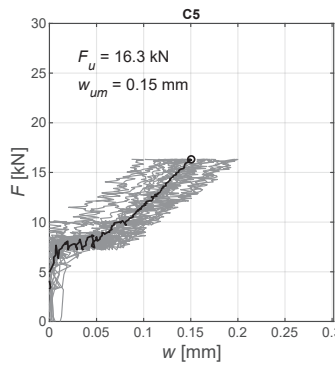
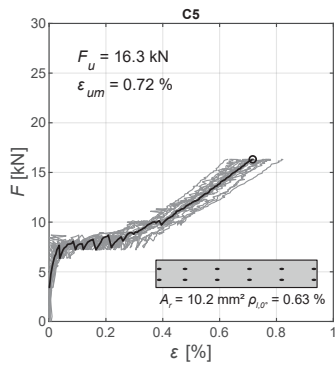
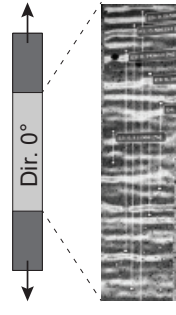
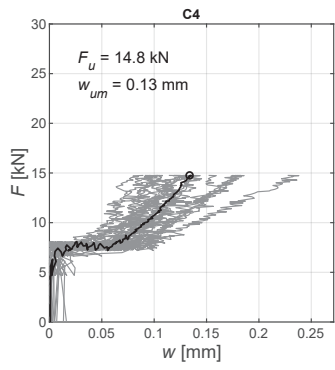
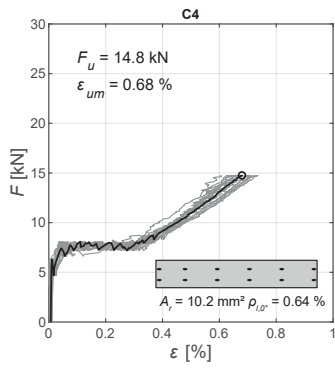
Fabric	Coating	Direction	Linear		Cross		Grid		Elastic		Standard		Strength		Standard		Straightening		Manufacturer
			name	type	α_r	λ_r	a_r	e_r	E_{rm}	$\sigma(E_r)$	f_{rm}	$\sigma(f_r)$	ϵ_{rom}	name					
[...]	[...]	[°]	[hex]	[mm ²]	[mm]	[GPa]	[GPa]	[MPa]	[MPa]	[%]	[...]								
CF01	-	00°	2×800	0.85	10.0	200	41.2	1900	337	0.04	Tissa								
CF01	-	90°	800	0.43	10.0	200	40.0	1900	384	0.01	Tissa								
CF02	SCS	00°	2×800	0.85	20.0	230	18.8	1700	226	0.11	S+P								
CF02	SCS	90°	1600	0.85	20.0	210	14.3	2000	288	0.18	S+P								
CF03	SCS	00°	2×1600	1.70	17.0	250	24.3	1700	351	0.10	S+P								
CF03	SCS	90°	3200	1.70	17.0	210	31.3	2000	157	0.05	S+P								
CF04	SBR	00°	3200	1.70	12.5	220	68.5	1550	280	0.11	Fraas								
CF04	SBR	90°	800	0.43	18.0	245	13.4	1700	112	0.01	Fraas								
CF05	SBR	00°	3200	1.70	12.5	165	14.4	1540	196	0.04	Fraas								
CF05	SBR	90°	3200	1.70	12.5	155	11.7	1550	32	0.00	Fraas								
GF06	SBR	00°	2×2400	1.92	17.0	56	3.0	617	67	0.03	Fraas								
GF06	SBR	90°	2×1200	0.96	17.0	51	2.2	610	30	0.00	Fraas								
GF07	epoxy	00°	2×1200	0.96	10.0	54	2.5	600	32	0.00	Kast								
GF07	epoxy	90°	2×1200	0.96	12.5	52	4.3	650	94	0.00	Kast								

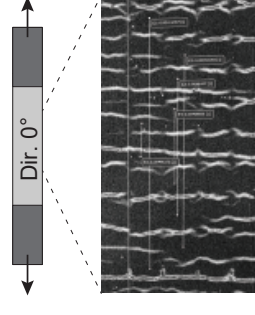
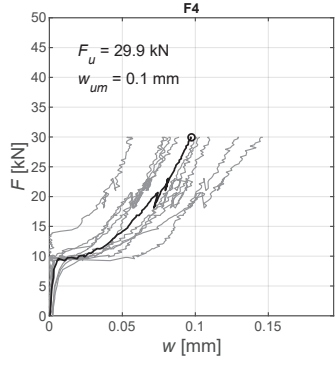
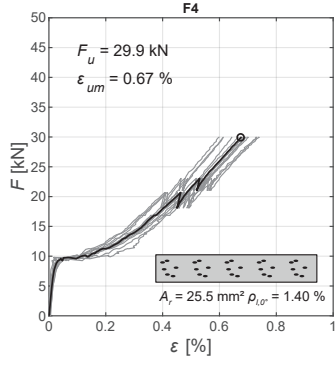
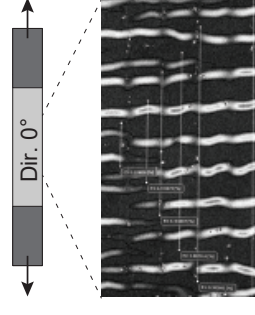
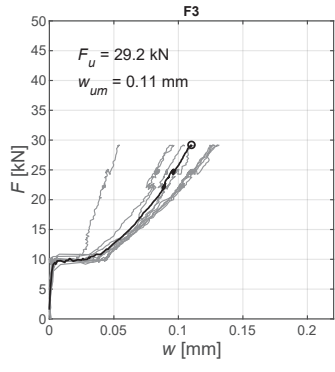
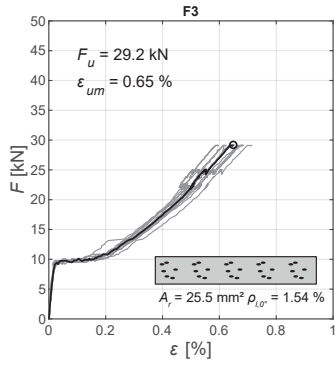
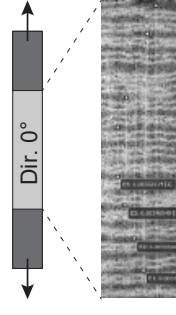
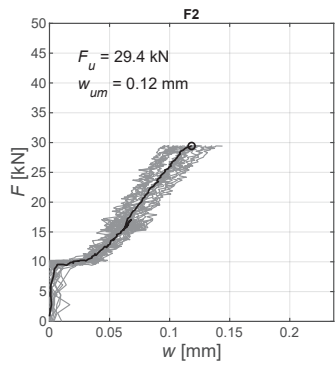
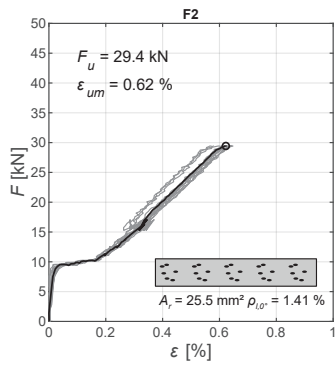
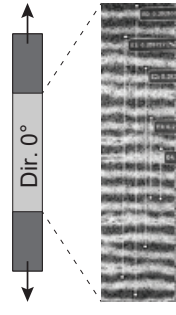
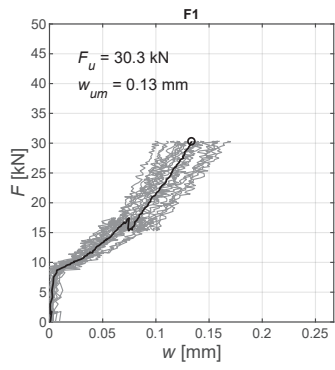
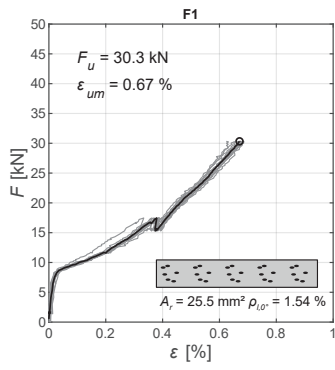
Composite tension tests

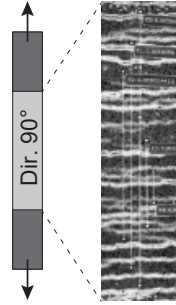
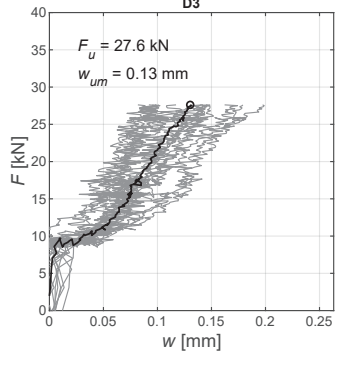
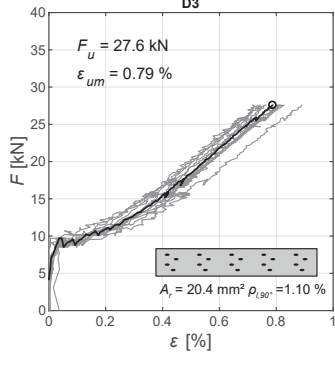
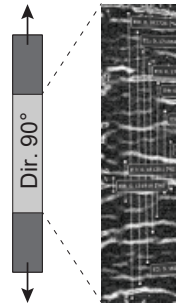
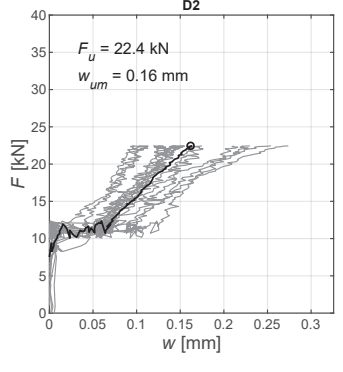
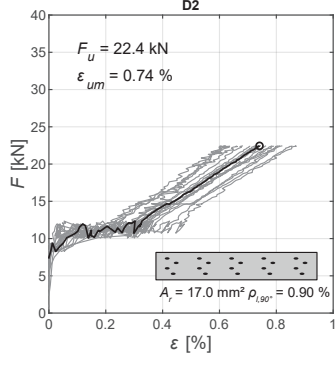
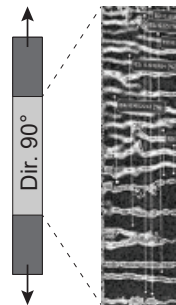
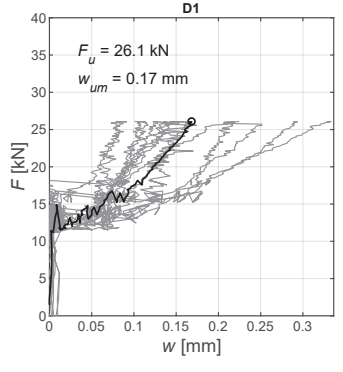
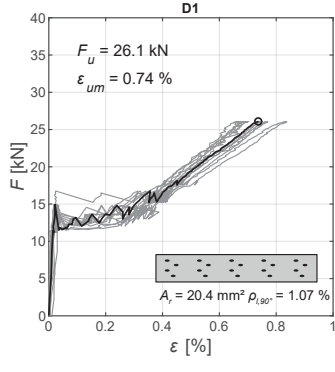
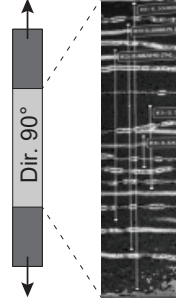
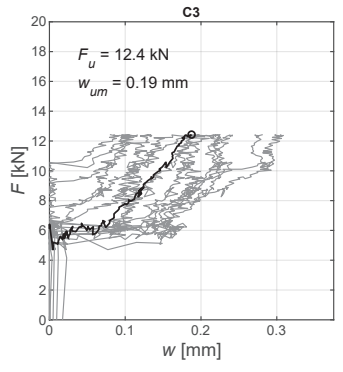
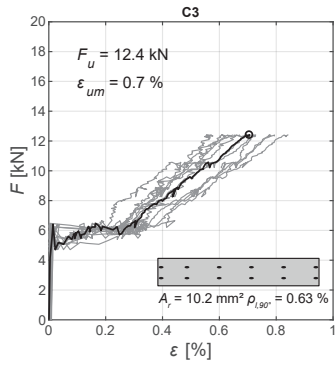
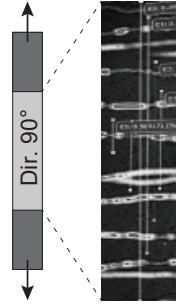
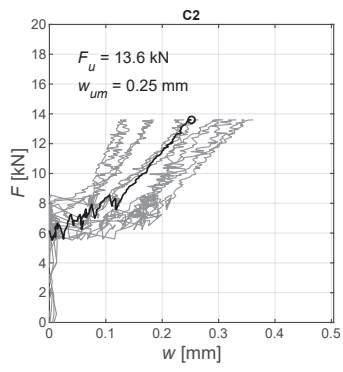
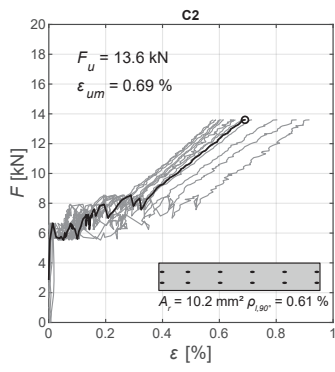
Results of composite tension tests. In the force-strain diagram, the light grey curves correspond to a single virtual extensometer defined in the Digital Image Correlation analysis (these correspond to different lengths and locations but cross at least two cracks). In the force-crack opening diagram, the light grey curves correspond to a single crack. The black curves correspond to the average values.

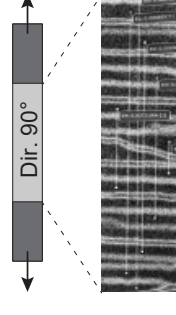
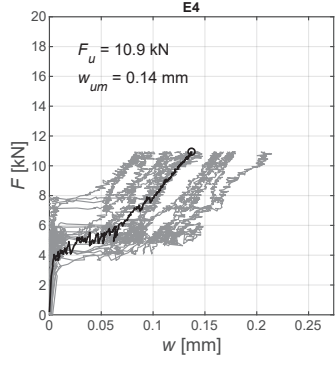
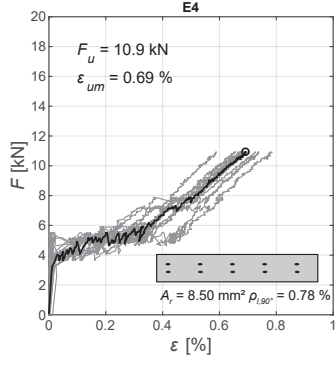
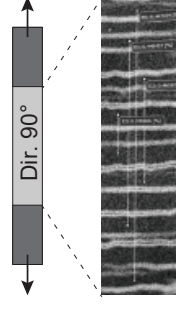
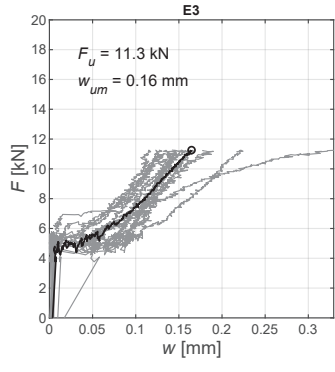
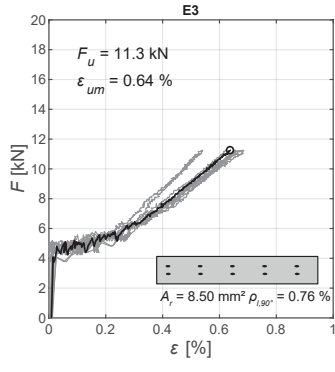
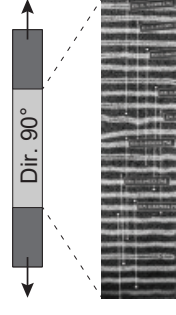
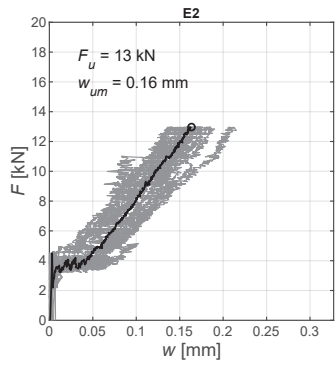
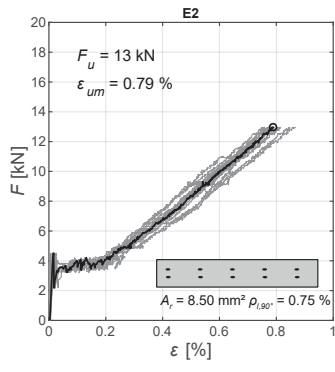
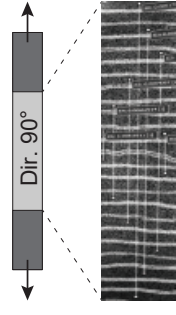
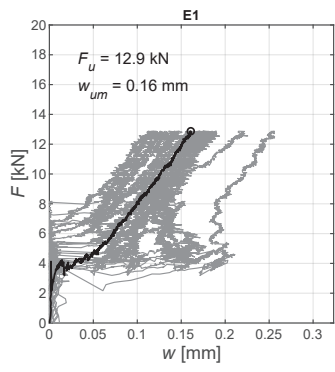
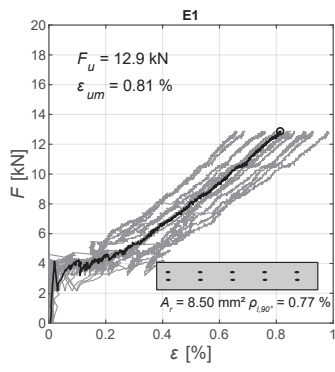


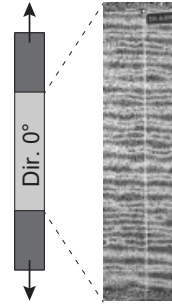
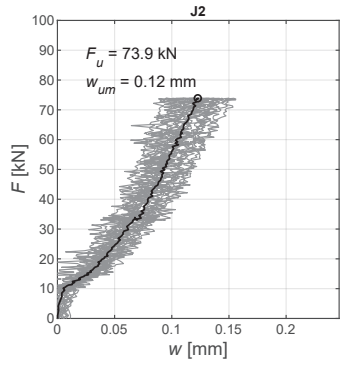
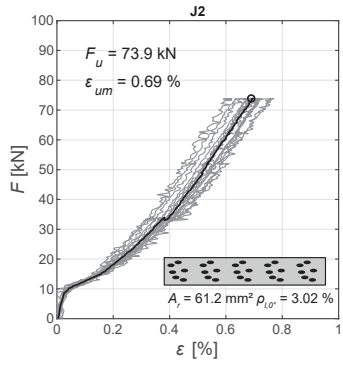
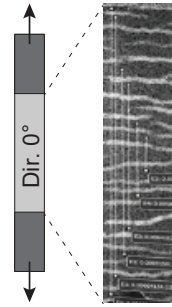
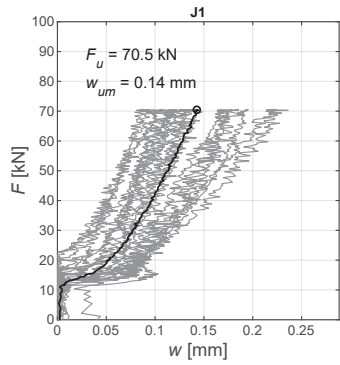
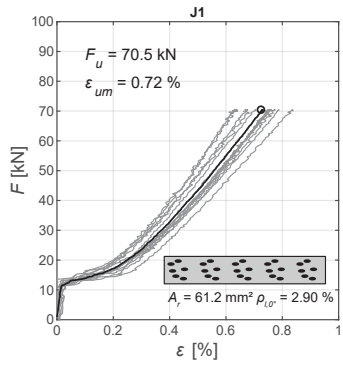
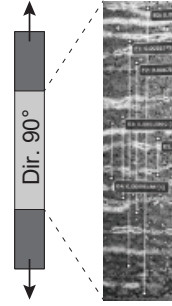
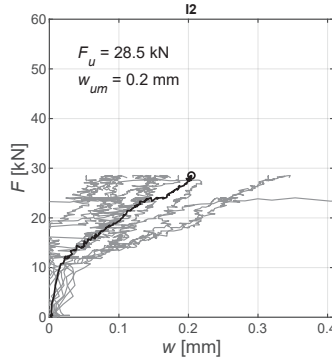
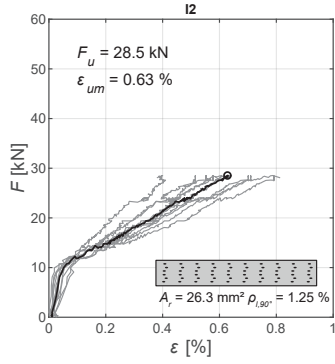
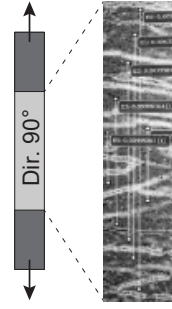
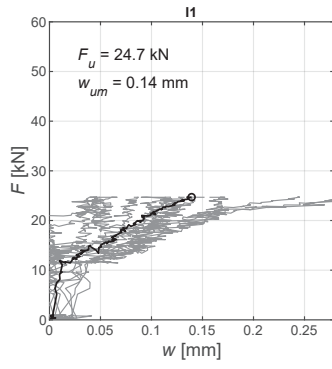
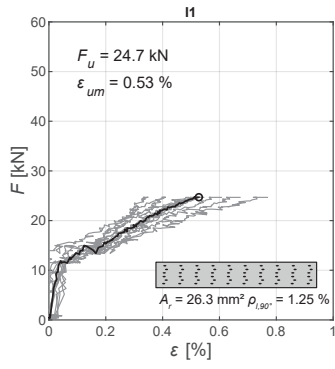






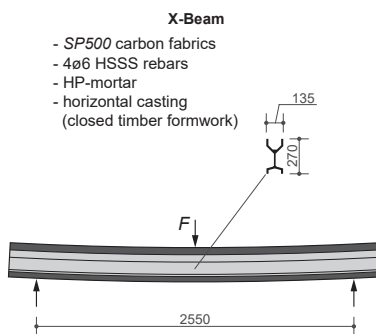
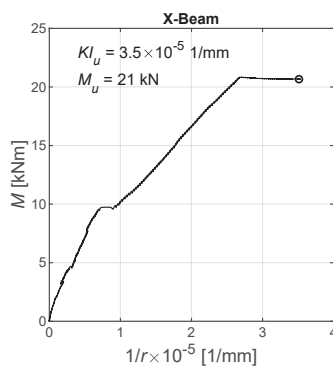
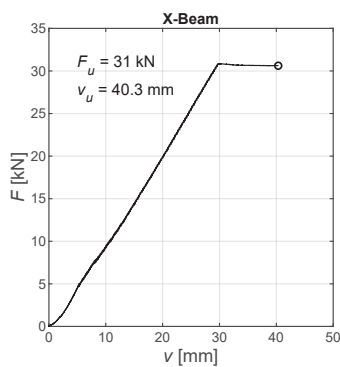
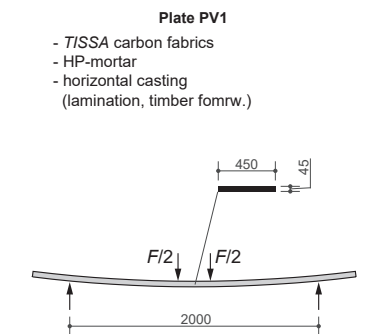
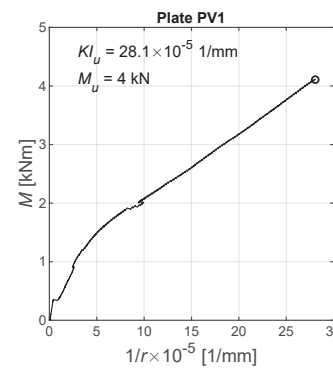
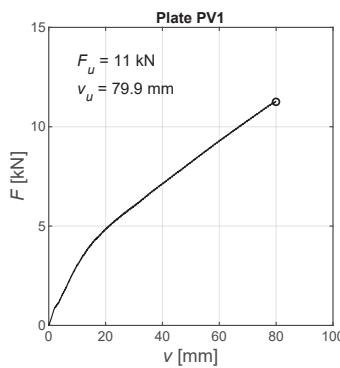
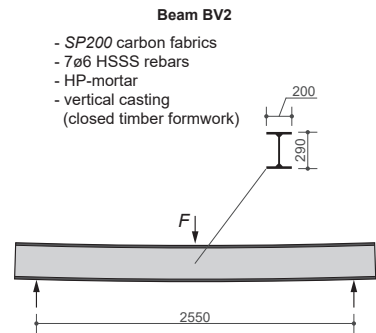
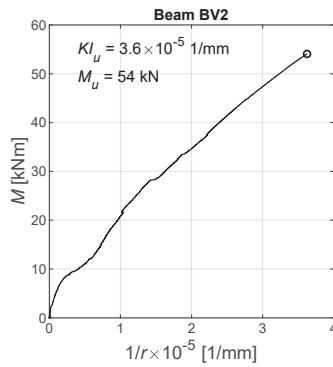
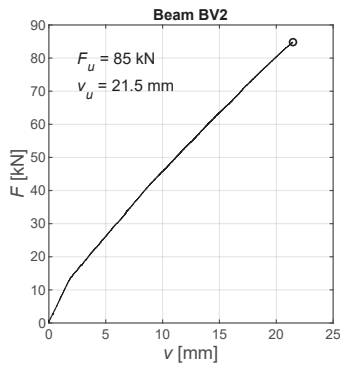
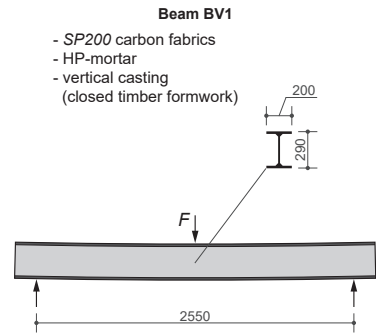
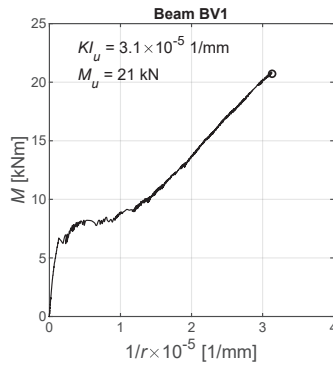
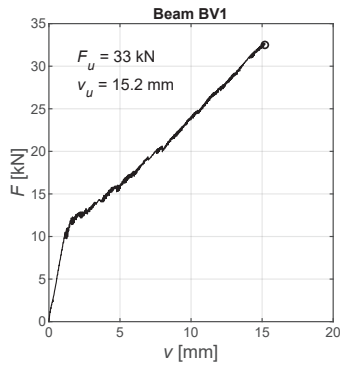


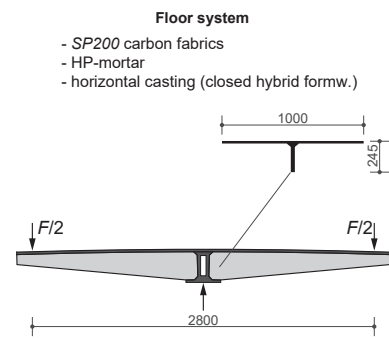
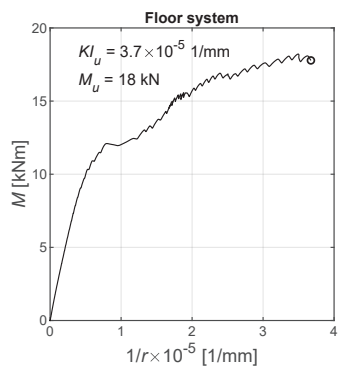
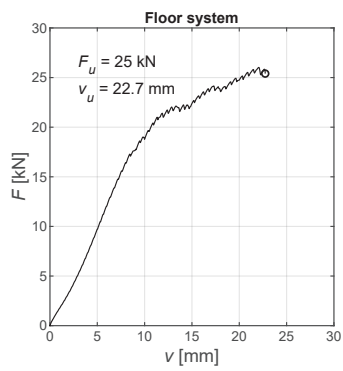
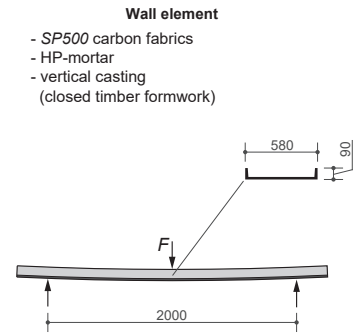
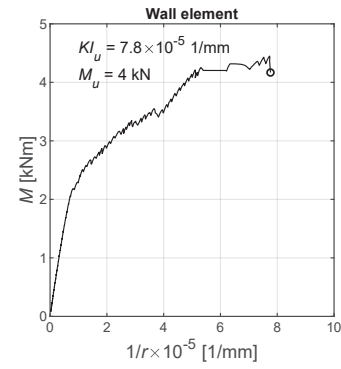
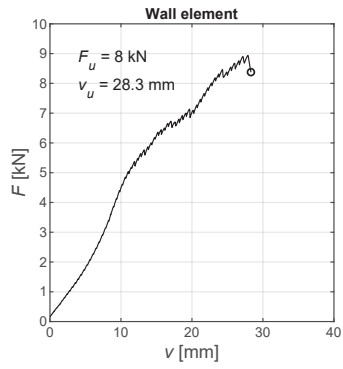
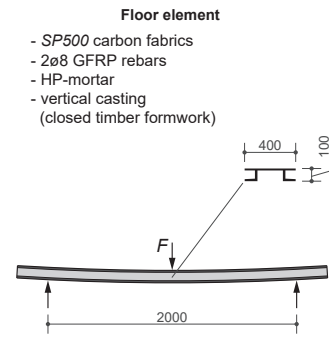
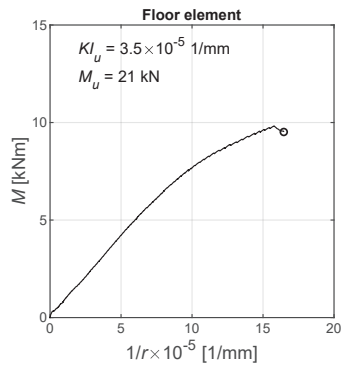
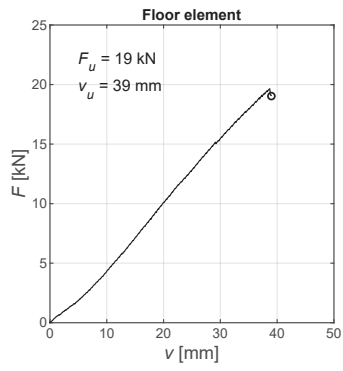


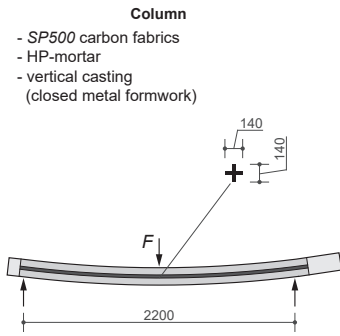
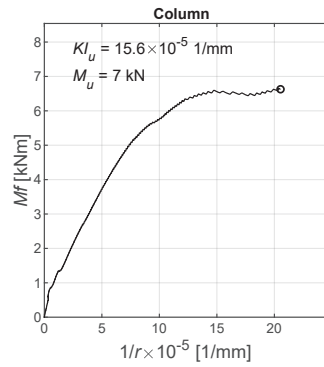
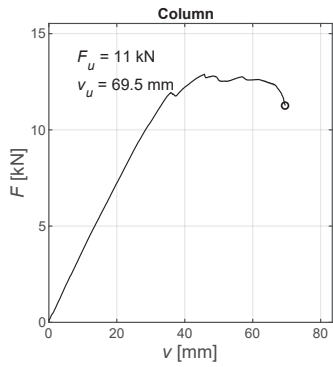
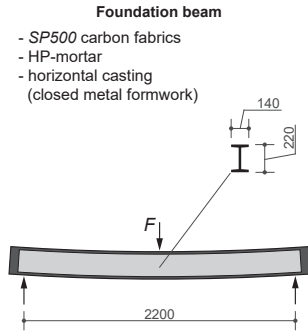
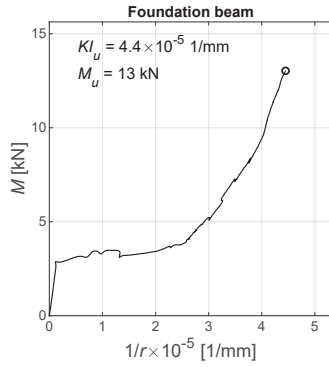
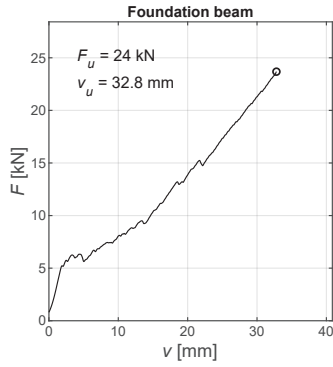
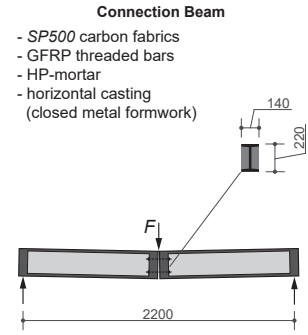
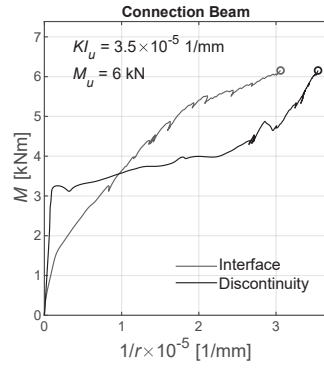
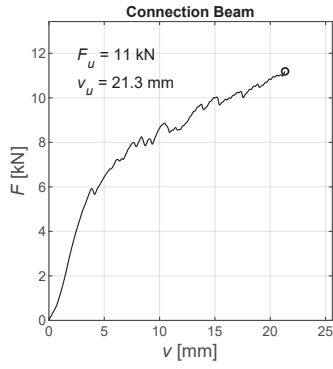


Load tests

Results of all structural load tests performed in the framework of this dissertation.



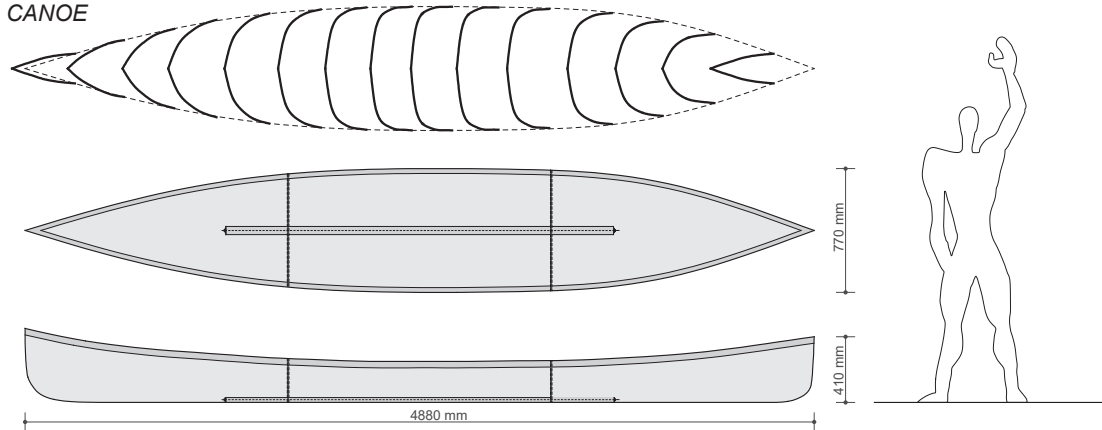




Construction experiences

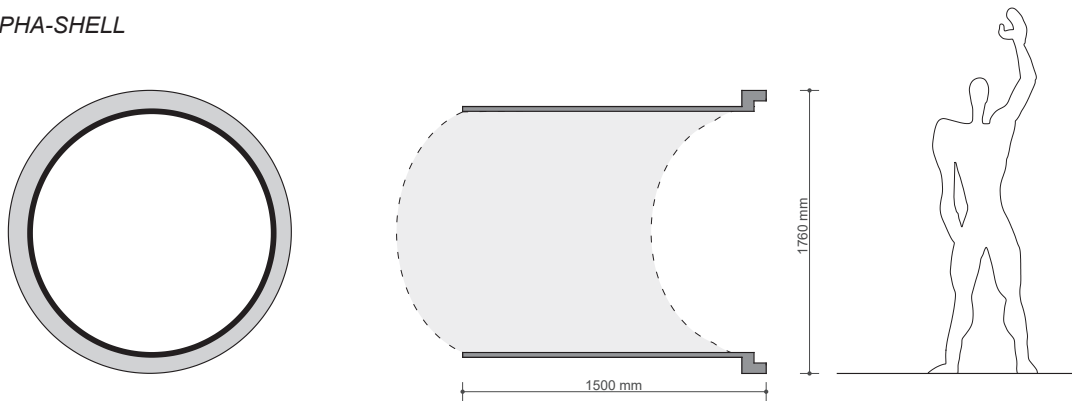
Structures realised within student projects.

CANOE

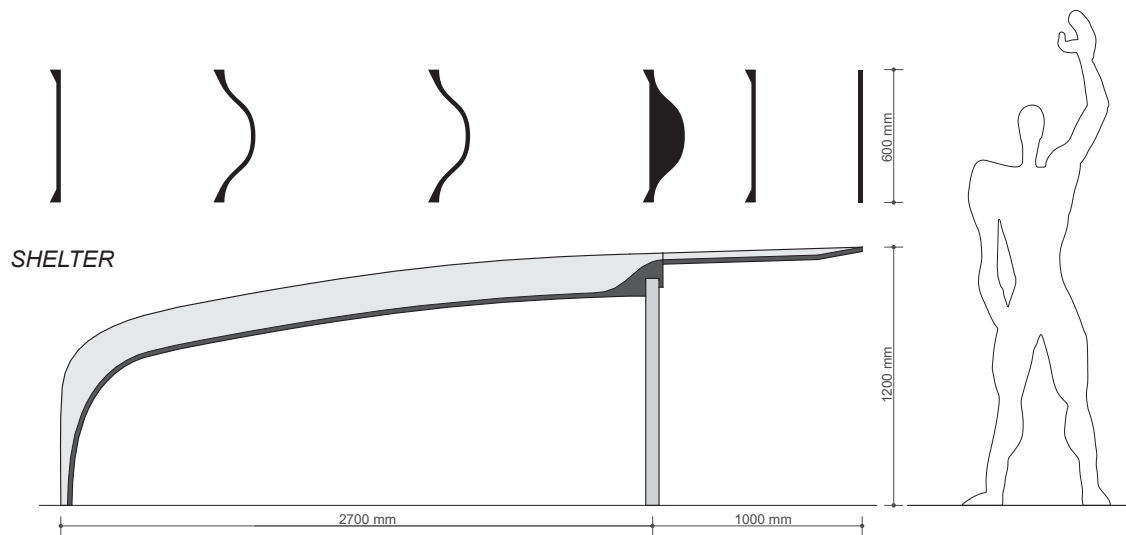


YEAR:	2017
LOCATION:	Structural Concrete Laboratory, EPFL, Lausanne (Switzerland)
CASTING METHOD:	Lamination
FORMWORK:	Rubber sheet sustained by a timber shell
REINFORCEMENT:	Tissa uncoated carbon fabrics (CF01)
MORTAR:	Ultra High Performance Mortar

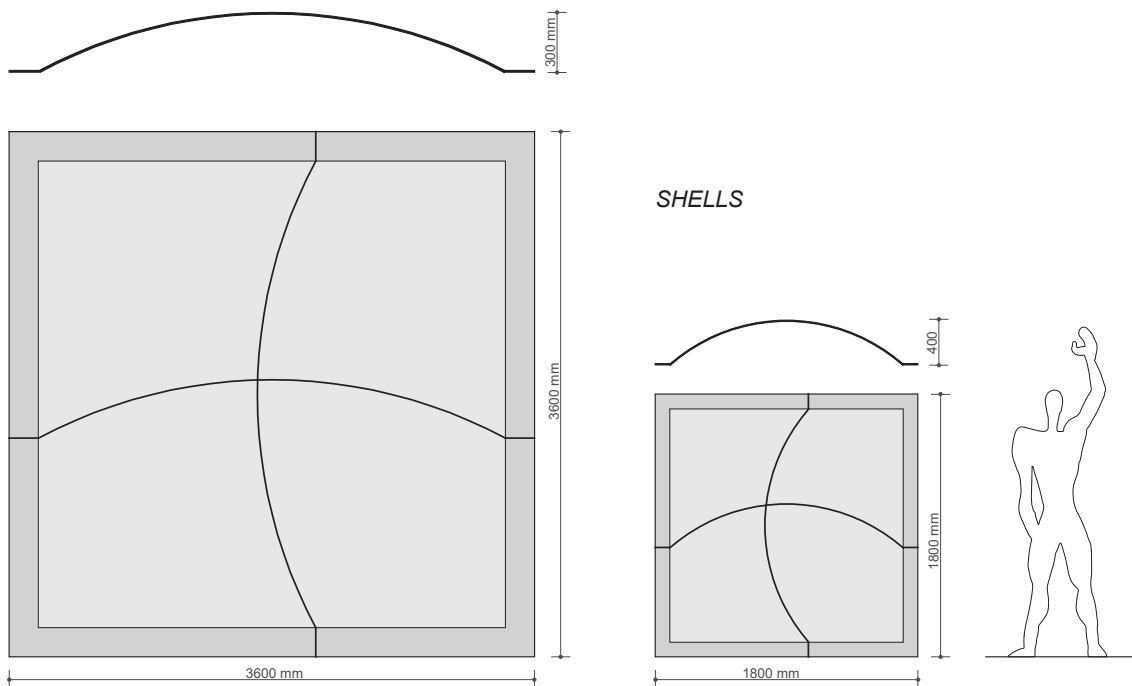
ALPHA-SHELL



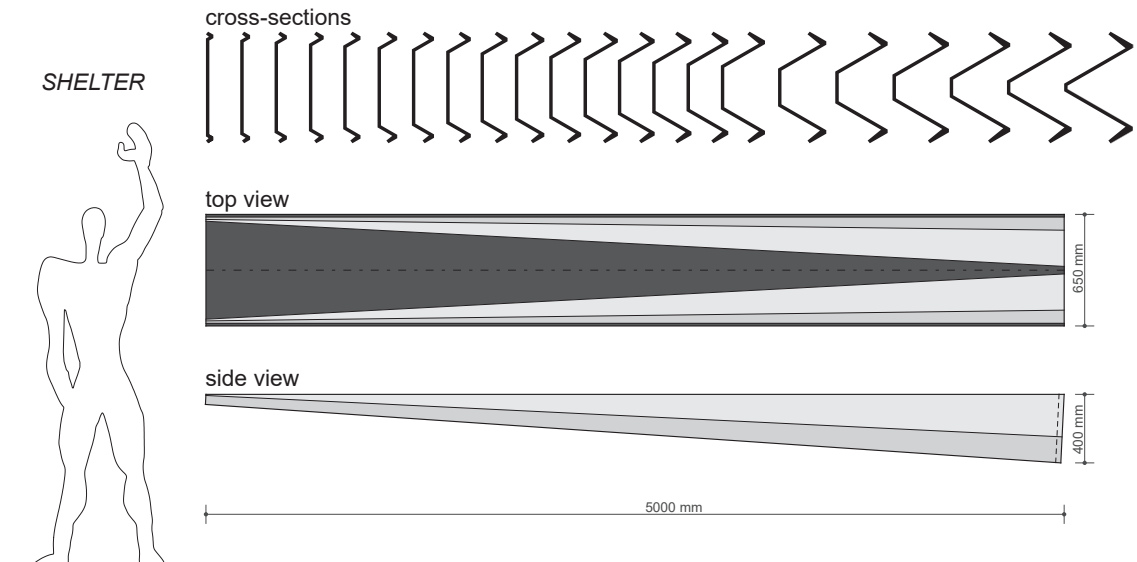
YEAR:	2018
LOCATION:	Structural Concrete Laboratory, EPFL, Lausanne (Switzerland)
CASTING METHOD:	Pouring
FORMWORK:	Plywood stiffened with timber rings
REINFORCEMENT:	Tissa uncoated carbon fabrics (CF01)
MORTAR:	High Performance Mortar



YEAR: 2018
LOCATION: Structural Concrete Laboratory, EPFL, Lausanne (Switzerland)
CASTING METHOD: Lamination
FORMWORK: Rubber sheet sustained by styropor blocks and a timber truss
REINFORCEMENT: Tissa uncoated carbon fabrics (CF01)
MORTAR: High Performance Mortar



YEAR: 2019
LOCATION: Open City Research Platform, Valparaiso (Chile)
CASTING METHOD: Lamination
FORMWORK: Flexible geotextile formwork
REINFORCEMENT: Tissa uncoated carbon fabrics (CF01)
MORTAR: Cement with dune sand (water and superplasticizer)



YEAR:	2020
LOCATION:	Atelier POP-UP, Halle Bleu, Fribourg (Switzerland)
CASTING METHOD:	Pouring
FORMWORK:	Folded steel sheets casting mould
REINFORCEMENT:	S&P coated carbon fabrics (CF03)
MORTAR:	High Performance Mortar

PATRICK VALERI

📍 Route de Cossonay 20, CH-1008 Prilly

🌐 [linkedin.com/in/patrickvaleri](https://www.linkedin.com/in/patrickvaleri)

✉ valeri.patrick@yahoo.it

☎ +41 76 804 0338

<https://orcid.org/0000-0002-1966-1939>



EDUCATION

2020 PhD-candidate **Swiss Federal Institute of Technology EPFL (CH)**

2011 MSc in Civil Engineering **Politecnico di Milano (I)**

2010 ATHENS | Nonlinear computational mechanics **Paris Mines Tech (F)**

2010 ERASMUS **Technische Universität Graz (A)**

2009 BSc in Civil Engineering **Politecnico di Milano (I)**

2005 High-school diploma **European School Varese (I)**

EMPLOYMENT

2015-2020 PhD-candidate **Swiss Federal Institute of Technology EPFL (CH)**

2014-2015 Civil engineer **Zilch+Müller Ingenieure GmbH, München (DE)**

2011-2014 Structural engineer **Jauslin+Stebler Ingenieure AG, Basel (CH)**

ACTIVE MEMBERSHIPS

2018 Convener of the **Swiss Young Members Group** of the International Federation for Structural Concrete *fib-CH*

PRICES | AWARDS | FELLOWSHIPS

2019 *fib* selection Award: *fib*-Conceptual design Symposium, Madrid **(ES)**

2019 ENAC Exploratory Grant Co-applicant for the construction of a pavilion

2018 ENAC special equipment funding Main applicant for laboratory equipment

2018 *fib* Special Mention Award 12th *fib* PhD Symposium, Prague **(CZ)**

2018 *cemsuissse* research grant Co-applicant for project #201801

2018 BASF Excellence Award 12th *fib* PhD Symposium, Prague **(CZ)**

2016 ENAC Seed Money Co-applicant for the Social Concrete project

SKILLS

Languages English (C1) | French (B1) | Italian (native) | German (native) | Spanish (A1)

Software MS Office | Adobe Photoshop | InDesign | Illustrator | LaTeX
MatLab | Python | Wolfram Mathematica | Autocad | Sofostik | Cubus

INTERESTS

Photography Member of *Club-Photo EPFL*

Cycling International bikepacking tours (annually, since 2013)

Hiking Level 1 ASGM certified on avalanche safety *Swiss Mountain Training*

Climbing Completion of the 54th alpine and safety course at *CAI-SEM Silvio Saglio* Milano

PERSONAL DATA

Born 1985 in Cologne, Germany | German nationality | Swiss resident permit **B** | Driver license **B**